Universidade de Aveiro Departamento de Química
2011

Dora Salomé Correia Coelho

Novos materiais poliméricos furânicos baseados na reacção reversível de Diels-Alder

Novel furan polymer materials based on the reversible Diels-Alder reaction

Universidade de Aveiro Departamento de Química
2011

Dora Salomé Correia Coelho

Novos materiais poliméricos furânicos baseados na reacção reversível de Diels-Alder

Novel furan polymer materials based on the reversible Diels-Alder reaction

Dissertação apresentada à Universidade de Aveiro para cumprimento dos requisitos necessários à obtenção do grau de Doutor em Química, realizada sob a orientação científica do Doutor Alessandro Gandini, Investigador Coordenador do CICECO/Departamento de Química da Universidade de Aveiro, e do Doutor Armando Jorge Domingues Silvestre, Professor Associado com Agregação do Departamento de Química da Universidade de Aveiro

Apoio financeiro do POCTI no âmbito do III Quadro Comunitário de Apoio.

Apoio financeiro da FCT e do FSE no âmbito do III Quadro Comunitário de Apoio.

Ciência.Inovação 2010 Programa Operacional Ciência e Inovação 2010
MINISTÉRIO DA CIÊNCIA, TECNOLOGIA E ENSINO SUPERIOR

Ao meu pai…

“O valor das coisas não está no tempo que elas duram, mas na intensidade com que acontecem. Por isso, existem momentos inesquecíveis, coisas inexplicáveis e pessoas incomparáveis.”

Fernando Pessoa

"I believe in intuition and inspiration. Imagination is more important than knowledge. For knowledge is limited, whereas imagination embraces the entire world, stimulating progress, giving birth to evolution. It is, strictly speaking, a real factor in scientific research."

"The important thing is not to stop questioning.
Curiosity has its own reason for existing."

Albert Einstein

o júri

presidente

Doutor José Rodrigues Ferreira da Rocha
professor catedrático da Universidade de Aveiro

Doutor Júlio San Román del Barrio
professor catedrático do Instituto de Ciencia y Tecnología de Polímeros do Consejo Superior de Investigaciones Científicas, Madrid, Espanha

Doutora Verónica Cortés de Zea Bermudez
professora associada com agregação da Universidade de Trás-os-Montes e Alto Douro

Doutora Maria do Rosário Gomes Ribeiro
professora auxiliar do Instituto Superior Técnico da Universidade Técnica de Lisboa

Doutora Ana Margarida Madeira Viegas de Barros-Timmons
professora auxiliar da Universidade de Aveiro

Doutor Alessandro Gandini
investigador coordenador da Universidade de Aveiro

Doutor Armando Jorge Domingues Silvestre
professor associado com agregação da Universidade de Aveiro

agradecimentos

A todos aqueles que, directa ou indirectamente, contribuíram para a realização desta tese, assim como para o meu "crescimento" académico e pessoal, gostaria de expressar aqui os meus sinceros agradecimentos.

Em primeiro lugar, aos meus orientadores, Prof. Dr. Alessandro Gandini e Prof. Dr. Armando Silvestre, não só pela oportunidade de trabalhar nesta área fascinante, mas também pela excelente orientação científica, pela disponibilidade constante, pelo incentivo e entusiasmo demonstrados, pelo apoio incansável, e, sobretudo, pela amizade ao longo destes anos. Por tudo o que me ensinaram, por acreditarem e confiarem em mim e nas minhas capacidades, um eterno muito obrigada!

A todos os membros do Departamento de Química que, de alguma forma, contribuíram para a realização deste trabalho, em particular, ao Prof. Dr. Dmitry Evtyugin pelas análises de GPC, aos técnicos Hilário Tavares pelas inúmeras análises de RMN, Celeste Azevedo pela ajuda e ensinamentos nas análises de FTIR e UV/Vis, Sandra Magina pelas análises térmicas, e, sem esquecer, ao Sr. Morais e ao Pedro Alves pelo material de vidro, nomeadamente no apoio dado nas emergências de vidro partido. A todos, agradeço também a incansável disponibilidade, o apoio e a paciência dispensados, bem como a amizade e boa disposição.

A todos os colegas e amigos do grupo "Lignomacro" e do Laboratório Associado CICECO, pela amizade, boa disposição constante e alegria contagiante e inspiradora, e também pelo apoio e colaboração prestados durante a execução deste trabalho. Obrigada por terem tornado os dias de trabalho mais agradáveis e divertidos! Especialmente, quero agradecer à Andreia, Fabiane, Gisela, Liliana, Mónica, Paula Pinto, Ricardo, Sandra, Sónia e Vera, não só pela vossa amizade e boa disposição, mas também pelos conselhos, pelo apoio e pelo encorajamento nas horas mais difíceis. Muito obrigada por me aturarem e aceitarem tal como sou, por me ouvirem, compreenderem e me deixarem partilhar com vocês as minhas alegrias e tristezas.
À Mónica e à Belinda, tenho ainda que agradecer o apoio e a disponibilidade face às dificuldades e imprevistos ocorridos durante a parte experimental deste trabalho. Obrigada pela vossa ajuda, amizade e paciência!

A todos os meus amigos e aquelas pessoas especiais (vocês sabem quem são!) que, independentemente da "posição geográfica", me acolheram e acompanharam durante todo ou parte deste percurso, um muito obrigada repleto de carinho por estarem presentes, por proporcionarem momentos únicos de alegria, descontracção e diversão, e por me ouvirem, apoiarem e aturarem.

Por último, mas não menos importante, agradeço à minha família, e, em especial, ao Roberto, por tudo o que significa para mim! Um eterno uito obrigada por tudo o que fizeram por mim, por confiarem e acreditarem que eu iria conseguir, pela paciência, compreensão e força, e por, simplesmente, estarem presentes na minha vida e ajudarem a superar com sucesso cada desafio que surge.

Desejo expressar ainda o meu agradecimento ao Departamento de Química da Universidade de Aveiro, ao CICECO e à plataforma IDPoR por possibilitarem a execução deste trabalho, e à Fundação para a Ciência e a Tecnologia (FCT) pelo apoio financeiro através da concessão da bolsa de Doutoramento SFRH/BD/28271/2006 e pelo Programa Nacional de Re-equipamento Científico (PNRC) REEQ/515/CTM/2005.

A todos, o meu Muito Obrigada!

palavras-chave

Recursos renováveis, Furfural, polímeros furânicos, maleimida, reacção de Diels-Alder, reacção de retro-Diels-Alder, policondensação, macromoléculas lineares, ramificadas e reticuladas, reversibilidade térmica.

resumo

A futura e inevitável escassez dos recursos fósseis, juntamente com o aumento imprevisível dos seus preços, levou, nas últimas décadas, a um aumento impressionante de iniciativas dedicadas não só à procura de fontes alternativas de fornecedores de energia, mas também de produtos químicos e polímeros a partir de fontes renováveis, em particular da biomassa vegetal. Entre estes, os polímeros derivados de monómeros furânicos constituem uma classe única de materiais cujas estruturas podem, em princípio, simular virtualmente os seus homólogos actualmente derivados de recursos fósseis.

O anel furânico é uma estrutura heterocíclica com um carácter diénico pronunciado, o que torna-o um dieno particularmente apropriado para a reacção de Diels-Alder (DA) com dienófilos como a maleimida. Um dos aspectos mais relevantes da reacção de DA é a sua reversibilidade em função da temperatura, a qual permite que os aductos sejam facilmente revertidos nos seus precursores por aumento da temperatura (reacção de retro-DA). No caso específico da combinação furano-maleimida, a formação do aducto predomina até cerca de 60ºC, enquanto a reacção inversa é dominante acima de 100ºC. A combinação desta característica da reacção de DA com a química de compostos furânicos pode abrir um novo caminho para a preparação de materiais macromoleculares funcionais com base em fontes renováveis e com aplicações promissoras como auto-reparação e reciclabilidade. O principal objectivo desta Tese, é a síntese e caracterização de novos materiais poliméricos termo-reversíveis, aplicando a reacção de DA a monómeros complementares com estruturas dos tipos furânico (o dieno, designado por A) e de maleimida (o dienófilo, designado por B).

A primeira etapa neste trabalho envolveu a síntese, purificação e caracterização de novos monómeros furânicos e de maleimida do tipo AA, A_3, BB, B_3, AB, AB_2, cada um com diferentes grupos separadores das funções reactivas. Posteriormente, estes monómeros foram polimerizados e despolimerizados por ciclos de DA/retro-DA utilizando diferentes combinações. A formação e dissociação de todos os aductos de DA foram seguidas por ambas espectroscopias de UV e RMN de ^{1}H.

O primeiro sistema de DA estudado foi uma combinação modelo entre reagentes mono-funcionais (-A+-B), nomeadamente o acetato furfurílico (FA) e a *N*-metilmaleimida (MM), ambos comercialmente disponíveis. O objectivo desta abordagem foi estudar a cinética e o equilíbrio da formação/dissociação dos aductos de DA e obter indicações sobre as condições mais adequadas a serem usadas na preparação dos correspondentes novos materiais macromoleculares. Além disso, pretendia-se verificar a presença ou ausência de reacções secundárias que poderiam intervir em ambas as vias directa e inversa das reacções, mesmo após vários ciclos. A espectroscopia de UV forneceu informação quantitativa sobre a cinética de formação do aducto

através da diminuição progressiva da absorvência máxima a 293 nm correspondente ao grupo maleimida, a diferentes temperaturas (35, 50, 65 ºC) Reciprocamente, a correspondente reacção de retro-DA foi seguida a 90 ºC através do aumento do mesmo pico. A reversibilidade destes sistemas foi verificada com sucesso após uma sequência de ciclos de DA/retro-DA. Adicionalmente, verificou-se que os espectros originaram um ponto isosbéstico, provando que estes sistemas não envolvem quaisquer reacções secundárias. Uma vez que foi usado um excesso de FA, as reacções de DA modelo apresentaram um comportamento cinético de pseudo-primeira ordem, com a constante de velocidade *k* mais alta ($2.1x10^{-5}$ $dm^3mol^{-1}s^{-1}$) para T=65 ºC. A correspondente energia de activação foi de 39.0 $kJ.mol^{-1}$. A reacção de retro-DA seguiu um comportamento de primeira ordem, com constante de velocidade de $1.6x10^{-6}$ s^{-1}. A evolução deste sistema por RMN de ^1H a 65ºC deu-nos informações mais detalhadas sobre a sua evolução estrutural, ou seja, à medida que a intensidade dos picos atribuídos à formação do aducto aumentaram progressivamente ao longo do tempo, os pertencentes aos reagentes iniciais diminuiram proporcionalmente. O "rendimento final", calculado após 20 dias à temperatura ambiente, foi de aproximadamente 70%. A reacção de retro-DA foi depois seguida a 90ºC, observando-se tal como na espectroscopia de UV, o deslocamento da reacção no sentido da regeneração dos reagentes de partida. A viabilidade de múltiplos ciclos de DA/retro-DA estabelecidos pela espectroscopia de UV foi igualmente confirmada por RMN de ^1H.

O passo seguinte envolveu o estudo de um sistema de policondensação linear baseado no crescimento gradual por reacção de DA entre um monómero bisfurânico A-A e um do tipo bismaleimida B-B, seguindo a mesma abordagem que no sistema modelo. O poliaducto linear foi obtido a partir de soluções equimolares dos monómeros, por reacção de DA a 65ºC. O progresso desta polimerização foi seguido por espectroscopia de UV e RMN de ^1H e, mais qualitativamente, pelo aumento da viscosidade do meio. A reacção seguiu um comportamento de segunda ordem, com uma constante de velocidade de $9.4x10^{-6}$ $dm^3mol^{-1}s^{-1}$, e observou-se novamente um ponto isosbéstico nos dados de UV. Os espectros de RMN apresentaram o padrão esperado, nomeadamente o aumento progressivo dos sinais associados ao aducto e a correspondente diminuição dos grupos furano e maleimida livres. A despolimerização do poliaducto através da reacção de retro-DA foi seguida a 110ºC usando as mesmas técnicas. Os dados de UV mostraram o retorno progressivo da absorção dos grupos de maleimida, seguindo um comportamento cinético de primeira ordem, com constante de velocidade de $2.5x10^{-6}$ s^{-1}, até à completa regeneração de ambos os monómeros. Os espectros de RMN providenciaram mais uma vez informação estrutural sobre o progresso da despolimerização, a qual foi acompanhada por uma diminuição progressiva da viscosidade. Adicionalmente, para seguir a retro-DA, adicionou-se um excesso de composto furânico monofuncional, nomeadamente o 2,5-dimetilfurano (DMFu), ao sistema de modo a bloquear as funções maleimida complementares, evitando assim a repolimerização após arrefecimento. Os productos isolados foram então o monómero bisfurânico AA, DMFu que não reagiu e o bisaducto não-polimerizável de BB com DMFu. Este resultado indicou claramente que o polímero foi de facto revertido nos seus monómeros durante a reacção de retro-DA.

O terceiro sistema estudado foi outra polimerização linear, seguindo as mesmas condições experimentais que os anteriores, mas com uma estratégia diferente de modo a contornar o problema clássico de assegurar a estequiometria exacta dos monómeros. As estruturas dos monómeros utilizados incorporam ambos os grupos reactivos, i.e, moléculas do tipo A-B. A polimerização prematura destes monómeros intrinsecamente reactivos foi evitada com a protecção do grupo maleimida na forma de um aducto de DA com furano, até a incorporação do substituinte furânico na outra extremidade. Portanto, a policondensação destes monómeros foi iniciada após a desprotecção *in situ* deste composto mediante aquecimento, seguido de arrefecimento até à temperatura adequada para polimerizar. Os resultados obtidos por UV e RMN sugerem que de facto o uso de monómeros do tipo A-B oferece um melhor sistema linear.

Em seguida, foram estudados sistemas de policondensação não-linear por reacção de DA, entre monómeros (um ou ambos) com funcionalidade superior a dois, nomeadamente sistemas do tipo A_3+B-B ou A-A+B_3, seguindo

mais uma vez as mesmas condições experimentais. Uma vez que utilizam monómeros complementares contendo, em média, mais de duas funcionalidades, estes sistemas conduzem a materiais reticulados. Nestes estudos, foram usadas três razões molares de [maleimida]/[furano], nomeadamente 1.0, 0.75 e 0.5, de modo a estudar ambas as situações de não-gelificação e reticulação. Ambos sistemas apresentaram um comportamento regular e boa reciclabilidade quer para gerar situações que possam conduzir à formação de redes a diferentes graus de conversão, ou que possam parar antes da sua obtenção, conforme previsto pela equação de Flory-Stockmayer. Como esperado, a utilização de grupos complementares em quantidades estequiométricas produziu o espessamento mais rápido e a reticulação quase completa; à medida que a quantidade relativa de monómero trifuncional decresceu, as reacções pararam antes da reticulação, ou seja, originaram meios altamente viscosos contendo polímeros solúveis altamente ramificados. As reacções de retro-DA a 110 ºC conduziram à gradual dissolução das partículas de gel (quando presentes), tendo sido comprovado pelos espectros de UV e de RMN de ^{1}H, evidenciado a regeneração dos monómeros. Tal como no sistema do tipo A-A+B-B, a reacção de retro-DA foi seguida adicionando um excesso de DMFu ao sistema reaccional. Como esperado, os produtos finais foram os monómeros furânicos, o DMFu em excesso e o trisaducto ou o bisaducto maleimida-DMFu, o que confirma a eficiência da despolimerização com regeneração dos monómeros iniciais.

O último sistema de policondensação por reacção de DA envolveu um monómero assimetricamente substituído do tipo AB_2, capaz de originar estruturas macromoleculares hiper-ramificadas que não reticulam. Este estudo preliminar deste sistema foi seguido nas mesmas condições experimentais que os anteriores, apresentando um comportamento com as características esperadas.

keywords

Renewable resources, Furfural, furan polymers, maleimide, Diels-Alder reaction, retro-Diels-Alder reaction, polycondensation, linear, branched and crosslinked macromolecules, thermal reversibility.

abstract

The inevitable future scarcity of fossil resources, together with their skyrocketting prices, has led in the last decades to a dramatic increase of initiatives devoted not only to the search for alternative sources of energy providers, but also to the search for chemical commodities and polymers from renewable resources, namely the vegetable biomass. Among these, polymers from furan monomers constitute a unique class of materials whose structures can in principle simulate virtually all their current fossil-derived counterparts.

The furan heterocycle displays a pronounced dienic character, which makes it highly suitable as diene in the Diels-Alder (DA) reaction, with dienophiles like maleimide. One of the most relevant aspects of the DA reaction is its thermal reversibility, which allows the adducts to be readily reverted to their precursors as the temperature is raised (retro-DA reaction). In the specific case of the furan-maleimide combination, the adduct formation dominates up to ca. 60ºC, whereas the reverse reaction is overwhelming above ca. 100ºC. The coupling of this DA feature with the furan chemistry can open a new way to prepare functional macromolecular materials based on renewable resources with novel properties and promising applications like mendability and recyclability. In this Thesis, the main goal is the synthesis and characterisation of novel thermoreversible polymer materials by means of the DA reaction, using complementary monomers bearing furan (the diene, assigned as A) and maleimide (the dienophile, assigned as B) moieties.

The first step in this study was the synthesis, purification and characterization of new furan and maleimide monomers, viz. AA, A_3, BB, B_3, AB, AB_2, each bearing different spacing moieties separating the reactive functions. They were then polymerized and depolymerised using different modes of DA/retro-DA cycles. The formation and decoupling of all the DA adducts were followed by both UV and ^{1}H NMR spectroscopy.

The first DA system investigated was on a model combination of monofunctional reagents (-A+-B), namely the commercially available furfuryl acetate (FA) and *N*-methylmaleimide (MM). The purpose of this approach was to study the kinetics and the equilibrium of the formation/decoupling of the DA adducts and to provide clear indications about the most appropriate conditions to be applied in the preparation of the corresponding novel macromolecular materials. Additionally, it aimed at verifying that no detectable side reactions intervened in both forward and backward pathways, even after several cycles. The UV spectroscopy provided quantitative information on the kinetics of the DA adduct formation by monitoring the progressive decrease in the maximum absorbance at 293 nm related to the maleimide moiety, at different temperatures (35, 50, 65ºC). Conversely, the corresponding retro-DA reaction was followed at 90ºC through the increase of the same peak. The reversibility of these systems was successfully checked over a couple of cycles. Additionally, all set of spectra gave rise to an isosbestic point, which proved

that these systems did not involve any side reactions.Since an excess of FA was used here, these model DA reactions displayed a pseudo-first order behaviour, with the highest rate constant *k* ($2.1x10^{-5}$ $M^{-1}.s^{-1}$) for T= 65ºC. The corresponding activation energy was found to be 39.0 $kJ.mol^{-1}$. The retro-DA reaction followed a first order behaviour, with a rate constant of $1.6x10^{-6}s^{-1}$.The evolution of the same system followed by ^1H NMR spectroscopy at 65ºC gave a detailed insight into its structural evolution, viz. as the intensity of the peaks assigned to the adduct formation progressively increased with time, those belonging to the initial reagents decreased correspondingly. The “final yield” taken after 20 days at room temperature, was approximately 70%. The retro-DA reaction was then carried out at 90ºC, and showed the same features as its UV counterparts, namely the displacement of the reaction towards the regeneration of the initial reagents. The feasibility of multiple DA/retro-DA cycles established by UV spectroscopy was confirmed here.

The subsequent stage involved the study of a linear polycondensation system based on the stepwise DA growth between a difuran monomer A-A and a complementary bismaleimide B-B, following the same approach as the model system. The formation of the linear DA polyadduct was achieved by letting equimolar solutions evolve at 65 ºC. The progress of this polymerization was followed by UV and ^1H NMR spectroscopy and, more qualitatively, by the increase in the viscosity of the medium. The reaction followed a second order behaviour, with a rate constant of $9.4x10^{-6}$ $M^{-1}.s^{-1}$, and again, a characteristic isosbestic point was observed in the UV data. The NMR spectra gave the expected pattern, namely the progressive increase in the signals associated with the adduct and the corresponding decrease of those attributed to the unreacted furan and maleimide cycles. The depolymerization of the polyadduct through the retro-DA reaction was followed at 110ºC by the same techniques. The UV time scans showed the progressive return of the absorption due to maleimide moieties following a first-order kinetic pattern, with a rate constant of $2.5x10^{-6}$ s^{-1}, until both monomers were fully regenerated. The ^1H NMR spectra provided once more structural information about the course of this depolymerization, which was accompanied by a progressive decrease in viscosity. Additionally to follow the retro-DA, an excess of a monofunctional furan compound, namely 2,5-dimethylfurfural (DMFu), was added to the system in order to block the complementary maleimide functions, thus avoiding the repolymerisation after cooling. The isolated products were then the difuran monomer AA, the unreacted DMFu and the non-polymerizable bisadduct of BB with DMFu. This result clearly indicated that the polymer had indeed reverted to its monomers during the retro-DA.

The third system studied was another linear polymerization, following the same experimental conditions as the previous, but with a different strategy, in order to avoid the classical problem of ensuring the exact monomer stoichiometry. Here, the monomers incorporated both reactive moieties in their structures, i.e. A-B molecules. Here, the premature polymerization of these intrinsically reactive monomers was avoided by protecting the maleimide group in the form of a furan-DA adduct, until the incorporation of the furan moiety. Therefore, the polycondensation of these monomers was initiated after the *in situ* deprotection of this compound through heating, followed by the cooling to appropriate temperature for polymerization. The results obtained by both UV and NMR spectroscopy suggested that indeed the use of an A-B monomer provides a better linear system.

Non-linear DA polycondensations between monomers (one or both) with functionality higher than two, viz. A-A+B_3 or A_3+B-B systems, were then studied, following once more the same experimental conditions. The use of complementary monomers bearing on average more than two functionalities lead to crosslinked materials. In these systems, three [maleimide]/[furan] molar ratios, viz. 1.0, 0.75 and 0.50, were applied in order to examine both non-gelling and crosslinking situations. Both types of systems displayed a clean-cut behaviour and good recyclability to generate situations either leading to the formation of a network at different degrees of conversions, or ending before its attainment, as predicted by the Flory-Stockmayer equation. As expected, the use of complementary moiety stoichiometry produced the most rapid thickening and near-complete crosslinking, whereas as the relative amount of trifunctional monomer was decreased, the reactions stopped short of crosslinking, i.e. gave highly viscous media containing soluble highly branched polymers. The retro-DA reactions at 110ºC revealed the gradual dissolution of

the gel particles (when present), while the UV and ^{1}H NMR spectra gave, once more, the details of the depolymerization processes leading the systems steadily back to the monomers. As in A-A+B-B depolymerization, to follow the retro-DA, an excess of DMFu DA trap, was added to the systems under the same conditions. As expected, the final products were the furan monomers, the unreacted DMFu and the non-polymerizable trisadduct or the bisadduct of maleimide-DMFu, confirming the efficiency of the retro-DA depolymerisation in the regeneration of the starting monomers.

The last DA polycondensation system involved an assymmetrically substituted monomer of the AB_2 type, capable of generating hyperbranched macromolecular structures that do not crosslink. This preliminary study was followed by the experimental approach applied above and the behaviour of the system displayed the expected features.

Abbreviations and symbols

Δ: Heating

A: Furan moiety

AA: Bisfuran monomer

A_3: Trisfuran monomer

AB: Furan-Maleimide monomer

AB_2: Furan-Bismaleimide monomer

Ac_2O: Acetic anhydride

Abs: Absorvance

***β*-ALA**: *β*-alanine

B: Maleimide moiety

BB: Bismaleimide monomer

B_3: Trismaleimide monomer

b.p.: Boiling point

d: Doublet

dd: Doublet of doublets

DA: Diels-Alder reaction

DCC: *N,N'*-Dicyclohexylcarbodiimide

DMA: Dimethylacetamide

DMAP: 4-Dimethylaminopyridine

DMF: *N,N'*-Dimethylformamide

DMFu: 2,5-Dimethylfuran

DSC: Differential Scanning Calorimetry

ε: Molar extinction coefficient

ESI- HRMS: Electrospray Ionization - High Resolution Mass Spectroscopy

FTIR-ATR: Fourier Transform Infrared Spectroscopy - Attenuated Total Reflectance

F: Furfural

FA: Furfuryl acetate

FCDA: 2,5-Furancarboxydialdehyde

FDCA: 2,5-Furandicarboxylic acid

FMO: Frontier Molecular Orbital (theory)

GPC: Gel Permeation Chromatography

HMF: 5-Hydroxymethylfurfural

HOMO: Highest-Occupied Molecular Orbital

***J*:** Coupling constant (^{3}J: vicinal coupling constant; ^{4}J: long-range allylic coupling constant)

***k*:** Rate constant

***k'*:** *pseudo*-Rate constant

LUMO: Lowest-Unoccupied Molecular Orbital

m: Multiplet

MF: 5-Methylfurfural

MM: Methylmaleimide

MO: Molecular Orbital

m.p.: Melting point

Mn: Number average molecular weight

Mw: Weight average molecular weight

NaOAc: Sodium acetate

^{1}H NMR: Proton Nuclear Magnetic Resonance

^{13}C NMR: Carbon-13 Nuclear Magnetic Resonance

Retro-DA: Retro-Diels-Alder reaction

r.t.: Room temperature

ρ: Crosslinking parameter

PD: Polydispersity

Pc: crosslinking critical point

***r* :** Functional stoichiometric ratio

s: Singulet

SEC: Size-Exclusion Chromatography

t: Triplet

T: Temperature

TCE: 1,1,2,2-Tetrachloroethane

TCE-d_2: Deuterated 1,1,2,2-tetrachloroethane

THF: Tetrahydrofuran

Tg: Glass transition temperature

Tm: Melting temperature

TMS: Tetramethylsilane

UV/vis: Ultraviolet-visible Spectroscopy

I: Difurfuryl adipate

II: *N,N'*-difurfuryl-4,7,10-trioxa-1,13-tridecanediimine

III: *N,N'*-difurfuryl-4,7,10-trioxa-1,13-tridecanediamine

IV: tris(2-(*N*-furfurylideneamino)ethyl)amine

V: *N,N',N''*-tris(furfurylideneamino) Jeffamine derivative

VI: tris(*N*-furfuryl-2-aminoethyl)amine

VII: *N,N',N''*-trisfurfuryl Jeffamine derivative

VIII: 1,6-hexyl-bismaleamic acid

IX: 1,6-bismaleimidohexane

X: tris(2-(exo-3,6-epoxy-1,2,3,6-tetrahydrophthalimido)ethyl)amine

XI: tris(2-maleimidoethyl)amine

XII: 3-(exo-3,6-epoxy-1,2,3,6-tetrahydrophthalimido)propanoic acid

XIII: furfuryl-3-(exo-3,6-epoxy-1,2,3,6-tetrahydrophthalimido)propanoate

XIV: *N*-furfuryl-3-(exo-3,6-epoxy-1,2,3,6-tetrahydrophthalimido)propanamide

XV: 3-(furfurylideneamino)-1,2-propanediol

XVI: 3-furfurylamino-1,2-propanediol

XVII: 3-furfurylamino-1,2-propanediyl-bis(3-(exo-3,6-epoxy-1,2,3,6-tetrahydrophthalimido) propanoate)

XVIII: Model FA-MM DA adduct

XIX: Linear **I+IX** polymer (A-A+B-B system)

XX: IX-DMFu DA bisadduct

XXI: Linear **III+IX** polymer (A-A+B-B system)

XXII: Linear **XIII** polymer (A-B system)

XXIII: Linear **XIV** polymer (A-B system)

XXIV: Non-linear **I+XI** polymer (A-A+B_3 system)

XXV: Non-linear **VI+IX** polymer (A_3+B-B system)

XXVI: Non-linear **VII+IX** polymer (A_3+B-B system)

XXVII: Non-linear **XVII** polymer (AB_2 system)

Contents

Part II: Synthesis and characterization of dienes and dienophiles

Part III: Polymerization by the Diels-Alder reaction

Part IV: Experimental

GENERAL INTRODUCTION

GENERAL INTRODUCTION

Since the prehistory, renewable sources of energy such as food, fire, wood, animals, water, wind and sun, have been widely used by mankind for its sustenance and well-being [1-3]. Indeed, until the mid-19th century, firewood was the main energy source [3,4]. However, great many changes, especially in what concerns to energy sources, were brought about by the onset of the Industrial Revolution in the late 18th century [1,3]. For the first time, non-renewable energy sources, viz. coal, began to be exploited in large quantities, gradually replacing woody biomass [1,3,5]. As a result, coal became the leading primary energy source until the mid 20th century (Figure 1), when it was supplanted by oil and natural gas [2,3,6,7].

Thus, within a relatively short period of about 150 years [7], the fossil resources, namely coal, oil and natural gas, became the dominant precursors in the realm of energy and chemical commodities (Figure 1), with only modest contribution from renewable counterparts [2,4,7,8,9]. Indeed, they currently supply more than 90% of the world's energy needs and organic chemicals, against less than 10% for renewable resources [2,7,8,10,11].

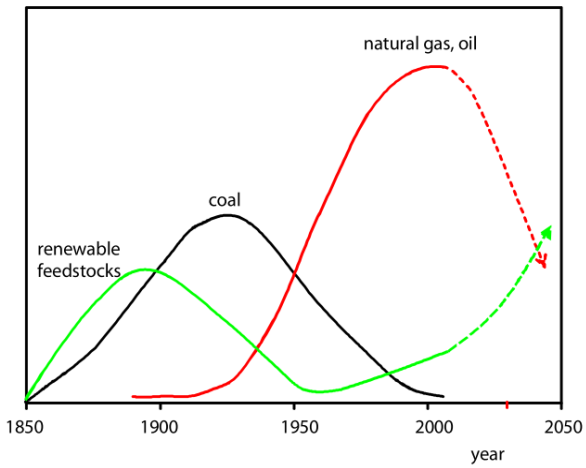

Figure 1. Raw materials basis of the chemical industry in historical perspective [6].

The fossil fuel era has had a huge impact on civilization and industrial development [5], but with the First Oil Shock in the 1970s [4,12-14], it became clear that the fossil resources are finite and subject to depletion as they are consumed [7,10,12,15], and hence, serious questions about the medium-term pursuit of their exploitation, whether as a source of energy or as purveyors of organic commodities and materials, begun to arise with the additional concern of the ecological impact related to their exploitation and consumption [4,6,16,17]. Thus, the progressive dwindling of fossil resources, together with their unpredictable price fluctuations [4,16,18,19], has led to a burgeoning surge of activities in the last couple of decades, devoted not only to the search for alternative energy sources, but also to the context of chemicals and polymers from renewable resources, namely the biomass [12,16,17,20-24].

Unlike fossil resources, the biomass is ubiquitous and essentially independent of geographical context and economic situation of countries [12,20,24-26], albeit with variable specific species. It has the basic advantage to be a naturally abundant resource, not only cheap, but also sustainable, environmentally friendly, and renewable in the sense that only a short period of time is needed to replace what is used [3,12,15,25]. Its wide array of sources includes virgin biomass, forestry and agricultural residues, municipal solid waste, biosolids (sewage), animal wastes (manures) and residues, industrial wastes and residues from paper manufacturing, food processing, wood mills, etc [4,12,15,27-30]. The use of biomass wastes and by-products has the advantage of not jeopardizing the food and feed supply, forests, and biodiversity in the world, and moreover, can lead to a substantial reduction in the overall amount of wastes requiring final disposal, and consequently reduce the greenhouse gas emissions [15,28].

The terrestrial biomass is considerably more complex than fossil raw materials, consisting of a multifaceted array of low- and high-molecular-weight substances, like sugars, hydroxy and amino acids, lipids, and biopolymers such as cellulose, hemicelluloses, chitin, starch, lignin and proteins. By far the most important class of these natural products, in terms of volume produced, is constituted by carbohydrates. Indeed, they represent the major feedstock from which industrial and economically viable organic chemicals and materials are developed that can replace those derived from petrochemical sources [31].

To be converted into fuel, power, and value-added products, the biomass feedstock can be treated and refined by systems analogous to the petrochemical refinery, known as "biorefinery" [20,22,25,29,32-34]. As shown in Figure 2, two main biorefinery platforms can be considered: (*i*) the *Chemical/biochemical platform*, based on biological and/or chemical conversion processes, viz. the treatment of sugars extracted from biomass; and (*ii*) the *Thermochemical platform*, based on heat and pressure-based conversion processes, viz. gasification or pyrolysis of biomass feedstock, producing *syngas* or bio-oil, respectively [19,25,35-37].

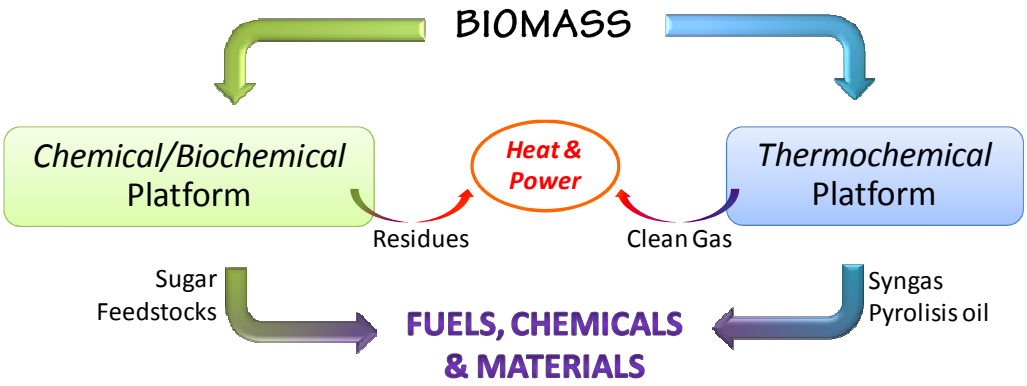

Figure 2. Simplified scheme of the biorefinery concept, adapted from [35].

In spite of this vigorous tendency to swing the world economy back towards renewable biomass resources, its industrial transition is still hindered by a set of obstacles [6,38-40], namely the facts that fossil raw materials are still more economic and their process technology is well-developed and basically different from that required for transforming biomass [6,40]. Hence, the basic question today is "*when will fossil raw materials have become so expensive that biofeedstocks are an economically competitive alternative?*" [6,40]; according to experts, the end of the cheap oil should occur by the year 2050 (Figure 1) [6,14,15].

This context clearly contributes to the development of a more sustainable and competitive "biobased" industry by using renewable feedstock as prime resource bases in the production of chemical commodities and materials. Within the realm of monomers and polymers from renewable resources [17,20,21], furan derivatives and furan chemistry

occupy a unique position, since they encompass a wide variety of structures that can simulate virtually all their current fossil-derived counterparts [16,17,21,41,42].

The main purpose of the present investigation is the synthesis and characterization of novel thermoreversible polymers through the Diels-Alder (DA) reaction, using complementary monomers bearing furan and maleimide moieties. The thermal reversibility of the DA reaction makes this work particularly attractive, because it enables the materials to be reverted to their precursors by increasing the system temperature (retro-DA reaction), and then, when the temperature is decreased, the original material can be recovered. The use of furan derivatives here is perfectly justified by their pronounced dienic character (compared with that of their thiophene and pyrrole homologues). In addition, the application of the DA reaction to macromolecular chemistry opens new ways to synthesize materials with unique properties, such as self-mendability and network recyclability, with the advantage of being based on renewable resources on the part of the furan precursors.

This manuscript is divided into three main parts, as follows:

Part I – "Bibliographic Review", where the more important aspects of furan chemistry, as well as the main aspects of the DA reaction, and its application in the organic and macromolecular syntheses, are expounded.

Part II – "*Synthesis and characterization of diene and dienophile monomers*", which includes the discussion of the synthesis and characterization of new furan and maleimide monomers of different types, namely AA, A_3, BB, B_3, AB, AB_2, each one bearing different spacing moieties between the reactive functions.

Part III – "*Polymerization by the Diels-Alder reaction*", that includes the study of the kinetics and equilibrium of DA polycondensation reactions involving the furan and maleimide moieties. Following an initial investigation of a simple -A+-B system involving model compounds, the linear polymerizations of difunctional A-A and B-B monomers are tackled. Thereafter, the study of linear polycondensations is described using monomers bearing both reactive moieties in their structures, i.e. A-B type molecules, which avoids the problem of functional stoichiometry. Non-linear DA polycondensations using complementary monomers bearing more than two functionalities are next developed, which lead to branched or crosslinked materials and finally, the preparation of

hyperbranched macromolecular structures by the polymerisation of asymmetrically substituted monomers (AB_2) concludes this research effort. All the ensuing polymers are characterized in terms of the structure and molecular weight, glass transition temperature, among others. Also, a clear-cut assessment of the parameters associated with the multiple-cycle thermal reversibility (DA/retro-DA cycle) is studied for each system.

The conclusions and the experimental part complete the manuscript.

PART I

BIBLIOGRAPHIC REVIEW

1 FURAN CHEMISTRY

The interest in the chemistry of the furan heterocycle and, hence, in the synthesis of a variety of furan derivatives begun around the middle of the 19th century and witnessed an important development in the first half of the 20th century [41,43], as beautifully and comprehensively detailed by Dunlop and Peters in their classical monograph [44]. Since then, broader extensive studies have regularly enriched this field, particular in such areas as synthons, pharmaceuticals and other fine chemicals, as well as in polymer science and technology [17,23,41,42,45,46], as evidenced by the growing number of publications, and patents.

1.1 THE SOURCE OF FURAN DERIVATIVES

The global biosynthetic production of renewable biomass is estimated on 200 billion tons per year [6,32,40,47]. Of these, only 4% is used by man for feed, food, fibre, energy, and materials [6,15,47], the rest being exploited in a low-value or relatively unproductive ways [25], or left in the growth areas where natural decomposition occurs [4,6,15].

A wide range of biomass resources are available worldwide. Among them, forestry and agricultural residues, namely corn cobs, oat and rice hulls, sugarcane bagasse, wheat and rice straw, cotton seeds, olive husks and stones, wood chips, as well as naturally growing vegetation, switchgrass, fast-growing trees, etc, are the major plant biomass feedstock [20,25,27,44,45,48]. Of their estimated annual production, 75% are carbohydrates, mainly in the form of cellulose, starch and saccharose, 20% lignin and only 5% other natural compounds, such as fats and oils, proteins and various substances bearing different chemical structure [6,32,34,40,47,49].

The biomass carbohydrates are mainly constituted by two types of sugars, pentoses (C_5-sugars) and hexoses (C_6-sugars). Their acid-catalyzed dehydration leads to the formation of

two important basic non-petroleum chemicals (Figure 3), viz. furfural (**F**) arising from pentoses, mainly xylose, and 5-hydroxymethylfurfural (**HMF**) arising from hexoses, mainly glucose and fructose [6,16,20,21,45,47,50,51].

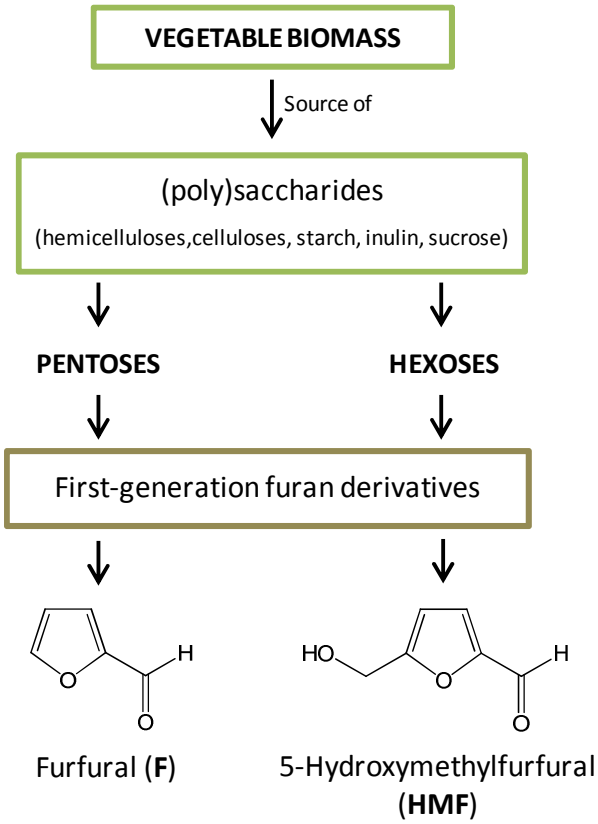

Figure 3. From vegetable biomass to **F** and **HMF**, the two first-generation furan compounds.

These two chemicals are then used as precursors of a large array of furan structures, including monomers which are suitable for any type of polymerization process and capable of simulating virtually all their current fossil-derived counterparts, hence making them an attractive alternative to petroleum-based materials [20,23,26,45,51].

1.1.1 Furfural

F was first obtained in the early 19th century and has interested chemists ever since [44,45]. However, it only became an industrial commodity about a century later, when the Quaker Oats Company began its mass-production by treating oat hulls from their cereal

mill at Cedar Rapids, Iowa [52-54]. The worldwide production of this renewable chemical is currently more than 300 000 tons per year, and its market price is close to $1 per kg [41,45]. In terms of world market, **F** has many applications, namely as a chemical feedstock for other furan and non-furan derivatives, in the refining of lubricant oils and rosins, in the synthesis of pharmaceuticals and agrochemicals [41,45,52-56], as well as a flavouring agent in foodstuff [53].

This first-generation furan derivative can be quite readily prepared from xylose, the main sugar present in raw materials rich in pentosans, such as corn cobs, oat hulls, sugarcane bagasse, wood chips, through an acid-catalyzed dehydration sequence (Figure 4) [41,45,50,53,57]. In this process, a smaller proportion of 5-methylfurfural (**MF**) is obtained from some rhamnose present, which is then separated by distillation [41], and used as a high value flavour compound or monomer precursor [53].

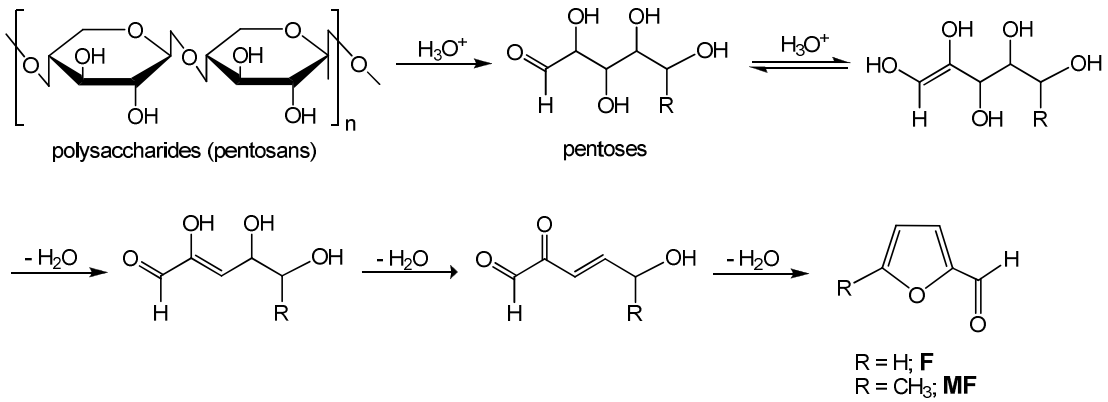

Figure 4. The mechanism of formation of furfural (R = H) and 5-methylfurfural (R = CH_3) from xylose and rhamnose, respectively.

The chemistry of **F** is well developed and provides a host of versatile industrial chemicals by simple straightforward operations [57]. Within the present context, it is obviously the monomeric structures that are relevant. Figure 5 provides a non-exhaustive array of such structures, which have all been already synthesized, characterized and polymerized [6,41,50]. Among these, furfuryl alcohol is still today the most important industrial and commercially available furan derivative, since more than 80 per cent of the world production of **F** is converted into this derivative by catalytic reduction [45,52,54,57]. In terms of general applications, furfuryl alcohol is used in the production of resins for

sand binders for the foundry industry, mortar, surface coatings, pharmaceuticals, resistant floor grouting, adhesives for cores and moulds, electrodes, etc [41,45,53,55].

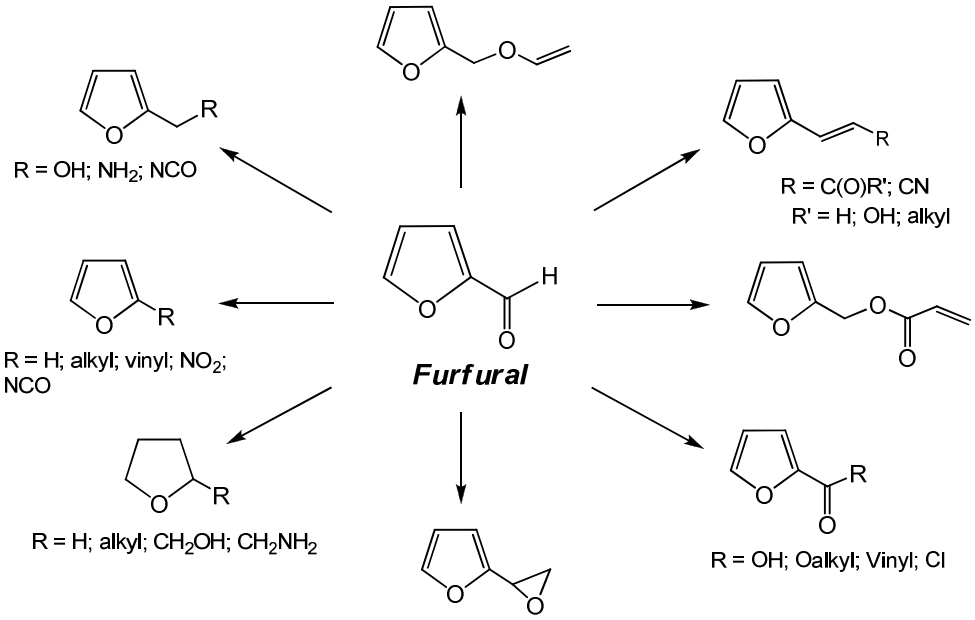

Figure 5. A selection of monomers derived from furfural (**F**).

Although, the structures present in Figure 5 are specifically suited for chain-growth polymerizations [45,46], they can also be converted into bifunctional monomers through the acid-catalyzed condensation of the corresponding 2-substituted furan derivative with an aldehyde or ketone, as shown in Figure 6. As a result, the ensuing monomers become suitable for step-growth polymerizations [41,43,45,51,58,59].

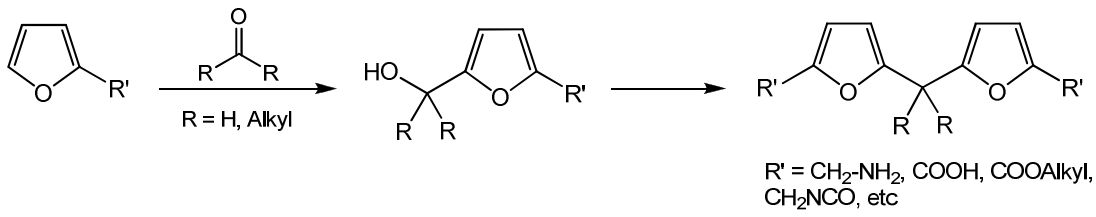

Figure 6. Synthesis of difuran monomers from **F** derivatives.

Whereas the monomers shown in Figure 5 give rise to polymers or copolymers with the furan ring pendant to their backbone, the monomers shown in Figure 6 generate macromolecules in which the furan moieties are an integral part of the chain's backbone [41,43]. This is a viable alternative for the preparation of a wide variety of difunctional monomers, while waiting for the commercial availability of the other first-generation furan derivative, **HMF** [41,43]. It is important to emphasize that all these monomers have already been prepared and characterized [23,41,43,45,51].

1.1.2 5-Hydroxymethylfurfural

HMF is mostly prepared from fructose, but also inulin and glucose (Figure 7) [23,50], following a mechanism analogous to that shown in Figure 4 for **F** [41,47].

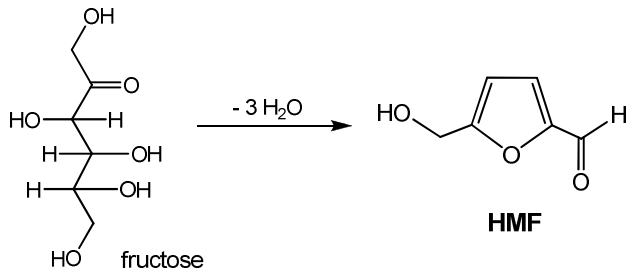

Figure 7. Conversion of C_6-sugars into 5-hydroxymethylfurfural (**HMF**).

Despite its high potential as precursor of fine chemicals and monomers [41,47,50], **HMF** is not yet produced on an industrial scale [41,51], because of the difficulties associated to its synthesis (low yields) and storage (proneness to degradation) [23,41,51]. Furthermore, the economic preconditions of its bulk-scale production are not yet favourable enough, viz. the estimated market price of HMF is around $3 per kg [60], which makes it too expensive against the corresponding competitive petrochemical raw materials [50,60]. Nevertheless, within the last several years, a sudden surge of research in numerous laboratories has been devoted to the optimization of its synthesis and stability [23,45], which suggest that **HMF** will be a commercial commodity soon [41]. It seems likely moreover that its commercialization will involve its preliminary transformation into stable

derivatives, e.g. by its *in situ* oxidation to either the dialdehyde or the diacid (Figure 8) [23].

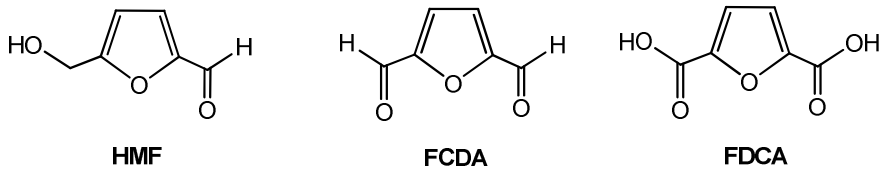

Figure 8. **HMF** and its corresponding dialdehyde (**FCDA**) and diacid (**FDCA**) derivatives.

A wide variety of bifunctional furan monomers have been obtained from **HMF**, some of which are shown in Figure 9. These structures can be used in step growth reactions, giving rise to macromolecules with the furan moieties as an integral part of the backbone structure [41,43,46].

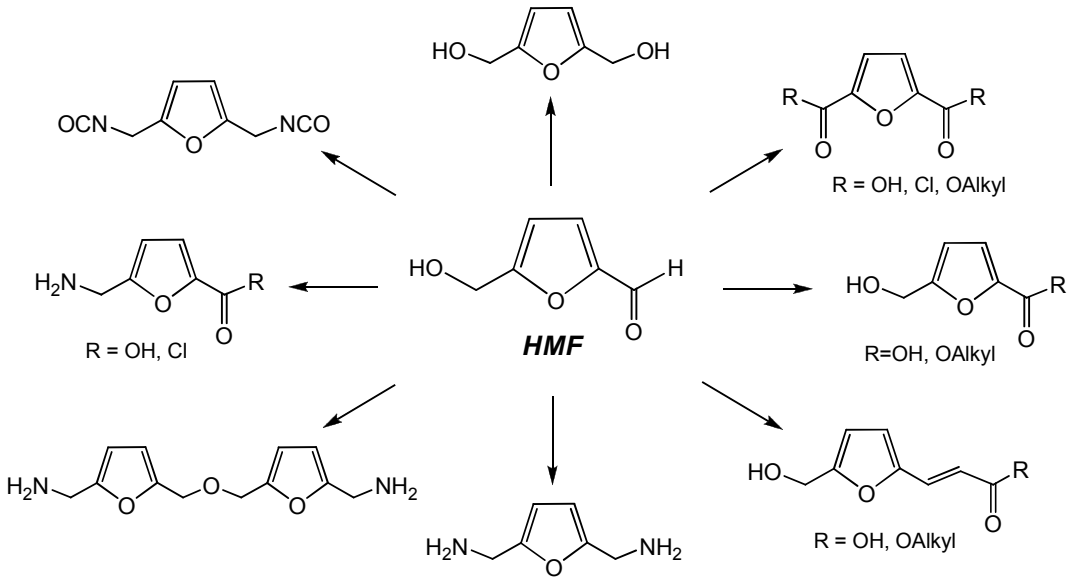

Figure 9. A selection of monomers derived from **HMF**.

These 2,5-disubstituted furan derivatives can replace their corresponding aromatic counterparts in the preparation of such important materials as polyesters, polyamides and polyurethanes, as well as phenolic and epoxy resins [51,56].

1.2 THE FURAN RING: STRUCTURE AND REACTIVITY

The furan ring (**1**) is a well-known representative of the five-member unsaturated heterocyle family, which includes several others, in particular pyrrole (**2**) and thiophene (**3**) [41,43-45,61]:

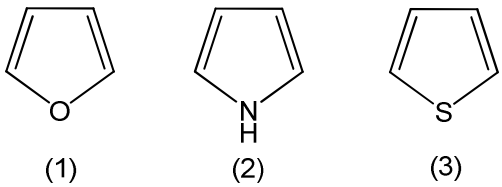

(1) (2) (3)

Furan, which was first prepared in 1870 by Heinrich Limpricht, who called it *tetraphenol* [44], is a volatile colourless liquid with an aromatic scent and boiling point near to room temperature [41]. It is a planar molecule, whose dimensions have been determined from electron diffraction data [44]:

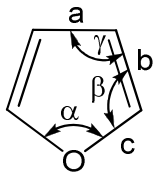

a = 1.46 Å
b = 1.35 Å
c = 1.41 ± 0.02 Å

$\alpha = 107 \pm 4^{o}$
$\beta = 109 \pm 3^{o}$
$\gamma = 107 \pm 2^{o}$

Molecular orbital calculations provide the set of resonance-contributing structures shown in Figure 10 for the furan heterocycle [41,44,45].

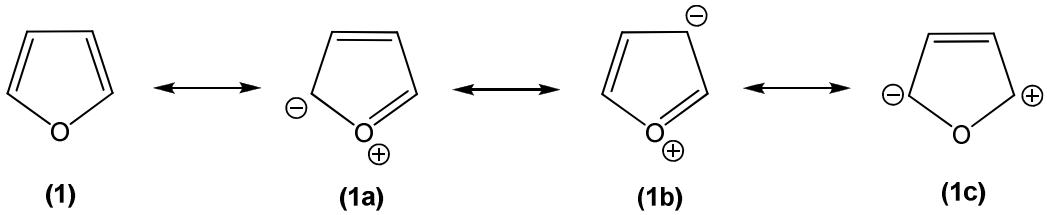

(1) **(1a)** **(1b)** **(1c)**

Figure 10. The mesomeric forms of furan.

In furan chemistry, substitution reactions, such as alkylation, halogenation, sulfonation and nitration, occur regioselectively at the C-2 and/or C-5 positions when these are not

already substituted, suggesting that the structure **1a** in Figure 10 is the dominant charged resonance structure [41,45].

Compared with its classical homologues pyrrole (**2**) and thiophene (**3**), furan displays the lowest aromatic and the highest dienic character, as illustrated in Figure 11 [41,43,45], where the two limiting structures of benzene and cyclopentadiene are also represented.

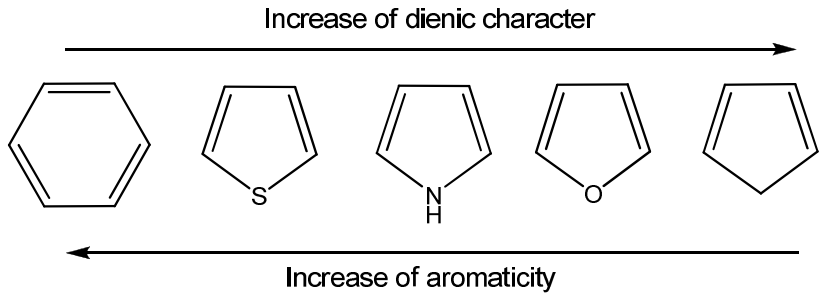

Figure 11. Aromatic and dienic characteristics of the heterocyclic furan homologues.

The pronounced dienic character of furan is a peculiar chemical feature that bears important mechanistic consequences in both organic and macromolecular chemistry. One of the most exemplary of these consequences is the ease with which furan and some of its derivatives undergo the Diels-Alder reaction as dienes, to the point of being given as typical examples in organic chemistry textbooks, typically with maleic anhydride as the dienophile [41,42,46,62].

Another well-known chemical feature of the furan ring is its sensitivity to acid-catalyzed hydrolysis, which can lead to the destruction of the heterocycle with the formation of aliphatic carbonyl compounds, as illustrated in the Figure 12 [41].

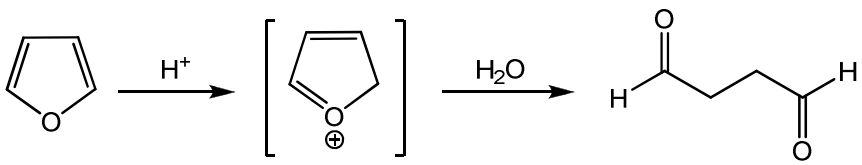

Figure 12. The overall pathway to ring opening in the acid-catalyzed hydrolysis of furan.

In conclusion, the chemical behaviour of furan and its derivatives displays a variety of features which are associated with both the structure and properties of the heterocycle and the specific nature and position of the substituents appended to it [43-45]. Thus, its presence within the main chain or as a side function can provide original and valuable properties to the ensuing macromolecular materials [55].

2 DIELS-ALDER REACTION

The Diels-Alder (DA) reaction is one of the most fundamental and useful reactions in synthetic organic chemistry, because it provides simple, efficient, and clean procedures to generate new bonds by inter- or intra-molecular coupling [63,64]. The DA reaction was discovered in 1928 by Otto Diels and Kurt Alder [65], who were awarded the 1950 Nobel Prize in chemistry. Since then, this reaction has received a great deal of attention, which is clearly shown by the numerous publications concerning its synthetic, mechanistic and theoretical aspects [63,64,66-80].

The classical DA reaction is a [4+2] cycloaddition between a conjugated diene and a second component, called dienophile, to give a stable cyclohexene derivative (the adduct) [63,64,81]. This reaction presents a thermally reversible character, which allows the decoupling of the adduct to take place by increasing the temperature, and hence, the equilibrium is displaced to the left with regeneration of the initial reagents (Figure 13). The reverse reaction is called retro-Diels-Alder (retro-DA) reaction [63,68,72].

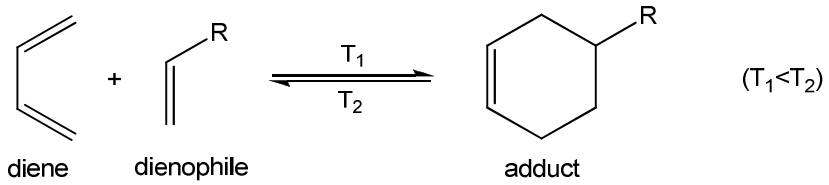

Figure 13. DA/retro-DA reaction.

2.1 DIENES

The *diene* has two conjugated double bonds and contributes with 4π electrons in the DA reaction. A great variety of conjugated dienes have been used, and can be classified as indicated in Table 1 [63,64,77].

Table 1. Representative dienes.

Open chain	Inner ring	Outer ring	Inner-Outer ring	Across rings
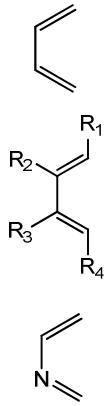	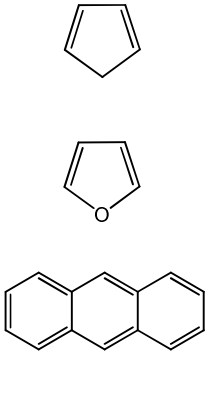	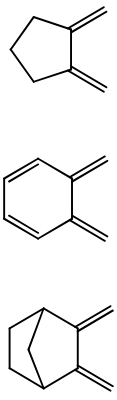	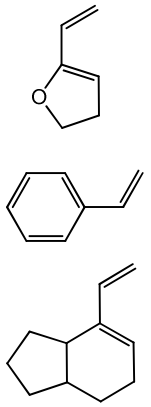	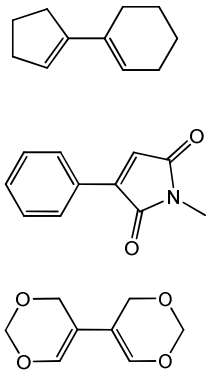

Open-chain dienes can adopt two conformations, viz. *s-cis* and *s-trans*. However, in order to participate in a DA reaction, the diene must be in the *s-cis* conformation. Although the *s-trans* conformation is the more stable form, it leads to an energetically unfavourable six-membered adduct and, therefore, it does do not undergo the DA reaction. Hence, the open-chain dienes must be frozen into the *s-cis* conformation or be able to achieve it during the reaction (Figure 14) [63,77,82,83].

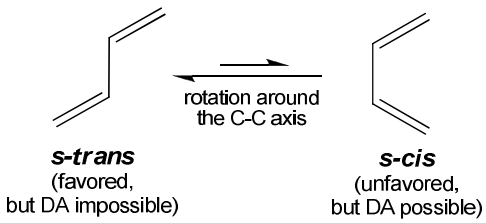

Figure 14. Conversion of the *s-cis* and *s-trans* conformations [82].

Cyclic dienes that are permanently in the *s-cis* conformation are significantly more reactive than the corresponding open-chain structures, which have to achieve this rotational conformation change. The cyclic dienes that are in the *s-trans* conformation and cannot adopt the *s-cis* one will not undergo the DA reaction [63,64,77,82]. Aromatic compounds also behave as dienes, but are generally less reactive than their non-aromatic homologues

towards to the same dienophile. However, certain heterocyclic aromatic rings, principally furans, also intervene readily in DA reactions [77].

2.2 DIENOPHILES

The *diene* counterpart in the DA reaction is the *dienophile,* which contributes with 2π electrons. It can be either an alkene or alkyne derivative. The classification of the dienophiles is difficult because of their large number and variety. Table 2 illustrates some examples of these structures [63,77,81].

Table 2. Representative dienophiles.

Acyclic	Cyclic
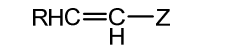 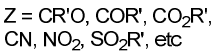 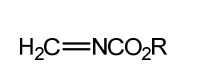 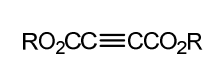 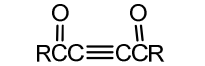 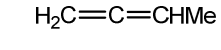 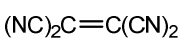 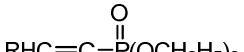 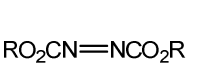 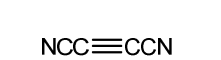	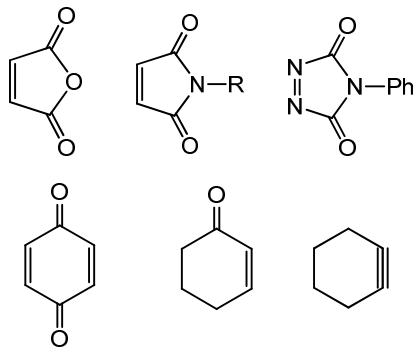

2.3 MECHANISM

There have been many investigations on the mechanism of the DA reactions [79,80,84-91], with a general debate on whether these reactions take place in a concerted fashion, or in a stepwise process [70,77,91,92]. Classically, three mechanisms have been considered.

The first mechanism involves a cyclic transition state and no intermediate (Figure 15). The reaction is concerted and occurs in a one step process, with simultaneous formation of both new bonds [77,81,82].

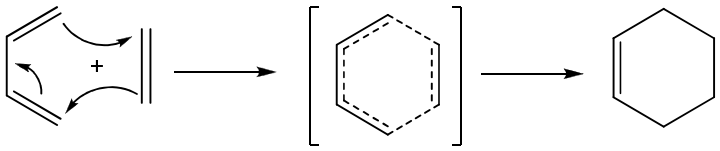

Figure 15. Mechanism of a concerted DA reaction.

The other two mechanisms occurs both in a two-step process with the formation of an intermediate, which may be either diradical or zwitterionic (Figure 16) [63,70,77].

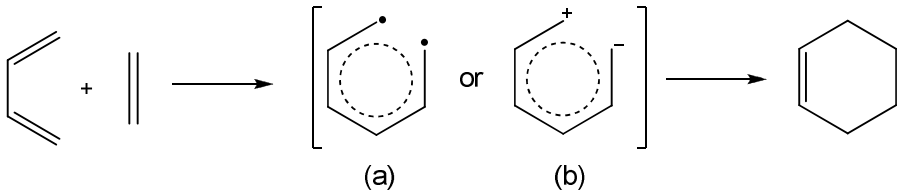

Figure 16. Mechanism of an (**a**) radical and (**b**) ionic DA reaction.

Most of the DA cycloadditions are described by a concerted mechanism (Figure 15). In the 1960s, Woodward and Hoffmann [93,94] showed that these reactions proceed through a cyclic transition state with conservation of the orbital symmetry. Usually, the approach between diene and dienophile occurs on the same side on both components, viz. through a *suprafacial* interaction, with retention of the orientation of the reactant substituents when forming the adduct. Thus, the DA reactions are almost always stereospecific [77,80,81,89].

According to the Frontier Molecular Orbital (FMO) heory, in a concerted DA cycloaddition, the bonding interaction can only take place between the highest-occupied molecular orbital (HOMO) of one reactant and the lowest-unoccupied molecular orbital (LUMO) of the other, which are the closest in energy (Figure 17) [77,95,96].

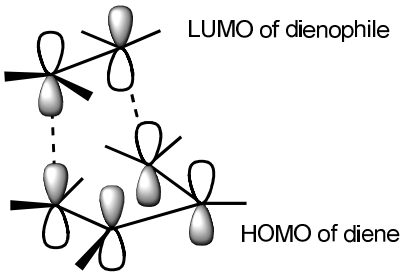

Figure 17. Interaction between LUMO of dienophile and HOMO of diene in the DA reaction [67].

The FMO theory has been also used successfully to explain and predict the reactivity and selectivity (both *regio* and *stereo*) phenomena of the DA cycloadditions [63,89,95], as follows.

2.4 REACTIVITY AND SUBSTITUENT EFFECTS

The DA reactions can be classified into three types, depending on the three possible arrangements of the HOMO and LUMO of the reactants [63]. These three situations are termed (*i*) *"normal" electron demand*, in which the dominating orbital interaction is the HOMO diene-LUMO dienophile interaction; (*ii*) *"inverse" electron demand*, controlled by LUMO diene-HOMO dienophile interaction; and (*iii*) *"neutral" electron demand*, where neither MO interactions dominates [63,77,97].

Thus, the reactivity of the DA reaction depends on the lowest HOMO-LUMO energy separation that can be achieved by the reactants [63]. Hence, any factor, electronic and steric, that lowers the energy difference between these orbitals, increases the reaction rate, because the stability of the transition state is greater [63,64,75].

The effects of the substituents on both diene and dienophile strongly influence the reactivity of the reaction. In general, electron-withdrawing groups, like carbonyl, nitrile, nitro or sulfonyl, lower the energy of both HOMO and LUMO, whereas electron-donating groups, like alkyl, alkoxy, or dialkylamino, raise their energies (Figure 18) [63,81,89,97].

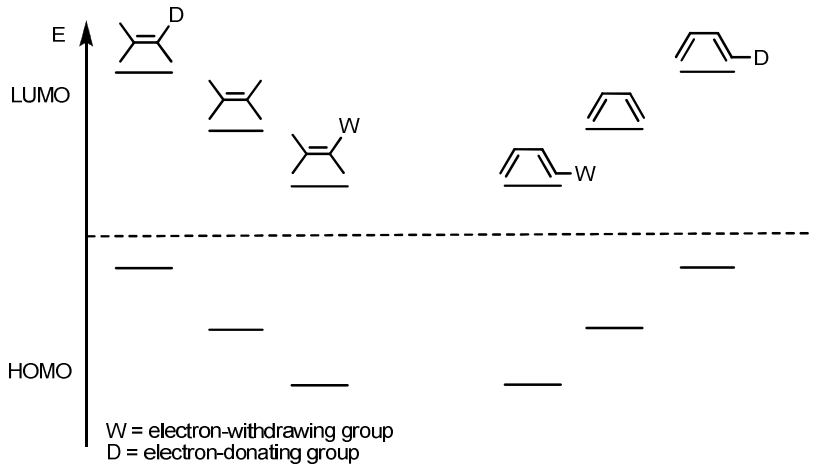

Figure 18. Electronic substituent effects on orbital energies [63].

The *normal electron demand* DA reactions (HOMO-diene controlled) are accelerated by electron-donating substituents in the diene and electron-withdrawing substituents in the dienophile. These are the most common DA reactions. The reverse substituent pattern, viz. electron-withdrawing groups in the diene and electron-donating groups in the dienophile (LUMO-diene controlled), is much less common than the previous, since they require more powerful donor and acceptor groups, and are not as effective (*inverse electron demand* DA reactions). The *neutral electron demand* DA reaction is controlled by both frontier orbital interactions, and is insensitive to the presence of substituents in either diene or dienophiles [63,64,77,81,89,98].

2.5 REGIOSELECTIVITY

The DA reaction of unsymmetrical dienes and dienophiles can give two regioisomer adducts, resulting from the two different orientations of the reactants (Table 3). However, in practice, one of them is often strongly favoured.

The relative position of the substituents in the adduct is indicated as *ortho*, *meta*, and *para*. In the DA cycloadditions, the "*ortho*" and "*para*" orientations are generally prefered (*ortho-para* rule), as shown in Table 3. Independently of the electronic nature of the substituent, the '*ortho*' adduct is predicted to be the major product for combinations with 1-substituted dienes, whereas the '*para*' adduct is predicted for 2-substituted dienes [63,64,77,81,89].

Exceptions to the "*ortho-para"* rule have been observed, e.g. the DA combination of an electron-donating-1- or 2-substituted diene and an electron-donating dienophile will lead to the "*meta*" adduct. Thus, the prediction of the regiochemistry is still a stimulating challenge, since it depends not only on the number and nature of substituents on both diene and dienophile, but also on the reaction conditions (catalyst, temperature, pressure, solvent, etc) [63,64].

Table 3. Regioselectivity of the Diels-Alder reaction; the *ortho* and *para* orientations in products are favored over the *meta* orientation.

***ortho*-type orientation**	***para*-type orientation**
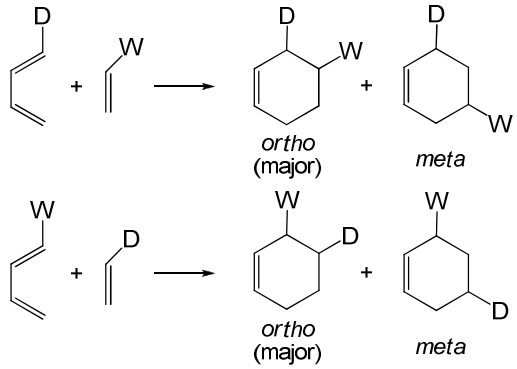	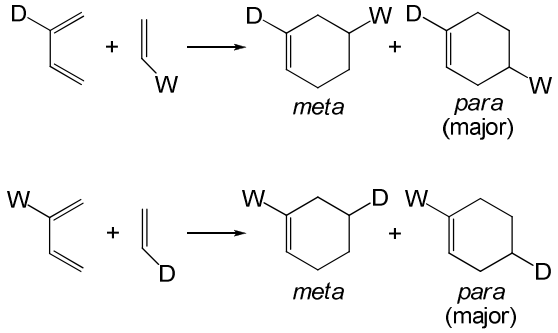

W = Electron-withdrawing group; D = Electron-donating group

2.6 STEREOSELECTIVITY

The DA reaction is a stereospecific *syn* addition of the diene with respect to dienophile and vice-versa, because it occurs suprafacially on each component, with preservation of the relative substituents' configuration of the reactants in the DA adduct (Figure 19). This observation is known as the *cis* principle [63,77,81,89].

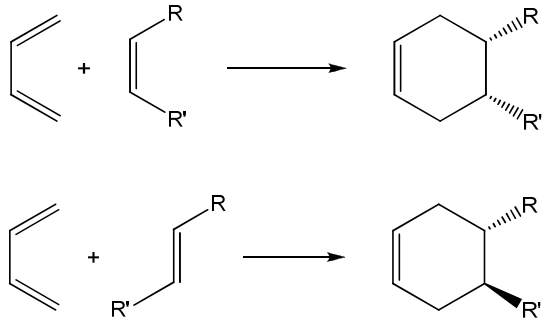

Figure 19. Stereochemistry retention of the reactants' substituents in the adduct.

Moreover, the two DA components, approaching each other in parallel planes, *a priori* may interact in two different orientations, affording *endo* and *exo* adducts (Figure 20). In the *endo* addition, the bulkier sides of both diene and dienophile lies one above the other,

whereas in the *exo* mode the bulkier side of one component is under the smaller side of the other [63,77,81]. Thus, the *exo* mode is expected to be preferred, because it suffers fewer steric repulsive interactions. In general, however, the *endo* adduct is the major product, because of its more stable transition state. This preference is known as *Alder's* rule [63,64,80,89,99-101].

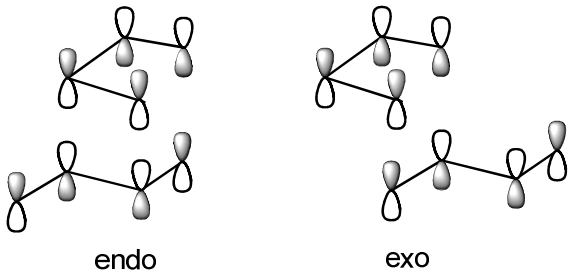

Figure 20. *Endo* and *exo* approach [99].

Commonly, a ratio of *exo/endo* adducts is obtained in the DA reactions. The *endo* isomer is generally formed more rapidly at low temperatures, thus being kinetically more favourable. However, for longer reaction times, as well as at higher temperatures, the *exo* isomer is preferred, since it is thermodynamically more stable. Further, the *endo* isomer can be then easily converted into the *exo* through a retro-DA followed by re-addition (Scheme 1) [64,77,89,102].

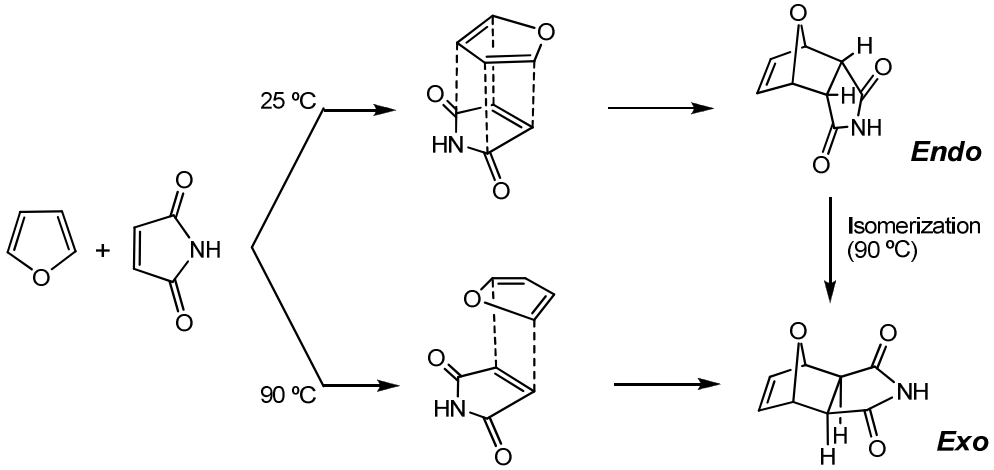

Scheme 1. *Endo-exo* addition for the DA reaction between furan and maleimide [103].

2.7 EXTERNAL FACTORS

The rate, route and equilibrium of the DA reactions can be increased by several external factors such as catalyst, temperature, pressure, solvents. Further, these conditions also allows the reactions to be carried out under milder conditions, and the use of less-reactive reactants [64,67,69,75,80,104].

2.7.1 Catalysts

In 1960, Yates and Eaton [105] first reported the remarkable acceleration of the reactions of anthracene with maleic anhydride catalyzed by aluminium trichloride. Since then, the use of Lewis acids as catalysts in the DA reaction has received increasing attention [106-113]. The interaction between the catalyst and the dienophile gives a more reactive complex toward the diene, which leads to a sharp acceleration of the reaction. Thus, catalyzed DA reactions can be carried out under mild conditions, and weakly reactive dienes and dienophiles can be used. Furthermore, an increase in stereoselectivity and regioselectivity of this reaction is also observed. The more commonly used catalysts are strong-to-medium Lewis acids such as $AlCl_3$, $TiCl_4$, $SnCl_4$, $ZnCl_2$, $ZnBr_2$, BF_3, etc. [63,64,67,89,114].

Nevertheless, the use of classical Lewis acids has some limitations, viz. they cannot be used with acid-sensitive reactants [64], and the reaction medium generally must be strictly anhydrous, or else the reaction stops, because most of these acids immediately react with water rather than substrates, even if a small amount of water is present [109,111]. To overcome these limitations, alternative catalysts have been used in DA reactions, namely transition-metal-based catalysts (lanthanide) [115-118], radical cations [119], chiral catalysts [112,120-123], solid-phase supported catalysts, such as clays [124], zeolites [125], silica or alumina [126], or dendrimers [127].

2.7.2 Temperature

Until the first report on the acceleration of the DA reactions by Lewis acid catalysts [105], these reactions were essentially carried out under thermal conditions due to the simplicity of their accomplishing process [63]. Nevertheless, in many cases, rather long reaction times are required to successfully perform these cycloadditions, restricting their practical synthetic utility. Furthermore, the reversible character of the DA systems (see section **2.8**) and the possible degradation and/or polymerization of the initial reactants at high temperatures, are important aspects that have to be considered.

In recent years, microwave irradiation is gaining interest as an alternative to the classical thermal conditions, because it allows the formation of the DA adducts without using high temperatures and in short reaction times. Moreover, it enhances the reaction rate without decreasing the selectivity and minimizing the degradation of the reactants thanks to the instantaneous character of this heating process [63,128-131].

2.7.3 Pressure

The DA reactions can also be markedly influenced by high pressure (1-15 kbar), because the reaction rate is increased, as well as their selectivity, and the displacement of the equilibrium toward the formation of the adducts [64,132-138]. Moreover, high-pressure DA cycloadditions allow the use of heat-sensitive and/or weakly reactive reactants [63,64,104], and their kinetic studies can yield information on the structure and properties of the transition state [132].

The choice of the solvent is an important parameter for reactions carried out in solution, because of the pressure effect on freezing temperature of the solvent. To prevent the solvent from freezing under high pressure, temperature elevation is mostly used [64].

2.7.4 Solvents

Most of the DA reactions are carried out in solution using non-polar organic solvents, and, for a long time, they were believed to be insensitive to the nature of the solvent used

[139]. Nevertheless, after the discovery of a remarkable acceleration of DA reactions carried out in water by Breslow and co-workers [140], polar aqueous and non-aqueous solvents have been investigated as reaction media for some DA cycloadditions [64,141-146]. The use of water as solvent increases significantly the reaction rate, and enhances the selectivity of the reaction, mainly due to the hydrophobic effect on the transition state, viz. nonpolar structures tend to aggregate in aqueous solution, so as to decrease the hydrocarbon-water interfacial area [147-150]. An additional advantage related to the use of aqueous media is their *green* character.

These results have revolutionized the concept that the DA reactions are moderately affected by the solvent. Thus, the choice of the solvent is crucial for the success of the reaction, since it can strongly influence both reactivity and selectivity.

2.8 RETRO-DIELS-ALDER REACTION

The DA reaction is thermally reversible, which means that the adduct can be converted to its respective diene and dienophile by heating. The reverse reaction, called retro-DA reaction, has been known for almost as long as the DA itself, being discovered in 1929 by Diels and Alder, who observed the decomposition of the furan-maleic anhydride DA adduct at around 120ºC (Figure 21). Since then, this reaction has been the object of much research, however, in less numerous studies than the forward one [72,151-154].

If one or both the reactants are thermally stable, or can be easily removed or consumed in a subsequent step, the dissociation of the adduct is more favourable [64,82,83]. Furthermore, the retro-DA reaction occurs with conservation of the regioselectivity.

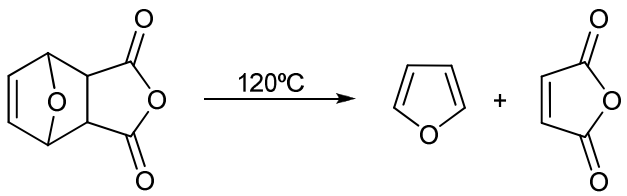

Figure 21. Retro-DA reaction of the adduct obtained from the DA reaction between furan and maleimide.

This reaction is frequently used in preparative organic chemistry in conjunction, or not, with the DA reaction, namely in the synthesis of structures that are difficult to obtain by conventional synthetic ways, or the protection of a sensitive double bond, which can be then deprotected by a simple retro-DA reaction. In some cases, when the retro-DA cannot readily occur, the decomposition or aromatization of the adduct is observed [64,72,83,153,155].

2.9 VARIATIONS ON THE DIELS-ALDER REACTION

There are many variants of the DA reaction (intermolecular), all bearing a high potential and useful applications in organic synthesis, namely the synthesis of complex molecules from simple starting materials [64,69,76]. The features described previously for intermolecular DA reactions can be applied in the following reactions.

Intramolecular Diels-Alder reaction

The intramolecular DA (IMDA) reaction deals with molecules incorporating both diene and dienophile moieties in their structures. This one step reaction produces two rings, but only one formed by the DA reaction, that can be fused if diene and dienophile are connected at the 1-position of the diene, or bridged, if the bond is at the 2-position of the diene [63,64,73]. The IMDA reaction can be used in the synthesis of natural products, namely stereochemically complex polycyclic compounds [69,73,76,156-159].

Homo-Diels-Alder reaction

The *homo*-DA-reaction is a [2+2+2] cycloaddition of a 1,4-diene with a dienophile, giving rise to a cyclopropane ring. Generally, open-chain dienes produces central-bridged six-membered rings, whereas inner-ring dienes produce a six-membered ring fused with another ring whose size depends on the initial cyclodiene. The use of 1,4-dienes has been limited mainly to bridged cyclohexa-1,4-dienes and almost exclusively to norbornadienes, which implies few synthetic applications [64,72,77].

Hetero-Diels-Alder reaction

The *hetero*-DA reactions have been intensively studied, since they represent one of the most important methods for the synthesis of heterocycles, and also natural products, like carbohydrates, alkaloids, terpenes, etc. The reactivity of these reactions is very specific, depending on the hetero-system diene-dienophile used, while their selectivity is generally remarkable. Typical heterodienophiles are ketones and aldehydes [64,130,159-164].

Multiple Diels-Alder reactions

The usual procedure for the synthesis of complex molecular structures is the stepwise formation of the individual bonds in the target molecule. However, it would be much more efficient if multiple carbon-carbon bonds could be formed sequentially in one-pot process without isolating any intermediates, changing the reaction conditions, or adding reagents during the process [63,64,73,76,165,166]. Thus, multiple DA reactions are described as a sequence of two DA cycloadditions, in which the initial monoadduct is involved, directly or after some other transformation, in the second cycloaddition that affords the final polycyclic bisadduct. This one-pot multistep process has been named in various ways, viz. *domino*, *timed*, *tandem*, *cascade*, etc [63,64].

3 FURAN CHEMISTRY AND DIELS-ALDER REACTION AT THE SERVICE OF MACROMOLECULAR MATERIALS

During the past decades, numerous studies on the application of the reversible DA reaction to the realm of furan polymers have bloomed, because of its potential in the preparation of a wide variety of novel macromolecular materials possessing, among others, the common and peculiar feature of thermal reversibility within a readily accessible domain of temperatures, as well as promising applications like self-mendability and network recyclability. These original materials have also the advantage of being based on renewable resources on the side of the furan precursors [17,21,23,41,43,45,51,167,168].

As previously referred, the furan heterocycle and many of its derivatives display the most pronounced dienic character, when compared with that of their thiophene and pyrrole homologues, which makes it highly suitable to intervene as a diene in the DA reaction. Indeed, among the different types of system representing the DA reaction, those involving furan derivatives as dienes and maleic anhydride or maleimide derivatives as dienophiles are undoubtedly the most classical examples. In furan macromolecular synthesis, the furan-maleimide couple (Figure 22) is the most frequently used diene-dienophile combination, due to the low temperature required for the DA and retro-DA and the high yield of products [41,61,64,86,87,103,167,169-172].

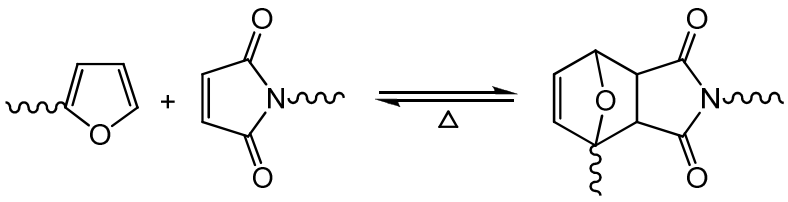

Figure 22. DA equilibrium between growing species bearing, respectively, furan and maleimide endgroups.

The proportion of the adduct *endo*- and *exo*- forms (see Scheme 1) varies as a function of the specific structure of both reagents and the system conditions. However, whereas the relative abundance of the isomeric adducts play a significant role in both synthetic and fundamental organic chemistry, it becomes irrelevant in the macromolecular context, since it does not affect the outcome of the forward and backward processes, and hence, what counts is the actual global yield of the adducts. In this context, the DA equilibrium can therefore be expressed as the more general form of Figure 22 [41,42,64,167].

The temperatures associated with the DA furan-maleimide equilibrium depend on the desired rates of either forward or backward reactions. Typically, temperatures up to 65 ºC insure a reasonably high forward (polymerization) rate and a negligible retro-DA contribution, whereas temperatures above 100ºC are quite adequate to revert the situation (depolymerization) to a fast and essentially complete adduct decomposition. In addition to this thermal reversibility, the DA reaction is also remarkable for its clean-cut character as regards the usual absence of side events perturbing its course. Further, in these conditions, the reproducibility of forward/backward cycles is insured [16,23,42,46,167].

The exploitation of the DA cycloaddition in macromolecular synthesis generally follows two approaches, namely (*i*) the construction of polymers where the backbone itself is built up through successive DA coupling reactions involving multifunctional complementary monomers; and (*ii*) the chemical modification of polymers bearing pendant DA-reactive moieties, with, e.g., formation of networks [45,168]. In both instances, the polymers can, on the one hand, be readily reverted to their precursors through the retro-DA reaction and this feature can be exploited in recycling, “mending” or phase-changing network-based material, or, alternatively, suffer an irreversible transformation of the adducts into aromatic moieties by catalyzed dehydration (Figure 23), and, in this context, the ensuing materials can be used, e.g., as thermally stable polymers (heat-resistant materials) [23,43,62,167,168].

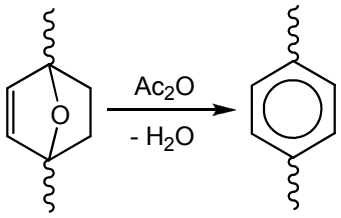

Figure 23. Conversion of a reversible DA adduct into a stable moiety by thermal aromatization.

3.1 LINEAR STEP-GROWTH SYSTEMS

The linear polymerization of bifunctional monomers bearing complementary DA functions, like difurans (A-A) and bismaleimides (B-B) (Figure 24), was first tackled some 20 years ago [173,174]. Since then, numerous studies concerning on linear A-A+B-B systems have been published with different monomer combinations and different approaches both in terms of the experimental conditions and the characterization and purpose of the ensuing materials [41,45,123,167,175-181]. Nevertheless, on the whole, the focus of these studies has been essentially on the qualitative polymerization-depolymerization features of polymer synthesis and thermal degradation, with little or no emphasis on detailed structural analyses, kinetic aspects and materials properties [23,41,45,167]. Some examples of bifunctional monomers used in these works are illustrated in Table 4.

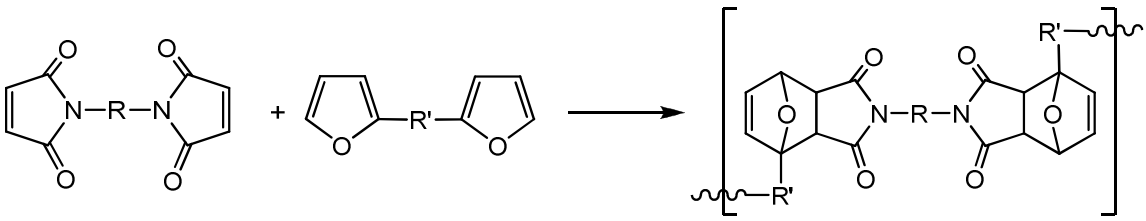

Figure 24. Classical linear polycondensation of A-A+B-B systems.

Table 4. Structure of some difunctional monomers used in the linear DA polycondensation.

R (central chain of B-B monomer)	R' (central chain of A-A monomer)	Ref.
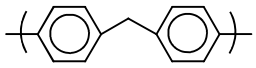	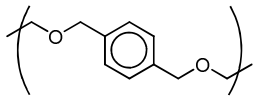	[123]
	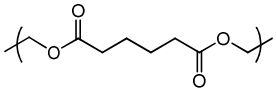	[178]
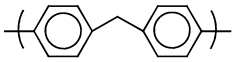		[179]
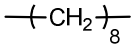		
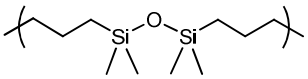	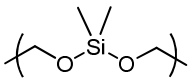	[182]

Linear macromolecular structures can also be prepared by using a single monomer molecule incorporating both furan and maleimide moieties, viz. A-B monomers (Figure 25). The use of these A-B type systems represents an interesting alternative to the previous linear DA polymerization, because it ensures the ideal initial stoichiometry [21,23,51,167].

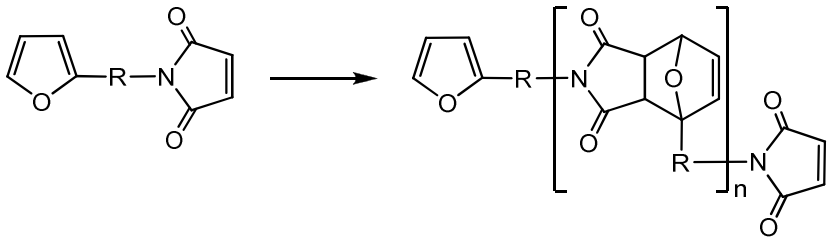

Figure 25. DA polycondensation of an A-B type monomer.

The first attempts to prepare furan-maleimide A-B structures emerged in the early 1990s [176,183,184], however the results obtained did not provide convincing evidence in favour of the expected structures [62]. A few years later, this same issue was briefly investigated by Goussé and Gandini [185], who prepared, characterized and polymerized the simplest A-B monomer of this series, viz. *N*-2-furfurylmaleimide, but the single methylene bridge joining the two complementary DA rings made the molecule difficult to

handle, and hence the study was not pursued [41,167]. These A-B systems were also tackled by Gaina and Gaina [186], who focussed, however, their attention on the aromatization of the ensuing DA adducts leading to thermally stable polymers [167].

3.2 NON-LINEAR SYSTEMS: NETWORK AND DENDRIMERS

The DA-based polymerizations applied to multifunctional furan and maleimide monomers, viz. A_n+B_m systems with *n* and/or *m* higher than two, leads to highly cross-linked macromolecular structures (networks) [187], whose interest lies on the preparation of "mendable" materials, due to the thermally reversible character of the adduct formation [41,167,187,188]. Moreover, these materials can also be prepared from the DA coupling of a linear polymer or copolymer bearing pendant furan or maleimide moieties with complementary difunctional reagents as cross-linker, or from complementary modified polymer (Figure 26) [51,167,168,188-203].

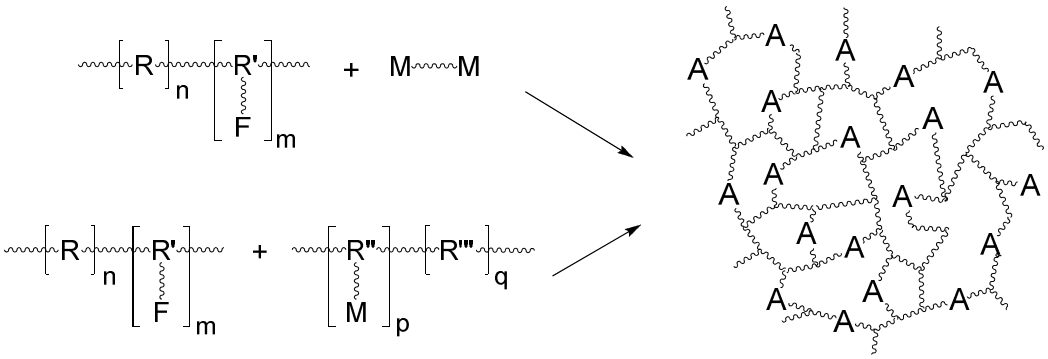

Figure 26. Schematic representation of the synthesis of macromolecular networks by the DA reaction, where F = furan, M = maleimide, and A = adduct [182].

Figure 27 shows the synthesis of one such polymer involving an A_4+B_3 monomer combination. This highly cross-linked structure was recently reported by Wudl's group [187,188], and since then, several studies based on the DA polycondensation between multifunctional furans and maleimides have appeared, including interesting applications in the realm of thermally removable foams and adhesives [167,204-207].

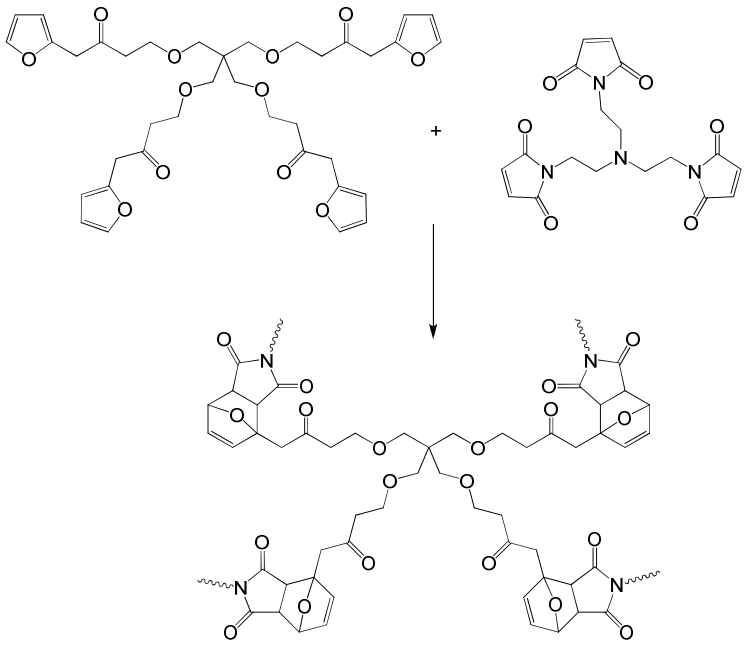

Figure 27. Non-linear DA polymerization of an A_4+B_3 system [188].

Another interesting application of the reversible DA reaction describes the synthesis of thermally responsive hyperbranched polymers, as well as dendrons and dendrimers, through the formation of adducts [41,51,167,168,208-214]. These non-linear macromolecular materials do not crosslink and are prepared from the DA polycondensation of asymmetrically substituted AB_n or A_nB monomers (n >1) [41,167]. The first example of a dendritic structure obtained by this approach [210] involved an AB_2 monomer with formation of a third generation architecture (Figure 28), which could be progressively reduced to lower generations through the retro-DA reaction [62,167].

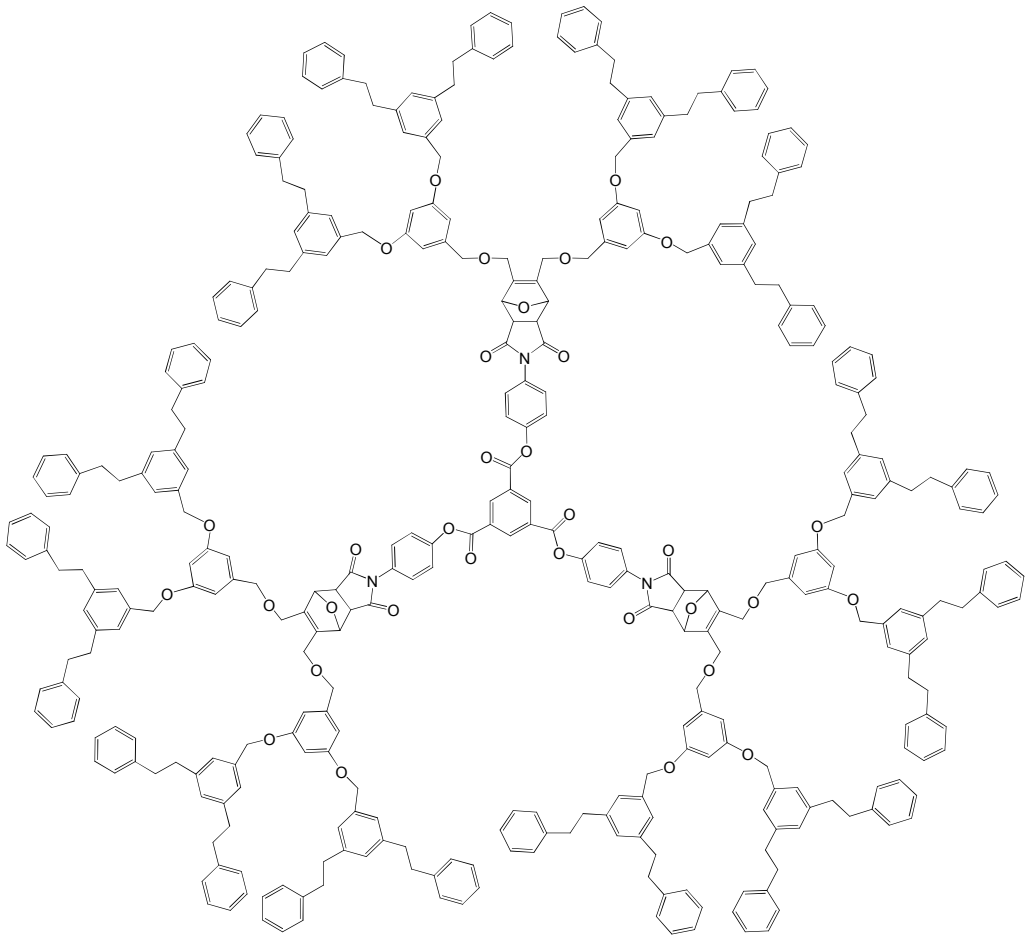

Figure 28. Structure of a third generation DA-based dendrimer [210].

3.3 REVERSIBLE POLYMER CROSS-LINKING

The preparation of thermoreversible crosslinked materials through the DA reaction was first mentioned in the late 1970s [195], but it was only in the early 1990s that this issue was investigated more systematically. Nevertheless, in the last years, these polymer systems have acquired an enhanced relevance, as reflected by the numerous publications dealing with such materials [41,42,51,167,168,187-201,204-213,215-235]. Among these, the preparation of linear polymers bearing pendant furan or maleimide moieties and their DA-based crosslinking with the complementary bifunctional reagent (Figure 29), viz. a bismaleimide or difuran compound, respectively, is perhaps the most active topic within this important area [41].

The growing interest in these crosslinked systems is related, as previously referred, to their thermoreversible character, which allows them to be readily reverted into their precursors through the retro-DA reaction. This original feature is particularly interesting in applications such as polymer recycling, mendable polymers or phase-changing materials [51,62,167]. Indeed, one of their promising applications is the possibility of recycling *tyres*, an industrial and ecological problem with no viable solution to date. Moreover, any fissure or other damage to the DA crosslinked materials can be mended by heating and subsequent cooling them to room temperature to restore the pristine material. In principle, this can go through repeated cycles of cracking and re-mending at the same site, if no barring unwelcome side reaction occurs [21,62,167].

The feasibility of the reversible pathway of these systems can be tested by an original approach, involving the addition to the decrosslinking medium of an excess of a complementary mono-functional DA reagent, which will trap the liberated difunctional cross-linker (Figure 29), thus avoiding a subsequent reconstruction of the network upon cooling, and hence, the original polymers can be completely recovered [21,41,45,167,189-191].

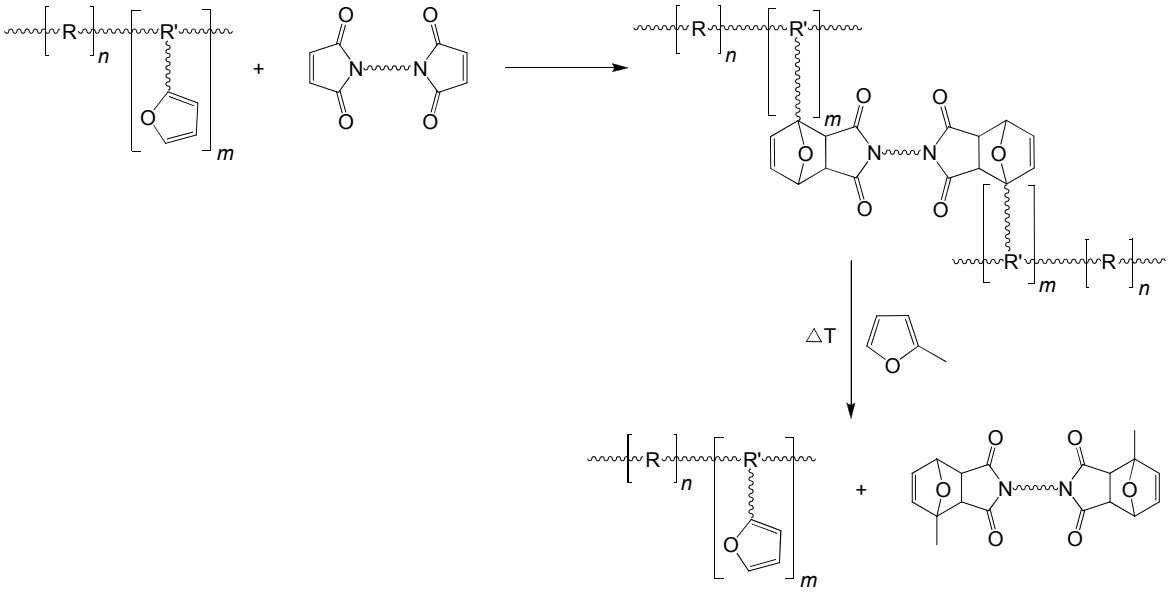

Figure 29. DA-based crosslinking of a furan-substituted linear polymer with a bismaleimide, followed by the retro-DA reaction in the presence of 2-methylfuran [41].

3.4 OTHER APPLICATIONS

The furan-maleimide DA/retro-DA principle is not strictly related only to polymers [167]. Ingenious applications of this approach include, among others, thermally cleavable surfactants [236], paper additives [237], reversible fluorescent structures [238,239] and drug-delivery vehicles [240,241]. Although these systems fall outside the scope of the present study, they illustrate a rich variety of applications, which provide original solutions to technical situations. Thus, for example, the possibility of eliminating *in situ* the surface energy decrease induced by the presence of a surfactant (impossible to remove by conventional means) through the decomposition of its molecule at moderately high temperatures, represent an extremely useful application in such major industrial operations as paper recycling.

PART II

SYNTHESIS AND CHARACTERIZATION OF DIENES AND DIENOPHILES

1 INTRODUCTION

As mentioned previously, the DA reaction needs two “partners” to form the adduct: the diene and the dienophile. The furan heterocycle is particularly suitable for this reaction as the diene, while maleimides represent a typical family of complementary reagents because of their strong dienophilic character [167].

This chapter describes the characterization of the synthesized monomers, namely AA, BB, A_3, B_3, AB and AB_2 type structures, where A and B denote, respectively, the reactive diene (furan) and dienophile (maleimide) moieties, which will be then used in the synthesis of linear, branched or cross-linked polymers through the DA reaction. Thus, three main topics divide this part, viz.

(i) synthesis and characterization of furan monomers (A_n);
(ii) synthesis and characterization of maleimide monomers (B_n);
(iii) synthesis and characterization of furan-maleimide monomers (AB_n).

Each type of these structures comprises monomers bearing different moieties (bridges) separating the reactive groups, viz. aliphatic domains bearing ether, ester or amide functions. The use of these spacers bearing different stiffness will thus lead to macromolecular materials with different properties and hence, different applications**.**

2 SYNTHESIS AND CHARACTERIZATION OF FURAN MONOMERS

As described in the *Experimental* part (p.159), the furan monomers (Figure 30) were synthesized by two different procedures, namely:

(i) one to produce a difunctional AA structure, using an acyl chloride as precursor;

(ii) and the other to produce another AA-type structure, as well as tri-functional monomers (A_3), using amine derivatives as precursors.

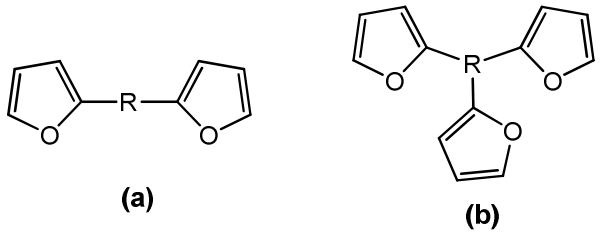

Figure 30. Representative structures of (**a**) difunctional and (**b**) trifunctional dienes.

2.1 AA MONOMERS

2.1.1 Difurfuryl adipate

The synthesis of the first difuran monomer (**I)** followed a procedure previously reported [178], in which an acyl chloride derivative reacted with furfuryl alcohol (Scheme 2). The final product was obtained in good yield (75%) as a viscous brown liquid, and its main features are summarized in Table 5.

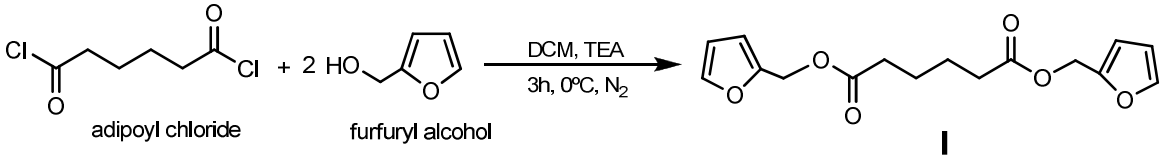

Scheme 2. Synthesis of the difuran monomer **I**.

Figure 31 shows the FTIR spectrum of monomer **I**, where the furan heterocycle bands at 3117, 1350, 1010, 918, 736, 597 cm^{-1}, and the ester C=O and C-O bands at 1732 and 1141 cm^{-1}, respectively, are clearly observed [185,189,242].

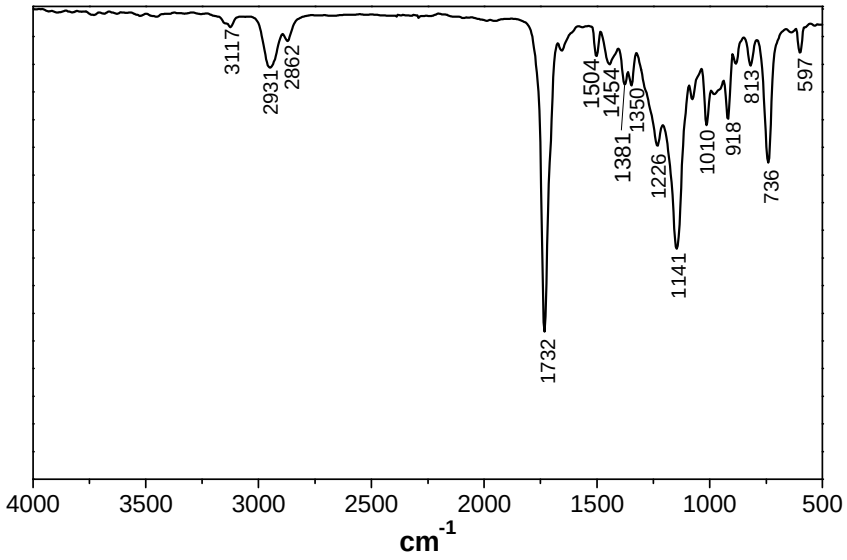

Figure 31. FTIR-ATR spectrum of the monomer **I**.

Its ^{1}H NMR spectrum (Figure 32) confirmed the expected structure due to the presence of furan peaks at δ 7.4, 6.4 and 6.3 ppm, and those of the methylene group adjacent to oxygen atom, viz. furfuryl moiety, at 5.0 ppm, as a singlet. The other methylene groups are displayed at δ 2.3 and 1.6 ppm, being the first shift assigned to protons next to carbonyl group [185,243,244].

The expansion shown in Figure 32 illustrates the proton region of the monosubstituted furan ring of **I**. The peak at δ 6.35 ppm, assigned to proton $H_{4'}$, appears as a doublet of doublets with vicinal coupling constants (^{3}J) 3.3 and 1.8 Hz, arising from its interaction with the adjacent protons H-3' and H-5', respectively. On the other hand, proton H-3'

appears at δ 6.4 ppm as a broad doublet with ^{3}J value 3.3 Hz, due to its interaction with H-4', whereas H-5' (δ 7.4 ppm), which was expected to be a doublet, appears as a doublet of doublets with *J* values 2.0 and 0.8 Hz, arising respectively from its vicinal coupling (^{3}J) with H-4', and long-range allylic coupling (^{4}J) with H-3'. In this case, the proton H-3' is less shielded than H-4', and thus, its signal appears at higher chemical shift. Nevertheless, all these values are in agreement with those referred in the literature [243-246].

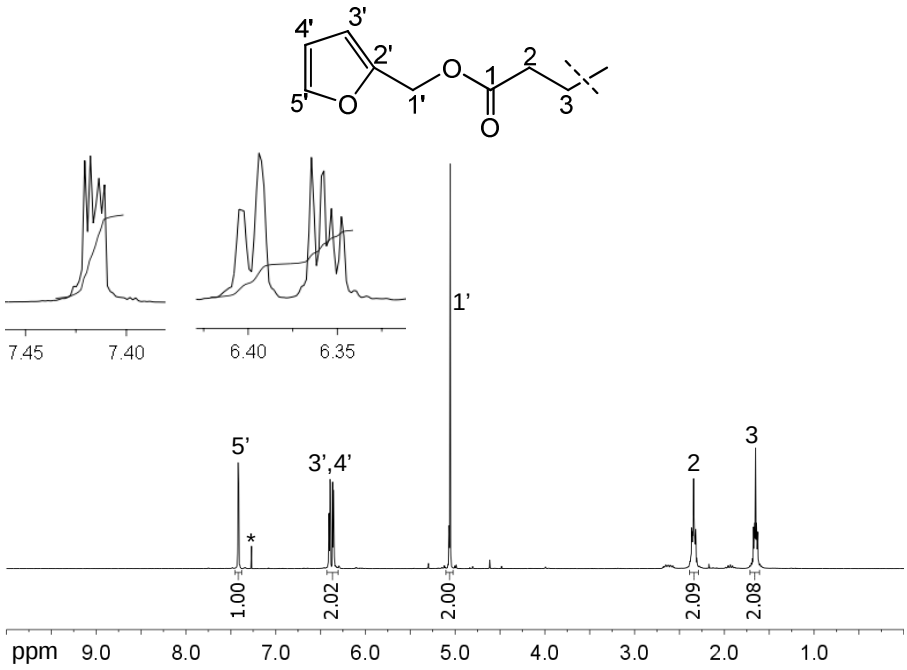

Figure 32. ^{1}H NMR spectrum of monomer **I** in *$CDCl_3$.

The ^{13}C NMR spectrum of **I**, shown in Figure 33, displays the carbonyl carbon resonance at δ 172 ppm and those of the furan ring at δ 149, 143 and 110 ppm, corroborating the previous results. The methylene carbon of the ester function appears at δ 58 ppm, whereas the carbon next to carbonyl group appears at 33 ppm. The peak at 24 ppm is assigned to the remaining methylene carbon [243,244,247].

Additionally, ESI-HRMS data (Table 5) favoured the molecular formula $C_{16}H_{18}O_6$ for **I,** which is in agreement with the expected structure [248].

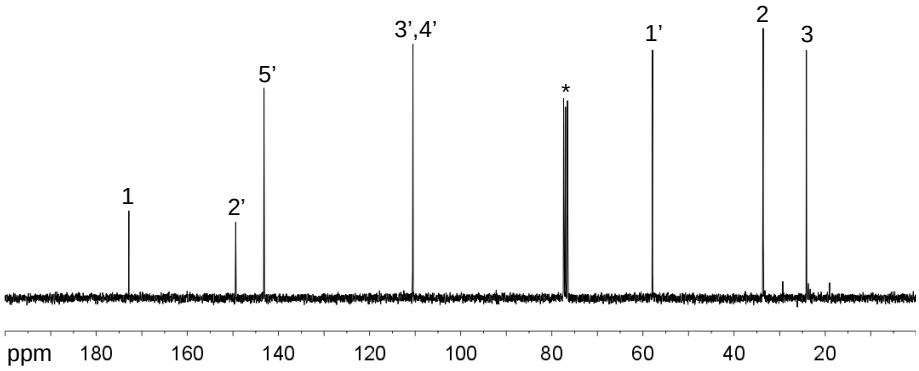

Figure 33. ^{13}C NMR spectrum of monomer **I** in *$CDCl_3$.

Table 5. Characterization of **I**.

Analysis		I
FTIR-ATR (cm^{-1})	ν =CH $_{furan}$	3117
	$\nu_{as\ s}$ CH_2	2931, 2862
	ν C=O	1732
	ν C=C $_{furan}$	1589, 1504, 1381
	ν C-O	1226, 1141
	δ CH_2, CH $_{furan}$	1454, 1350
	furan ring breathing	1010
	$\delta_{out\text{-}of\text{-}plane}$ CH $_{furan}$	918, 813, 736
	furan ring deformation	597
^{1}H NMR (ppm)	H-5'	7.42 (dd; *J*=2.0, 0.8; 1H)
	H-3'	6.40 (d; *J*=3.3; 1H)
	H-4'	6.36 (dd; *J*=3.3, 1.8; 1H)
	H-1'	5.06 (s; 2H)
	H-2	2.34 (m; 2H)
	H-3	1.65 (m; 2H)
^{13}C NMR (ppm)	C-1	172.8
	C-2'	149.4
	C-5'	143.2
	C-3', C-4'	110.5,110.4
	C-1'	57.9
	C-2	33.6
	C-3	24.1

DSC Tg (ºC)		-63.4
ESI-HRMS Calculated found	$C_{16}H_{18}O_6Na$ $[M+Na]^+$	 329.09956 329.09926

2.1.2 *N,N'*-difurfuryl-4,7,10-trioxa-1,13-tridecanediamine

The synthesis of the other AA monomer (**III**) took place in a two-step procedure previously reported [249,250], where first a Schiff base derivative was prepared, and then *in situ* reduction was applied (Scheme 3). The ensuing product was obtained as a brown viscous liquid with an overall yield of 80%.

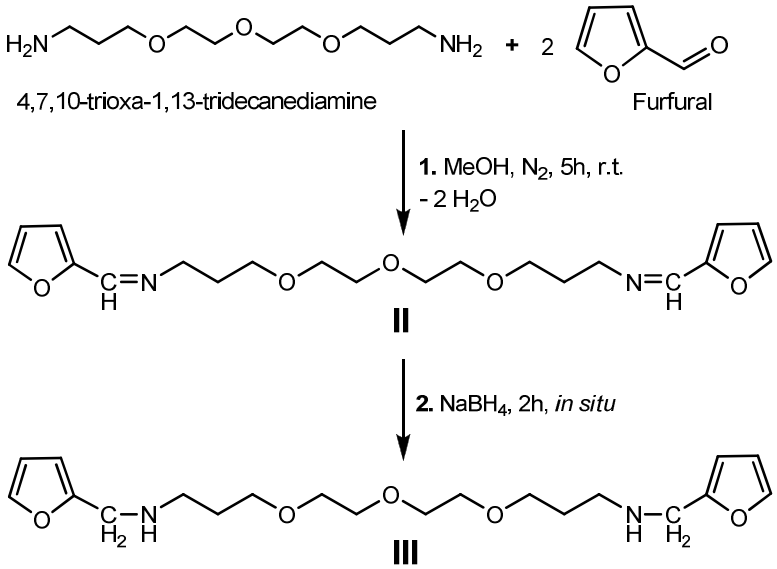

Scheme 3. Preparation of the (**1**) Schiff base **II** and (**2**) its corresponding reduced structure **III**.

*2.1.2.1 Schiff base **II***

The structure of a Schiff base is characterized by the presence of an imine *CH=N* group [242,248,250], resulting from the condensation of a primary amine and a carbonyl group. In this study, 4,7,10-trioxa-1,13-tridecanediamine and furfural were the reagents used (Scheme 3).

The FTIR spectrum of **II** (Figure 34) clearly shows a C=N band at 1643 cm^{-1}, as well as the C-O band at 1099 cm^{-1} and furan ring bands at 3109, 1014, 748, 594 cm^{-1} [242,250].

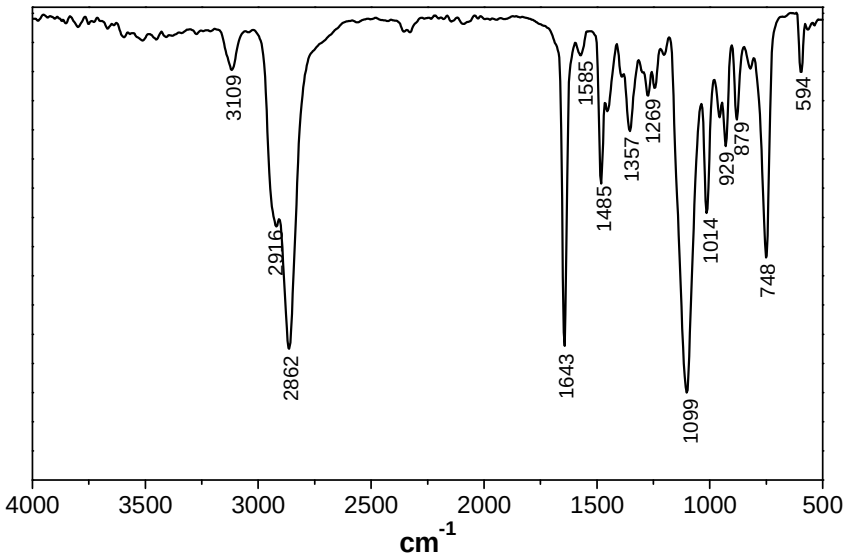

Figure 34. FTIR-ATR spectrum of the structure **II**.

As expected, the ^{1}H NMR spectrum of **II** (Figure 35) showed the imino proton peak (H-1') at δ 8.1 ppm as a singlet, and those of the furan ring at δ 7.5, 6.7 and 6.4 ppm, respectively assigned to protons H-5' (a doublet with ^{3}J value 1.6 Hz), H-3' (a doublet with ^{3}J value 3.4 Hz), and H-4' (a doublet of doublets with ^{3}J values 3.4 and 1.8 Hz). In this case, the long-range allylic coupling between H-5' and H-3' is not clearly observed. The methylene protons next to oxygen and nitrogen atoms appear as multiplets between δ 3.7 and 3.5 ppm, while the remaining methylene group appears as a quintet with ^{3}J value of 6.5 Hz, at lower chemical shift (δ 2.0 ppm). These attributions and values are in agreement with the literature [243,244,246,250].

Its ^{13}C NMR spectrum (Figure 36) corroborates the synthesized structure, mainly by the presence of the imino carbon peak at δ 150 ppm, and the furan ring carbons at δ 151, 144, 113 and 111 ppm. The methylene carbons next to oxygen appear between δ 71 and 68 ppm, whereas the methylene group attached to the nitrogen appears at a slightly lower chemical shift (δ 58 ppm) due to the lower electronegativity of the nitrogen atom. The remaining carbon appears at 30 ppm [244,247,250].

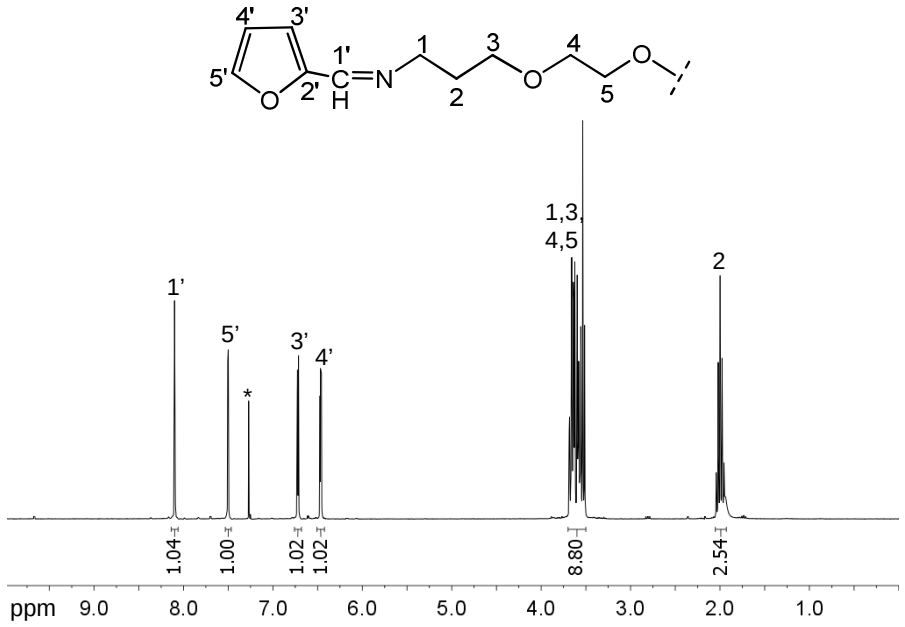

Figure 35. ^{1}H NMR spectrum of the Schiff base **II** in *$CDCl_3$.

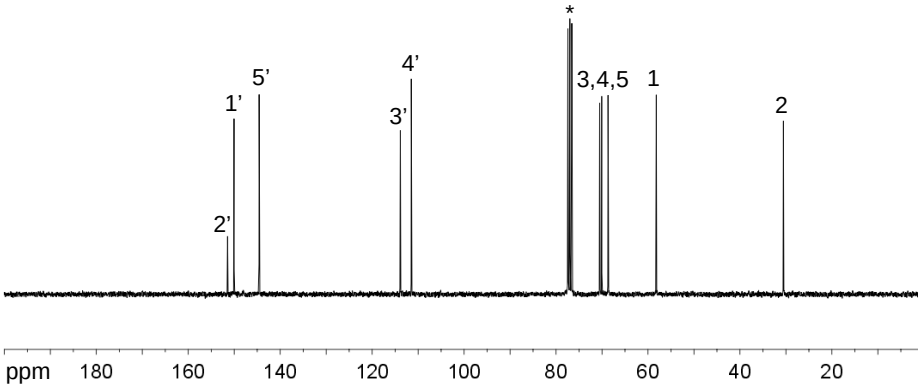

Figure 36. ^{13}C NMR spectrum of the Schiff base **II** in *$CDCl_3$.

*2.1.2.2 Reduced Schiff base **III***

When the reduction was applied to compound **II** (Scheme 3), the imine *CH=N* group was readily converted into the corresponding secondary amine *CH_2-NH* in compound **III** (Figure 37).

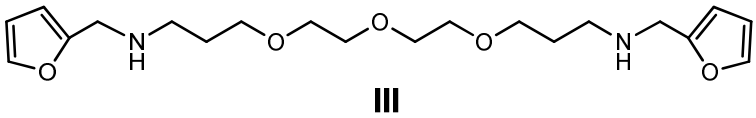

III

Figure 37. Structure of the reduced Schiff base **II**.

The comparison between the FTIR spectra of **III** before (Figure 34) and after reduction (Figure 38) confirms the success of the reaction, because of the disappearance of the characteristic bands of the imine group, viz. absence of the C=N band at 1643 cm^{-1}, as well as the presence of those related to the amino group, viz. 3305, 1598, 1145 cm^{-1} [242,250].

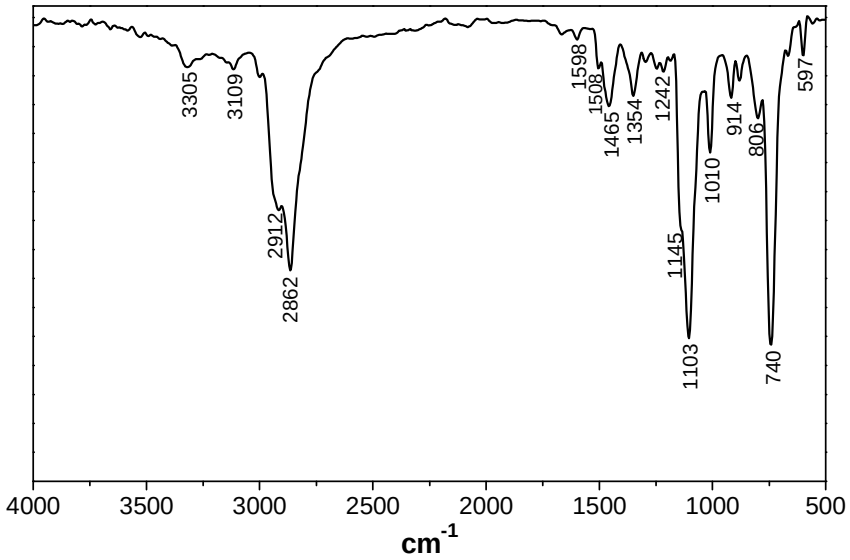

Figure 38. FTIR-ATR spectrum of the reduced Schiff base **III**.

The ^{1}H NMR spectrum of **III** (Figure 39) confirms its structure, since the imino peak at δ 8.1 ppm disappears, whereas a new resonance assigned to methylene protons of the corresponding amino moiety (H-1'), viz. between both furan and NH moieties, appears at δ 3.7 ppm (singlet). The chemical shift of the furan protons is not significantly changed. Furan H-5' (δ 7.3 ppm) appears as a double of doublets with ^{3}J value 1.6 Hz and ^{4}J value 0.8 Hz, arising respectively from its interaction with H-4' and H-3'. The peak at δ 6.3 ppm is assigned to H-4', which appears as a double of doublets with ^{3}J values of 3.1 and 1.9 Hz, whereas the peak at lowest chemical shift (δ 6.1 ppm) is assigned to H-3', which appears as a doublet with ^{3}J value 2.9 Hz. The methylene protons next to oxygen appear as a

multiplet at δ 3.7-3.4 ppm, whereas the group next to nitrogen appears at δ 2.70 ppm as a triplet with ^{3}J value 6.9 Hz. The remaining methylene group (δ 1.7 ppm) appears as a quintet with ^{3}J value 6.6 Hz. Additionally, a broad singlet peak is observed at δ 1.6 ppm, being assigned to the NH proton [243,244,246,250].

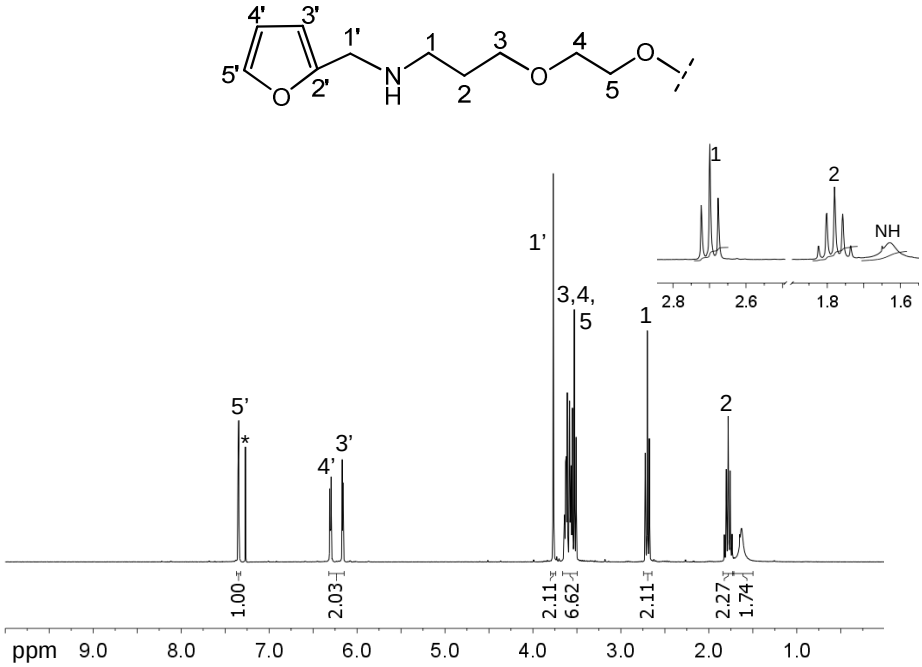

Figure 39. ^{1}H NMR spectrum of the reduced Schiff base **III** in *$CDCl_3$.

The ^{13}C NMR spectrum of **III**, shown in Figure 40, further corroborates the expected structure with the absence of the imino carbon peak at 150 ppm, and the presence of the corresponding amino carbon (C-1') at 46 ppm, which is at the same shift of the methylene group on the other side of the nitrogen (C-1). Furan carbons (δ 154, 141, 109 and 106 ppm), as well as methylene carbons (δ 71-69 and 29 ppm), do not suffer significant change in their chemical shifts [244,247,250].

The main features of both **II** and **III** structures are summarized in Table 6. According to ESI-HRMS data (Table 6), the favoured molecular formula $C_{20}H_{32}N_2O_5$ for **III** is in agreement with the expected results [248].

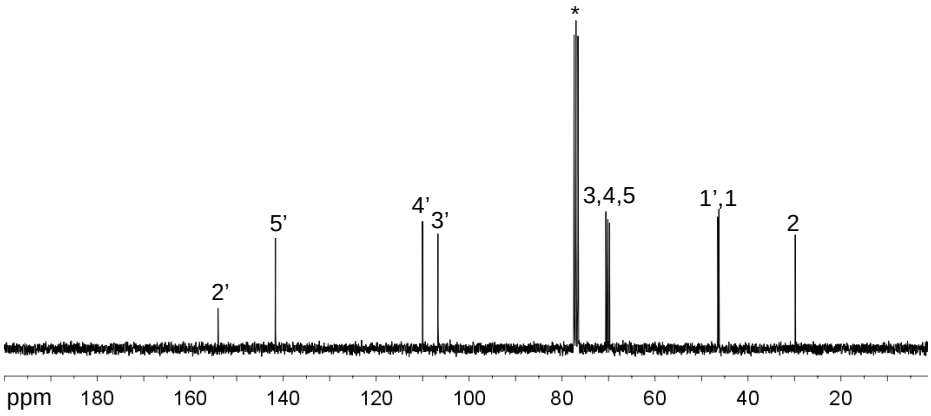

Figure 40. ^{13}C NMR spectrum of the reduced Schiff base **III** in *$CDCl_3$.

Table 6. Characterization of **II** and **III**.

Analysis		II	III
FTIR-ATR (cm^{-1})	ν NH	-	3305
	ν =CH $_{furan}$	3109	3109
	$\nu_{as,s}$ CH_2	2916, 2862	2912, 2862
	ν CH=N	1643	-
	ν C=C $_{furan}$	1585, 1469, 1396	1508, 1384
	δ NH, ν C-N	-	1598, 1145
	ν C-O	1269, 1099	1242, 1107
	δ CH_2, CH $_{furan}$	1481, 1357	1465, 1354
	furan ring breathing	1014	1014
	$\delta_{out\text{-}of\text{-}plane}$ CH $_{furan}$	929, 879, 748	914, 806, 740
	furan ring deformation	594	597
^{1}H NMR (ppm)	H-1'	8.10 (s; 1H)	3.77 (s; 2H)
	H-5'	7.50 (d; *J*=1.6; 1H)	7.35 (dd; *J*=1.6, 0.8; 1H)
	H-3'	6.72 (d; *J*=3.4; 1H)	6.16 (d; *J*=2.9; 1H)
	H-4'	6.46 (dd; *J*=3.4, 1.8; 1H)	6.30 (dd; *J*=3.1, 1.9; 1H)
	H-3, H-4, H-5	3.51-3.68 (m; 8H)	3.66-3.48 (m; 6H)
	H-1		2.70 (t; *J*=6.9; 2H)
	H-2	2.0 (quintet; *J*=6.5; 2H)	1.78 (quintet; *J*=6.6; 2H)
	NH	-	1.63 (br s; 1H)

^{13}C NMR (ppm)	C-2’ C-1’ C-5’ C-3’, C-4’ C-4, C-5 C-3 C-1 C-2	151.4 150.0 144.6 113.7, 111.0 70.5, 70.1 68.7 58.2 30.5	154.0 46.5 141.6 110.0, 106.7 70.6, 70.1 69.8 46.2 29.8
DSC Tg (ºC)		-	-70.8
ESI-HRMS calculated found	$C_{20}H_{33}N_2O_5$ $[M+H]^+$	-	381.23840 381.23769

2.2 A_3 MONOMERS

The procedure followed to obtain both A_3 monomers was similar to that used in the synthesis of the previous monomer **III**, i.e., first a Schiff base was synthesized and then *in situ* reduction was applied (Scheme 4). However, in this case, trisamine derivatives were used as precursors, namely tris-(2-aminoethyl)amine and jeffamine T-403. The final products were both obtained as brown viscous liquids, with an overall yield higher than 90%.

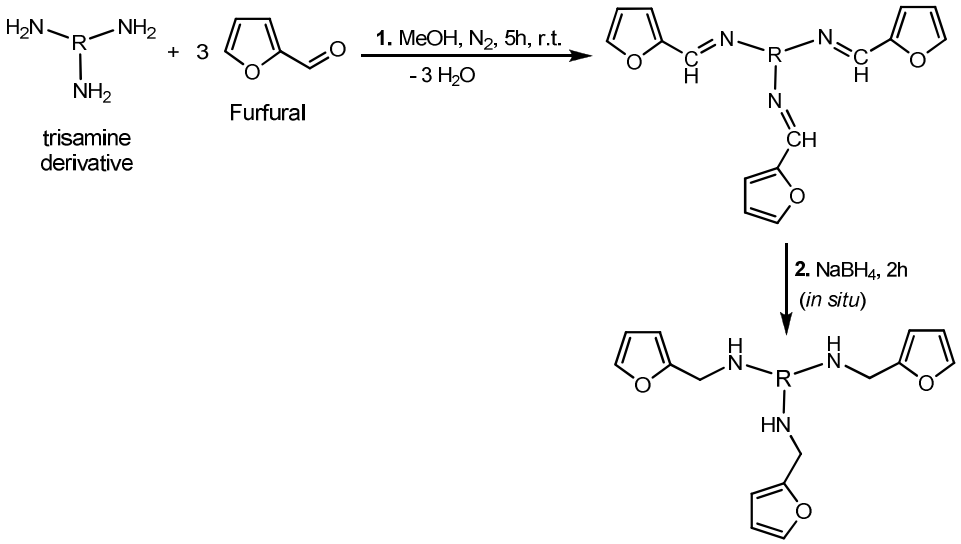

Scheme 4. Preparation of (**1**) Schiff bases from tris-amines, followed by (**2**) their reduction.

2.2.1 Schiff bases IV and V

The structures of the synthesized Schiff bases, **IV** and **V**, are shown in Figure 41, and their features are summarized in Table 7 and Table 8, respectively. As previously referred, the success of these reactions is confirmed by the presence of the characteristic peaks of the imine *CH=N* group (Scheme 4), viz. around 1640 cm^{-1} and δ 8.0 ppm in the FTIR and ^{1}H NMR spectra, respectively [242,248,250].

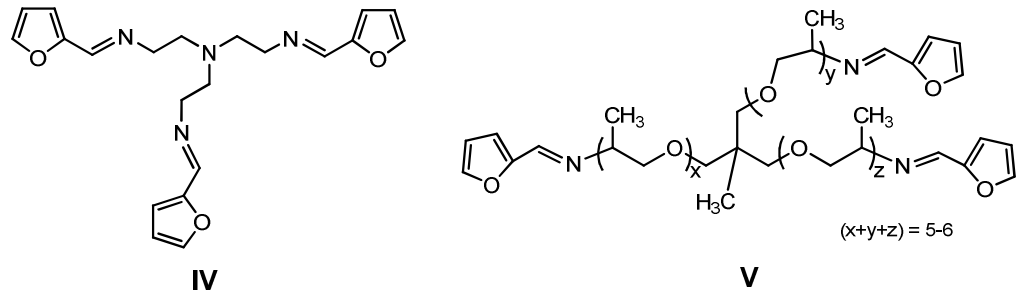

Figure 41. Structure of the Schiff base from tris-(2-aminoethyl)amine **(IV**) and from jeffamine (**V**).

The FTIR spectra of **IV** and **V** showed clearly the presence of the imino group band at 1643 cm^{-1} for both structures, and the furan ring bands at 3108, 1012, 930, 816, 743, 595 cm^{-1} for **IV** and at 3117, 1011, 930, 818, 747, 596 cm^{-1} for **V** [242,250].

Figure 42 shows the ^{1}H NMR spectrum of the Schiff base **IV**, whose pattern is similar to that obtained for **II**, namely the proton of the imino group is clearly observed at δ 7.9 ppm (singlet), whereas those of the furan ring appear at δ 7.4, 6.5 and 6.4 ppm, respectively assigned to proton H-5' (a doublet with ^{3}J value 1.5 Hz), H-3' (a doublet with ^{3}J value 3.4 Hz), and H-4' (a doublet of doublets with ^{3}J values 3.4 and 1.7 Hz). The methylene protons next to the trisamine group appear at 3.6 ppm as a triplet with ^{3}J value 6.0 Hz, whereas those next to the imine appears at lower chemical shift (δ 2.8 ppm) also as a triplet with ^{3}J value 6.4 Hz [243,244,246,250].

Its ^{13}C NMR spectrum confirmed its structure with the peak at δ 150 ppm for the imine carbon. The furan ring carbons appear at δ 151, 144, 113 and 111 ppm, whereas the methylene carbons appear at δ 59 and 55 ppm, respectively assigned to carbons next to the imino and trisamino group [244,247,250].

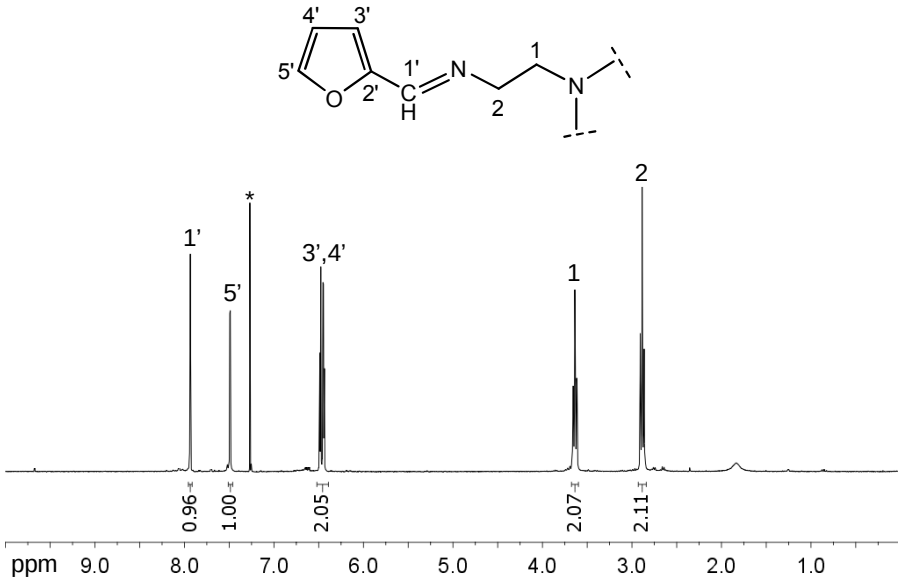

Figure 42. ^{1}H NMR spectrum of the Schiff base **IV** in *$CDCl_3$.

The ^{1}H NMR spectrum of the second A_3 Schiff base **V** (Figure 41) is shown in Figure 43. As the previous structure **IV**, the imine proton peak appears at δ 8.1 ppm, whereas those of the furan ring appear at δ 7.4, 6.7 and 6.4 ppm, respectively assigned to H-5', H-3', and H-4' protons, whose coupling constants could not be calculated due to overlapping signals. Due to its complex structure, Jeffamine core protons are only indicated to appear in the range δ 1.0-4.0 ppm, without further specification.

In the ^{13}C NMR spectrum of **V**, the imino carbon (δ 149 ppm), as well as furan carbons resonances (δ 151, 144, 114 and 111 ppm) are observed, and the Jeffamine core carbons appear between δ 80 and 0 ppm [243,244,250].

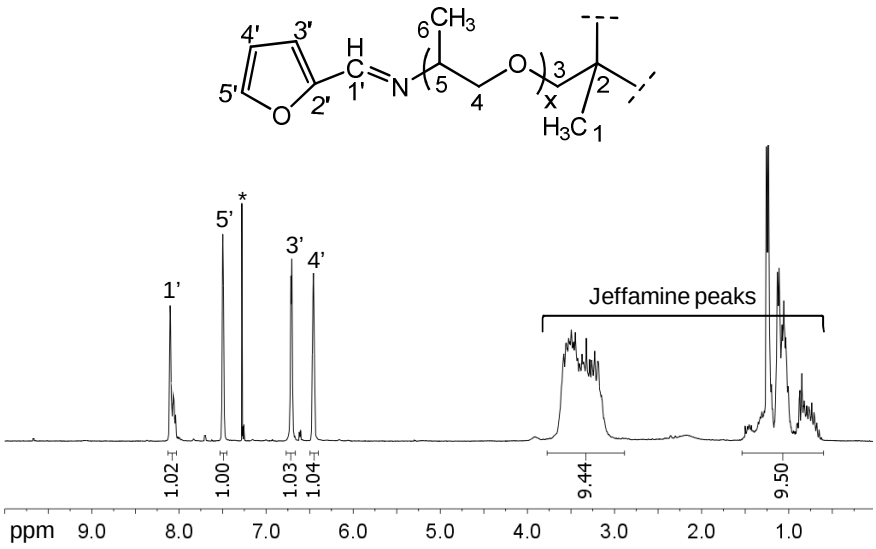

Figure 43. ^{1}H NMR spectrum of the Schiff base **V** in *$CDCl_3$.

2.2.2 Reduced Schiff bases, VI and VII

As previously discussed, the reduction step (Scheme 4) implies the disapperance of the characteristic peaks of the imine *CH=N* group at 1643 cm^{-1} and 8.1 ppm in the FTIR and ^{1}H NMR spectra, respectively, as well as the concurrent appearance of peaks related to the amine *CH_2-NH* group, viz. 3335 cm^{-1} and 3.76 ppm. Both reduced Schiff base's structures, **VI** and **VII**, are represented in Figure 44.

The FTIR spectra of both these structures showed clearly the success of the reduction, mainly due to the absence of the imine band at 1643 cm^{-1} [242,250].

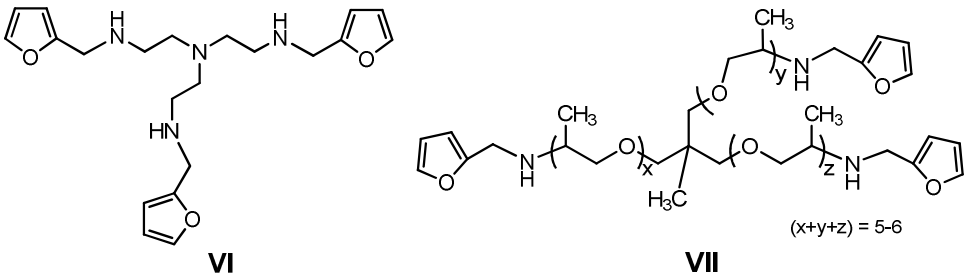

Figure 44. Structure of the reduced Schiff base **VI** and **VII**.

Figure 45 shows the ^{1}H NMR spectrum of **VI**. When compared with its spectrum before reduction (Figure 42), it is possible to conclude that the imino proton peak previously at δ 7.93 ppm, now appears at δ 3.74 ppm, which is assigned to the corresponding methylene protons attached to both furan and NH moieties (H-1'). Furan ring protons do not suffer significant changes, viz. H-5' appears at δ 7.3 ppm, as a double of doublets with ^{3}J value 1.8 Hz and ^{4}J value 0.9 Hz; proton H-4' appears a δ 6.2 ppm, as a double of doublets with ^{3}J values of 3.0 and 2.1 Hz; and H-3', assigned to the peak at δ 6.1 ppm, appears as a double of doublets with ^{3}J value 3.2 Hz. The two methylene groups now appear at δ 2.6 and 2.5 ppm, each one as a triplet with ^{3}J value of 5.8 and 5.9 Hz, respectively. A broad singlet peak is also observed at 2.0 ppm, which is assigned to the NH proton [243,244,246,250]. Its ^{13}C NMR spectrum confirmed the occurrence of the reduction, because of the absence of the imino carbon peak at δ 150 ppm, and the presence of the corresponding amino carbon peak at 46.6 ppm (C-1'). The chemical shifts of the remaining structure, namely furan and methylene carbons, are not significantly changed [244,247,250].

Furthermore, ESI-MS data of **VI** (Table 7) were in agreement with the expected results, with favouring the molecular formula $C_{20}H_{32}N_2O_5$ [248].

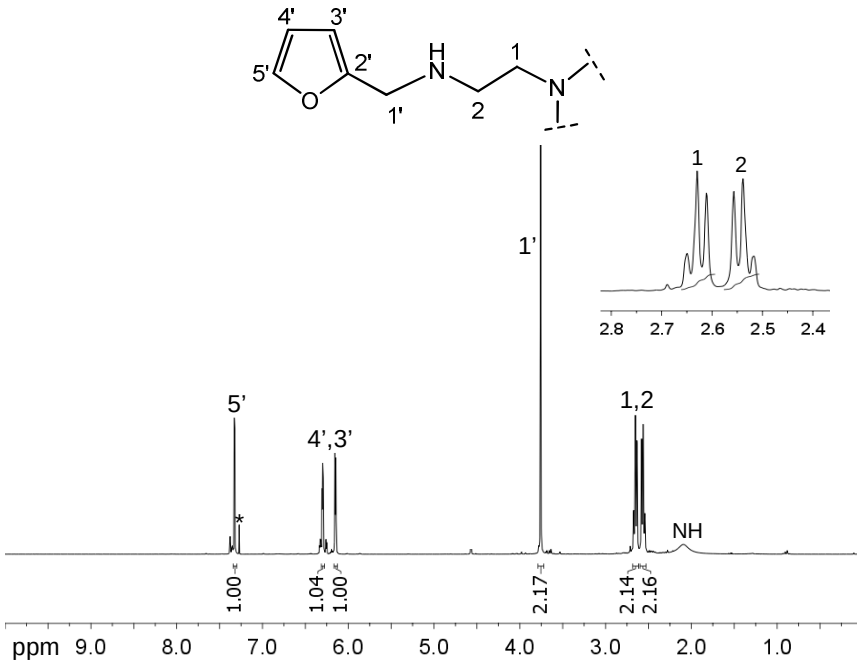

Figure 45. ^{1}H NMR spectrum of monomer **VI** in *$CDCl_3$.

The main features of **VI** are summarized in Table 7, together with those related to structure **IV**.

Table 7. Characterization of the A_3 monomer **VI**, before and after reduction

Analysis		IV	VI
FTIR-ATR (cm^{-1})	ν NH	-	3305
	ν =CH $_{furan}$	3108	3113
	$\nu_{as\,s}$ CH_2, ν CH	2940, 2883, 2836	2923, 2819
	ν CH=N	1643	-
	ν C=C $_{furan}$	1568, 1439, 1388	1504, 1384
	δ NH	-	1590, 1146, 1051, 880
	ν C-N	1153, 1060,881	
	ν C-O	1269	1192
	δ CH_2, CH $_{furan}$	1482, 1346	1452, 1330
	furan ring breathing	1012	1008
	$\delta_{out\text{-}of\text{-}plane}$ CH $_{furan}$	930, 816, 743	916, 796, 728
	furan ring deformation	595	598
^{1}H NMR (ppm)	H-1’	7.93 (s; 1H)	3.78 (s; 2H)
	H-5’	7.49 (d; *J*=1.5; 1H)	7.33 (dd; *J*=1.8, 0.9; 1H)
	H-3’	6.48 (d; *J*=3.4; 1H)	6.14 (d; *J*=3.2; 1H)
	H-4’	6.44 (dd; *J*=3.4, 1.7; 1H)	6.29 (dd; *J*=3.0, 2.1; 1H)
	H-2	3.64 (t; *J*=6.0; 2H)	2.68 (t; *J*=5.8; 2H)
	H-1	2.89 (t; *J*=6.4; 2H)	2.56 (t; *J*=5.9; 2H)
	NH	-	2.06 (br s; 1H)
^{13}C NMR (ppm)	C-2’	151.6	153.9
	C-1’	150.5	46.7
	C-5’	144.5	141.6
	C-3’, C-4’	113.8, 111.5	110.0, 106.8
	C-2	59.7	54.2
	C-1	55.3	46.0
DSC Tg (ºC)		-	-61.6
ESI-HRMS calculated found	$C_{21}H_{31}N_4O_3$ $[M+H]^+$	-	387.23907 387.23855

The spectroscopic data related to the second reduced Schiff base **VII** (Figure 44) are similar to those obtained for **VI**, namely the imino proton peak at δ 8.1 ppm disappears and a new one appears at δ 3.8 ppm assigned to the corresponding methylene protons. However, unlike previous Schiff base structures where it appears as a singlet, in this case, the new peak appears as an AB "quartet" (^3J value 14.4 Hz), which means that it is coupling with adjacent NH [244,248]. The furan ring protons appear at δ 7.4, 6.7 and 6.4 ppm, respectively assigned to H-5', H-3', and H-4' protons, however, their coupling constants could not be calculated due to overlapping signals.

The ^{13}C NMR spectrum of **VII** corroborated these results, mainly by the absence of the imino carbon peak at δ 150 ppm [243,244,247,250]. Moreover, its ESI-MS data (Table 8) suggests that indeed the expected structure was obtained by favouring the molecular formula $C_{42}H_{72}N_3O_{10}$ or $C_{44}H_{75}N_3O_{11}$ for $(x+y+z)$ =5 or 6, respectively [248].

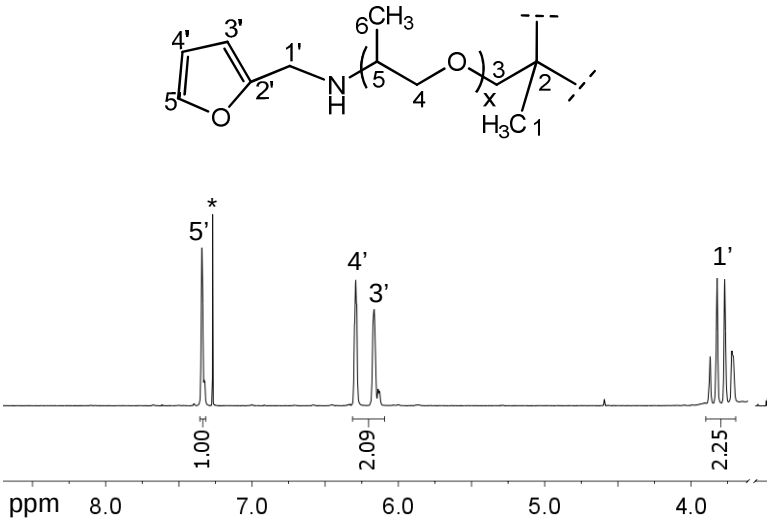

Figure 46. ^1H NMR spectrum of monomer **VII** in *$CDCl_3$ omitting the range δ 3.5-0 ppm.

The main features of **VII**, together with those related to the corresponding Schiff base **V**, are summarized in Table 8.

Table 8. Characterization of the A_3 monomer **VII** before and after reduction

Analysis		V	VII
FTIR-ATR (cm^{-1})	ν NH	-	3315
	ν =CH $_{furan}$	3117	3113
	$\nu_{as\ s}$ CH_2, ν CH_3	2967, 2931, 2867	2966, 2938, 2867
	ν CH=N	1643	-
	ν C=C $_{furan}$	1560, 1482, 1376	1488, 1374
	δ NH	-	1585
	ν C-N	1100, 880	1131, 880
	ν C-O	1268, 1100	1248, 1095
	δ CH_3, CH_2, CH $_{furan}$	1453, 1372	1449, 1374, 1331
	furan ring breathing	1011	1009
	$\delta_{out\text{-}of\text{-}plane}$ CH $_{furan}$	930, 818, 747	914, 802, 730
	furan ring deformation	596	599
^{1}H NMR (ppm)	H-1'	8.13 (s; 1H)	3.80 (*AB 'quartet'*; *J*=14.5; 2H)
	H-5'	7.49 (s; 1H)	7.34 (s; 1H)
	H-3'	6.70 (s; 1H)	6.15 (m; 1H)
	H-4'	6.45 (s; 1H)	6.29 (m; 1H)
	NH	-	2.0 (br s; 1H)
	core jeffamine protons	3.77-2.89 (m; 9H)	3.61-2.80 (m; 9H)
		1.54-0.60 (m; 9H)	1.46-0.71 (m; 9H)
^{13}C NMR (ppm)	C-2'	151.5	154.6
	C-1'	149.2	44.1
	C-5'	144.5	142.0
	C-3', C-4'	114.2, 111.4	110.5, 107.0
	core jeffamine protons	80-10	80-10
DSC Tg (ºC)		-	-60.1
ESI-HRMS	$[M+CH_3]^+$		
calculated	For (*x*+*y*+*z*)=5,		778.52122
found	$C_{42}H_{72}N_3O_{10}$	-	778.52029
calculated	For (*x*+*y*+*z*)=6,		836.56309
found	$C_{45}H_{782}N_3O_{11}$		836.56344

3 SYNTHESIS AND CHARACTERIZATION OF MALEIMIDE MONOMERS

As described in the *Experimental* part (p.159), two different procedures were applied to synthesize maleimide monomers (Figure 47), namely:

(i) one to synthesize the difunctional BB monomer, using a diamine derivative as precursor;

(ii) and the other to synthesize the trifunctional monomer B_3, using a trisamine derivative as precursor.

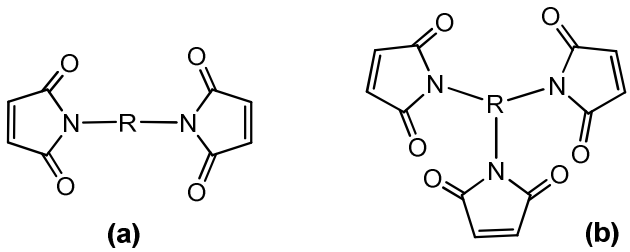

Figure 47. Representative structures of (**a**) difunctional and (**b**) trifunctional dienophiles.

3.1 BB MONOMER

The bismaleimide monomer was prepared by a two-step procedure [251-255], namely first a bismaleamic acid was formed by the reaction of a diamine derivative with maleic anhydride (Scheme 5); and then the ensuing product was converted into the corresponding maleimide through intramolecular cyclization in the presence of anhydrous sodium acetate and acetic anhydride (Scheme 6).

3.1.1 *N,N'*-hexamethylenebismaleamic acid

1,6-hexamethylenediamine was used to prepare the bismaleamic acid **VIII** (Scheme 5), which was obtained as white crystals with a yield higher than 80%.

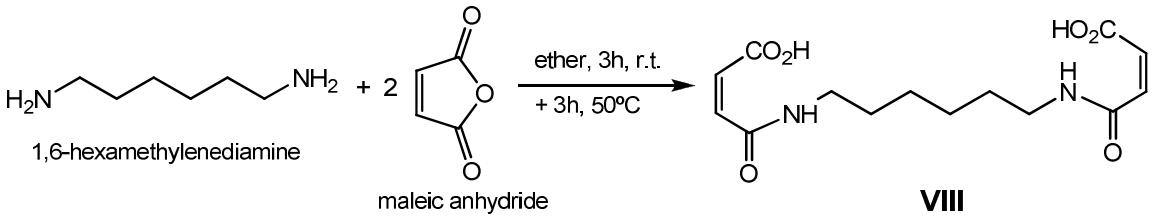

Scheme 5. Synthesis of the bismaleamic acid from **VIII**.

In the FTIR spectrum of **VIII** (Figure 48), the presence of the characteristic carbonyl bands at 1705 and 1627 cm^{-1} corresponding to the acid and amide groups, respectively, as well as the OH and NH bands at 3300 and 3286 cm^{-1}, respectively, confirms the expected structure. Further, C-O and C-N vibrations are also observed at 1469 and 1531 cm^{-1}, respectively [189,242,256].

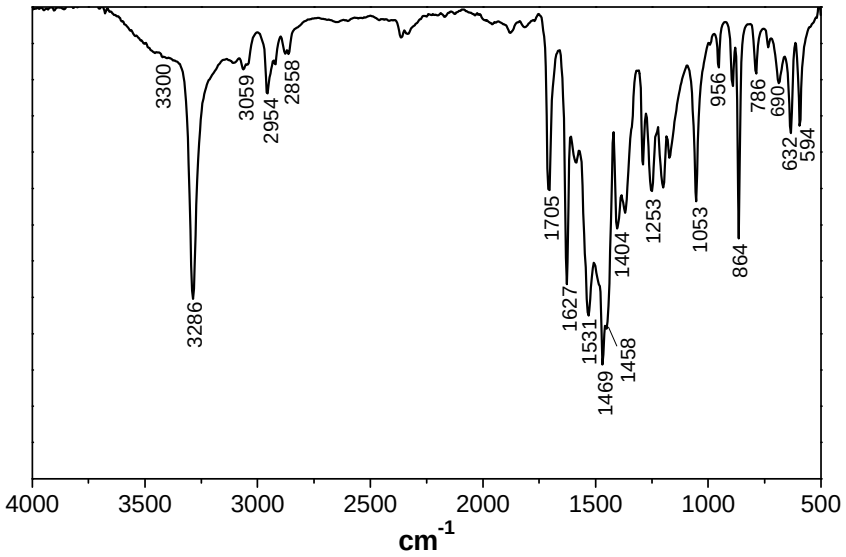

Figure 48. FTIR-ATR spectra of bismaleamic acid **VIII**.

The ^{1}H NMR spectrum of **VII** (Figure 49) confirms its structure, due to the presence of two doublets at δ 6.43 and 6.26 ppm, both with ^{3}J value around 12.6 Hz. These peaks are assigned to the protons of the asymmetric C=C moiety. The methylene protons appear at δ 3.3, 1.6 and 1.4 ppm, being the first value assigned to that next to the amide group. In this case, the NH peak is not observed. Furthermore, its ^{13}C NMR corroborated the formation of the maleamic acid **VII** by the presence of two carbonyl peaks at δ 168 and 167 ppm, as well as, two peaks at δ 134 and 133 ppm corresponding to the insaturation carbons [189,243,244,247].

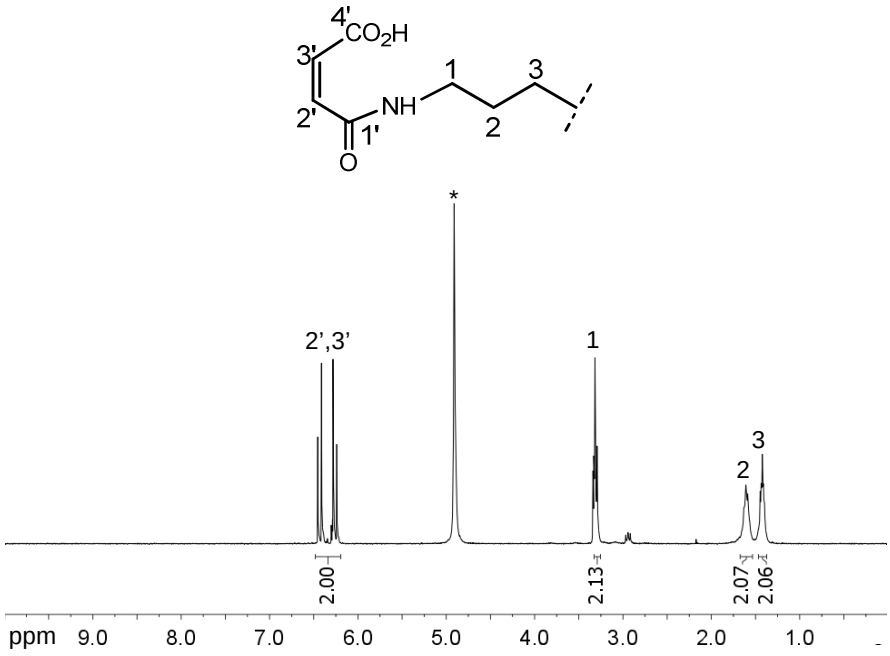

Figure 49. ^{1}H NMR spectrum of the bismaleamic acid **VIII** in *methanol-d_4.

3.1.2 *N,N'*-hexamethylenebismaleimide

As referred previously, the bismaleamic acid, **VIII**, was converted into the corresponding maleimide, **IX**, by cyclization using anhydrous sodium acetate and acetic anhydride (Scheme 6). The former was used in excess to guarantee that all terminal groups would react [203,252,254]. The ensuing product was obtained as a brown viscous liquid, which after further purification by column chromatography gave a white solid. The product

yields of this step were around 50%, mainly due to the product solubility in water during the washing of the excess of acetic anhydride and the purification.

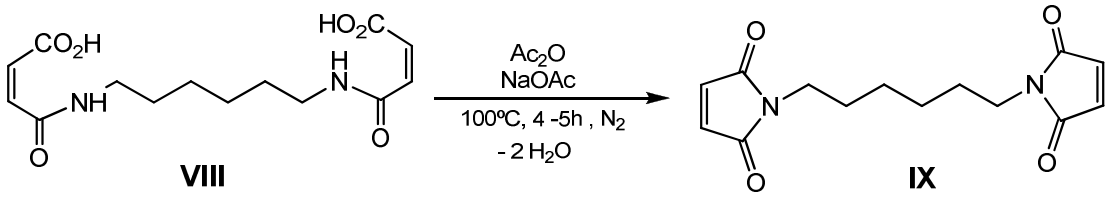

Scheme 6. Cyclization of bismaleamic acid **VIII**, with formation of the corresponding bismaleimide.

The comparison between the FTIR spectra of **IX** before (Figure 48) and after cyclization (Figure 50) shows the presence of a typical intense doublet peak at 1747 and 1687 cm^{-1}, arising from the C=O group of the maleamide cycle, instead of the two bands in the maleamic acid spectrum, as well as the disappearance of the characteristic maleamic acid bands at 3300, 3286, 1531, 1469, 1253, 956 and 690 cm^{-1} [189,242,252,255,256].

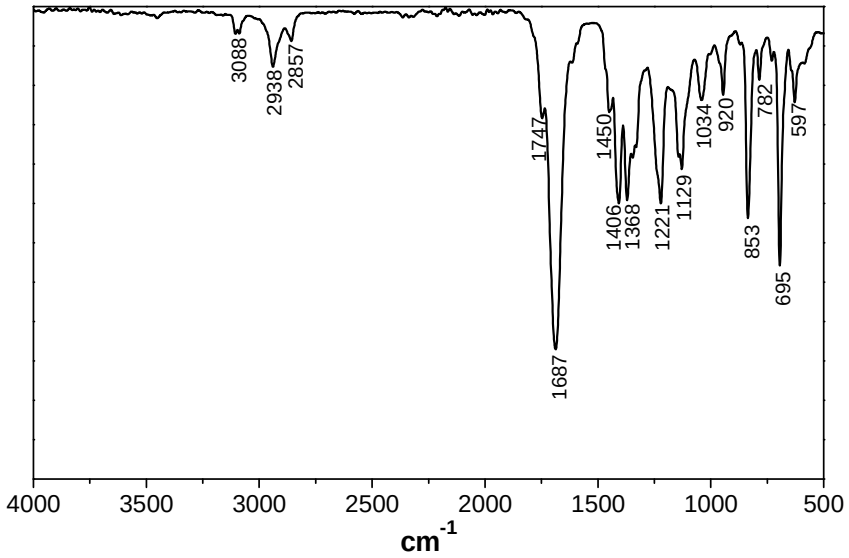

Figure 50. FTIR-ATR spectra of the monomer **IX**.

The ^{1}H NMR spectrum of **IX** (Figure 51) confirms its structure by the presence of a singlet peak at δ 6.6 ppm for the insaturation protons, instead of the two doublets in the corresponding maleamic acid (Figure 49). The methylene protons next to nitrogen appear

at δ 3.5 ppm as a triplet with ^{3}J value 7.2 Hz, whereas the other methylene groups appear each as a multiplet at δ 1.5 and 1.2 ppm, respectively [189,243,244,255]. Its ^{13}C NMR spectrum corroborated these results, due to the presence of only one carbonyl and insaturation carbons at δ 170 and 134 ppm, respectively. The methylene carbons appear at δ 37, 28 and 26 ppm [189,243,244,247,255].

Although unknown impurities were detected in both spectra, even after the purification process, they do not interfere in the subsequent DA reactions, as will be seen later in the part *III* (p. 95).

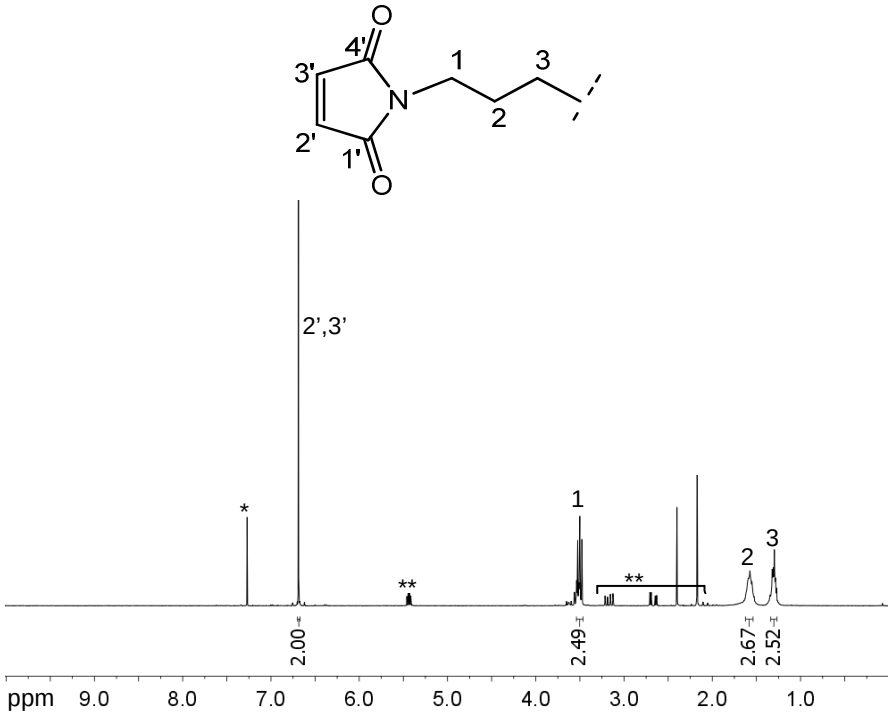

Figure 51. ^{1}H NMR spectrum of **IX** in *$CDCl_3$ (**unknown impurities).

The ESI-HRMS data (Table 9) for **IX** favoured the molecular formula $C_{14}H_{16}N_2O_4$ [248]. The characteristics of the monomer **IX**, before and after cyclization, are summarized in Table 9.

Table 9. Characterization of the monomer **IX**, before and after cyclization.

Analysis		VIII	IX
FTIR-ATR (cm^{-1})	ν OH, NH	3300, 3286	-
	ν =CH	3059	3088
	$\nu_{as\ s}\ CH_2$	2954, 2858	2938, 2857
	ν C=O	1705, 1627	1747, 1687
	ν C=C	1458	1450
	δ NH	1531	-
	ν C-N	1372, 1053, 690	1368, 1326, 1129, 782
	δ OH, ν C-O	1469, 1253, 956	-
	δ CH	1404, 864, 786	1406, 853
	δ N-C=O	632, 594	695, 597
^{1}H NMR (ppm)	H-2',H-3'	6.43 (d; *J*=12.6; 1H) 6.26 (d; *J*=12.9; 1H)	6.69 (s; 2H)
	H-1	3.31 (t; *J*=4.8; 2H)	3.50 (t; *J*=7.2; 2H)
	H-2	1.66-1.55 (m; 2H)	1.60-1.52 (m; 2H)
	H-3	1.45-1.40 (m; 2H)	1.32-1.27 (m; 2H)
^{13}C NMR (ppm)	C-1',C-4'	168.7, 167.7	170.9
	C-2',C-3'	134.1, 133.5	134.0
	C-1	40.7	37.7
	C-2	29.7	28.3
	C-3	27.5	26.1
DSC m.p. (ºC)		-	115.5
ESI-HRMS calculated found	$C_{14}H_{17}N_2O_4$ $[M+H]^+$	-	277.11828 277.11839

3.2 B3 MONOMER

The trifunctional monomer was obtained by a procedure different from that described for the previous monomer **IX**, viz. tris-(2-aminoethyl)amine was reacted with furan-maleic anhydride DA adduct, following a previously described protocol [257,258]. In this case, the ensuing product (**X**) bore protected maleimide groups in the form of their furan-DA adduct, which were then deprotected at high temperature giving the actual B_3 structure, **XI**, as shown in Scheme 7.

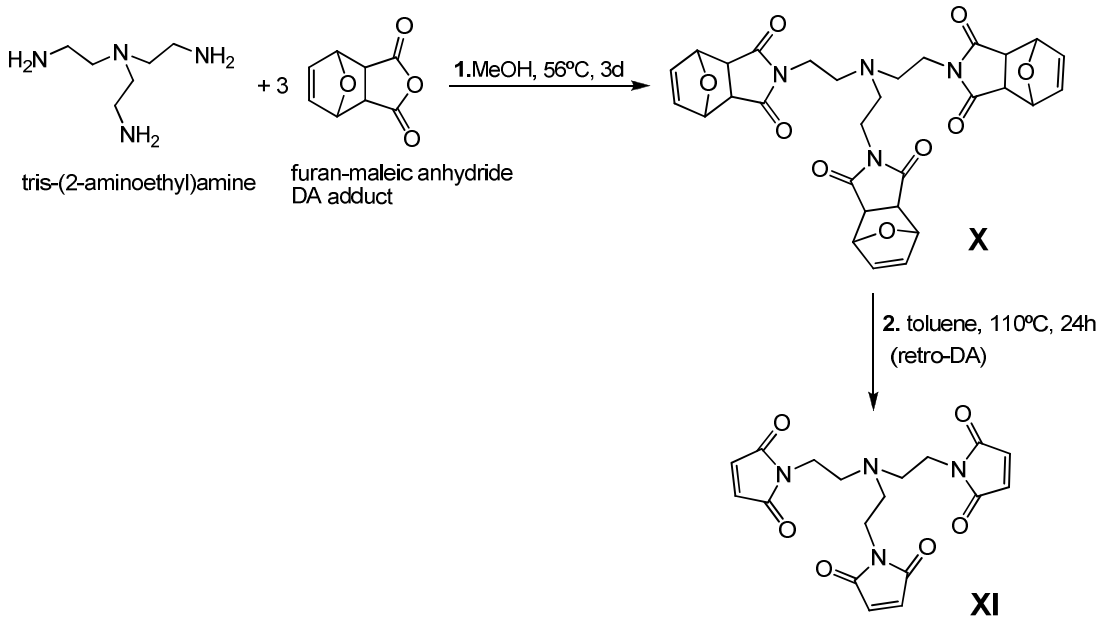

Scheme 7. Reaction of (**1**) the tris-(2-aminoethyl)amine and the furan-maleic anhydride DA adduct, followed by (**2**) the retro-DA reaction of the ensuing product, resulting the B_3 monomer **XI**.

The FTIR spectrum of the intermediate structure **X**, shown in Figure 52, clearly indicates the presence of the adduct due to the weak =CH band at 3017 cm^{-1}, the C=O peaks (*endo* and *exo* isomers) at 1767 and 1687 cm^{-1}, the C-O adduct band at 1018 cm^{-1}, as well as the absence of the NH_2 band at 3300 cm^{-1}, and characteristic maleimide bands at 3100, 1405, 826 and 691 cm^{-1} [179,189,191,203,242].

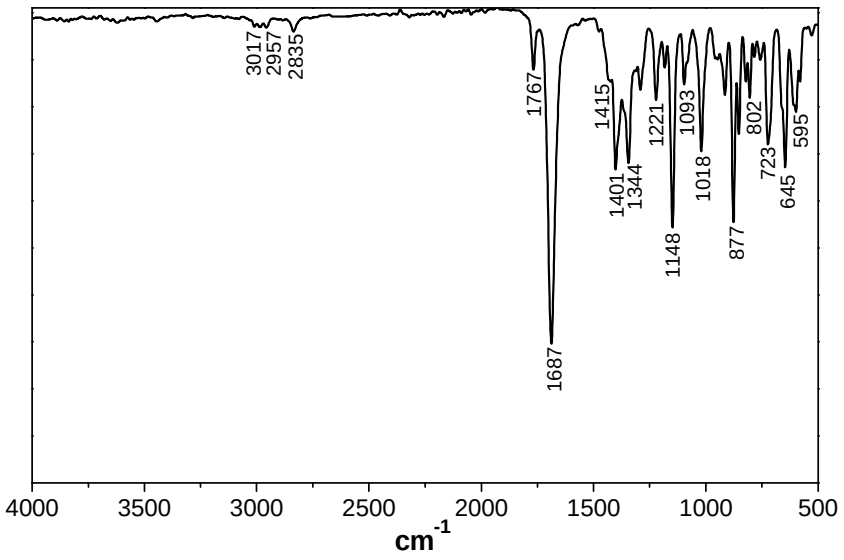

Figure 52. FTIR-ATR spectrum of **X**.

Its ^{1}H NMR spectrum, shown in Figure 53, confirmed the expected structure, with the peaks assigned to the adduct appearing at δ 6.5 ppm for the H-4’ and H-5’ protons of the double bond, at δ 5.2 ppm for the bridgehead H-3’ and H-6’ protons, and at 2.9 ppm for the H-2’ and H-7’ protons of the fused rings. The two methylene groups appear each one as a triplet with ^{3}J value 5.8 Hz (δ 3.4 ppm) for the protons next to maleimide moiety, and with ^{3}J value 5.9 Hz (δ 2.6 ppm) for those next to the trisamine group [179,189,191,243,244].

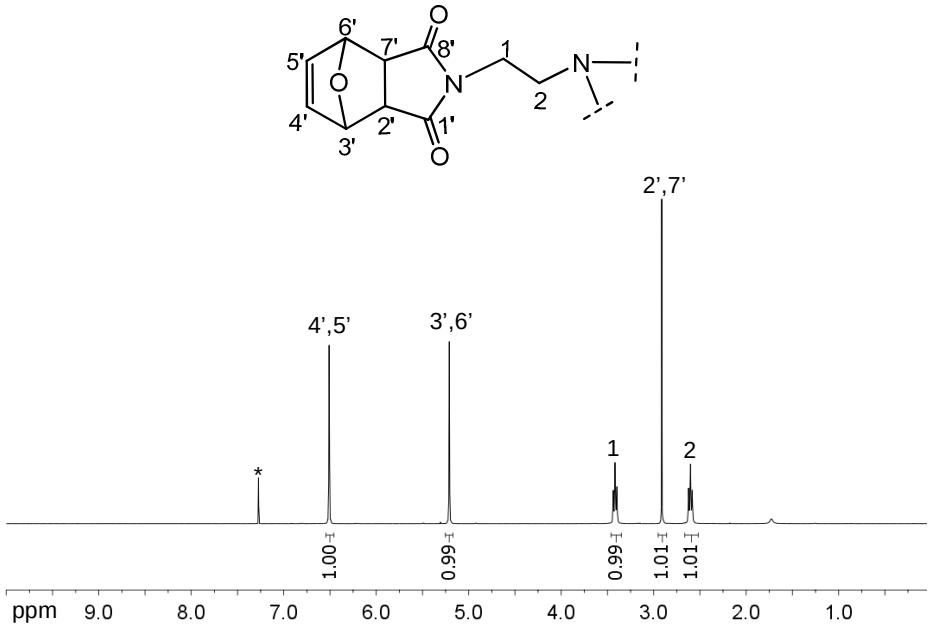

Figure 53. ^{1}H NMR spectrum of the structure **X** in *$CDCl_3$.

In the ^{13}C NMR spectrum of **X** (Figure 54), the adduct carbons are displayed at δ 136, 80 and 47 ppm, and only one carbonyl peak is observed at 176 ppm. The methylene carbons appear at δ 51 and 36 ppm, respectively [203,243,244].

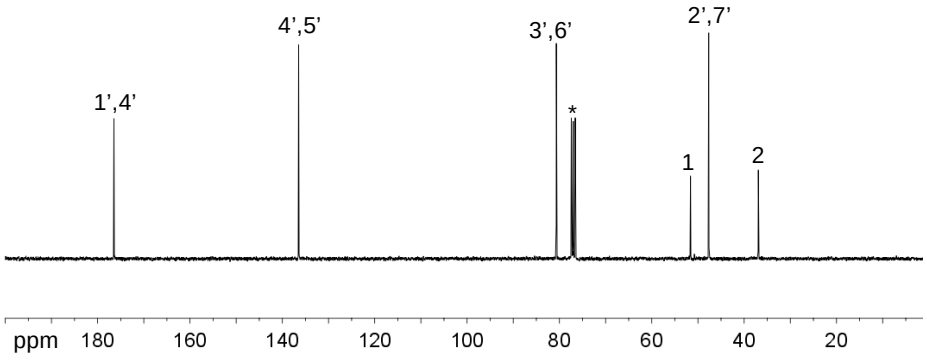

Figure 54. ^{13}C NMR spectrum of the structure **X** in *$CDCl_3$.

As previously mentioned, the maleimide terminals of **X** were deprotected through the retro-DA reaction, viz. by increasing the temperature to release the furan moiety (Scheme 7). The chosen solvent was toluene due to its high boiling point (110ºC) and the **X** solubility. The ensuing product, **XI**, was obtained as yellow solid with a yield around 96%.

Each adduct of **X** was thus reverted to the corresponding maleimide, as shown by the absence of the characteristic signals attributed to the adduct in the ensuing FTIR and NMR spectra. The FTIR spectrum of **XI**, shown in Figure 55, presents the characteristic bands of the maleimide, namely =CH at 3098 and 691 cm^{-1}, as well as the disappearance of the adduct bands at 3017 (=CH) and 1018 (C-O) cm^{-1} [203,242,252,255].

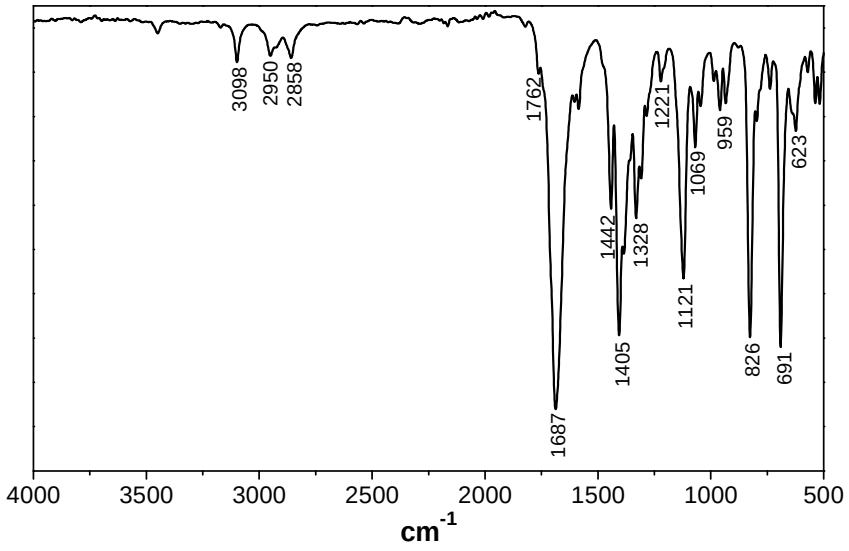

Figure 55. FTIR-ATR spectra of the B_3 monomer (**XI**) after the retro-DA reaction.

The ^{1}H NMR spectrum of **XI** (Figure 56) confirms the decoupling of the adducts by the retro-DA reaction, because the peaks related to the adduct (as discussed above) disappear, and a single peak is present at δ 6.67 ppm, corresponding to the protons of the maleimide insaturation. The chemical shift of the methylene groups is not significantly changed, and thus, each one appears as a triplet with ^{3}J value 6.6 for both [189,191,243,244].

Furthermore, its ^{13}C NMR spectrum displayed a single peak at δ 134 ppm assigned to the carbons of the maleimide insaturation, whereas those of the adduct (δ 136, 80, 47 ppm) disappears, thus corroborating the expected structure [203,243,244,247].

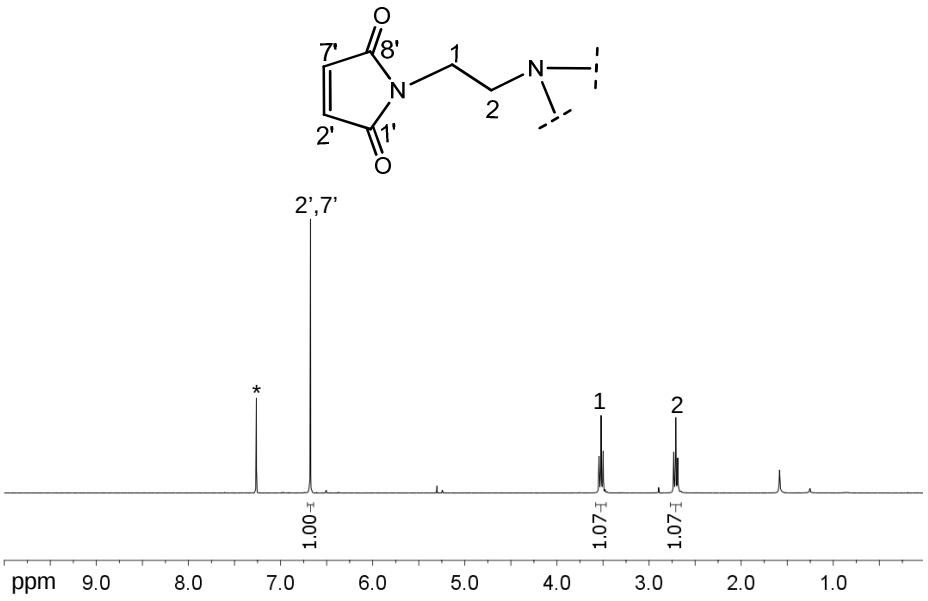

Figure 56. ^{1}H NMR spectrum of monomer **XI** in *$CDCl_3$.

In addition, ESI-HRMS data for **XI** (Table 10) corroborates the previous results, by favouring the molecular formula $C_{18}H_{18}N_4O_6$, which is in agreement with the expected structure [248]. Table 10 summarizes the main features of both structures, before (**X**) and after (**XI**) the retro-DA reaction.

Table 10. Characterization of the structures **X** and **XI**.

Analysis		X	XI
FTIR-ATR (cm^{-1})	ν =CH	3017	3098
	$\nu_{as\,s}$ CH_2	2957, 2835	2950,2858
	ν C=O	1767, 1687	1762, 1687
	ν C=C	1415	1442
	ν C-N	1344, 1148, 851, 723	1382, 1328, 1121, 734
	ν C-O	1018	-
	δ CH	1401, 877, 802	1405, 826
	δ N-C=O	645, 595	691, 620
^{1}H NMR (ppm)	H-4', H-5'	6.51 (s; 2H)	-
	H-3', H-6'	5.21 (s; 2H)	-
	H-1	3.42 (t; *J*=5.8; 2H),	3.52 (t; *J*=6.6; 2H)
	H-2', H-7'	2.91 (s; 2H),	6.68 (s; 2H)
	H-2	2.60 (t; *J*=5.9; 2H)	2.71 (t; *J*=6.6; 2H)
^{13}C NMR (ppm)	C-1', C-8'	176.5	170.6
	C-4', C-5'	136.5	-
	C-3', C-6'	80.7	-
	C-1	51.6	51.6
	C-2', C-7'	47.7	134.0
	C-2	36.9	35.7
DSC m.p. (ºC)		-	167.7
ESI-HRMS	$C_{18}H_{19}N_4O_6$ $[M+H]^+$	-	
calculated			387.12991
found			387.12924

4 SYNTHESIS AND CHARACTERIZATION OF FURAN-MALEIMIDE MONOMERS

The monomers described in the previous sections have only one type of functional group in their structure, that is, they bear only maleimide moieties or furan rings. As a result, the thermally reversible polymers which can be prepared from these monomers require the use of these complementary DA structures. As an alternative approach, we decided to explore also the preparation of single furan-maleimide monomers of the AB and AB_2 type, which ensure the ideal initial stoichiometry. The former type structures were the first to be synthesized and only later, a more complex structure was also studied, as described in the *Experimental* part (p.159).

4.1 AB MONOMERS

In this work, two AB type structures were synthesised using the aminoacid β-alanine (β-ALA) as precursor, providing on the one hand, stable monomers and on the other hand, the possibility of using further precursors from renewable resources.

The synthesis of these structures was carried out in two steps (Scheme 8), viz. (*i*) first, *β*-ALA reacted with the furan-maleic anhydride DA adduct, which originated a protected maleimide moiety [257,259]; (*ii*) then, the furan moiety was incorporated at the other end of the molecule by esterification with furfuryl alcohol or by amidation with furfuryl amine, both in the presence of *N,N'*-dicyclohexylcarbodiimide (DCC) and a catalytic amount of 4-dimethylaminopyridine (DMAP) [260,261].

In this case, one of the functionalities is maintained protected, until the incorporation of the other group, in order to avoid the DA polymerization during the synthesis, purification and storage.

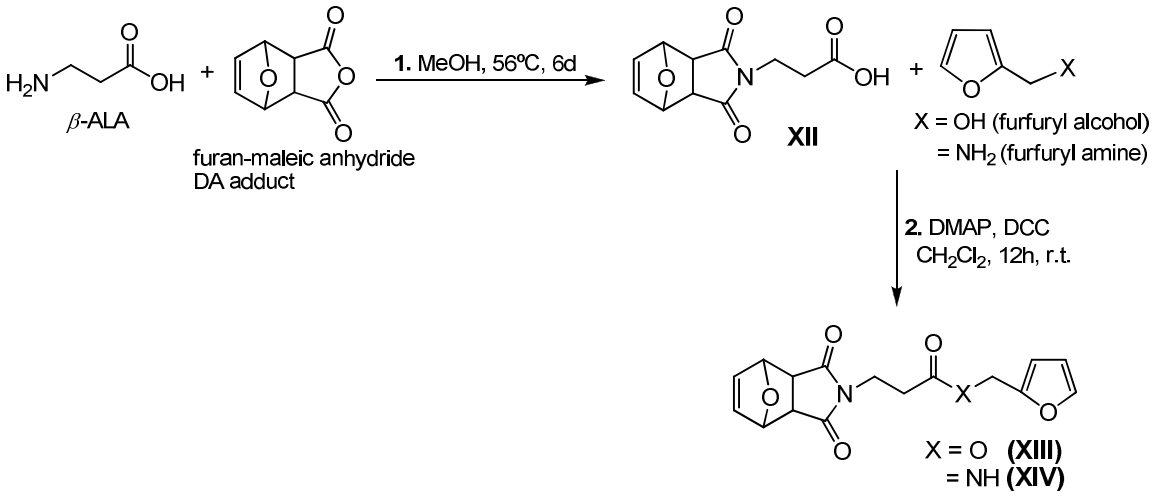

Scheme 8. Synthesis of the protected A-B type structures.

4.1.1 3-(exo-3,6-epoxy-1,2,3,6-tetrahydrophthalimido)propanoic acid

As shown in Scheme 8, the first step involves the reaction of *β*-ALA with the furan-maleic anhydride DA adduct. The ensuing compound, **XII**, was obtained as white crystals with a yield of 56%.

Its FTIR spectrum is shown in Figure 57, where the OH band, as well as the carbonyl bands at 1779 and 1690 cm^{-1} and C-O adduct band at 1012 cm^{-1}, are clearly observed. The C=O acid band is hidden by the strong 1690 cm^{-1} band [179,203,242,259].

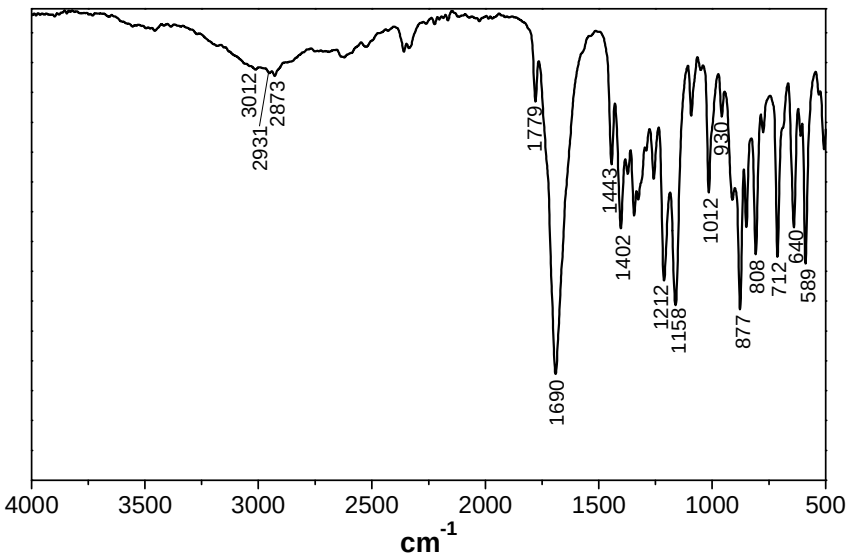

Figure 57. FTIR-ATR spectrum of **XII**.

In the ^{1}H-NMR spectrum of **XII** (Figure 58), the presence of typical signals of the adduct at δ 6.5, 5.1 and 2.9 ppm, respectively assigned to protons H-7 (double bond), H-6 (bridgehead) and H-5 (fused rings), confirms its expected structure. The methylene protons next to the maleimide moiety resonate at δ 3.6 ppm as a triplet with ^{3}J value 7.8 Hz, whereas those next to the carboxylic group appears at δ 2.5 ppm as a triplet with ^{3}J value 7.7 Hz [179,189,243,244,259].

Its ^{13}C NMR spectrum corroborated the previous results by the presence of two carbonyl peaks at δ 176 and 171 ppm, and adduct carbon resonances at δ 137 (C-7), 81 (C-6) and 48 ppm (C-5). The methylene carbons next to the maleimide moiety and carboxylic group appear at δ 34 and 32 ppm, respectively [203,243,244,247,259].

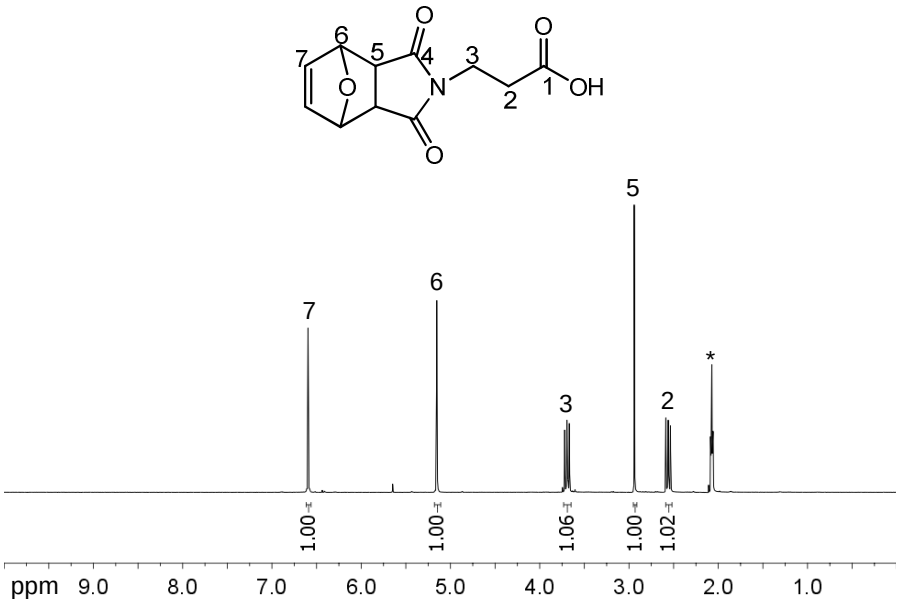

Figure 58. ^{1}H NMR spectrum of **XII** in *acetone-d_6.

4.1.2 Furfuryl-3-(exo-3,6-epoxy-1,2,3,6-tetrahydrophthalimido)propanoate

The first AB-type compound was prepared by reaction of the previous acid **XII** with furfuryl alcohol, as shown in Scheme 8. The ensuing product (**XIII**) was obtained as a brown solid with a yield of 90%, and its characteristics are summarized in Table 11.

The FTIR spectrum of **XIII** is shown in Figure 59, where the furan heterocycle bands at 3120, 1015, 915, 734, 593 cm^{-1} are accompanied by the C=O ester band at 1736 cm^{-1}, as

well as those of the maleimide moiety at 1775 and 1693 cm^{-1} (see Figure 57). Moreover, the C=O and OH bands of the acid group have disappeared [179,185,203,242].

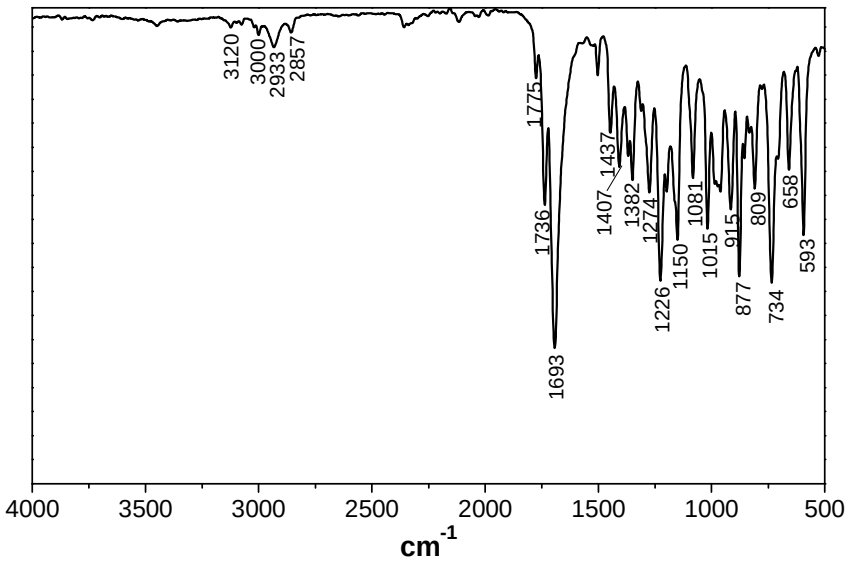

Figure 59. FTIR-ATR spectrum of the protected AB monomer **XIII**.

Besides the peaks of the precursor acid structure (see Figure 58), the ^{1}H NMR spectrum of **XIII** (Figure 60) displays also the signals of the furan ring at δ 7.4, 6.4 and 6.3 ppm, respectively assigned to protons H-5' (double of doublets with ^{3}J value 1.6 Hz and ^{4}J value 0.6 Hz), H-3' (doublet with ^{3}J value 3.3 Hz), and H-4' (double of doublets with ^{3}J values of 3.2 and 1.9 Hz) protons. The methylene protons of the furfuryl moiety (H-1') appear as a singlet at δ 5.0 ppm, thus confirming the occurrence of the esterification [185,243-246].

Its ^{13}C NMR spectrum (Figure 61) corroborates the expected structure by the presence of two C=O peaks at δ 175 and 170 ppm and of the adduct carbons, as well as those of the furan carbons at δ 149, 143 and 110 ppm, and the methylene carbon of the furfuryl moiety at δ 58 ppm [203,243,244,247].

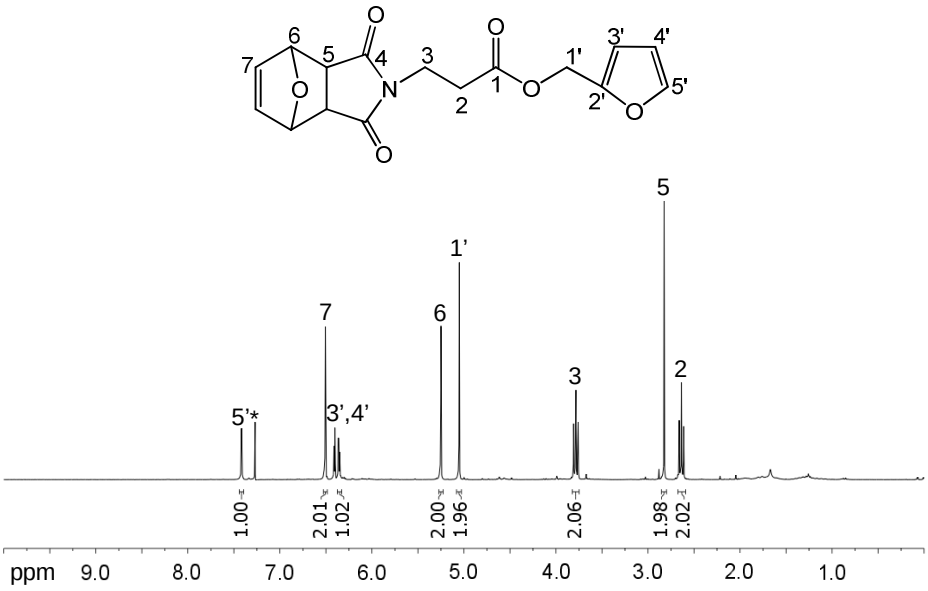

Figure 60. ^{1}H NMR spectrum of the protected AB monomer **XIII** in *$CDCl_3$.

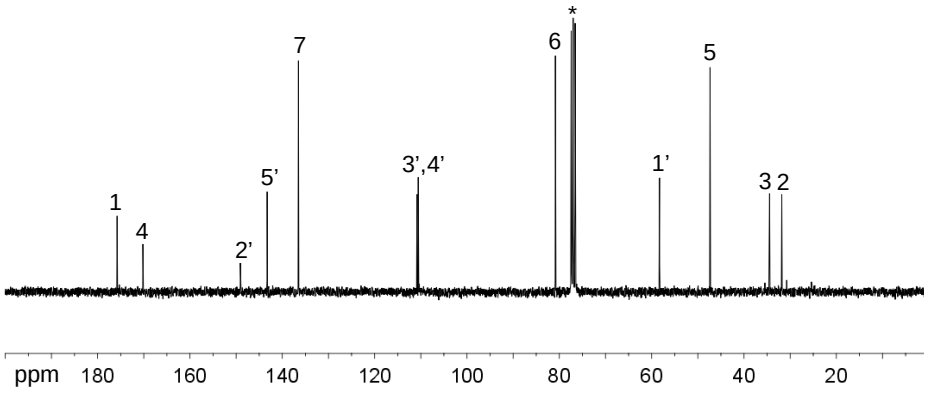

Figure 61. ^{13}C NMR spectrum of the protected AB monomer **XIII** in *$CDCl_3$.

4.1.3 *N*-furfuryl-3-(exo-3,6-epoxy-1,2,3,6-tetrahydrophthalimido) propanamide

The second AB structure was prepared by reaction of the previous acid **XII** with furfuryl amine (Scheme 8). The ensuing product (**XIV**) was obtained as a white solid with a yield of 97%, and its characteristics are summarized in Table 11.

The FTIR spectrum of **XIV**, shown in Figure 62, confirms the expected structure by the presence of the furan heterocycle bands at 3117, 1016, 918, 737, 598 cm^{-1}, and also the characteristic amide bands at 3337, 1644, 1539, 693 cm^{-1}. Moreover, the C=O and OH bands of the acid group have disappeared (see Figure 57) [179,185,203,242].

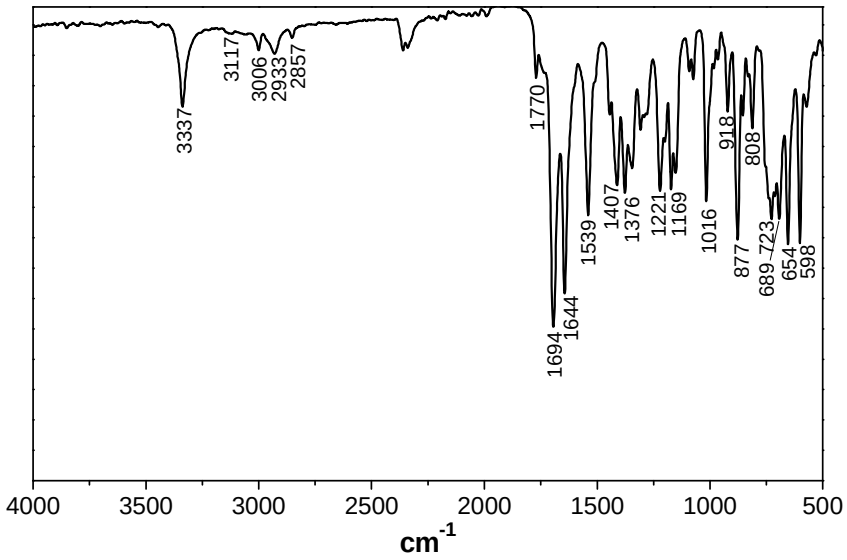

Figure 62. FTIR-ATR spectrum of the protected AB monomer **XIV**.

Its ^{1}H NMR spectrum (Figure 63), besides the peaks of the precursor acid structure (*see* Figure 58), bears also the signals of the furan ring at δ 7.3 (H-5', a double of doublets with ^{3}J value 2.0 Hz and ^{4}J value 0.8 Hz), 6.5 (H-4', a double of doublets with ^{3}J values of 3.2 and 1.8 Hz) and 6.2 (H-3', a doublet with ^{3}J value 3.6 Hz) ppm, as well as the methylene protons of the furfuryl moiety (H-1') at δ 4.4 ppm as a doublet (^{3}J value 5.5 Hz), which means that it is coupling with adjacent NH. Additionally, a broad singlet peak is observed at δ 6.0 ppm, corresponding to NH [185,243-246].

The ^{13}C NMR spectrum of **XIV** (Figure 64) corroborates the expected structure by the presence of the C=O peaks at δ 175 and 169 ppm and of the adduct carbons, as well as those of the furan carbons at δ 151, 142, 110 and 107 ppm, and the methylene carbon of the furfuryl moiety at δ 32 ppm [203,243,244,247].

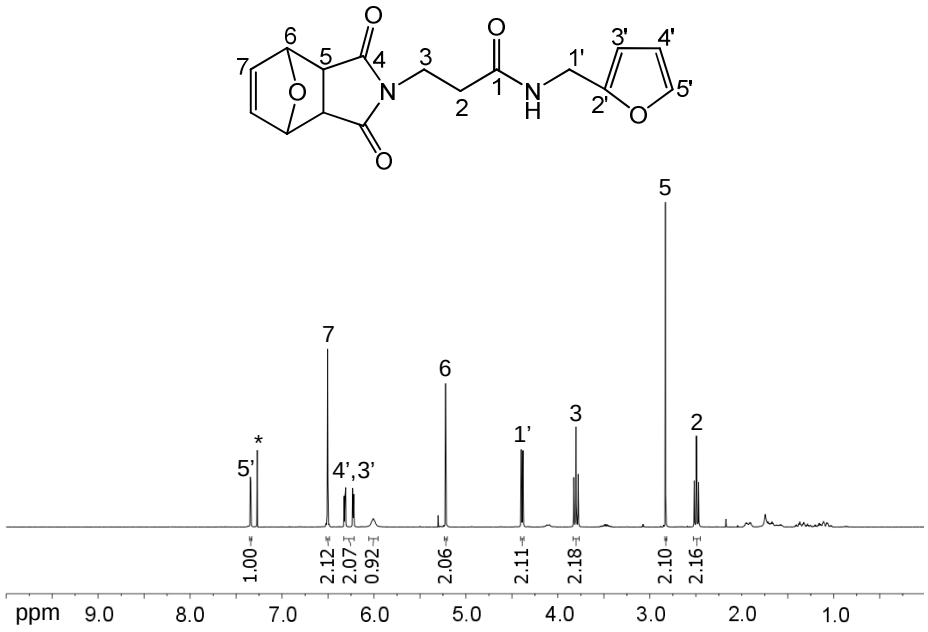

Figure 63. ^{1}H NMR spectrum of the protected AB monomer **XIV** in *$CDCl_3$.

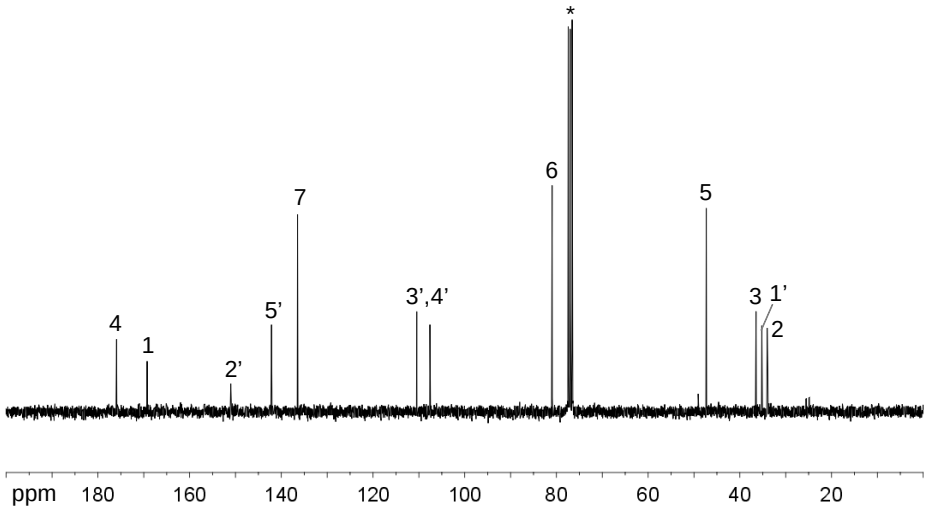

Figure 64. ^{13}C NMR spectrum of the protected AB monomer **XIV** in *$CDCl_3$.

Furthermore, for both AB structures **XIII** and **XIV**, ESI-MS data corroborates the previous results as shown in Table 11, by favouring the molecular formula $C_{18}H_{18}N_4O_6$, which is in agreement with the expected structure [248].

Table 11 summarizes the main features of the monomers **XIII** and **XIV**, as well as their precursor **XII**.

Table 11. Characterization of the protected AB monomers **XIII** and **XIV**, and their precursor **XII**.

Analysis		XII	XIII	XIV
FTIR-ATR (cm^{-1})	ν OH	3000-3100	-	-
	ν NH	-	-	3337
	ν =CH	3012	3120, 3000	3117, 3006
	$\nu_{as\,s}$ CH_2	2931, 2873	2933, 2857	2933, 2857
	ν C=O	1779, 1690	1775, 1736, 1693	1770, 1694, 1644
	ν C=C	1443	1437, 1382	1429, 1376
	δ NH	-	-	1539, 723
	ν CN	1341, 1158, 712	1347, 1150	1340, 1169, 851
	ν C-O, δ COH	1443, 1212,	-	-
	ν C-O	1012, 954,	1274, 1226, 1015	1221, 1016
	δ CH	1402, 877	1407, 915, 877, 734	1407, 918, 877
	δ N-C=O	640, 589	658, 593	689, 654, 598
^{1}H NMR (ppm)	H-5’	-	7.41 (dd; *J*=1.6,0.6; 1H)	7.34 (d; *J*=2.0; 1H)
	H-7	6.58 (s; 2H)	6.51 (s; 2H)	6.50 (s; 2H)
	H-3’	-	6.41 (d; *J*=3.3; 1H)	6.23 (d; *J*=3.6; 1H)
	H-4’	-	6.36 (dd; *J*=3.2,1.9; 1H)	6.32 (dd; *J*=3.2,1.8; 1H)
	NH	-	-	6.01 (br s; 1H)
	H-6	5.13 (s; 2H)	5.26 (s; 2H)	5.22 (s; 2H)
	H-1’	-	5.05 (s; 2H)	4.39 (d; *J*=5.5; 2H)
	H-3	3.67 (t; *J*=7.8; 2H)	3.78 (t; *J*=7.4; 2H)	3.80 (t; *J*=7.1; 2H)
	H-5	2.92 (s; 2H)	2.83 (s; 2H)	2.83 (s; 2H)
	H-2	2.55 (t; *J*=7.7; 2H)	2.64 (t; *J*=7.3; 2H)	2.49 (t; *J*=7.1; 2H)
^{13}C NMR (ppm)	C-1	176.8	175.8	175.9
	C-4	171.9	170.2	169.3
	C-2’	-	149.0	151.0
	C-5’	-	143.3	142.1
	C-7	137.3	136.5	136.5
	C-3’,C-4’		110.9, 110.6	110.5, 107.6
	C-6	81.7	80.8	80.9
	C-1’	-	58.3	35.2
	C-5	48.2	47.3	47.3
	C-3	34.8	34.4	36.4
	C-2	32.0	31.8	34.0
DSC m.p. (ºC)			67.4	138.3
ESI-HRMS calculated found			$C_{16}H_{15}NO_6Na$ 340.07916 $[M+Na]^+$ 340.07908	$C_{16}H_{17}N_2O_5$ 317.11320 $[M+H]^+$ 317.11317

4.2 AB_2 MONOMER

Unlike the previous monomers, the preparation of the AB_2-type monomer **XVII** (Scheme 9) was only a preliminary survey. Its synthesis followed a three-step procedure previously reported [249,250], where the commercial 3-amino-1,2-propanediol was used as precursor.

In a general way, the first two steps involved the synthesis of a Schiff base derivative and its reduction with an overall yield of 84%. The ensuing product was then esterified with the previous synthesized acid **XII**, in the presence of DCC and a catalytic amount of DMAP [260,261]. The protected AB_2 monomer, **XVII**, was thus obtained as a sticky brownish-yellow solid with a yield of 30%, and its characteristics are summarized in Table 12, together with those of the intermediate structures.

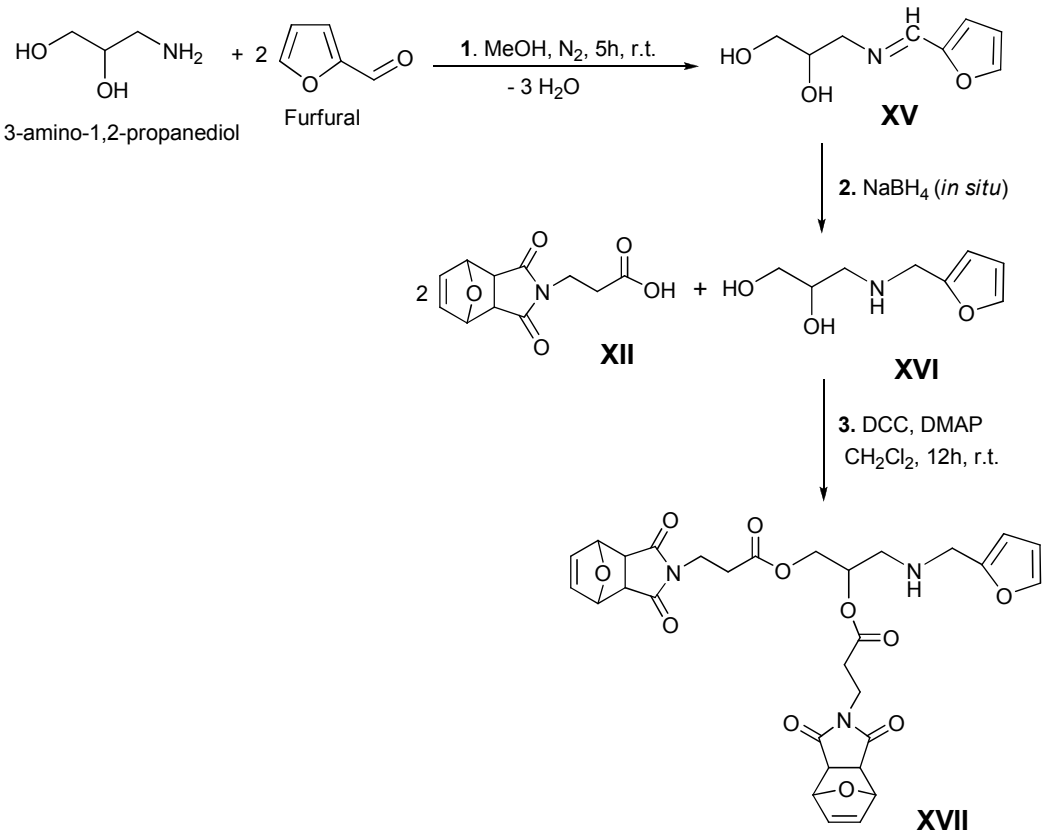

Scheme 9. Synthesis of the protected AB_2 monomer **XVII**.

As shown in Scheme 9, the first step involved the synthesis of the Schiff base **XV**, whose success was confirmed by the presence of the characteristic imine (*CH=N*) peaks. In general, the spectroscopic data obtained to this compound are similar to those described previously (section **2.1.2** and **2.2**).

The FTIR spectrum of **XV** (Figure 65) shows clearly the imino band at 1643 cm^{-1}, as well as those of the furan ring at 3112, 1014, 931, 883, 746 and 592 cm^{-1}. The broad band in the range 3500-3000 cm^{-1} corresponds to the OH groups [242,248,250]. Furthermore, its ^{1}H NMR and ^{13}C NMR spectra (see Table 12) confirmed the expected structure, due to the presence of the imino proton and carbon peak at δ 8.10 and 152 ppm, respectively. The furan ring protons and carbons appear in the expected chemical shifts, viz. δ 7.52, 6.78, 6.47 ppm, and 151, 145, 114, 111 ppm, respectively [243,244,246,247,250].

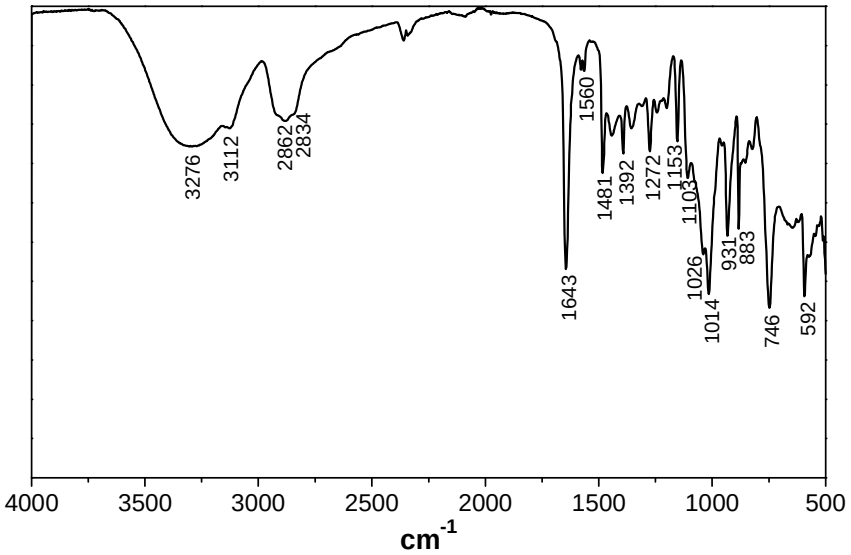

Figure 65. FTIR-ATR spectrum of the Schiff base **XV**.

When the reduction was applied to the previous compound **XV**, the imine group was readily converted into the corresponding secondary amine **XVI** (Scheme 9), which was confirmed by the disappearance of the characteristic imino peaks as well as the presence of those related to the amino CH_2-NH group.

The FTIR spectrum of **XVI** (Figure 66) shows clearly the absence of the imino C=N band at 1643 cm^{-1}, and also the presence of those related to the amino group, viz. 1569,

1180 cm^{-1}. In this case, the NH band is hidden by the strong hydroxyl (OH) band [242,250].

Moreover, both its ^{1}H NMR and ^{13}C NMR spectra confirmed the expected structure, because the typical peaks at δ 8.1 and 152 ppm, respectively assigned to the imine proton and carbon, disappeared, whereas a new resonance corresponding to the amino (CH_2-NH) moiety appeared at δ 4.0-3.4 and 53.4 ppm. The chemical shifts of the furan ring do not suffer significantly changes, viz. the protons appear at δ 7.36, 6.30 and 6.20 ppm, and the carbons at δ 153, 141, 110, 107 ppm [243,244,246,247,250].

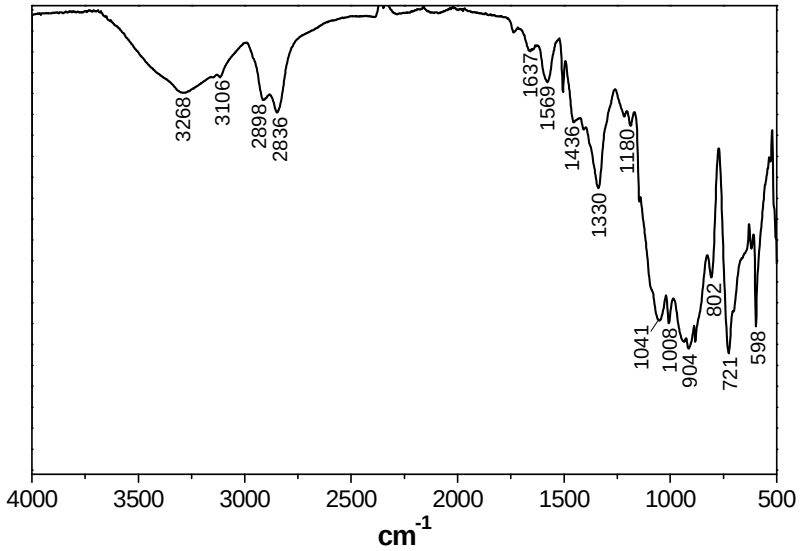

Figure 66. FTIR-ATR spectrum of the reduced Schiff base **XVI**.

The last step leading to the final AB_2 structure involved the esterification of the acid **XII** with the previously prepared aminodiol **XVI**, as shown in Scheme 9.

In the FTIR spectrum of the structure **XVII** (Figure 67), the furan heterocyclic bands at 3069, 1015, 732, 592 cm^{-1} are accompanied by the ester band at 1732 cm^{-1}. Moreover, the alcohol bands, namely OH, have disappeared, and those related to the furan-maleimide adduct, namely at 3069, 1161, 1084, 876, 647 cm^{-1}, are now observed [242,248,250].

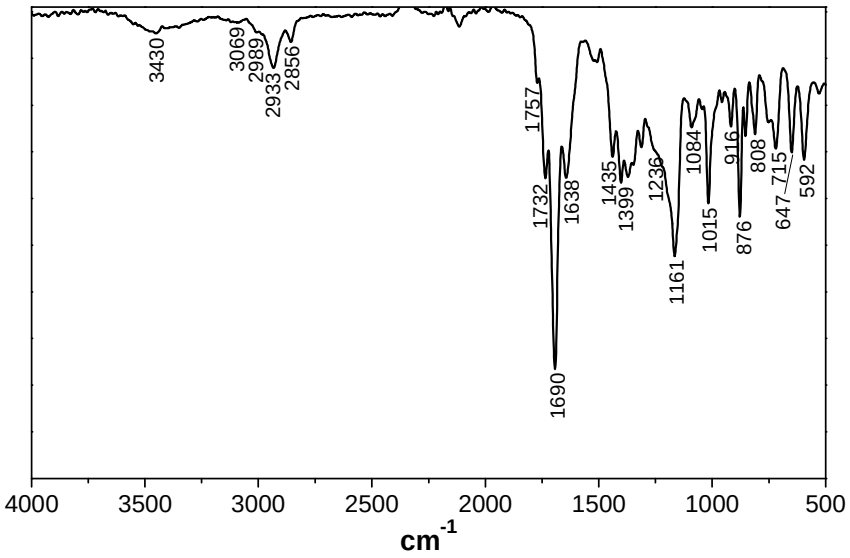

Figure 67. FTIR-ATR spectrum of the protected AB_2 monomer **XVII**.

Its ^{1}H NMR spectrum (Figure 68), besides the peaks of the precursor acid structure, also bears the signals of the furan ring at δ 7.4, 6.3 and 6.2 ppm, as well as those of adduct protons at δ 6.5, 5.2 and 2.8 ppm, whose integration indicates the possible presence of unreacted acid **XII** or a monosubstituted structure, viz. AB-type compound [243,244,246,247,250]. Further, its spectrum also presents a significant quantity of DCU (range δ 2.0-1.0 ppm) and other unknown impurities, which means that the purification process was not efficient, and thus need to be improved. Nevertheless, these impurities will not react or interfere with the polymerization of **XVII**, as shown in part *III* (p. 95).

The ^{13}C NMR spectrum of **XVII** corroborated these results by the presence of carbonyl peaks at 176 and 170 ppm, adduct carbons at 136, 81 and 47 ppm, and furan carbons at 149, 143 and 110 ppm, besides the peaks of the precursor acid structure [244,247,250].

Moreover, ESI-HRMS data for **XVII** (Table 12) favoured the molecular formula $C_{30}H_{31}N_3O_{11}$, which is in agreement with the expected structure [248].

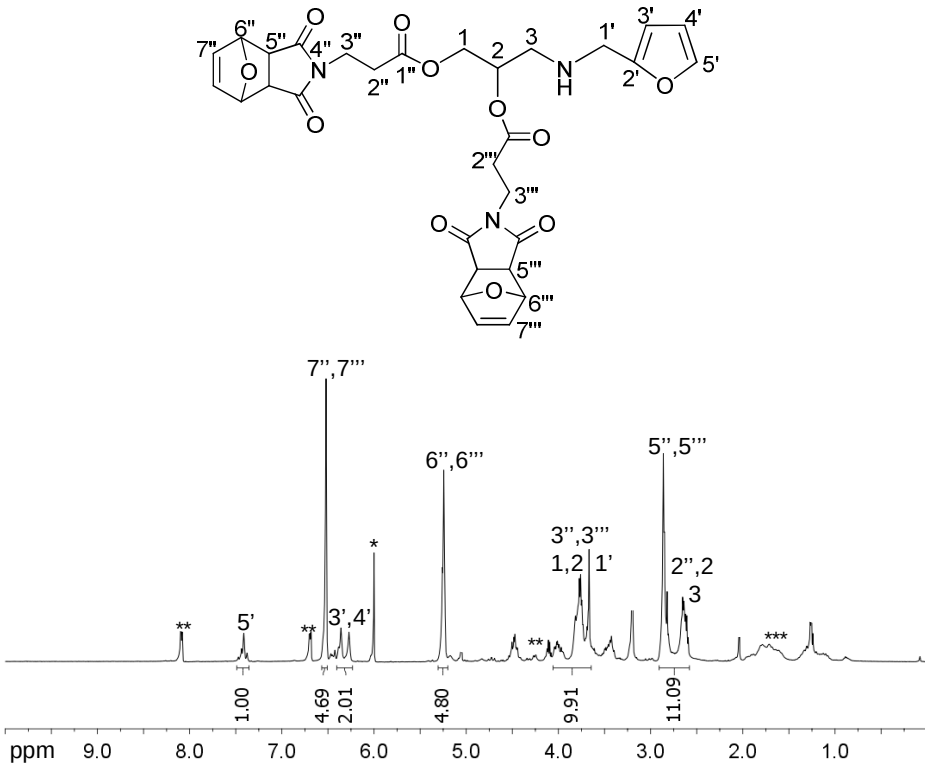

Figure 68. ^{1}H NMR spectrum of the protected AB_2 monomer **XVII** in *TCE-d_2 (**unknown impurities and ***DCU).

Table 12. Characterization of structures **XV**, **XVI** and **XVII**.

Analysis		XV	XVI	XVII
FTIR-ATR (cm^{-1})	ν OH	3500-3100	3500-3100	-
	ν NH			3430
	ν =CH $_{furan}$	3112	3106	3069, 2989
	ν CH, $ν_{as\,s}$ CH_2	2862, 2839	2898, 2836	2933, 2856
	ν C=O	-	-	1757, 1732, 1690
	ν CH=N	1643	-	-
	ν C=C $_{furan}$	1560, 1481, 1392	1504, 1388	1435,1363
	δ NH, ν C-N	-	1569, 1180	1589, 1341, 1161, 715
	δ OH	1348, 1272, 1103, 1026	1330, 1041	-
	ν C-O			1307, 1236, 1084
	furan ring breathing	1014	1008	1015
	δ CH	1418, 931, 883, 746	1436, 914, 802, 721	1399, 916, 876, 732
	δ N-C=O	-	-	647
	furan ring deformation	592	598	592

^{1}H NMR (ppm)	H-1’	8.10 (s; 1H)	4.11-3.39 (m; 6H)	
	H-5’	7.52 (d; *J*=1.8; 1H)	7.36 (d; *J*=1.9; 1H)	7.41 (s; 1H)
	H-7’’	-	-	6.52 (m; 5H)
	H-3’	6.78 (d; *J*=3.3; 1H)	6.30 (d; *J*=3.3; 1H)	6.36-6.26 (m; 2H)
	H-4’	6.48 (dd; *J*=3.1,1.6; 1H)	6.20 (dd; *J*=3.2,2.0; 1H)	
	H-6’’	-	-	5.25 (m; 5H)
	H-1, H-2, OH	4.05-3.70 (m; 5H)	4.11-3.39 (m; 6H)	4.06-3.64 (m; 10H)
	H-3’’, H-1’	-	-	
	H-5’’, H-2’’	-	-	2.91-2.58 (m; 11H)
	H-3	2.84 (m; 2H)	2.69 (m; 2H)	
^{13}C NMR (ppm)	C-4’’,C-1’’	-	-	176.2, 176.0, 170.7
	C-1’	152.0	53.5	52.2
	C-2’	151.1	153.5	149.6
	C-5’	145.1	141.9	143.3
	C-7’’	-	-	136.8
	C-3’, C-4’	114.9, 111.8	110.2, 107.2	110.8, 108.9
	C-6’’	-	-	81.1
	C-2	71.4	72.3	66.9
	C-1	64.9	66.2	58.6
	C-5’’	-	-	47.6
	C-3	64.1	46.2	46.4
	C-3’’	-	-	34.8
	C-2’’	-	-	32.1
DSC Tg (ºC)		-	-	-1.3
ESI-HRMS calculated found	$C_{30}H_{32}N_3O_{11}$ $[M+H]^+$	-	-	610.20314 610.20296

5 CONCLUSIONS

New furan and maleimide monomers bearing different bridging groups separating the reactive moieties, viz. aliphatic or oligoether domains, and, in some cases, ester and amide functions, were described in this chapter.

Four different structures containing two and three furan ring were synthesized. These compounds were obtained as highly viscous liquids, and showed low Tg values due to the flexible nature of the spacing moieties separating the reactive functions.

Only two complementary structures bearing two and three maleimide moieties were prepared, being both obtained as solids with high melting point.

The two furan-maleimide AB monomers prepared are the first examples of such feasible structures for DA polymerizations. Indeed, the protection of the maleimide group in the form of a furan-DA adduct, until the incorporation of the furan moiety, proved to be effective in the synthesis of these structures, because it avoided the DA polymerization of these intrinsically reactive monomers during their synthesis, purification and storage. Later, these compounds could easily be "activated" by their *in situ* deprotection trough heating (retro-DA).

A more complex furan-maleimide monomer, namely AB_2 type structure, was also synthesized. However, since only a preliminary study was followed, this approach pursues, namely in terms of final yield and purification.

PART III

POLYMERIZATION BY THE DIELS-ALDER REACTION

1 INTRODUCTION

As mentioned previously, in the last couple of decades, the reversible DA cycloaddition has been exploited in furan macromolecular chemistry with growing frequency, because it opens the way to original temperature-sensitive polymer materials with promising applications, like mendability and recyclability. Scheme 10 illustrates the essence of the mechanism involved in the DA and retro-DA reactions between a furan and a maleimide end-group. In the present context, the most relevant feature of the DA reaction is its reversible character, in which the reaction temperature is a key factor, viz. the equilibrium is progressively shifted to the left (retro-DA reaction) as the temperature is raised and vice-versa (Scheme 10). The stereochemical aspects related to the relative abundance of *exo* and *endo* forms of the adducts are not a relevant issue here, since both play the same role as chain links between monomer units. Hence, the results presented and discussed here refer to the formation or the decoupling of a given adduct as a whole.

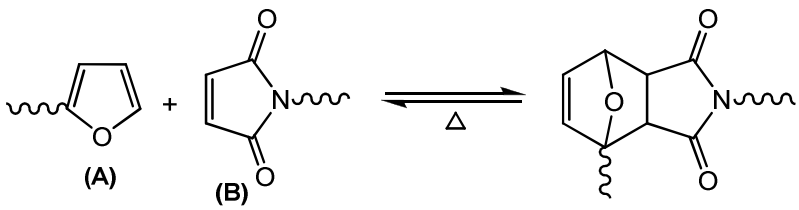

Scheme 10. The DA equilibrium between growing species bearing, respectively, furan (**A**) and maleimide (**B**) end-groups.

In this chapter, the synthesis and characterization of novel thermoreversible polymers through the DA reaction, using the previously synthesized furan and maleimide monomers (part *II*, p.45) are described, viz.

(i) Linear polymerizations involving difunctional A-A and B-B monomers, as well as A-B monomers;

(ii) Non-linear polymerizations involving complementary monomers bearing more than two functionalities, e.g. A-A+B_3 or B-B+A_3 systems, leading to branched or crosslinked materials, as well as an asymmetrically substituted monomer of the AB_2 type, which leads to hyperbranched structures.

The aspects related to the controlled thermal depolymerization of these systems, as well as their multiple-DA/retro-DA cycles, will be also presented and discussed.

Before the investigation of these systems, however, it was deemed necessary to conduct a systematic study of the equilibrium position and kinetic behaviour of the model furan-maleimide DA reaction "-A+-B", involving monofunctional compounds.

2 MODEL SYSTEM (-A+-B)

The study of the kinetics and the equilibrium of the formation and decoupling of the DA adducts is important to understand the behaviour of these systems. Therefore, the DA/retro-DA cyclic reaction was applied to a model monofunctional system (-A+-B).

The monofunctional model compounds (Scheme 11) chosen for the study were the commercially available furfuryl acetate (FA) and *N*-methylmaleimide (MM). This choice was based on the structure of the monomers studied later for the different DA polymerizations, both in terms of the nature of the DA reactive moieties and of them being monosubstituted at each relevant position.

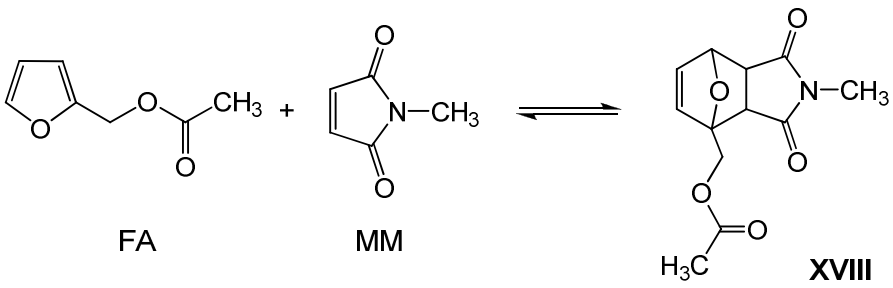

Scheme 11. Model DA reaction, involving monofunctional compounds.

The DA/retro-DA reactions in 1,1,2,2-tetrachoroethane (TCE) and TCE-d_2 were examined by both UV and ^{1}H NMR spectroscopy, respectively. In addition, a calibration curve was made previously using several standard solutions of MM in TCE. Obedience to the Beer-Lambert law was confirmed, and the value of the molar extinction coefficient, ε, was 720 $dm^{-3}\,mol^{-1}\,cm$.

2.1 UV SPECTROSCOPY

The DA reaction between FA and MM (Scheme 11) was followed by UV spectroscopy in TCE at three different temperatures, viz. 35, 50 and 65ºC, with initial concentrations of 2 M and 0.2 M, respectively.

The UV spectrum of FA in TCE did not show any absorption maximum above about 270 nm, with the tailing off of the ester carbonyl peak, whereas the MM solutions in the same solvent displayed the characteristic maximum at 293 nm arising from the conjugated effect of its ππ* (C=C) and nπ* (C=O) chromophore excitation (Figure 69).

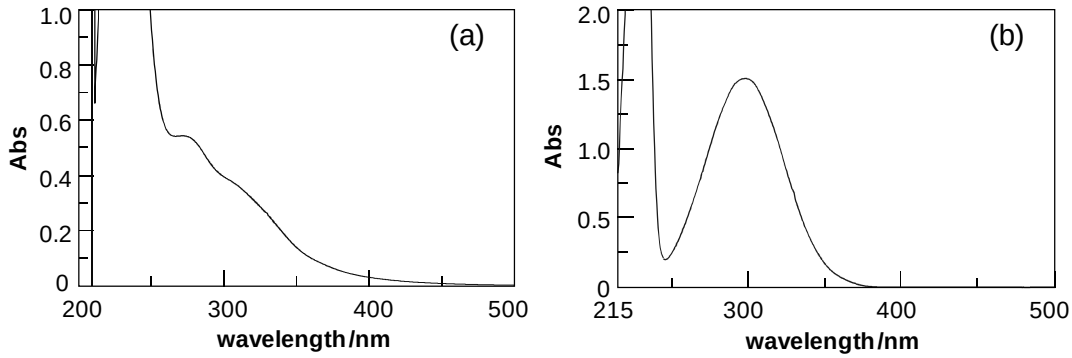

Figure 69. UV spectra of (**a**) FA 2 M and (**b**) MM 0.2 M in TCE taken with an optical path 0.01 cm.

When the model DA adduct is formed (Scheme 11), the conjugation between the two chromophores of the MM structure is broken, resulting in the displacement of the absorption, now limited to the unconjugated individual carbonyl excitation. The progress of both DA and retro-DA reactions could therefore be followed by monitoring the decrease or the increase, respectively, in the absorbance at 293 nm with time at different temperatures.

Figure 70, 71 and 72 show the UV results related to the reaction of MM with a tenfold excess of FA at 35, 50 and 65ºC, respectively. All the reactions gave the same behaviour pattern and the repetition of a given run reproduced its quantitative features. Furthermore, the progressive decrease of the MM peak was also accompanied by a corresponding increase in absorption below 260 nm, with the formation of an isosbestic point, indicating that the formation of the DA adduct was not accompanied by any side reaction.

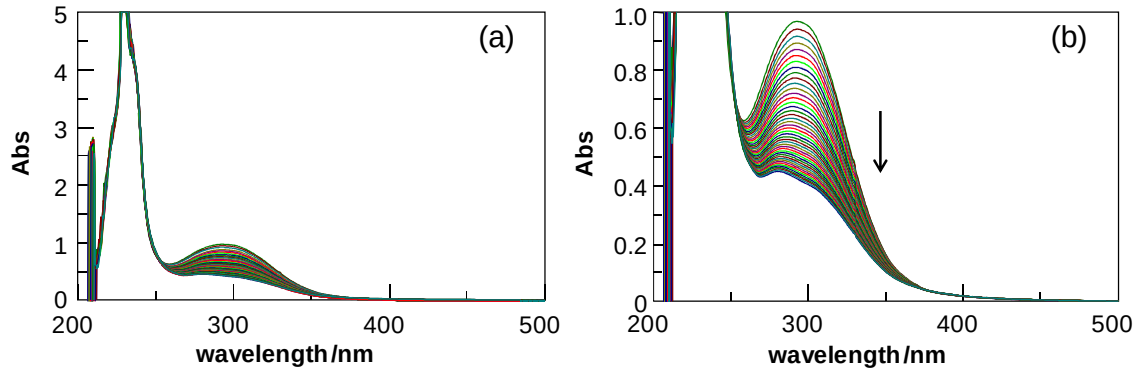

Figure 70. Evolution of the UV spectrum during the DA reaction between MM (0.2 M) and FA (2 M) at 35ºC in TCE with an optical path of 0.01 cm. Spectra were taken every 30 min during 24 h.

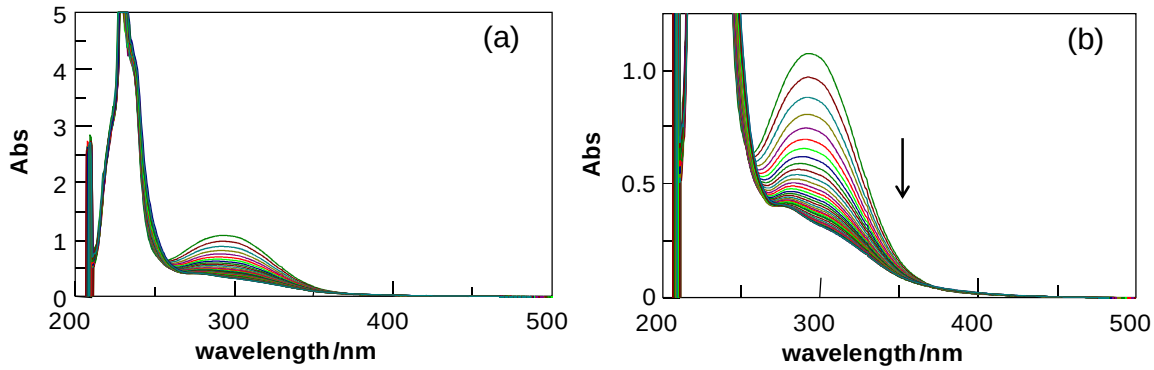

Figure 71. Evolution of the UV spectrum during the DA reaction between MM (0.2 M) and FA (2 M) at 50ºC in TCE with an optical path of 0.01 cm. Spectra were taken every 30 min during 24 h.

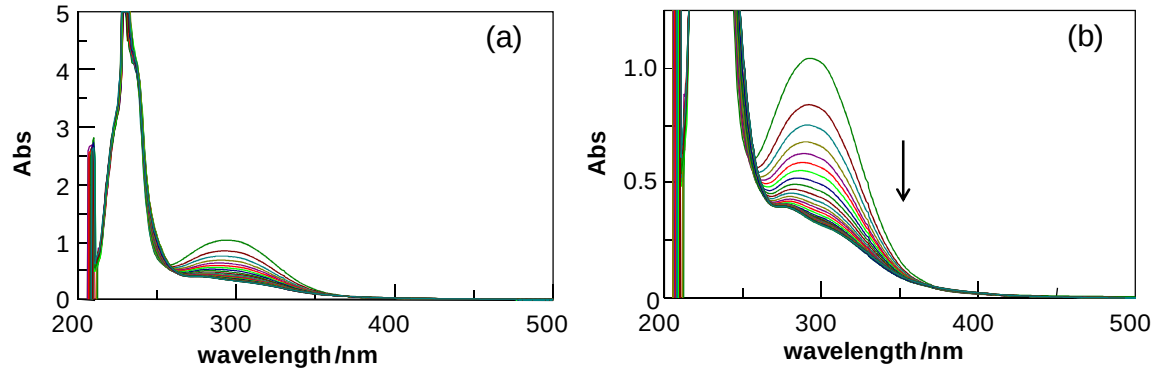

Figure 72. Evolution of the UV spectrum during the DA reaction between MM (0.2 M) and FA (2 M) at 65ºC in TCE with an optical path of 0.01 cm. Spectra were taken every 30 min during 24 h.

The results obtained from the UV experiments were used to evaluate the order of the reaction and the rate constant, *k*, for the formation and decoupling of the model adduct.

The DA reaction generally follows a second-order rate law [180]. In this case, however, given the excess of FA, the reaction followed a pseudo-first order kinetics (1), viz.

$$-d[MM]/dt \approx k[FA]_0[MM] = k'[MM] \qquad (1)$$

were $k' = k[FA]_0$

Figure 73 shows the good fit of the three runs conducted at different temperatures and Table 13 gives the corresponding values of *k'* and *k* for the adduct formation, which reflect the average constants for *endo*- and *exo*-adduct formation. The rate constants were calculated from the slopes of the fit lines, and are in agreement with data from the literature [172].

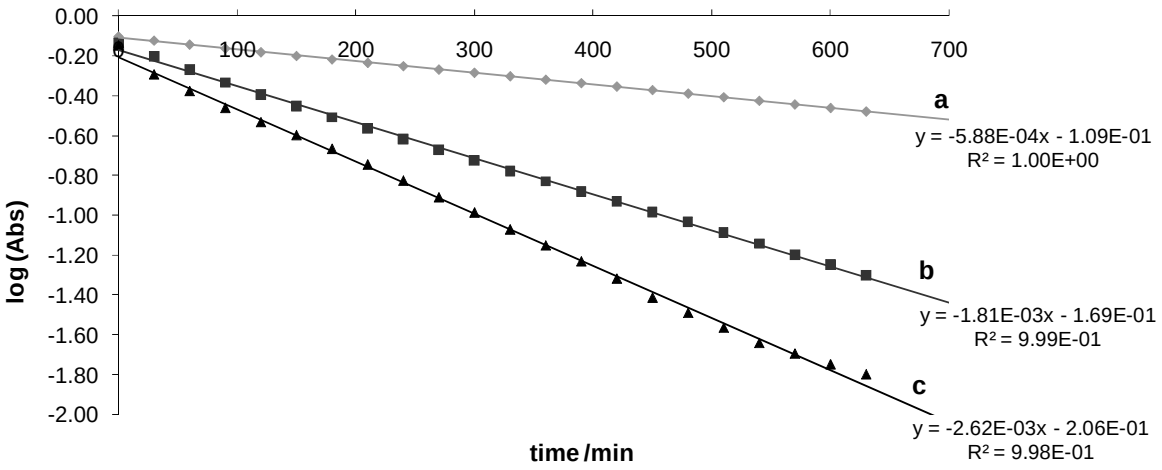

Figure 73. Pseudo-first-order plots based on the decrease of the absorption at 293 nm for the model DA reactions conducted in the conditions given in Figure 70, 71 and 72: **a**) 35; **b**) 50 and **c**) 65ºC.

Table 13. Values for the rate constants related to the model DA reactions, processed following Equation 1.

T /ºC	k' x 10^{-3} min^{-1}	k' x 10^{-5} s^{-1}	k_{DA} = k'/[FA] x10^{-5} $dm^3mol^{-1}s^{-1}$
35	0.59	0.98	0.47
50	1.81	3.02	1.46
65	2.62	4.37	2.11

From the Arrhenius plot of these DA rate constants (Figure 74), the activation energy (*Ea*) for this model reaction was calculated to be 39.0 kJ mol^{-1}.

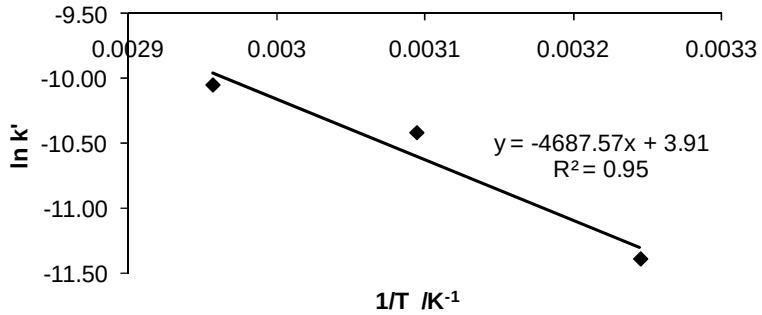

Figure 74. Arrhenius plot related to the pseudo-first-order rate constants obtained from Figure 73 and given in Table 13.

The retro-DA kinetics of the model system was also studied. Since an excess of FA was used, the ensuing adduct **XVIII** was precipitated into an excess of diethyl ether and dried under vacuum. Then, a 0.1 M solution of it in TCE was prepared and its retro-DA reaction monitored by UV spectroscopy at 90ºC during 24 hours. In this case, the shift of the equilibrium displayed the corresponding progressive increase in the absorption at 293 nm (Figure 75).

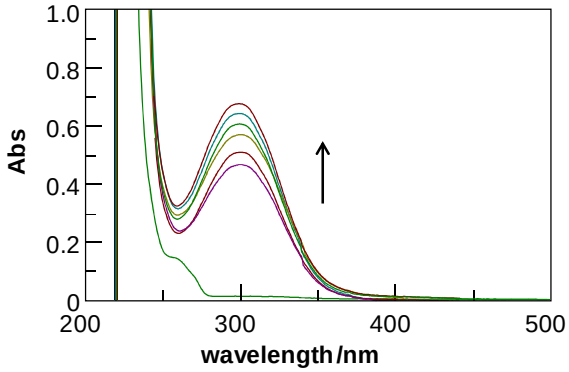

Figure 75. Evolution of the UV spectrum during the retro-DA reaction of the model system (the green line corresponds to the initial solution, while the red one corresponds to the same solution after 24 h at 90ºC).

Whereas the DA reaction follows a second-order rate law, the retro-DA is first order, given its monomolecular character [180]. From the plot in Figure 76, the rate constant *k* for the decoupling of the model adduct **XVIII** was determinated to be 1.6×10^{-6} s^{-1}.

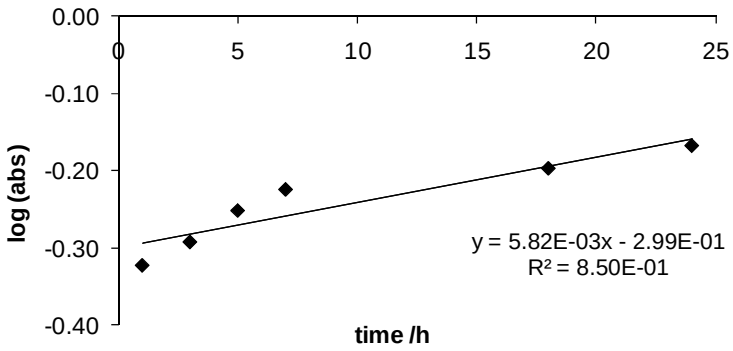

Figure 76. First-order plot based on the increase of the absorption at 293 nm for the model DA reactions conducted in the conditions given in Figure 75.

All these kinetic parameters are in agreement with the results obtained with similar systems [172,178], albeit in more polar solvents and mostly with *unsubstituted* reagents, i.e. in conditions less akin to our study.

2.2 NMR SPECTROSCOPY

Concurrently, the DA/retro-DA model reactions were also followed by ^{1}H NMR spectroscopy to assess the structural evolutions in a more detailed fashion. The reaction was followed using the proton assignments for the two reagents and the ensuing adduct (Scheme 12, Table 14).

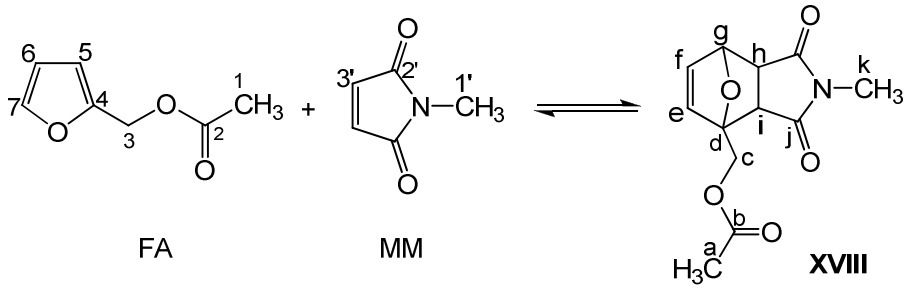

Scheme 12. Model DA reaction.

Table 14. Proton assignments for the DA reagents, FA and MM, and the corresponding adduct in TCE-d_2 (see also Scheme 12 and Figure 77).

	proton	FA	MM	XVIII
^{1}H NMR (ppm)	7	7.43 (d; *J*= 1.8Hz; 1H)	-	-
	3’	-	6.70 (s; 1H)	-
	5	6.41 (d; *J*= 3.2 Hz; 1H)	-	-
	6	6.38 (dd; *J*= 3.3, 1.9 Hz; 1H)	-	-
	f (*endo* + *exo*)	-	-	6.56 (dd; *J*= 5.7, 1.5; 1H) + 6.45 (dd; *J*= 5.8, 1.6; 1H)
	e (*endo* + *exo*)	-	-	6.42 (d; *J*= 5.6; 1H) + 6.31 (d; *J*= 5.8; 1H)
	g (*endo* + *exo*)	-	-	5.31 (dd; *J*= 5.5, 1.7; 1H) + 5.28 (d; *J*= 1.8; 1H)
	3	5.06 (s; 2H)	-	-
	c *endo*	-	-	4.95 (d; *J*= 12.9; 1H), 4.58 (d; *J*= 12.9; 1H)
	c *exo*	-	-	4.86 (d; *J*= 12.7; 1H), 4.46 (d; *J*= 12.7; 1H)
	h *endo*	-	-	3.67 (dd; *J*= 7.7, 5.5 Hz; 1H)
	i *endo*	-	-	3.40 (d; *J*= 7.7Hz; 1H)
	1’	-	3.01 (s; 2H)	-
	h *exo*	-	-	2.99 (d; *J*= 6.6 Hz; 1H)
	i *exo*	-	-	2.90 (d; *J*= 6.4 Hz; 1H)

	k (*endo* + *exo*)	-	-	2.97 (s; 3H) + 2.82 (s; 3H)
	1	2.08 (s; 3H)	-	-
	a (*endo* + *exo*)	-	-	2.14 (s; 3H) + 2.10 (s; 3H)

All kinetic experiments were performed directly in the NMR tubes under nitrogen in TCE-d_2 during 72 hours at a constant temperature of 65ºC. In this case, the concentration of both reagents was higher than in UV tests and the same, namely 0.6 M.

Figure 77 shows the evolution of the model DA system at 65ºC, which follows the expected pattern, viz. the signals associated with the adduct protons progressively increase, whereas those attributed to the initial reagents decrease correspondingly. More specifically, the peaks related to the furan ring at δ 7.4 (H-7), 6.4 (H-5) and 6.3 (H-6) ppm, as well as the maleimide unsaturation protons (H-3') at δ 6.7 ppm, decreased progressively during the formation of the DA adduct. Conversely, the resonances related to the protons of the adduct grow correspondingly at δ 5.3-5.2 for the bridgehead proton (H-g,), 6.5-6.3 for the protons of the double bond (H-e, H-f), and 3.7-3.4 and 3.0-2.9 ppm, respectively, for the protons of the *endo* and *exo* fused rings (H-h, H-i). The methylene protons of the furfuryl moiety, which resonated at δ 5.0 ppm as a singlet in the initial reagent (H-3), appears as a doublet at δ 5.0-4.0 ppm in the adduct (H-c). The chemical shift of the methyl groups does not suffer significant changes during the DA reaction [179,189,191,243].

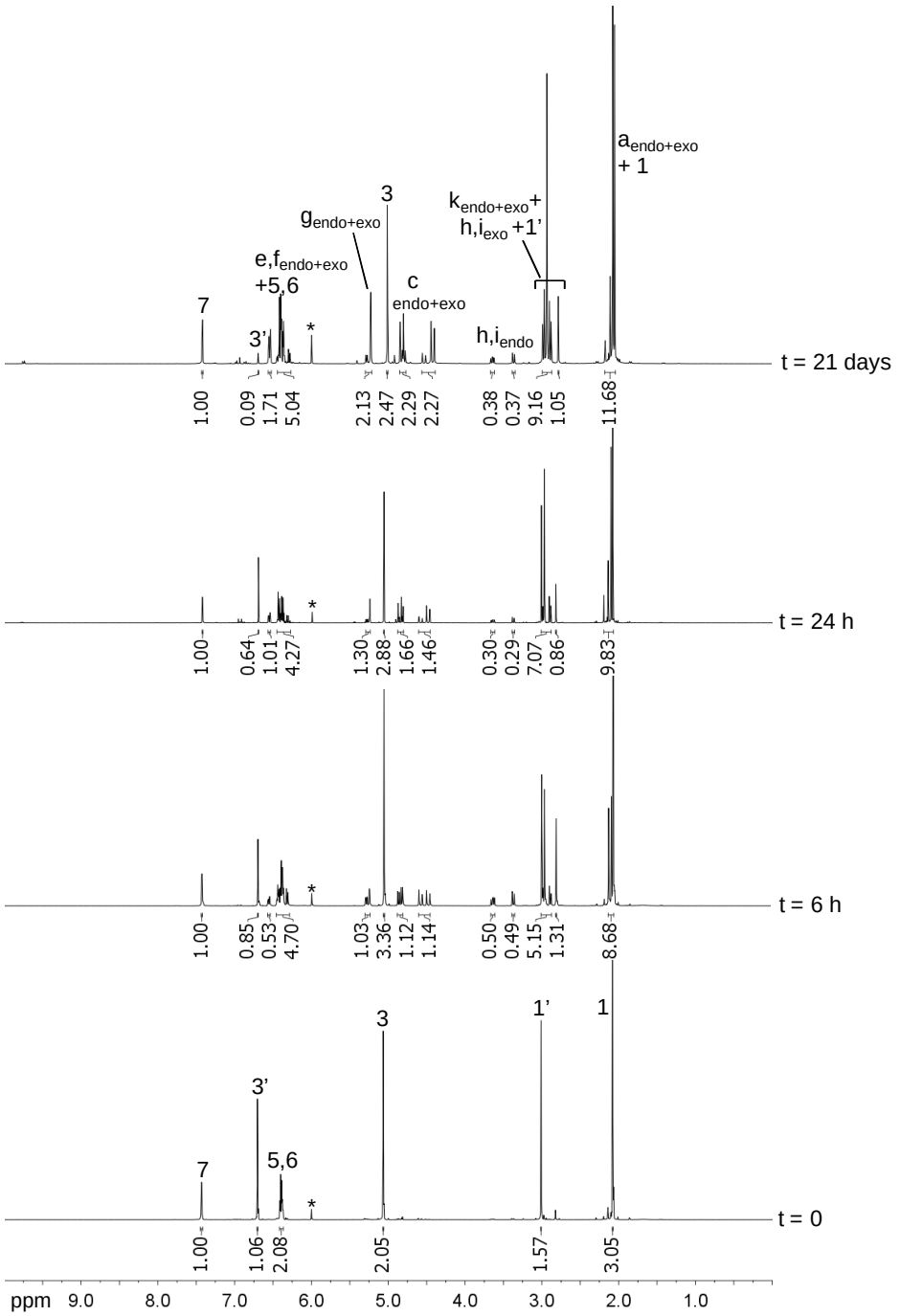

Figure 77. Evolution of the model DA reaction between MM (0.6 M) and FA (0.6 M) in *TCE-d_2 at 65ºC for 24 h. The top spectrum was taken after 20 days at room temperature. The peaks labeled with numbers and letters correspond to the reactants and adduct, respectively (see Scheme 12 and Table 14).

The reaction conversions (Table 15) were calculated by comparison of a specific integral, such as proton H-g (δ 5.3 ppm), with the standard, viz. that of the FA proton H-7

at δ 7.4 ppm, since during the whole reaction, the intensity decrease of H-7 was compensated by the corresponding increase in the signal of the analogous proton H-g of the adduct.

The initial spectrum at t=0 shows the mixture of monomers brought to 65ºC, and the time required to reach this temperature and run the spectrum (~10 minutes) was enough to reveal the presence of some adduct, corresponding to about 7% conversion (Table 15). The mixture attained some 50% conversion after just 6 hours at 65ºC, and when the reaction time reached 24 hours, 56% of adducts were present.

After the system had been left at 65ºC for 72 hours, it was allowed to return to room temperature and left for seven more days, when it reached 62% conversion. The solution was then left for 20 more days at room temperature and again a spectrum was run. The "final yield" at this point was calculated to be approximately 68%.

Table 15. Reaction conversions during time for the model DA reaction between FA+MM.

T /ºC	time /h	Área		% conversion
		H-7 (FA)	H-g (XVIII)	[XVIII] / ([FA]+[XVIII]) (%)
65	0	1.00	0.07	6.7
	3	1.00	0.74	42.5
	6	1.00	1.03	50.6
	24	1.00	1.30	56.4
r.t.	168	1.00	1.66	62.4
	480	1.00	2.13	68.1
90	0	1.00	2.13	68.1
	6	1.00	1.34	57.3
	24	1.00	0.69	40.8
r.t.	168	1.00	1.42	58.7
	288	1.00	1.82	64.6

After this forward reaction, the retro-DA of the model system was studied at 90ºC. As shown in Figure 78, the intensity of the peaks assigned to the individual reagents increases progressively with time to the detriment of those belonging to the adduct, which decrease correspondingly, as discussed above.

Nevertheless, the backward reaction did not progress completely, since after heating at 90ºC for 24 hours, 40% of the adducts (Table 15) (*exo* form since it is thermodynamically more stable) were still present in equilibrium, which clearly shows that the temperature chosen was not sufficiently high to shift the equilibrium toward to near-complete regeneration of the initial reagents. Hence, the reaction was slower than expected, although with good reversibility.

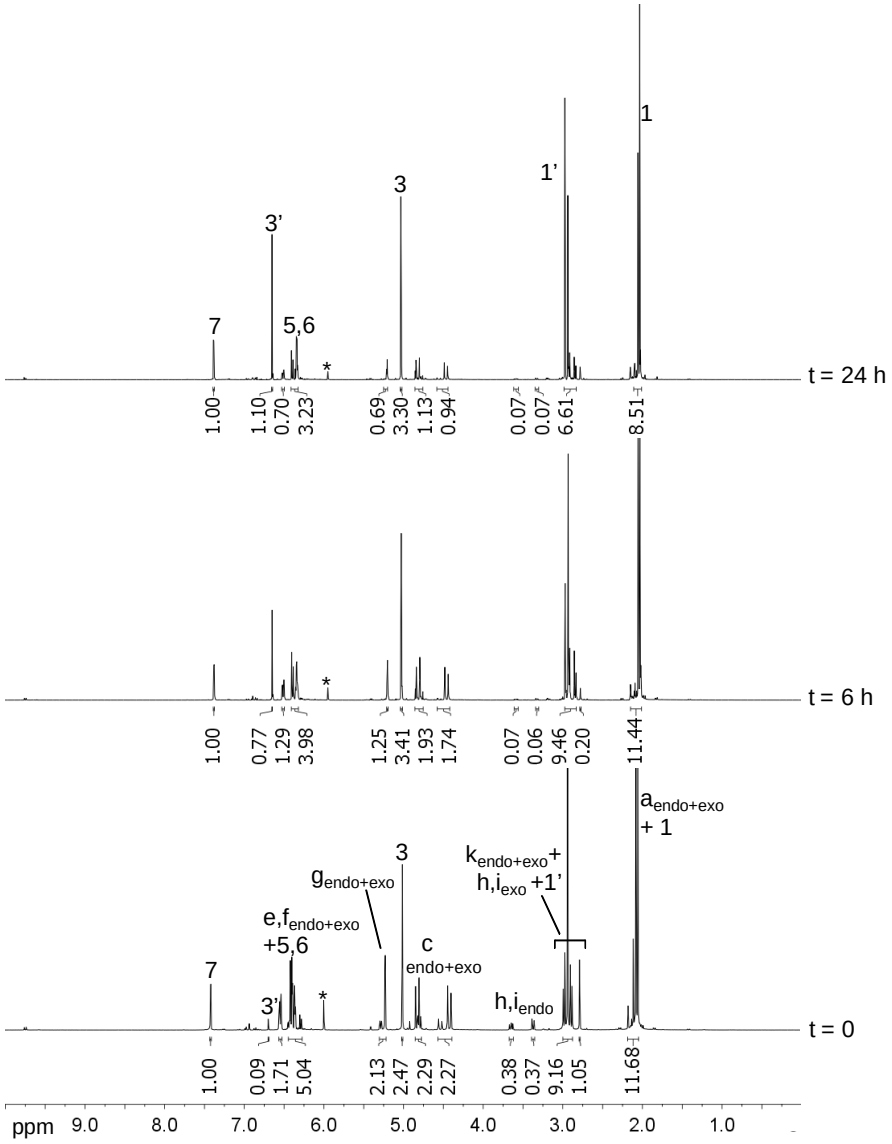

Figure 78. Retro-DA of the model system (Scheme 12) at 90ºC.

The system was then allowed to cool again to room temperature and left for twelve more days (Figure 79). The equilibrium was re-established with 64% conversion, which is

close to the value obtained before the retro-DA (Table 15). Furthermore, the growth of the signals related to the formation of the adducts and the corresponding decrease of those associated to the initial reagents were again clearly observed, as discussed above. The feasibility of multiple DA/retro-DA cycles was thus confirmed.

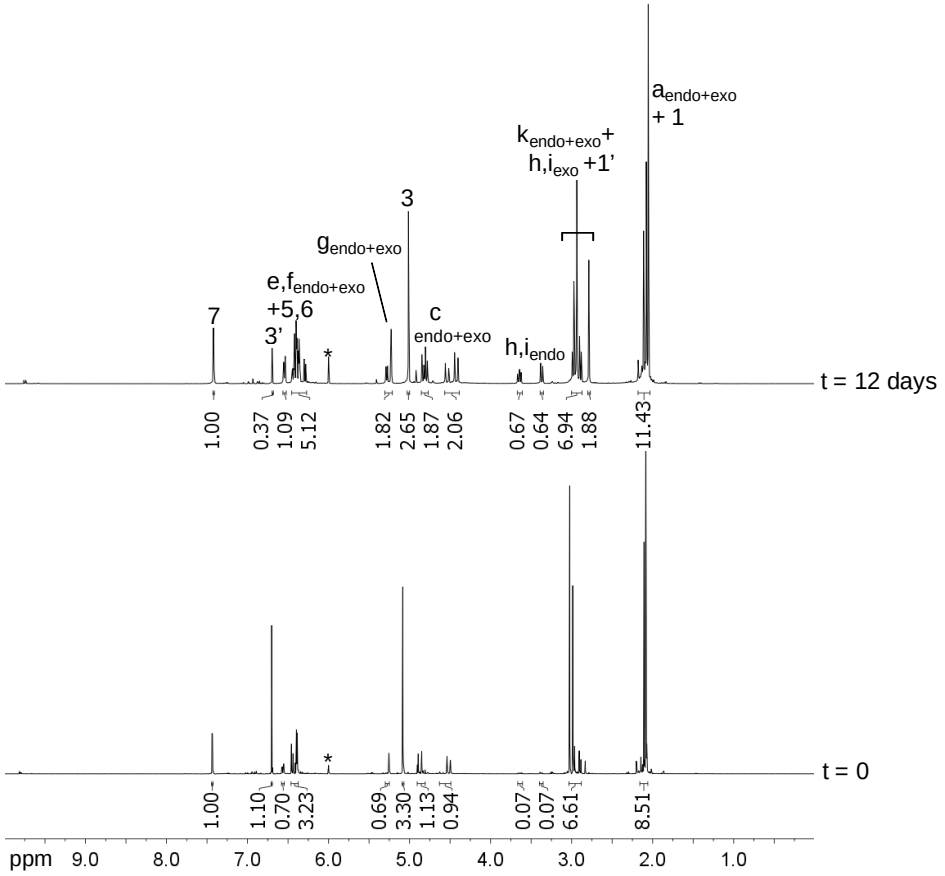

Figure 79. ^{1}H NMR spectra of the model DA system (Scheme 12) taken after the retro-DA reaction (t=0) and then after 12 days at room temperature.

After the second DA reaction, the model DA adduct **XVIII** was precipitated in diethyl ether, filtered and vacuum dried. Its FTIR spectrum is shown in Figure 80. The presence of the adduct moiety was clearly confirmed mainly by the presence of the weak =CH band at 3013 cm^{-1}, the imide and ester C=O bands at 1756, 1682 (*endo* and *exo* isomers) and 1734 cm^{-1}, the C-N and C-O bands at 1372 and 1039 cm^{-1}, respectively, as well as by the disappearance of the characteristic bands of the furan (3120, 1502, 1016, 918, 744 cm^{-1}) and maleimide (3100, 826, 691 cm^{-1}) rings [179,189,191,242].

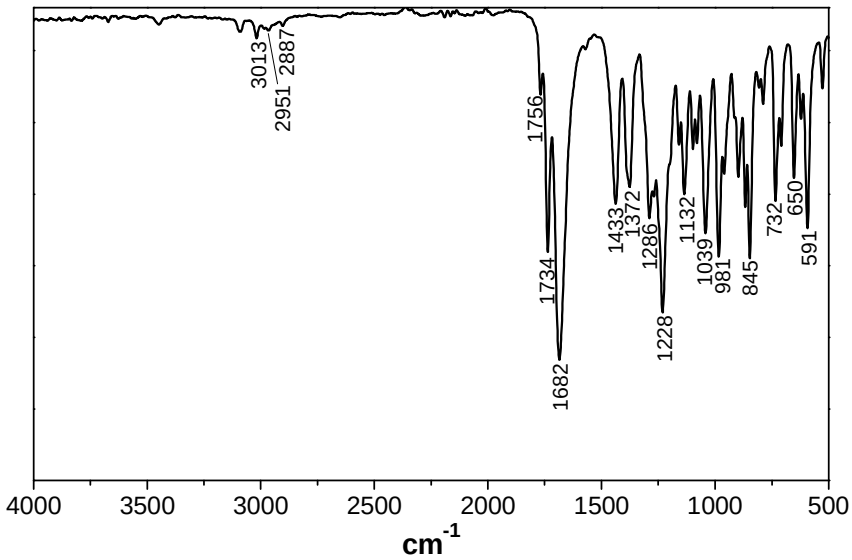

Figure 80. FTIR-ATR spectrum of the model DA adduct **XVIII**.

2.3 CONCLUSIONS

The study of the furan-maleimide DA model reaction provided clear indications about the most appropriate conditions to be applied in the preparation of the corresponding novel macromolecular materials, as well as clear-cut evidence of the intermediate structures involved and of the absence of significant side reactions in both forward and backward pathways, even after several cycles. These features are indeed crucial in the context of the corresponding polymerizations with multifunctional monomers, because they obviously play a determining role in optimizing the polymer molecular weight and the possibility of reverting to the starting or intermediate building blocks in a quantitative fashion over multiple cycles.

The original application of UV spectroscopy, coupled with the more classical use of the ^{1}H NMR counterpart, to follow the kinetics and equilibrium of formation and decoupling of the DA adducts, proved particularly valuable.

From this preliminary study, the choice of both forward and backward reaction temperatures was made for the subsequent polymerizations, viz. temperatures around 65ºC are best suited for the growth reactions, with relatively fast reaction rates (k_{DA} = 2.1x10^{-5} dm^{3}mol^{-1}s^{-1}), whereas the retro-DA reaction occurred at 90ºC, but was slower than

expected ($k_{retroDA}$ = $1.6x10^{-6}$ s^{-1}). As a consequence, it was decided to carry out the subsequent retro-DA reactions at 100-110ºC.

Furthermore, the thermoreversibility and reproducibility of these systems was also successfully checked over a couple of cycles.

3 LINEAR SYSTEMS

The subsequent step was to examine the behaviour of linear polymerization systems based on the stepwise DA growth following two approaches, one involving a difuran monomer A-A and a complementary bismaleimide counterpart B-B, and the other, monomers bearing both reactive moieties in their structures, i.e. A-B type molecules.

3.1 A-A+B-B SYSTEMS

The kinetic behaviour of a linear DA polymerization involving difunctional monomers was examined using monomers **I** and **IX** (Scheme 13) for this study, whose conditions were based on the preliminary investigation of the corresponding reaction of the monofunctional model compounds discussed above.

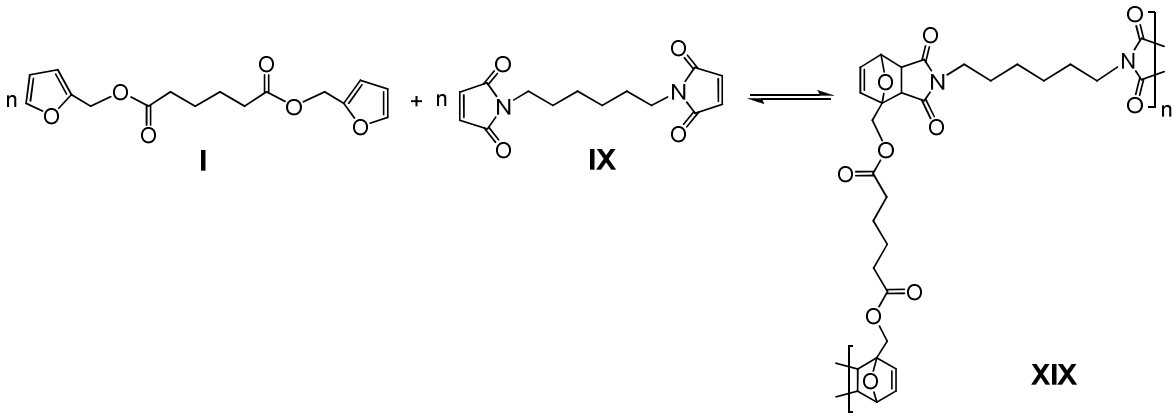

Scheme 13. DA polymerization mechanism of the two difunctional monomers **I** and **IX**.

The polymerizations of equal concentrations of **I** and **IX** in TCE or TCE-d_2, were followed by both UV and ^{1}H NMR spectroscopy at 65ºC, and more qualitatively by changes in the viscosity of the reaction medium as a function of time.

3.1.1 UV spectroscopy

The DA polycondensation between **I** and **IX** (Scheme 13) was followed by UV spectroscopy in TCE at 65ºC, with an initial concentration for both monomers of 0.2 M. The procedure used was similar to that followed for the model system. Again, the furan moiety did not show any absorption maximum above about 270 nm, while the bismaleimide monomer displayed the characteristic maximum at ~300 nm (Figure 81), as with its monofunctional model.

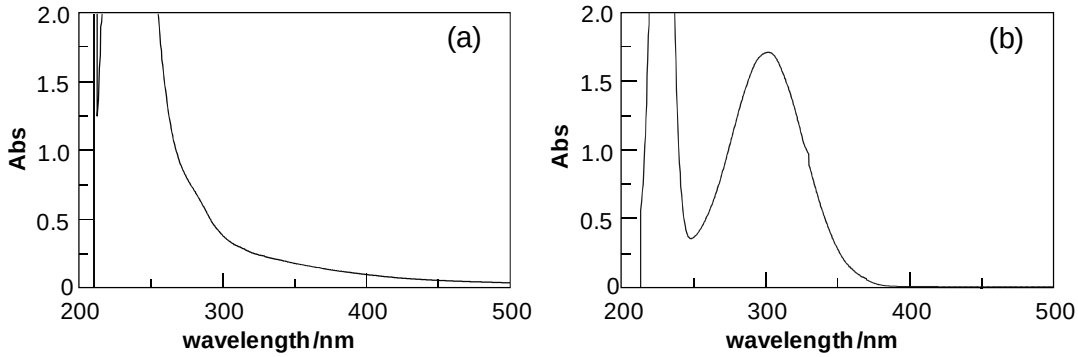

Figure 81. UV spectrum of (**a**) **I** 0.2M and (**b**) **IX** 0.2M taken with an optical path 0.01 cm.

The evolution of the DA polymerisation was thus monitored during 62 hours by the progressive decrease of the maleimide peak at 300 nm, associated with the corresponding loss of conjugation between the two carbonyl groups and the C=C unsaturation separating them, which accompanied the formation of the DA adduct. Figure 82 shows its set of spectra, and again the presence of an isosbestic point, common to all these experiments, clearly suggests that the polymerisation was not marred by side reactions.

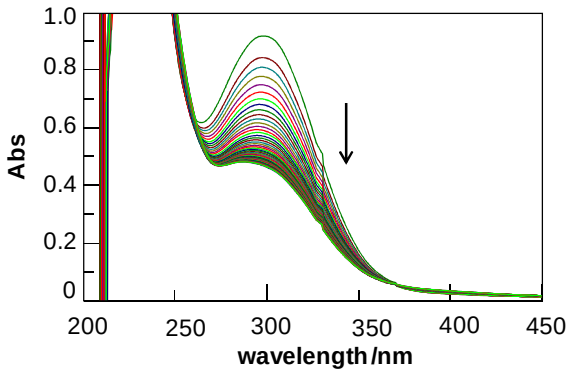

Figure 82. Progressive decrease in the absorbance of the maleimide peak following the progress of the DA polymerization of **I** (0.2 M) with **IX** (0.2 M) in TCE at 65ºC. Spectra were taken every hour during 62 h with an optical path of 0.01 cm.

This system displays the same behaviour as its model counterpart, although the use of equimolar solutions of both difunctional monomers (stoichiometric balance 1:1) resulted in a slower reaction, which, as expected, followed now a second order pattern, as shown by the corresponding linear and reproducible plot of *1/Abs* vs. *time* (Figure 83), giving a rate constant of 9.4×10^{-6} $dm^3mol^{-1}s^{-1}$. The twofold decrease in this value compared with that of the model reaction at the same temperature, viz. 2.1×10^{-5} $dm^3mol^{-1}s^{-1}$ (Table 13), is most probably associated with steric factors in the case of the growing chains.

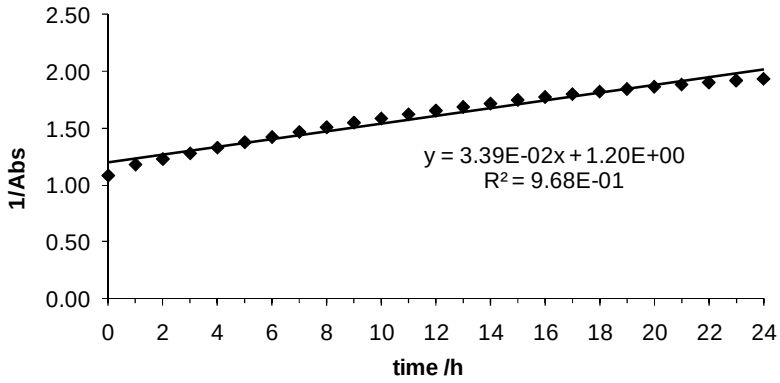

Figure 83. Second-order plot based on the decrease of the absorption at 300 nm for the DA polymerization conducted in the conditions given in Figure 82, for the first 24 h.

The retro-DA reaction of the ensuing polymer was also followed at 110ºC during 24 hours by taking spectra at regular time intervals. In this case, a progressive increase in the absorption at 300 nm was observed (Figure 84), due to the decoupling of the adducts along the DA macromolecules, generating furan and maleimide end-moieties. The reversibility of these systems was successfully checked over several cycles.

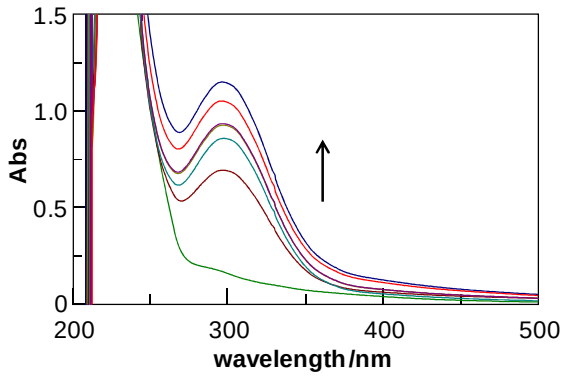

Figure 84. Progressive increase in absorbance following the progress of the DA depolymerization of **I**+**IX** (the green line corresponds to the initial polymer solution, while the blue one corresponds to the same solution after 24 h at 110ºC).

As expected, the retro-DA of the system **I**+**IX** displays a first order kinetic behaviour, with a corresponding rate constant of 2.5×10^{-6} s^{-1}. The increase in this value compared with that obtained with the model system, viz. $1.6\text{x}10^{-6}$ s^{-1}, is related to the corresponding increase in the temperature from 90 to 110ºC. No steric hindrance was expected here, since one is dealing with the statistical opening of adducts along the polymer chain, which does not differ topochemically from the corresponding opening of the single adduct moiety in the model system.

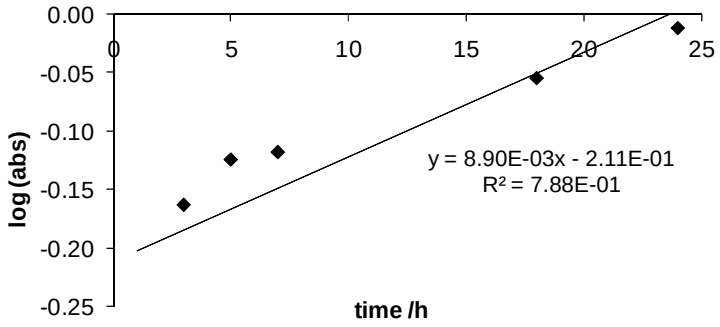

Figure 85. First-order plot based on the increase of the absorption at 300 nm for the retro-DA depolymerization conducted in the conditions given in Figure 84.

The second- and first-order rate constants obtained with the polymerisation and depolymerisation, respectively, are in agreement with those obtained previously (except for the increase in that of the retro-DA for the depolymerization at 110ºC already pointed out above) from the reaction of monofunctional model compounds in similar conditions. This observation is not surprising, since in both types of systems, the DA reaction involves the same diene and dienophile structures, i.e. a furan heterocycle substituted at C-2 with a methylene group and a maleimide ring *N*-substituted by the same moiety. In other words, the reactivity of both DA partners did not depend detectably on the nature of their substituents beyond their first carbon atom, which suggests that steric hindrance did not play a significant retarding effect in this context.

3.1.2 NMR spectroscopy

The evolution of the linear DA polymerization/depolymerization system **I**+**IX** was also followed by ^{1}H NMR spectroscopy. The solutions were prepared directly in the NMR tubes under nitrogen in TCE-d_2 and the spectra taken at a constant temperature of 65ºC during 72 hours. The concentration of both monomers was 0.6 M.

Figure 86 shows the ^{1}H NMR spectra of the polymerizing system, in which the expected pattern was again observed, namely the progressive increase in the signals related to the adduct protons at δ 5.3 (H-12), 6.6-6.2 (H-13, H-14), and 3.7-2.8 (H-10, H-11) ppm, and the corresponding decrease of those attributed to the unreacted furan [δ 7.4 (H-a), 6.4-6.3 (H-b,H-c) ppm] and maleimide (δ 6.6 ppm, H-A) cycles. The protons' chemical shift of

the aliphatic bridges between adduct moieties was not significantly altered during the DA reaction, except for the methylene protons of the furfuryl moiety, which resonates at δ 5.0-4.0 ppm as doublet in the adduct (H-16), instead of a singlet at δ 5.0 ppm for the difuran monomer (H-e) [179,189,191,243].

After the system had been kept at 65ºC for 72 hours, it was allowed to return to room temperature and left for seven more days, when its ^{1}H NMR spectrum suggested near-complete reaction. Moreover, the polymer growth was accompanied by a regular increase in the solution viscosity. As previously mentioned, monomer **IX** presented unknown impurities which however did not interfere in the DA reaction.

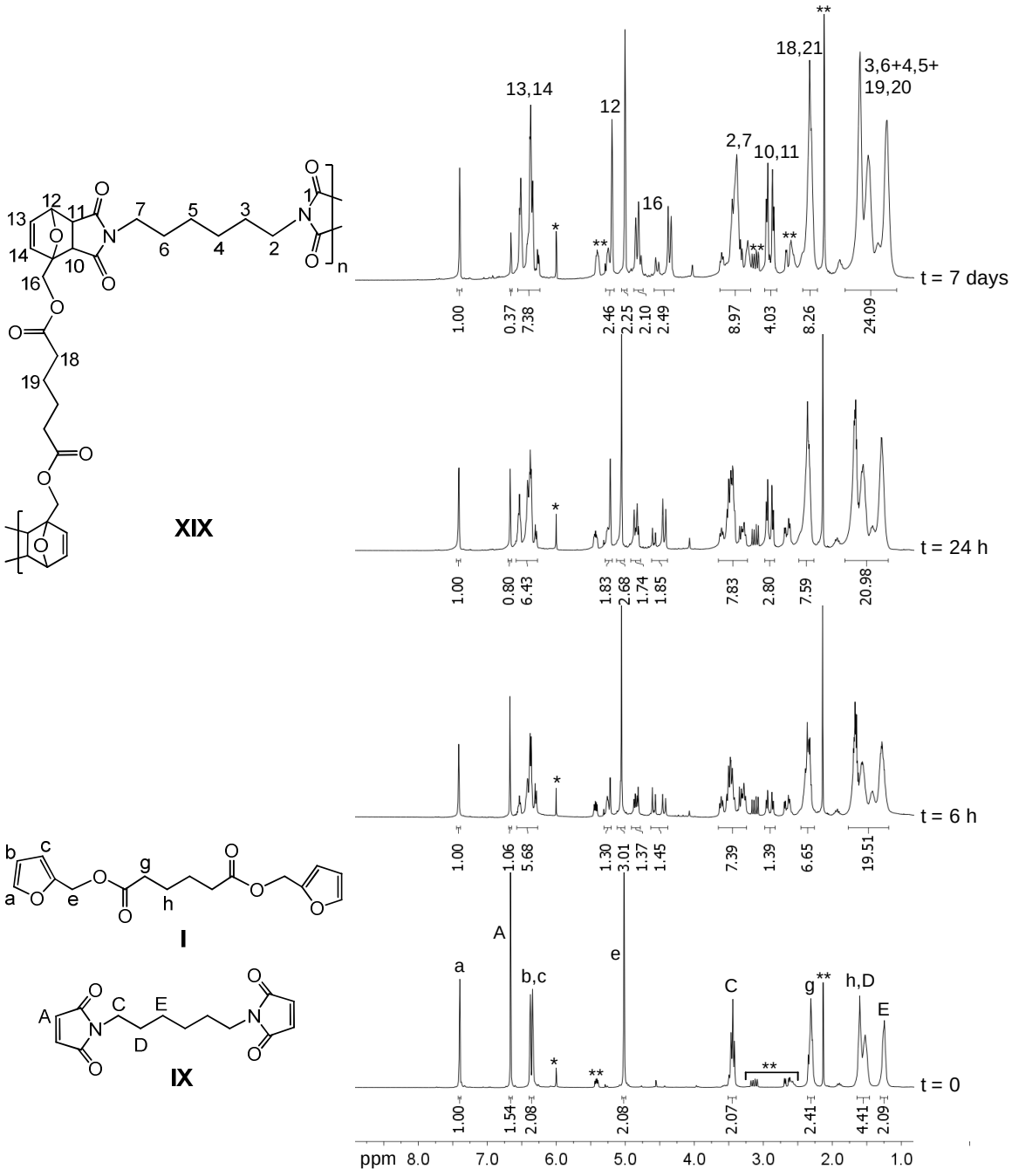

Figure 86. DA reaction between **I** (0.6 M) and **IX** (0.6 M) in *TCE-d_2 at 65ºC. The last spectrum was taken after the system had been kept at 65ºC for 72 h and left for seven more days at room temperature. The peaks labeled with letters and numbers correspond to the reactants and adduct, respectively.

Table 16 shows the reaction conversion of this linear system as a function of the reaction time, which reached more than 50% of adducts in only 6 hours at 65ºC and ~71% at the end of the experiment.

Table 16. Reaction conversions during time for the linear DA system **I**+**IX**.

T /ºC	time /h	Área		% conversion
		H-a (I)	H-12 (XIX)	[XIX] / ([I]+[XIX]) (%)
65	0	1.00	0.03	2.91
	6	1.00	1.30	56.52
	24	1.00	1.83	64.66
r.t.	168	1.00	2.46	71.10

After this study, the ensuing linear polymer, **XIX** was precipitated in petroleum ether and dried under vacuum. Figure 87 shows its FTIR spectrum, the presence of the adduct moieties was confirmed by the presence of their characteristic bands at 1736, 1692, 1349, 1073, 982, 885, 731, 646 cm^{-1}, as well as by the absence of the characteristic furan and maleimide ring bands (as discussed above for the model system) [179,189,191].

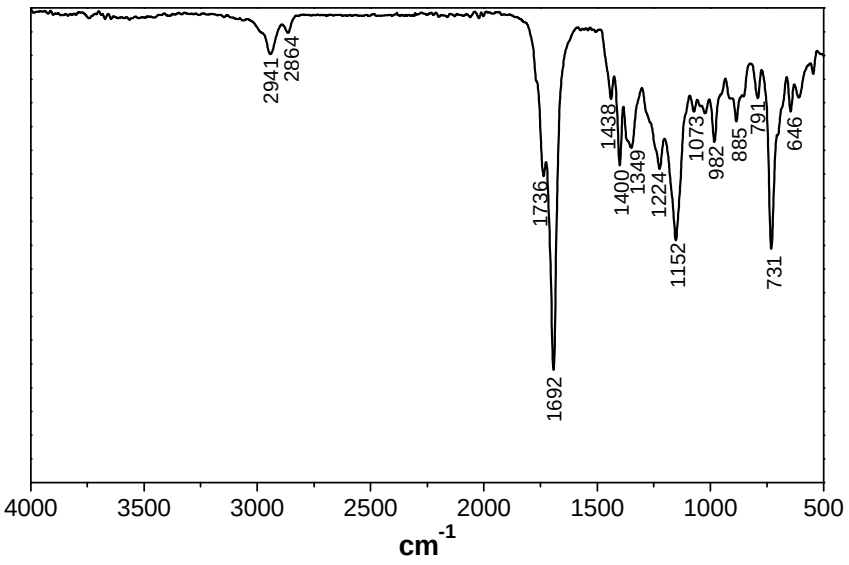

Figure 87. FTIR-ATR Spectrum of the linear DA polymer **XIX**.

The retro-DA depolymerisation of polymer **XIX** was then carried out following a strategy which had already been applied in the literature to avoid the return to a network structure after the decrosslinking of DA-based gels [189,190], as follows.

A fraction of polymer **XIX** was dissolved in toluene and then heated at 110ºC for 24 hours. After this time, a tenfold excess of a monofunctional compound, namely 2,5-

dimethylfuran (DMFu), was added to the solution and the temperature was decreased to 65ºC. The reaction was left for another 24 hours. The solvent choice was based in its high boiling point (110ºC) and the solubility of both the polymers and its monomers into it.

After the vacuum removal of toluene and the unreacted DMFu (b.p.= 92ºC), the residue was analysed by ^{1}H NMR spectroscopy and shown to be an equimolar mixture of monomer **I** and the bis-adduct of **IX** with DMFu (**XX**) (Figure 88), viz. the furan protons of **I** resonated at δ 7.4 (H-a), 6.4 (H-c) and 6.3 (H-b) ppm, and the methylene ones of the furfuryl moiety (H-e) at 5.0 ppm, whereas the peaks related to the disubstituted adduct moiety of **XX** appeared at δ 6.3 (H-3, H-4) and 2.8 (H-6) ppm, and the methyl groups at δ 1.8 ppm. Moreover, the maleimide protons at δ 6.7 ppm were not observed [179,189,191,243]. This result indicates that the polymer had indeed reverted to its monomers during the treatment in refluxing toluene, but the excess of DMFu had trapped the bismaleimide **IX** during the cooling process, by forming the corresponding bisadduct, thus inhibiting its DA repolymerisation with **I**. The regenerated bismaleimide monomer would in fact react preferentially with the excess of DMFu to form the corresponding bisadduct, instead of recondensing with the bisfuran monomer.

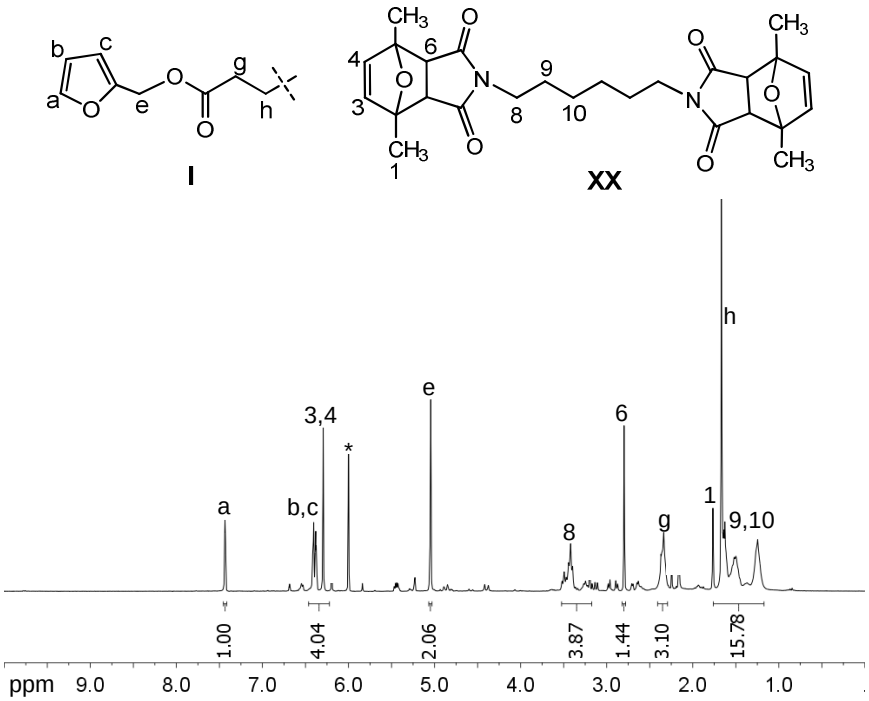

Figure 88. ^{1}H NMR of the mixture of monomer **I** and bisadduct **IX**+DMFu, with some residual amount of initial polymer **I**+**IX** in *TCE-d_2, after removing the toluene and the excess of DMFu.

3.1.3 Non-equimolar polymerizations

The linear polycondensations generally involve equimolar amounts of the difunctional monomers. Thus, the monomer's stoichiometry can influence the behaviour of these DA systems.

In this section, two linear systems, viz. difuran monomers **I** or **III** reacting with bismaleimide **IX**, were studied (Scheme 14).

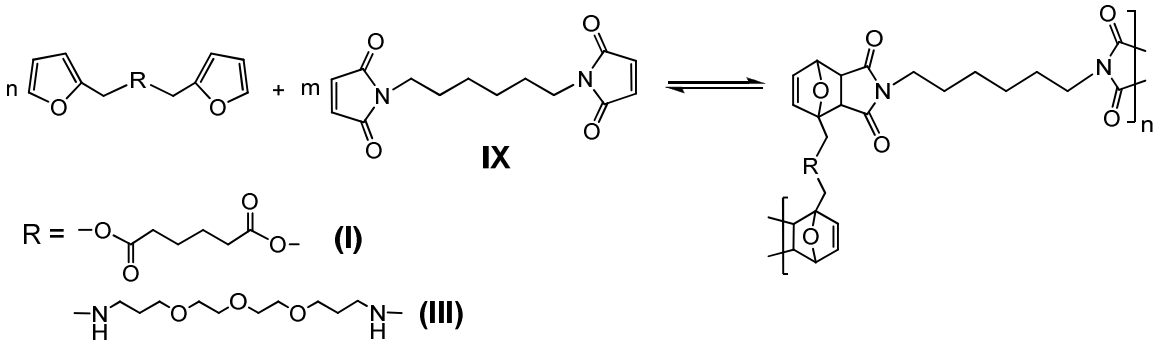

Scheme 14. DA polymerization of the linear **I+IX** and **III+IX** systems.

As previously referred, monomer **IX** contained unknown impurities which did not interfere with the DA reaction. However, the stoichiometry of the reaction would be influenced, viz. the real stoichiometry of these systems could not be established, and hence the reaction under stoichiometric conditions (1:1) contained a small excess of furan groups. Nevertheless, since it was not possible to quantify the proportion of impurities, which must have been quite low, a first approach was made, namely their contribution was not taken into account in the weighed amount of monomer **IX**, i.e. it was considered as "pure".

Given this approach, the linear systems were implemented with three different stoichiometric ratios, namely 1:1, 1:0.95 and 0.95:1, i.e. 5% deviation from stoichiometry both ways. The DA reactions were followed by ^{1}H NMR spectroscopy in TCE-d_2 at 65ºC, and the procedure was the same for all the experiments (*Experimental* Part, p.159). The evolution of these DA systems with reaction time gave the expected features, as discussed above, viz. a progressive increase in the signals related to the adduct protons resonances and a corresponding decrease of those attributed to the unreacted furan and maleimide cycles was again observed.

The characterization of the ensuing polymers was important to understand the influence of the monomers' stoichiometry. Thus, after the end of each reaction, the solutions were precipitated in an excess of petroleum ether and the ensuing products dried under vacuum. Polymers **XIX** and **XXI** (Figure 89) were then characterized by DSC and SEC. Given the occurrence of the retro-DA reaction, the range of temperatures considered for the DSC analysis was below 80ºC. The corresponding results are reported in Table 17.

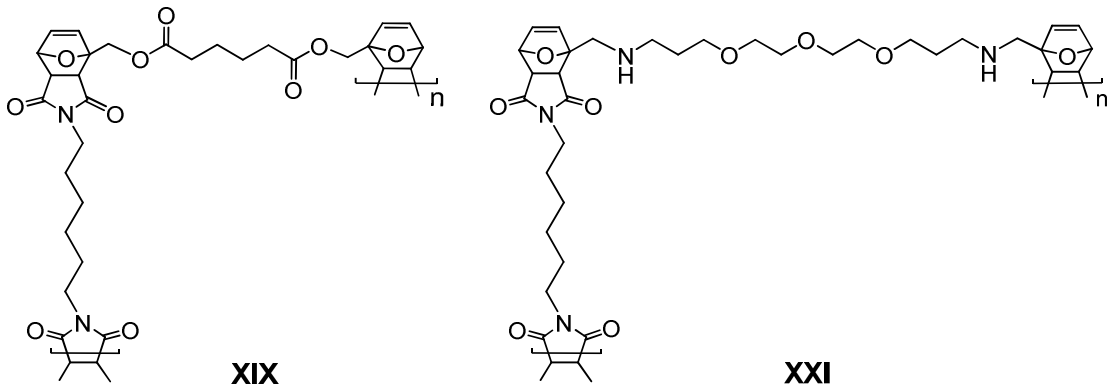

Figure 89. Structure of the linear polymers obtained from the systems **I+IX** and **III+IX**, respectively.

Table 17. DSC and SEC results for the linear polymers **XIX** and **XXI**.

polymer	Monomer proportion I or III : IX	Tg /ºC	Mw	Mn	PD = Mw/Mn
XIX	1 : 1	7	5514	2126	2.59
	1 : 0.95	13	6108	3017	2.02
	0.95 : 1	15	5991	3553	1.69
XXI	1 : 1	26	7380	4340	1.70
	1 : 0.95	17	7610	4710	1.62
	0.95 : 1	12	7310	4320	1.69

Both polymers **XIX** and **XXI** gave glass transition temperature (Tg) values mostly somewhat below room temperature, in tune with the fact that their adducts are linked with flexible segments, viz. aliphatic domains bearing ester or ether moieties, respectively. Their DSC thermograms are represented in Figure 90 and 91, respectively.

Although polymers **XXI** bore a highly flexible oligoether spacer, their slightly higher average Tg values, compared with those of **XIX** counterparts, were attributed to the presence of amine (-NH-) groups which generate intermolecular hydrogen bonding.

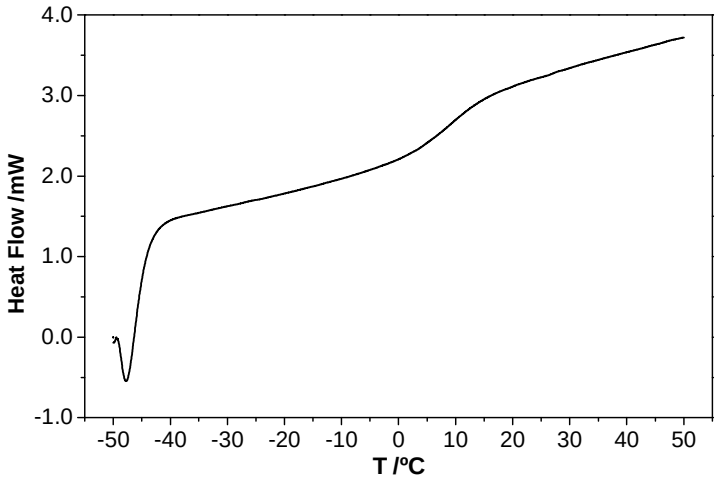

Figure 90. DSC thermogram for polymer **XIX** 1:1.

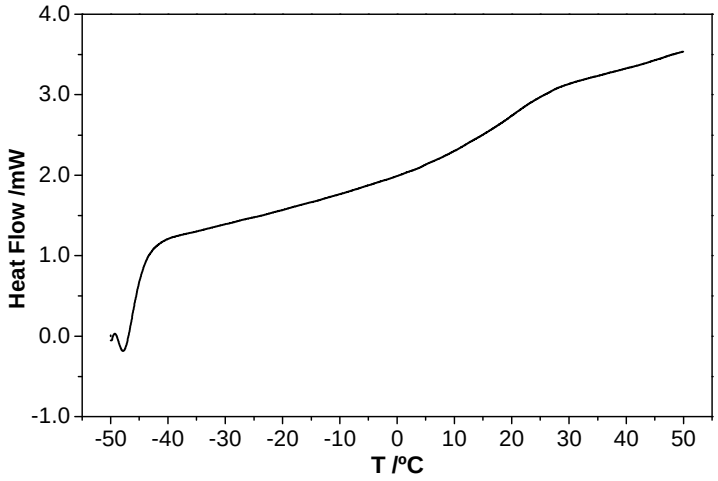

Figure 91. DSC thermogram for polymer **XXI** 1:1.

The Mw of these linear polymers are rather low, but their PD values around 2 are consistent with linear polycondensations (Table 17). More interestingly, their molecular weight distribution curves (Figure 92) were accompanied by several narrow peaks, each with a PD value around 1, i.e., corresponding to a specific compound instead of a distribution of homologues. These peaks are therefore assigned to cyclic oligomeric

structures formed during the DA polycondensation [262], since a growth associated exclusively with linear molecules of different size would not have yielded those peaks in the corresponding SEC tracings.

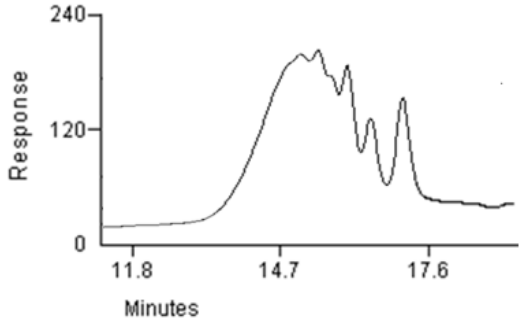

Figure 92. SEC tracing of the linear polymer **XIX**.

The formation of cycles in a polycondensation thus limits the molecular weight of the polymers (the chain growth stops) and hence the relatively low values of the measured molecular weights. Moreover, the polymer Tg tends to be lower in the presence of these structures, because they act as "plasticizers", i.e., they create gaps among polymer chains, thus increasing their mobility and reducing the interchain interactions, with a consequent increase in polymer flexibility (lower Tg).

Moreover, the formation of the cyclic oligomers makes the discussion of the monomer stoichiometry effect on the DA systems rather ambiguous, although, in a general way, the results obtained with 5% stoichiometry deviation (considering the approach made) (Table 17) did not bring about significant differences.

3.2 A-B SYSTEMS

Another type of linear polymerization system involves monomers bearing both reactive moieties in their structures, i.e. A-B molecules. As previously mentioned, the synthesis and polycondensation of these structures represents an interesting alternative for linear DA polymerizations, because it ensures the ideal initial stoichiometry.

In this section, two AB-type systems (Scheme 15) involving the previously synthesized monomers **XIII** and **XIV** will be described as sources of polymers **XXII** and **XXIII**, respectively. As shown in Scheme 15, one of the reactive moieties of the monomers is protected, viz. the maleimide is masked in the form of its furan-DA adduct, in order to obtain a stable structure and hence, avoid premature polymerization. The polycondensation of these monomers could then be achieved after the *in situ* deprotection of the maleimide moiety at high temperature, followed by cooling to the appropriate DA polycondensation temperature.

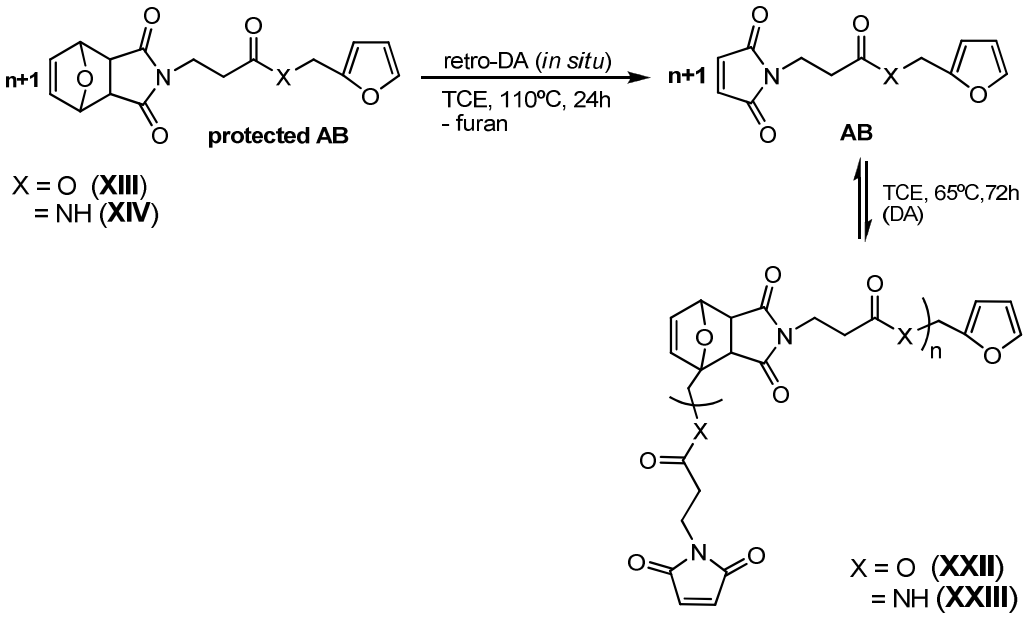

Scheme 15. Deprotection of the AB monomers and their linear DA polymerization.

As in the case of the previous linear systems, these DA polymerizations and depolymerisations were followed by both UV and ^{1}H NMR spectroscopy in TCE and TCE-d_2, respectively.

3.2.1 UV spectroscopy

Both AB polymerizations (Scheme 15) were followed by UV spectroscopy in TCE at 65ºC, with initial concentration of 0.2 M. As expected, the initial solutions did not show

any maximum absorption, because the maleimide moiety was protected. Nevertheless, after the *in situ* deprotection of the maleimide moiety at high temperature, viz. 110ºC for 24 hours under N_2, the systems displayed the characteristic maleimide peak at 293 nm. Thereafter, they were cooled to 65ºC to promote their DA polymerization. Their DA evolution was monitored for 72 hours by the progressive decrease of the maleimide peak intensity, showing a similar pattern to that observed in Figure 82.

Once again, the DA reactions were not accompanied by side reactions. However, in the case of **XIV**, the formation of a precipitate was observed during the reaction time, which affected the absorbance measurements of the solution.

3.2.2 NMR spectroscopy

The linear AB polymerizations were also followed by ^{1}H NMR spectroscopy at 65ºC in TCE-d_2, with 0.2 M solutions. As in the case of the UV study, first the monomer underwent the retro-DA reaction (110ºC for 24 hours under N_2) in order to deprotect the maleimide moiety, and making it available for subsequent DA polymerization. Thereafter, the solutions were cooled to 65ºC to initiate it.

Figure 93 shows the ^{1}H NMR spectra taken before and after the *in situ* retro-DA of **XIII**. Apart from traces of residual DCU (δ 1.0-2.0 ppm) and evidence of the incipient polymerization, the spectrum of this unprotected AB structure clearly confirms its presence through the maleimide C*H*=C*H* protons at δ 6.6 ppm, as well as the disappearance of the adduct peaks at δ 6.5 (H-7), 5.2 (H-6) and 2.8 (H-5) ppm [179,189,191].

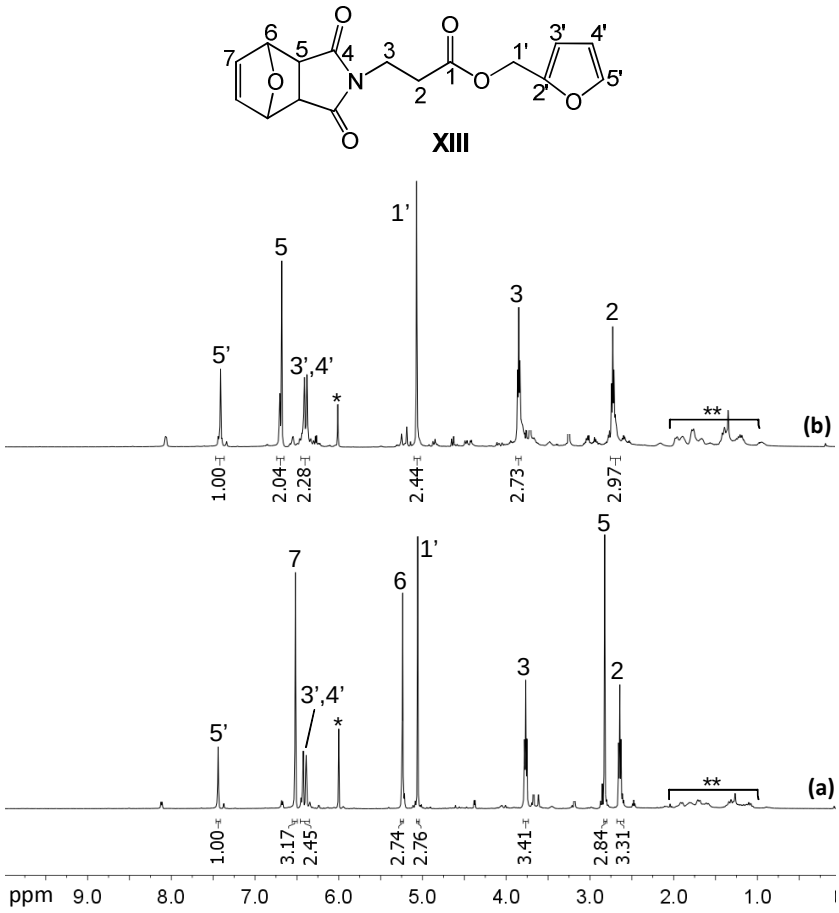

Figure 93. ^{1}H NMR spectra of **XIII** (0.2 M) in *TCE-d_2, (**a**) before and (**b**) after the *in situ* deprotection of the maleimide moiety by the retro-DA reaction (**traces of DCU).

Similar features were observed for compound **XIV**, as shown in Figure 94. Additionally, in this case, the methylene group between the furan ring and the amino group appears as a doublet, indicating that this proton is coupling with the amino proton.

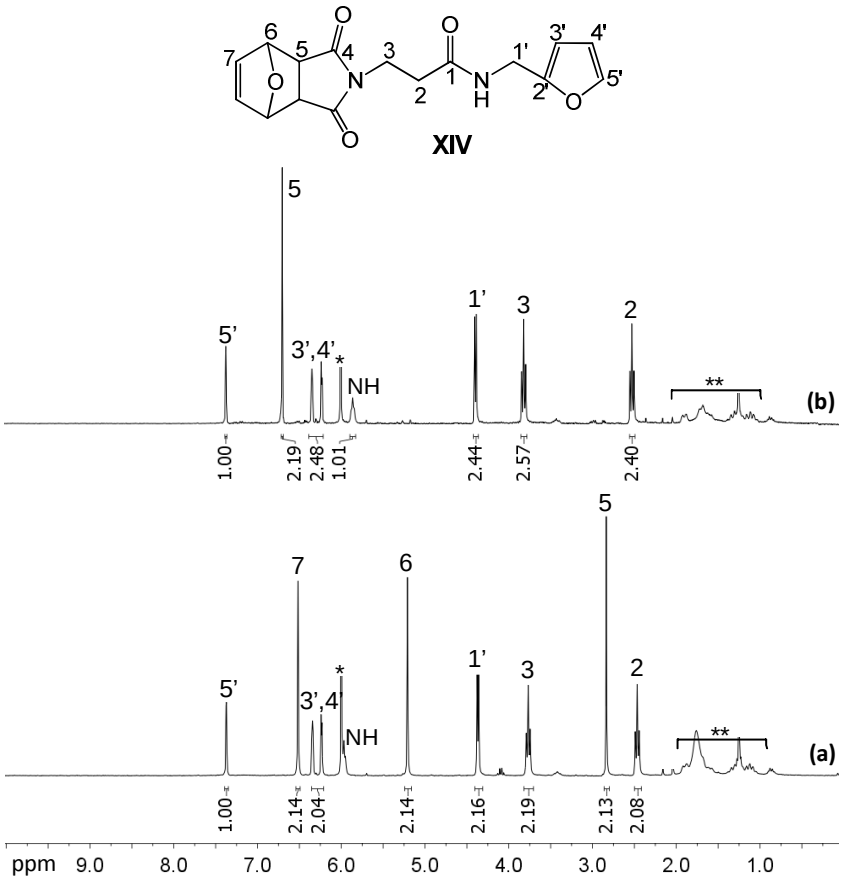

Figure 94. ^{1}H NMR spectra of **XIV** (0.2 M) in *TCE-d_2, (**a**) before and (**b**) after the *in situ* deprotection of the maleimide moiety by the retro-DA reaction (**traces of DCU).

As an example, the progress of the DA polycondensation of **XIII** is illustrated in Figure 95. The spectrum taken at t=0 corresponds to the monomer solution after the *in situ* deprotection of the maleimide moiety by the retro-DA reaction of its adduct with furan. The expected pattern was observed in both systems, namely the progressive decrease in the peak intensity of the monomer relevant protons [δ 7.4 (H-5'), 6.7 (H-5), 6.4-6.3 (H-3', H-4') ppm] and the corresponding increase in that of the peaks related to the corresponding formation of the adducts, viz. δ 5.3 (H-e), 6.5-6.2 (H-c, H-d), 3.6-2.9 (H-f, H-g) ppm. Concurrently, as the reaction proceeded, the viscosity of the medium also increased.

After 6 hours of reaction, the polycondensation of **XIII** had reached over 65% of conversion, and the "final yield" was calculated to be approximately 80% of adducts. In the case of **XIV**, as already mentioned, the precipitate formed during the reaction led to a general "disappearance" of the polymer peaks, because this was no longer in solution. Hence, the calculation of the adduct conversion was not possible in this situation.

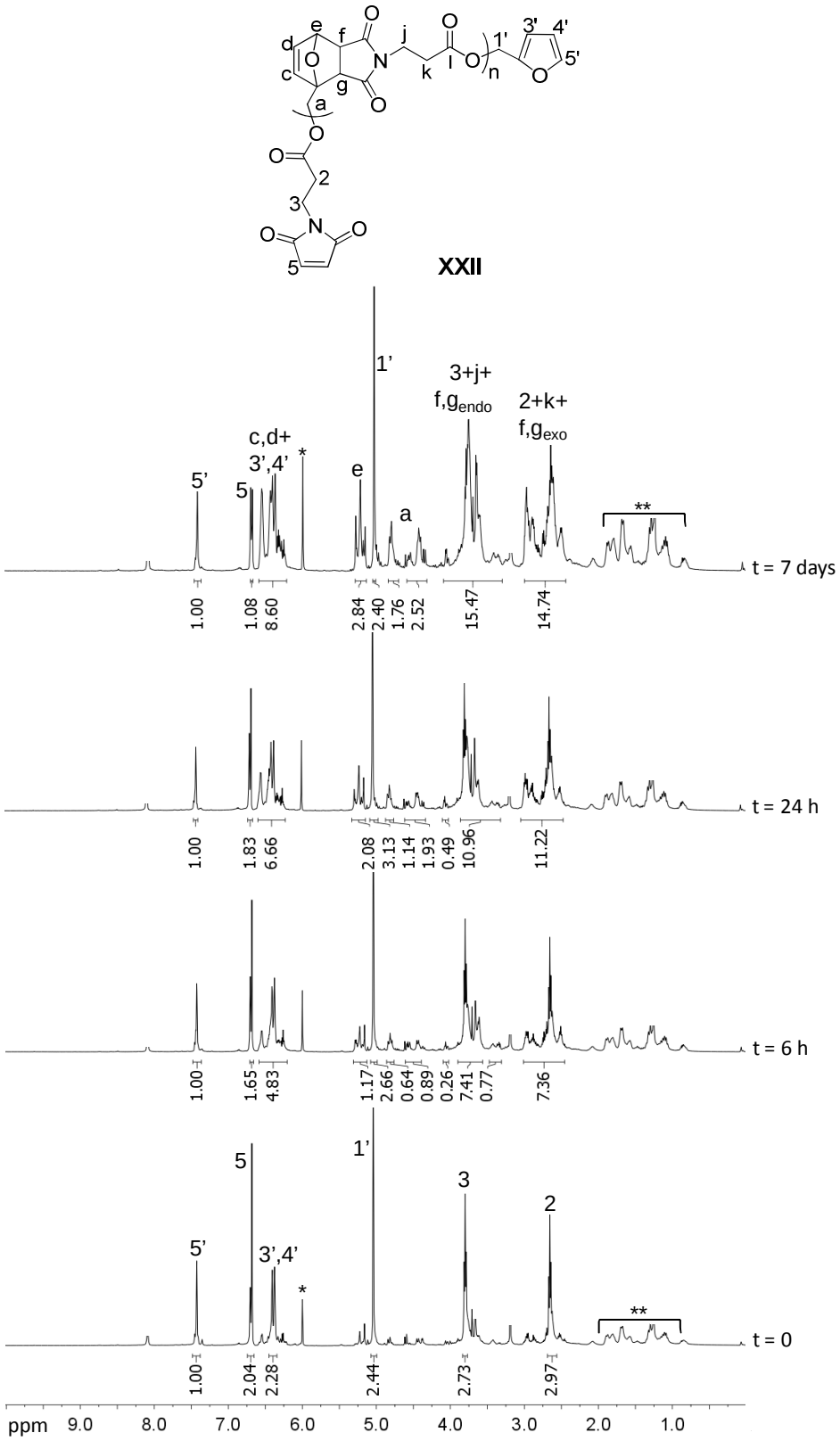

Figure 95. Time evolution of the ^{1}H NMR spectrum for the DA polimerization of **XIII** (0.2 M) at 65ºC in *TCE-d_2. The initial spectrum (t = 0), taken at room temperature, corresponds to the unprotected AB structure.

After these systems had reached high conversions, the retro-DA reaction was followed by ^{1}H NMR spectroscopy at 110ºC for 24 hours. Again, the expected behaviour was observed (Figure 96), viz. decrease in the adduct signals to the detriment of the corresponding growth of the unreacted furan and maleimide moieties, as discussed above. After 6 hours at 110ºC, 34% of adducts were still present, which was constant even after 24 hours at that temperature. This shows that the equilibrium was indeed shifted towards the starting compounds upon heating, but not completely.

Thereafter, the systems were allowed to cool again to 65ºC, and left for three more days and the systems returned to the original polymerized state (about 65% of conversion).

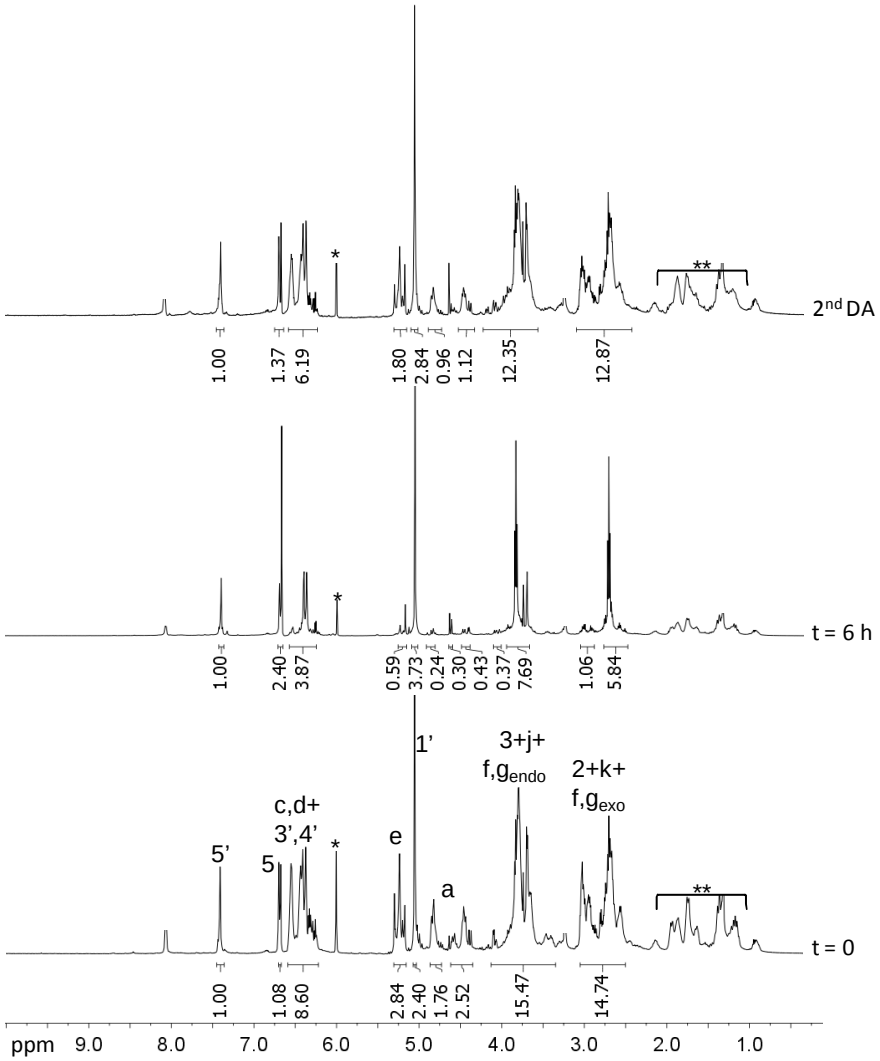

Figure 96. Time evolution of the ^{1}H NMR spectrum of the retro-DA depolimerization of AB-polymer **XXII** at 110ºC in *TCE-d_2, followed by the last ^{1}H NMR spectrum following the second DA polimerization at 65ºC.

3.2.3 Characterization of the AB polymers

The ensuing polymers **XXII** and **XXIII** (Figure 97) were precipitated in an excess of petroleum ether and dried under vacuum before being characterized by DSC and SEC.

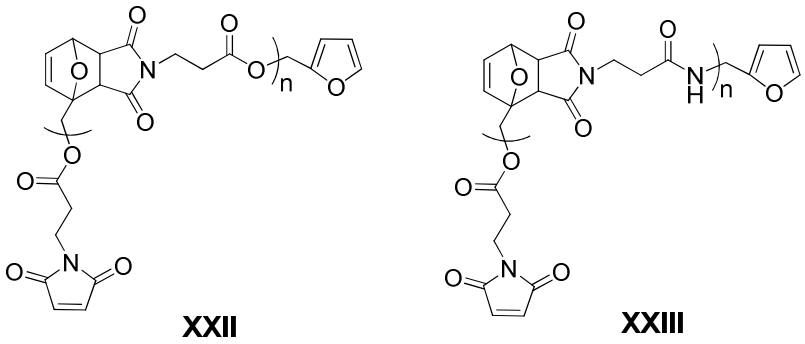

Figure 97. Structure of the synthesized linear A-B polymers.

As expected, the characteristic adduct moieties, namely at 1757, 1715, 1693, 1390, 1012, 977, 729, 641, 595 cm^{-1}, were observed in the FTIR spectra of these polymers. Moreover, the characteristic bands of the furan and maleimide rings were absent (as discussed above for the linear and model system) [179,189,191].

Table 18 gives the only detected Tg, together with the molecular weight distribution and polydispersity values for polymer **XXII**. As already mentioned, the range of temperatures considered for this study was below 80ºC given the occurrence of the retro-DA reaction above this temperature.

Table 18. DSC and SEC results for the linear polymer **XXII**.

polymer	Tg /ºC	Mw	Mn	PD = Mw/Mn
XXII	38	4200	1900	2.2

Polymer **XXII** gave a Tg higher than room temperature (Table 18), i.e. somewhat higher than those of the A-A+B-B counterparts, as indeed expected since here the aliphatic bridge between adducts was shorter and more polar. For polymer **XXIII**, it was not possible to determine the Tg nor melting point, since its DSC thermogram did not show

any relevant feature below 80ºC (Figure 98). The considerable increase in the Tg of **XXIII**, i.e. above 80ºC, can be explained by the presence of amide (-CONH-) groups in the backbone of this polymer, which strongly favors intermolecular hydrogen bonding, as in all polyamides, compared with the corresponding polyesters. The lack of melting features was complemented by an X-ray analysis of **XXIII,** which showed the typical features associated with a semi-cristalline material, viz. sharp peaks, as illustrated in Figure 99, in tune with the relative ease with which polyamides crystallize compared with polyesters for the same reason of ordered interchain packing through hydrogen bonding.

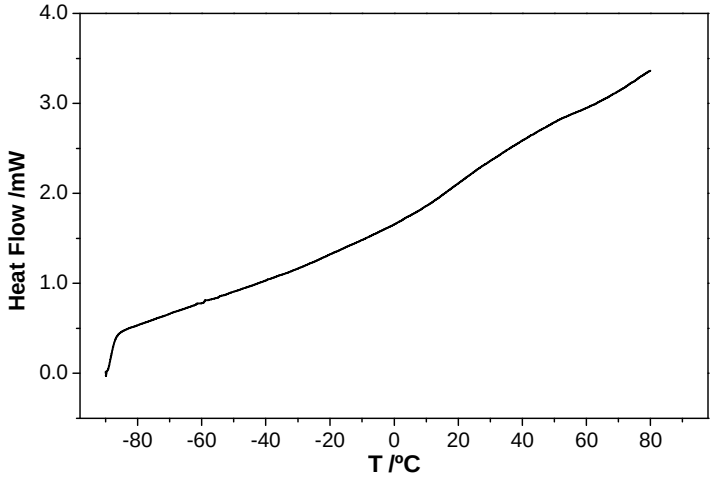

Figure 98. DSC thermogram of polymer **XXIII**.

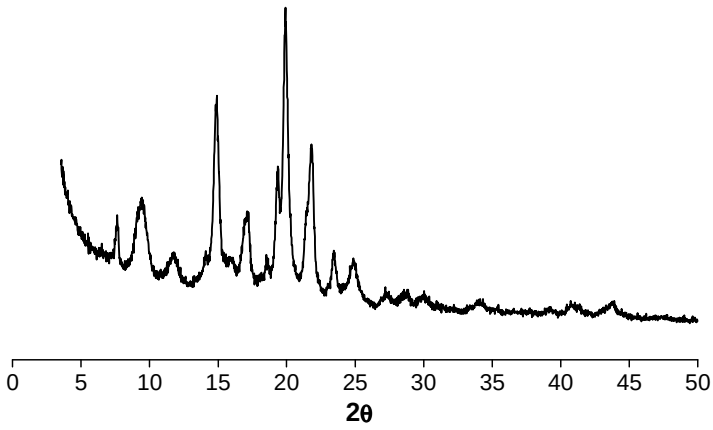

Figure 99. X-ray diffractogram of polymer **XXIII**.

The SEC tracing of polymer **XXII** gave low Mw value, but the PD value around 2 is consistent with a linear polycondensation. Once again, its distribution curve (Figure 100) was accompanied by narrow peaks, each with a PD value close to 1, assigned to cyclic oligomeric structures formed during the DA polycondensation.

Since polymer **XXIII** was not completely soluble (a precipitate was always formed) in any solvent used for the SEC analyses, it was not possible to determine its molecular weight and the possible presence of similar cyclic oligomers, although the sharp peaks observed in its X-ray diffractogram could also be attributed to these cyclic structures, and not only to the semi-crystalline features of the linear macromolecules. Further study is, however, required to confirm this hypothesis. The loss of solubility of the growing chains of **XXIII** clearly gave rise to modest molecular weigths, since the precipitated products could not pursue their polycondensation.

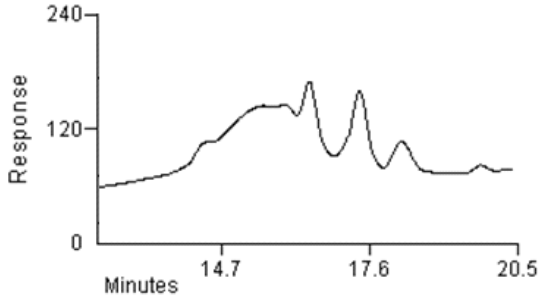

Figure 100. SEC tracing of polymer **XXII**.

3.3 CONCLUSIONS

The formation of linear macromolecules from the step-growth mechanism associated with the successive DA reactions was followed. First, equimolar and non-equimolar DA systems using difunctional A-A and B-B monomers, namely **I**+**IX** and **II**+**IX** systems, were considered. The ensuing polymers were then characterized in terms of structure and molecular weight, glass transition temperature and thermal depolymerisation by the retro-DA reaction.

The DA reaction of these systems was carried out at 65ºC with a reaction rate constant k of $9.4x10^{-6}$ $dm^3mol^{-1}s^{-1}$, and 71% of conversion into adducts, whereas the depolymerization took place at 110ºC with $k_{retroDA} = 2.5x10^{-6}$ s^{-1}. Furthermore, the DA polymerisation/depolymerisation cycles were applied reproducibly, without any side reactions. In order to avoid the return to the initial polymer, the DA/retro-DA cycle was interrupted by adding an excess of a monofunctional reagent (maleimide) to the system so that, upon cooling, this reagent acted as a trap by forming non-polymerizable adducts with the released monomer bearing the complementary moiety. This strategy was successfully applied in this study, and hence the thermal reversibility of these DA systems was confirmed.

These linear DA polymers exhibited Tg values close to room temperature, since both had flexible segments as bridging structures linking the adducts.

An additional challenge in the application of the DA reaction to furan polymers was the synthesis and polycondensation of monomers bearing both reactive moieties in their structures, i.e. AB molecules, since they avoid the problem of functional stoichiometry.

In this study, two linear DA polymers were prepared using A-B monomers with one of the reactive groups (maleimide) protected in the form of a DA adduct. This moiety was kept in a masked configuration in order to obtain a stable monomer and avoid premature polymerization. Their polycondensation could be then achieved after the subsequent *in situ* deprotection at high temperature, followed by the cooling to the appropriate temperature for the DA polymerization. Once again, the results obtained from both UV and ^1H NMR spectroscopy corroborated the thermal reversibility of these systems, as well as their reproducibility.

When compared with their A-A+B-B counterparts, these polymers exhibited higher Tg values, as expected, since here the aliphatic bridge between adducts was shorter and more polar. Moreover, the substitution of the ester linkage by an amide group in the A-B structures led to a considerable increase of the corresponding Tg, which is easily explained by the well-known intermolecular hydrogen bondings present in all polyamides, compared with the corresponding polyesters.

In addition, for all DA linear systems, since relatively low concentrations were used (<1M), a tendency to cyclization was observed, which influenced negatively their final polymer molecular weights, as well as lowered their Tg values, because they acted as “plasticizers”.

4 NON-LINEAR SYSTEMS: A_n+B_m AND AB_2

Non-linear DA polycondensations involving at least one monomer bearing more than two functionalities lead to highly branched or crosslinked structures, and thus can be applied in the preparation of "mendable" materials. Here, non-linear systems using the combination of a bisfuran and a trismaleimide (A_2+B_3), and also the reverse combination of a bismaleimide reacting with a trisfuran monomer (A_3+B_2), were studied in order to determine the conditions to obtain highly branched polymers or crosslinked counterparts.

Furthermore, an asymmetrically substituted monomer of the AB_2 type was used in the preparation of a hyperbranched macromolecular structure that does not crosslink.

4.1 A_2 + B_3 SYSTEM

The first non-linear system involves the DA reaction of the bisfuran **I** with the trismaleimide **XI** (Scheme 16).

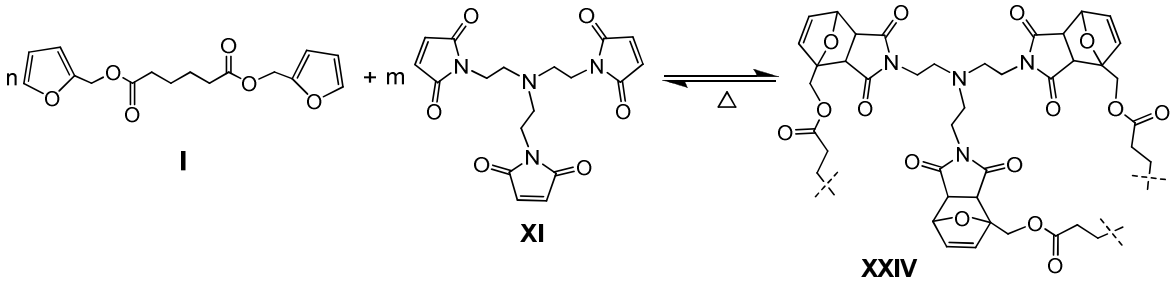

Scheme 16. Non-linear DA polycondensation between bisfuran **I** and trismaleimide **XI** monomers.

The relevant relationship providing the critical yield *Pc* associated with the inception of gel formation is the *Flory-Stockmayer equation* (2):

$$Pc = \frac{1}{[r + r\rho(m-2)]^{1/2}} \qquad (2)$$

In the present context, *m* was equal to 3 for the branching monomer **XI** and ρ was unity, because there is no other maleimide-type monomer in the system. As explained in *Experimental* part (p. 159), three [maleimide]/[furan] functional ratios *r*, viz. 1.0, 0.75 and 0.50 were applied, which, as indicated in Table 19, are associated with critical conversions, *Pc*, for network formation of 71, 81 and 100%, respectively, if intermolecular cyclisations are neglected.

Table 19. Stoichiometric ratios of the monomers **I** and **XI** and the corresponding yield expected for gel formation, according to *Flory-Stockmayer* equation.

r ($N_B/N_A < 1$)	Pc (%)
1.0	71
0.75	81
0.5	100

The initial monomer concentrations are given in Table 20, where the concentration of difuran **I** was the same for the three experiments. Due to the high concentration for the UV measurements, a fivefold dilution of each initial solution was applied (Table 20).

Table 20. Initial (^{1}H NMR) and fivefold dilution (UV) concentration of **I** and **XI** solutions in TCE for the three different stoichiometric ratios *r*.

Monomer	*r*	$[monomer]_{initial}$ /mol.dm^{-3}	$[monomer]_{dilution}$ /mol.dm^{-3}
I	1; 0.75; 0.5	1.2	0.24
XI	1	0.8	0.16
	0.75	0.6	0.12
	0.5	0.4	0.08

4.1.1 UV spectroscopy

The DA polycondensations between **I** and **XI** (Scheme 16), carried out with functional ratios *r* of 1.0, 0.75 and 0.5, were followed by UV in TCE at 65ºC using the diluted solutions (Table 20). As expected, the UV spectrum of **I** did not show any absorption maximum above about 270 nm, whereas **XI** displayed the characteristic maximum at about 300 nm for all concentrations (Figure 101).

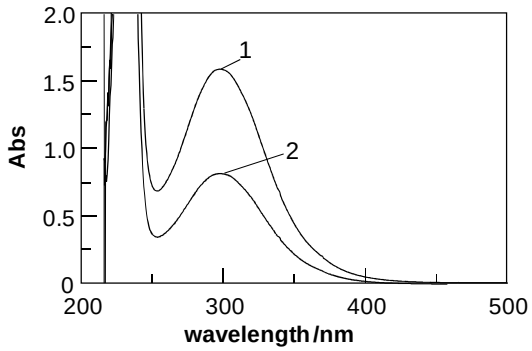

Figure 101. UV spectra of the TCE solutions 0.16 M (*1*) and 0.08 M (*2*) **IX**, with an optical path 0.01 cm.

The evolution of these DA reactions was again followed by monitoring the progressive decrease in the intensity of the maleimide peak at ~300 nm, associated with the corresponding loss of conjugation between the two carbonyl groups and the C=C unsaturation separating them, which accompanied the formation of the DA adduct.

The progress of the non-linear polymerization under stoichiometric conditions, viz. *r* = 1.0, is given in Figure 102 as an example of their typical behaviour. The three experiments displayed the same pattern, and the presence of an isosbestic point at ~260 nm, common to all, clearly indicated that the formation of the DA adducts were not accompanied by any side reaction.

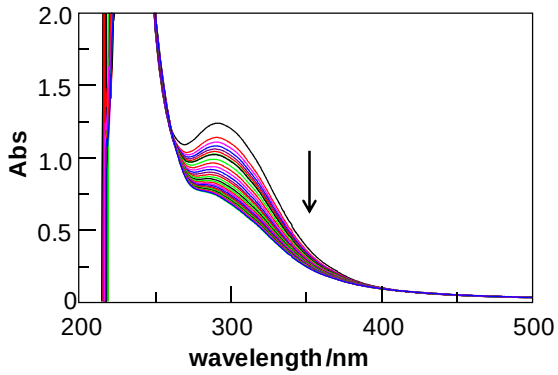

Figure 102. UV spectra of the DA evolution between **I** (0.24 M) and **IX** (0.16 M), viz. *r* = 1.0, at 65ºC in TCE with an optical path of 0.01 cm. Spectra were taken every hour during 24 h.

4.1.2 NMR spectroscopy

The non-linear **I**+**XI** system (Scheme 16) was also followed by ^{1}H NMR spectroscopy in TCE-d_2 at 65ºC to assess the structural evolutions in a more detailed way. The NMR measurements were performed with the different **XI**/**I** stoichiometric ratios *r*, viz. 1.0, 0.75 and 0.5. The monomers concentration for each experiment is given in Table 20.

Figure 103 shows the evolution of the DA polymerization under stoichiometric conditions, viz. *r* = 1.0. The other two systems (*r* = 0.75 and 0.5) exhibited similar features. The main evidence for polymer formation is the progressive decrease and growth related, respectively, to the peaks associated with furan [δ 7.4 (H-a), 6.4-6.3 (H-b,H-c) ppm] and maleimide (6.6 ppm, H-D) protons and to those of the ensuing adducts, namely at δ 5.2 (H-6), 6.5-6.2 (H-7,H-8), 4.3-4.8 (H-10) and 3.6-2.8 (H-4,H-5) ppm [179,189,191,243]. Furthermore, a considerable widening of all resonances was observed, reflecting a strong increase in molecular weight. Indeed, the last spectrum shown in Figure 103 was taken well after the formation of the network, i.e. with a mixture of crosslinked (*gel*) and branched (*sol*) macromolecules, and of course only the latter species were detected and displayed in this situation.

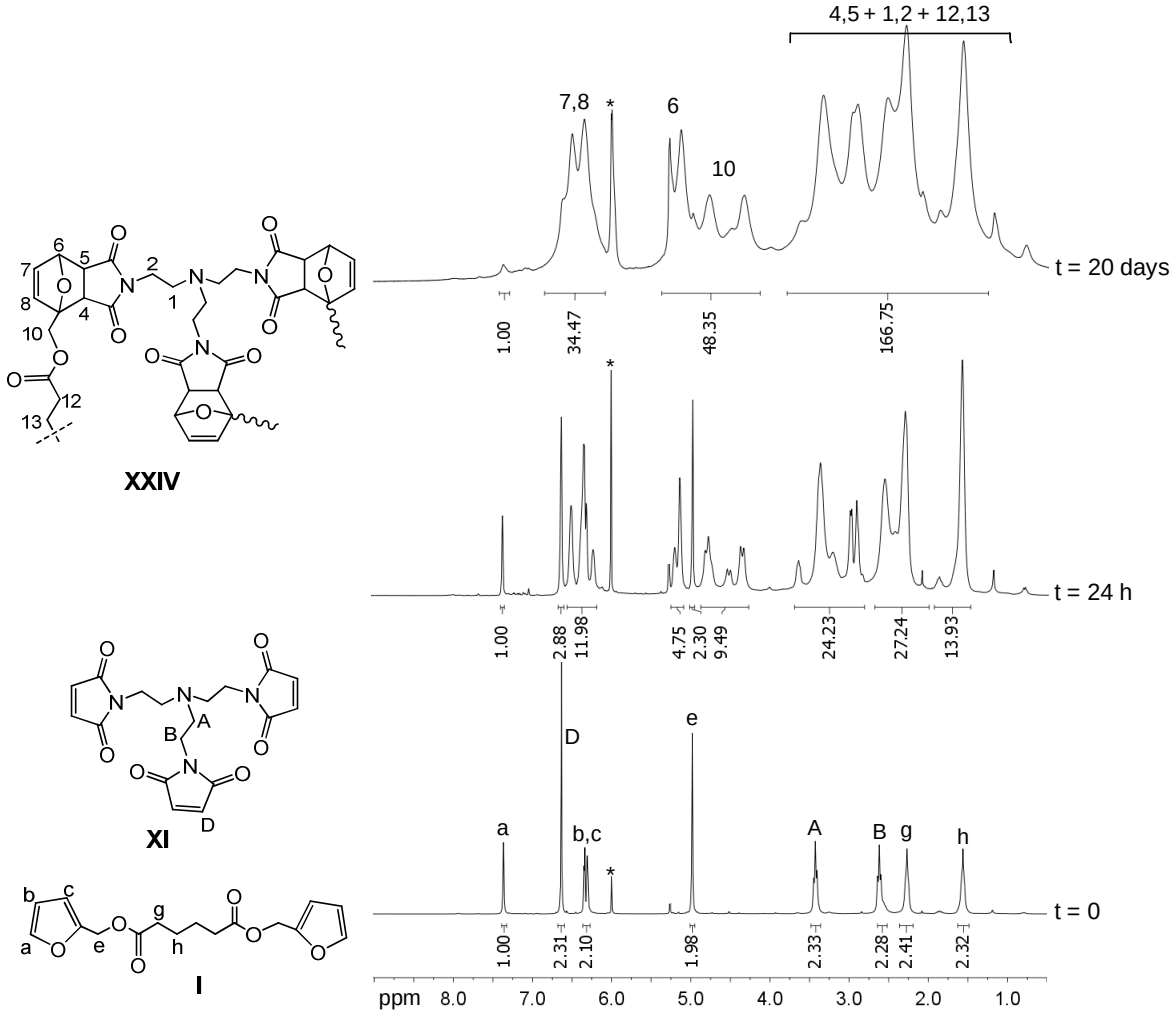

Figure 103. ^{1}H NMR spectra of the evolution of the non-linear polymerization **I**+**XI** for r = 1.0 with concentrations 0.24 M and 0.16 M, respectively, at 65ºC in *TCE-d_2. The peaks labeled with letters and numbers correspond to the monomer s and polymer protons, respectively.

These reactions were also accompanied by a progressive increase in viscosity, with formation of a gel (network) for molar rations *r* = 1.0 and 0.75, whereas for *r* = 0.5, a highly viscous liquid was obtained at the end of the reaction. The fact that crosslinking did not occur with the latter system was rationalized by considering that the gel point was predicted for 100% conversion in the absence of cyclization reactions, i.e. an ideal situation.

After reaching these non-linear polycondensations, the thermal reversibility of **I**+**XI** systems was studied. The solutions were heated at 110ºC and their ^{1}H NMR spectra revealed the occurrence of the retro-DA depolymerisation (Figure 104). Here, the reverse

sequence of that shown in Figure 103 was observed, namely the decrease in adduct peaks intensity and corresponding decrease of those attributed to the initial reagents, as discussed above. Concurrently, the viscosity of all media decreased progressively when the temperature was raised, viz. first the de-crosslinking of the network and then the depolymerization of the soluble macromolecules. At the same time, the spectra revealed a progressive sharpening of the peaks, viz. the reverse feature compared with that characterizing the DA polymerizations, corroborating the progressive decrease in molecular weight.

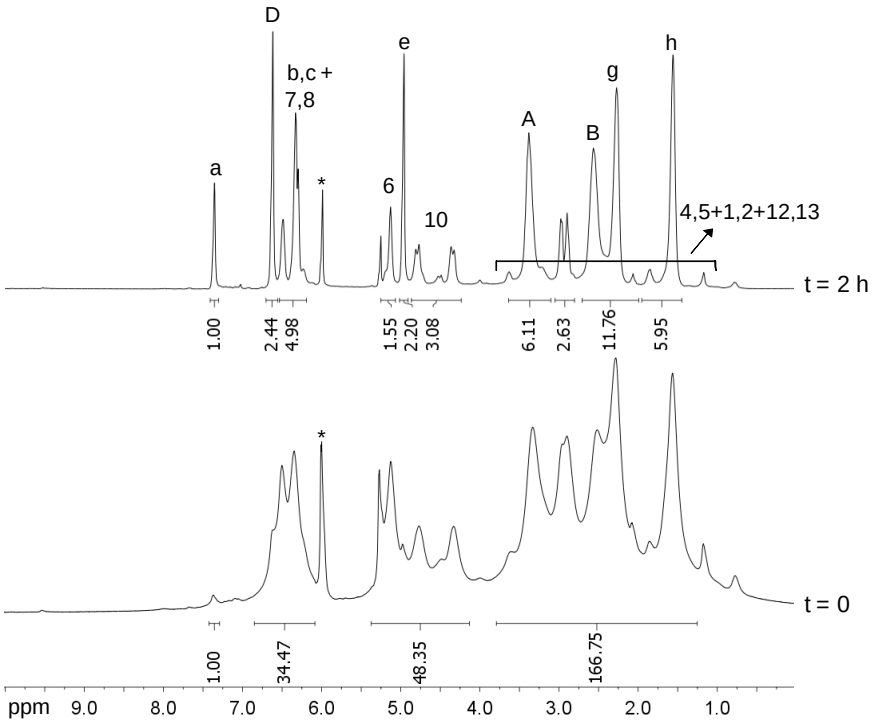

Figure 104. ^{1}H NMR spectra taken during the retro-DA depolymerization (24 h at 110ºC) of the polymerized and gelled **I**+**XI** system for r = 1.0 in*TCE-d_2. The spectrum run after 2 h shown here was essentially identical to that taken after 24 h. The peaks are labelled according to Figure 103.

After 24 hours at 110ºC, the systems were allowed to cool to 65ºC in order to confirm their cyclability, i.e., the DA polymerization was again applied. The ^{1}H NMR spectra taken after 72 hours at 65ºC (Figure 105) shows the increase in the peaks intensity associated with the formation of the adducts and the decrease of those related to unreacted furan and maleimide protons, as discussed above. Moreover, the viscosity of the media increased.

These results confirms that the solutions had indeed returned to their initial high-viscosity, with gelled material for r = 1 and 0.75. Thus, the feasibility of multiple DA/retro-DA cycles, already established by UV spectroscopy, was again confirmed.

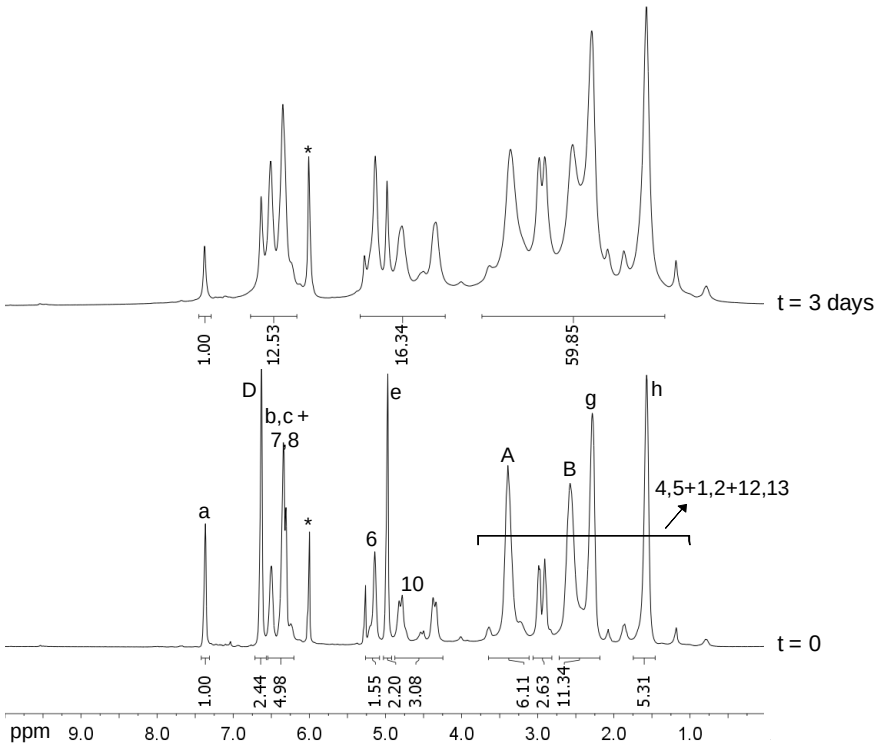

Figure 105. ^{1}H NMR spectra of the depolymerized *r* = 1.0 **I+XI** system heated at 65ºC for 3 days in *TCE-d_2. The top spectrum represents the second DA polycondensation. The peaks are labelled according to Figure 103.

4.1.3 Characterization of the A_2+B_3 polymers

The non-linear polymers **XXIV** (Figure 106) were precipitated in petroleum ether, filtered and washed with dichloromethane. The final products were then dried under vacuum and characterized in terms of structure, molecular weight and glass transition temperature.

The *r* = 1 and 0.75 systems gave mostly a *gel* fraction, and little or no *sol*. After drying, the swollen gel became a very stiff solid. For *r* = 0.5, the final product was a glassy polymer, since the critical crosslinking point was not reached.

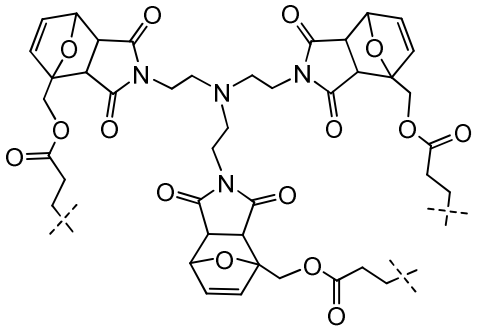

Figure 106. Structure of the non-linear polymer **XXIV**.

Their FTIR spectrum (Figure 107) confirmed the presence of the adduct moieties by the presence of their characteristic bands at 1756, 1718, 1690, 1016, 980, 879, 726, 643, 583 cm^{-1}, as well as by the absence of the characteristic furan and maleimide ring bands (as discussed above for the linear and model system) [179,189,191].

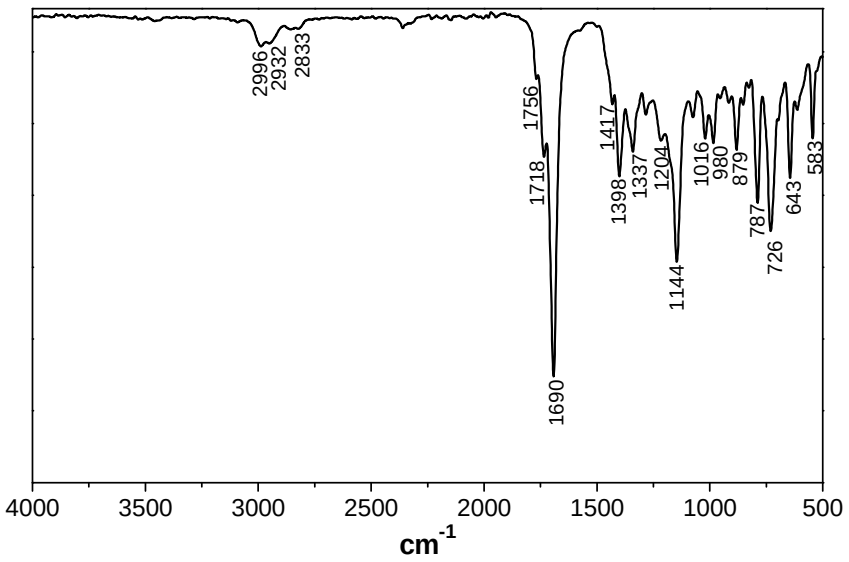

Figure 107. FTIR-ATR Spectrum of the non-linear DA polymers **XXIV**.

As in the linear **I**+**IX** system (Scheme 13), the retro-DA depolymerization of these systems was studied following a strategy which avoided the return to the network structure after its decrosslinking [189,190]. Thus, a fraction of polymer **XXIV**, either *sol* or *gel*, was depolymerised at 110ºC for 24 hours and allowed to cool to 65ºC, after adding a tenfold

excess of the DMFu DA trap. The solution was left to react at that temperature for a further 24 hours before vacuum removing the unreacted DMFu and part of the solvent.

As expected, the ^{1}H NMR spectrum of the ensuing mixture was similar to that obtained for the difunctional linear system (Figure 88), namely it displayed the resonances of monomer **I**, viz. the furan protons at δ 7.4 (H-a), 6.4 (H-c) and 6.3 (H-b) ppm, and the methylene ones of the furfuryl moiety (H-e) at 5.0 ppm, together with those of the **IX**-DMFu trisadduct, namely the adduct protons at δ 6.3 (H-3,H-4) and 2.8 (H-6) ppm and the methyl groups at δ 1.7 ppm [179,189,191,243], thus confirming the efficiency of the retro-DA depolymerisation in the regeneration of the starting monomers.

DSC analysis yielded no clear-cut evidence of a Tg in the temperature range -90ºC to 80ºC for all these polymers. This was interpreted as a confirmation of the high Tg associated with such rigid and highly branched macromolecular structures.

Additionally, the SEC tracing of *r* = 0.5 system (the only fully soluble polymer) shows the presence of cyclic oligomers (Figure 108), which leads to a lower polymer molecular weights (Table 21), as discussed above for the linear polymers.

Table 21. DSC and SEC results for non-linear polymers **XXIV**.

polymer	*r*	Mw	Mn	PD = Mw/Mn
XXIV	0.5	9622	5533	1.74

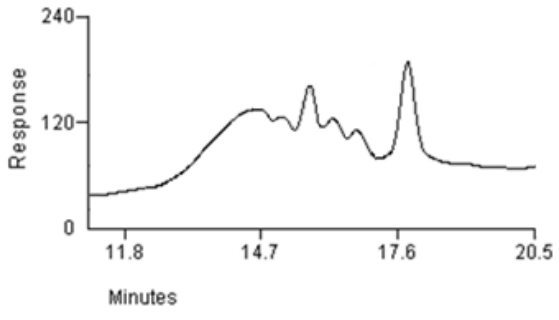

Figure 108. SEC tracing for *r* = 0.5 **I**+**XI** system.

4.2 $A_3 + B_2$ SYSTEMS

The second non-linear DA polymerization involves the reverse combination of a bismaleimide reacting with a trisfuran monomer, viz. A_3+B_2 system. In this case, two trisfuran monomers, viz. **VI** and **VII**, were used, and each one was reacted with the bismaleimide **IX** (Scheme 17).

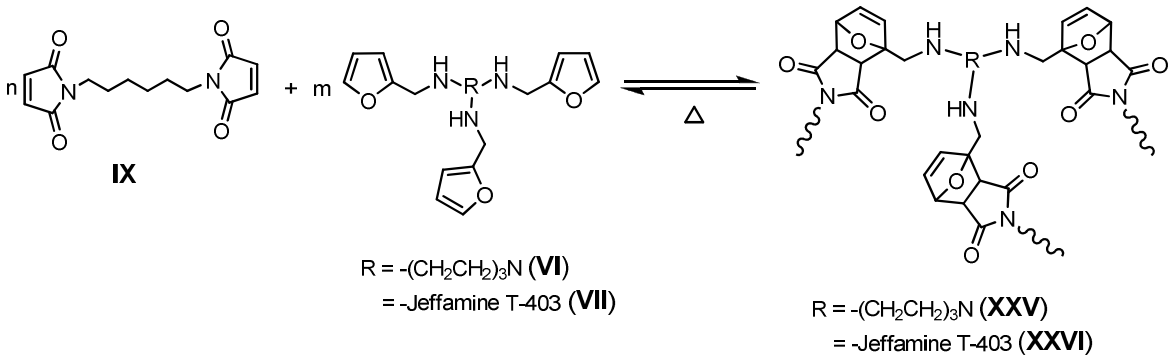

Scheme 17. Non-linear DA polycondensation between a trisfuran (**VI** or **VII**) and bismaleimide **IX**.

Three different [maleimide]/[furan] functional ratios *r*, viz. 1.0, 0.75 and 0.50, were also used here (Table 19). The monomer initial concentrations were the same as those used in the previous non-linear system (Table 20); however, in this case, it was the concentration of the bismaleimide **IX** that was kept the same in all the experiments.

4.2.1 UV spectroscopy

The non-linear **VI**+**IX** and **VII**+**IX** polymerizations, performed according to the different function molar ratios *r*, viz. 1, 0.75 and 0.5, were followed by UV spectroscopy at 65ºC in TCE. Again, due to their high concentration for UV measurements, a fivefold dilution of the original mixtures (Table 20) was made.

In this case, the concentration of the bismaleimide **IX** is the same for the three reactions, and as expected, its UV spectrum showed a characteristic maximum at around 300 nm.

The evolution of the DA reactions was then followed by monitoring the progressive decrease in the intensity of the maleimide peak. Figure 109 shows the progress of the non-linear **VI**+**IX** and **VII**+**IX** polymerizations under stoichiometric conditions, viz. r = 1. The other reactions gave this same behaviour pattern. Again, the presence of the characteristic isosbestic point at ~260 nm, common to all the experiments, clearly indicates that the formation of the DA adducts were not accompanied by any side reaction.

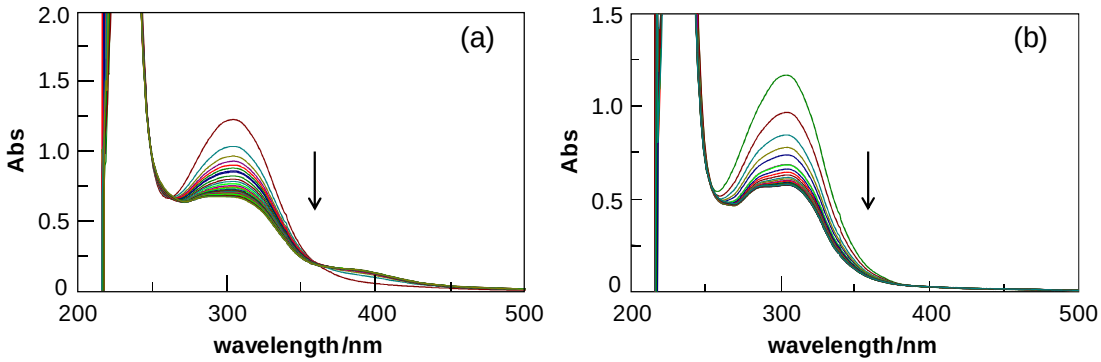

Figure 109. UV spectra of the DA evolution of the systems (a) **VI**+**IX** and (b) **VII**+**IX** with r = 1, at 65ºC in TCE with an optical path of 0.01 cm. Spectra were taken every hour during 24 h.

4.2.2 NMR spectroscopy

The DA progress of the non-linear **VI**+**IX** (Scheme 18) and **VII**+**IX** (Scheme 19) systems, with molar ratios r = 1.0, 0.75 and 0.5, was also followed by ^{1}H NMR spectroscopy in TCE-d_2 at 65ºC, using the initial monomer concentrations given in Table 20.

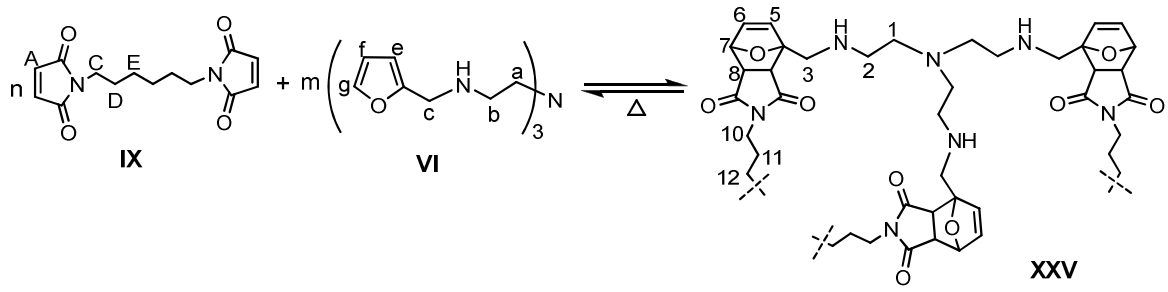

Scheme 18. Non-linear DA **VI**+**IX** polymerization.

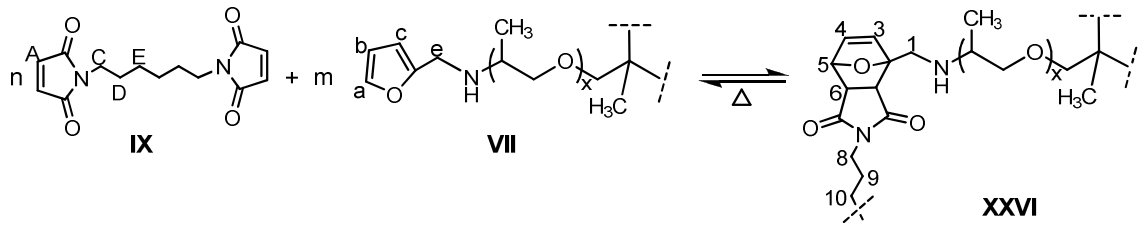

Scheme 19. Non-linear DA **VI**+**IX** polymerization.

These systems displayed features similar to that described for the previous non-linear system. Figure 110 and 111 show the changes with time of the DA polymerizations **VI**+**IX** and **VII**+**IX**, respectively, under stoichiometric conditions, viz. r = 1.0. In these set of spectra, apart from the progressive increase in the signals associated with the adduct protons and the corresponding decrease of those attributed to the unreacted furan and maleimide cycles (as discussed above for the other non-linear system), the other relevant phenomenon is the considerable widening of all resonances reflecting the considerable increase in molecular weight. Indeed, the last spectra were taken well after the formation of the network, i.e. a mixture of crosslinked (*gel*) and branched (*sol*) macromolecules, and of course only the latter species were detected and displayed in these spectra.

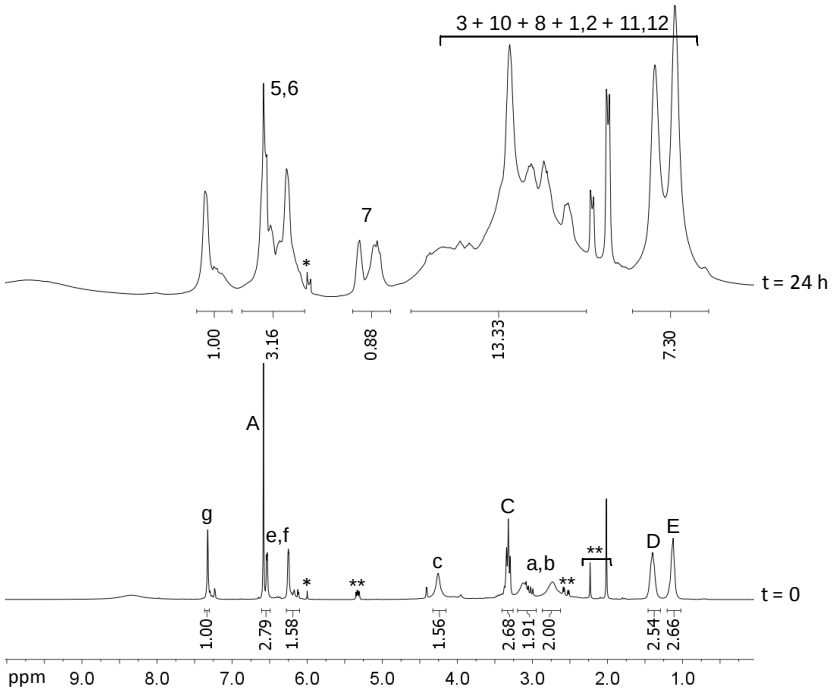

Figure 110. ^{1}H NMR spectra of the evolution of non-linear system **VI**+**IX** for r = 1, at 65ºC in *TCE-d_2 (**unknown impurities). The peaks are labeled according to Scheme 18.

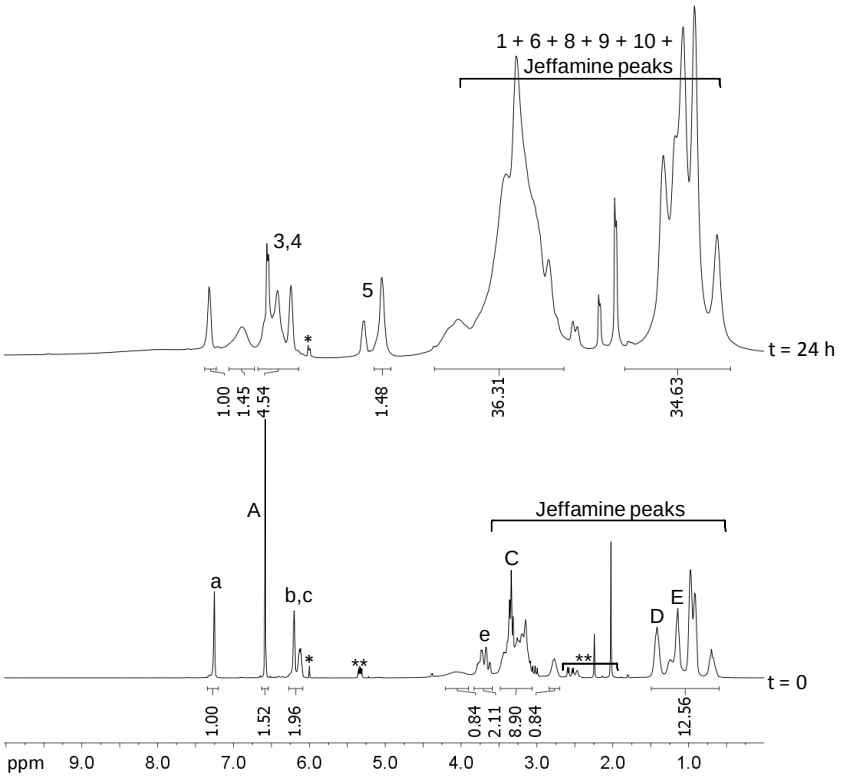

Figure 111. ^{1}H NMR spectra of the evolution of the non-linear ssytem **VII**+**XI** for *r* = 1, at 65ºC in *TCE-d_2 (**unknown impurities). The peaks are labeled according to Scheme 19.

As expected, a progressive increase in the medium viscosity accompanied these reactions, and a gelled material was formed for molar rations *r* = 1.0 and 0.75, whereas for *r* = 0.5, the reaction produced a highly viscous solution.

After these polymerizations, all the solutions were heated at 110ºC and their ^{1}H NMR spectra, taken after 24 hours at that temperature, confirmed the occurrence of the retro-DA depolymerisation. Thereafter, these same systems were allowed to cool to 65ºC and kept at that temperature for 3 days, and a second DA polymerization occurred. Figure 112 shows the ^{1}H NMR spectra taken after the retro-DA depolymerisation and the second DA reactions for the *r* = 1 **VI**+**IX** system. When the temperature was raised above 100ºC, the adduct peaks intensity progressively decreased, and correspondently those attributed to the initial reagents increased, as discussed above. Conversely, the reverse sequence was observed when the system was returned to 65ºC.

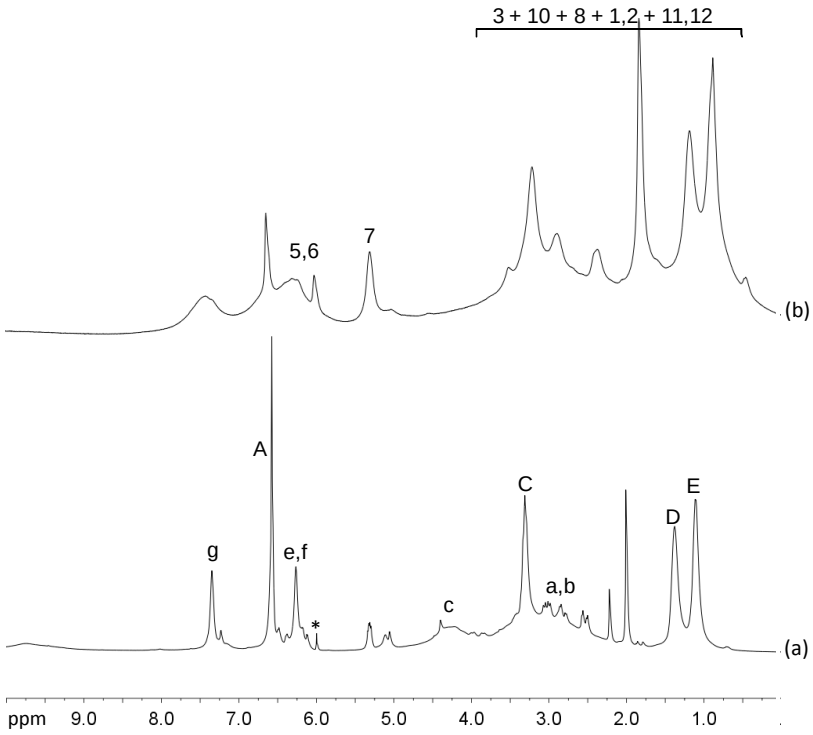

Figure 112. ^{1}H NMR spectra in *TCE-d_2 of the (**a**) depolymerized **VI**+**IX** system (r = 1.0) after the retro-DA reaction at 110ºC for 24 h, and the (**b**) corresponding solution taken after cooling the system again to 65ºC and keeping it at that temperature for 3 days, viz. second DA polycondensation. The peaks are labeled according to Scheme 18.

Concurrently, the retro-DA reactions were accompanied by a progressive dissolution of the gels and the subsequent decrease in the medium viscosity, leading to less viscous liquids, whereas cooling the systems again, allowed the returned to their initial high-viscosity and gel formation for the appropriate r values. Once again, the thermal reversibility and reproducibility of DA/retro-DA cycles was unambiguously confirmed.

4.2.3 Characterization of the A_3+B_2 polymers

Both non-linear polymers **XXV** (Scheme 18) and **XXVI** (Scheme 19) were precipitated in petroleum ether, filtered and washed with dichloromethane. Then, the ensuing products were dried under vacuum and characterized in terms of structure, molecular weight, and glass transition temperature, whose results are indicated in Table 22.

After drying, the gelled materials resulting from **XXV**, with both *r* = 1 and 0.75 became stiff solids, whereas the final product for *r* = 0.5 was a glassy polymer. For polymers **XXVI**, no gel was observed for the three molar ratios and the isolated polymers were rather soft materials. This can be explained by the lack of intermolecular organization in polymer **XXVI**, due to the specific irregular structure of the Jeffamine backbone.

As expected, the characteristic adduct bands, namely at 1756, 1718, 1690, 1016, 980, 879, 726, 643, 583 cm^{-1}, were observed in the FTIR spectrum of these polymers, whereas those characteristic of the furan and maleimide rings were absent (as discussed above for the linear and model system) [179,189,191].

DSC analyses of **XXV** yield no Tg value in the temperature range -90ºC to 80ºC for the three molar ratios, using either gel or sol fractions (Table 22). This suggests that their Tg was above 80ºC, which seems reasonable in view of their compact, stiff and highly branched macromolecular structure. For polymer **XXVI**, the Tg values fell around room temperature, i.e. much lower than those of polymers **XXV**, in agreement with the more flexible structure of the bridges.

Table 22. DSC and SEC results for non-linear polymers **XXV** and **XXVI**.

polymer	*r*	Tg /ºC	Mw*	Mn*	PD = Mw/Mn
XXV	1.0	n.d.	3950	3390	1.16
	0.75	n.d.	4620	3890	1.19
	0.5	n.d.	4750	3970	1.20
XXVI	1.0	18	6560	3970	1.65
	0.75	25	7070	4410	1.60
	0.5	25	7220	4410	1.64

(n.d.: not detected in the range -90 to 80ºC) (**sol* fraction)

The SEC tracings of the soluble portions of polymers **XXV** exhibited sharp peaks within the continuous trace, suggesting the presence of individual cyclized oligomers, together with the mixture of branched macromolecules. This explains the relatively low average values of molecular weights given in Table 22, and the equally low PD values, associated with the fact that those individual oligomers have a PD of unity by definition. Interestingly, the overall PD values for polymers **XXV** are quite low, approaching unity, in tune with the important contribution of cyclic structures, whereas those for the **XXVI**

counterparts are around 1.6, indicating that the proportion of cyclic oligomers is less important, as indeed expected for their more irregular architecture. Notwithstanding these comparisons, both sets of materials obviously contain a significant proportion of cyclic structures, since in their absence, the PD values would have been higher than 2, given the non-linear character of all these systems.

4.3 AB_2 SYSTEM

As already mentioned, the use of an asymmetrically substituted monomer, viz. AB_n or A_nB (with $n > 1$), allows the preparation of hyperbranched macromolecular structures that do not crosslink. In this study, the previously synthesized AB_2-type monomer **XVII** was used as a source of such type of polymer (Scheme 20).

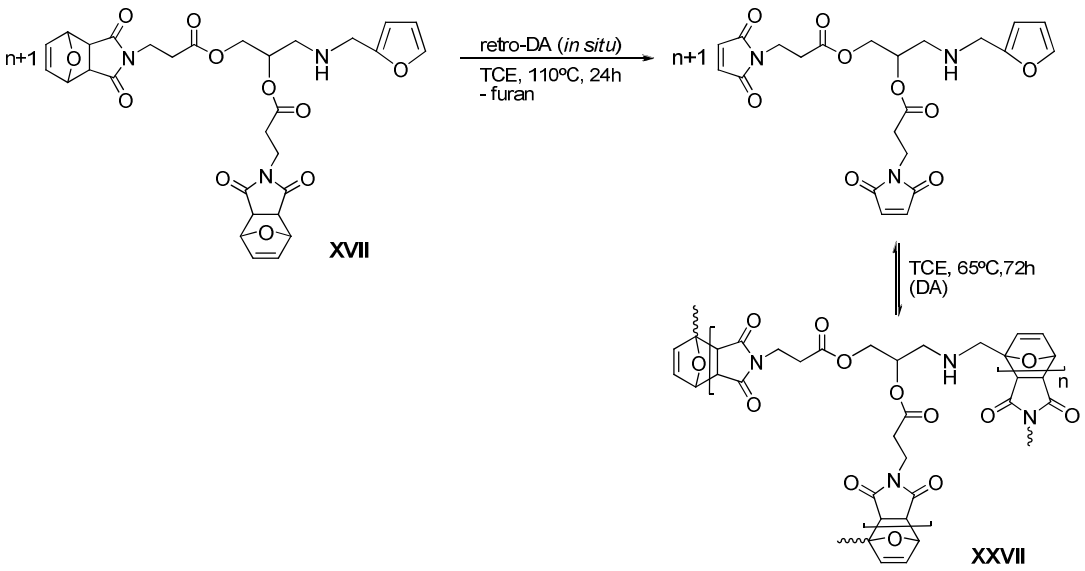

Scheme 20. Deprotection of the AB_2-type monomer, **XVII**, and its non-linear DA polymerization.

4.3.1 UV spectroscopy

The AB_2 polymerization (Scheme 20) was followed by UV spectroscopy in TCE at 65ºC, with initial concentration of 0.1 M. As expected, the initial solution did not show any maximum absorption, since the maleimide moieties were protected. However, when the *in*

situ deprotection by the retro-DA reaction at 110ºC for 24 hours was applied, the UV spectrum displayed the characteristic maleimide peak at ~300 nm.

After cooling the system to 65ºC, the DA polymerization was promoted, and its evolution monitored by the progressive decrease of the maleimide peak intensity, as shown in Figure 113. The presence of the characteristic isosbestic point indicates that the formation of the DA adducts were not accompanied by any side reaction.

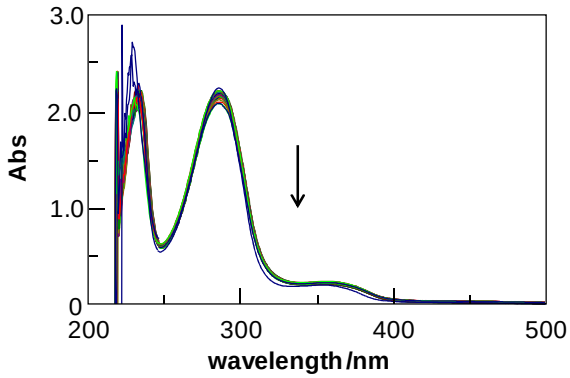

Figure 113. Typical initial decrease in the maleimide peak absorbance, reflecting the DA polymerization of monomer **XVII**, in TCE at 65ºC. Spectra were taken every hour during 24 h with an optical path of 0.01 cm.

4.3.2 NMR spectroscopy

Concurrently, the AB_2 polymerization was also followed by ^1H NMR spectroscopy at 65ºC in TCE-d_2, using a 0.1 M **XVII** solution. As in UV measurements, first the monomer underwent the retro-DA reaction (110ºC for 24 hours under N_2) and thereafter, its DA reaction by cooling the system to 65ºC. Figure 114 shows the NMR spectra taken before and after the *in situ* deprotection of **XVII**.

Apart from traces of residual DCU (δ 1.0-2.0 ppm) and evidence of the incipient polymerization, the spectrum of the unprotected monomer confirms its structure due to the presence of the maleimide C*H*=C*H* protons at δ 6.7 ppm, as well as the disappearance of the adduct peaks at δ 6.5 (H-7''), 5.2 (H-6'') and 2.8 (H-5'') ppm [179,189,191].

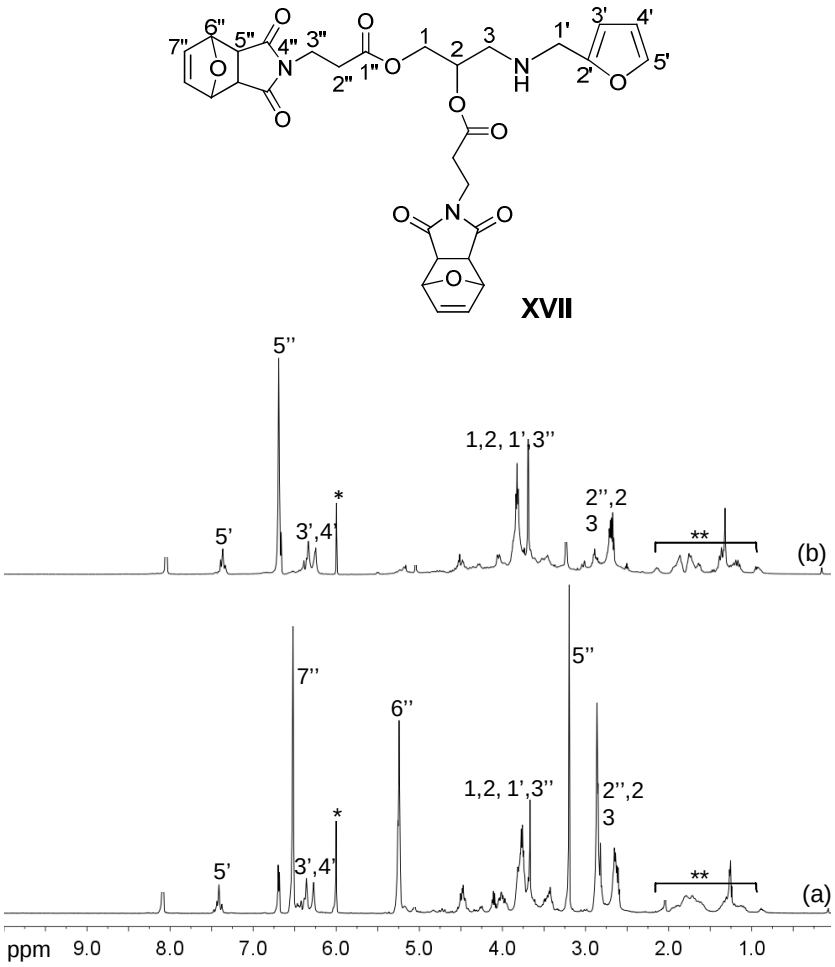

Figure 114. ^{1}H NMR spectra of monomer **XVII** in *TCE-d_2, (**a**) before and (**b**) after the *in situ* deprotection of the maleimide moieties by the retro-DA reaction (**traces of DCU).

The progress of the non-linear DA polycondensation of unprotected **XVII** is illustrated in Figure 115. The spectrum taken at t=0 is related to the monomer solution after its *in situ* deprotection by the retro-DA reaction. The expected pattern is observed, namely the progressive decrease of in the peak intensity of the monomer's relevant protons and the corresponding increase in that of the peaks related to the corresponding formation of the adducts, as discussed above.

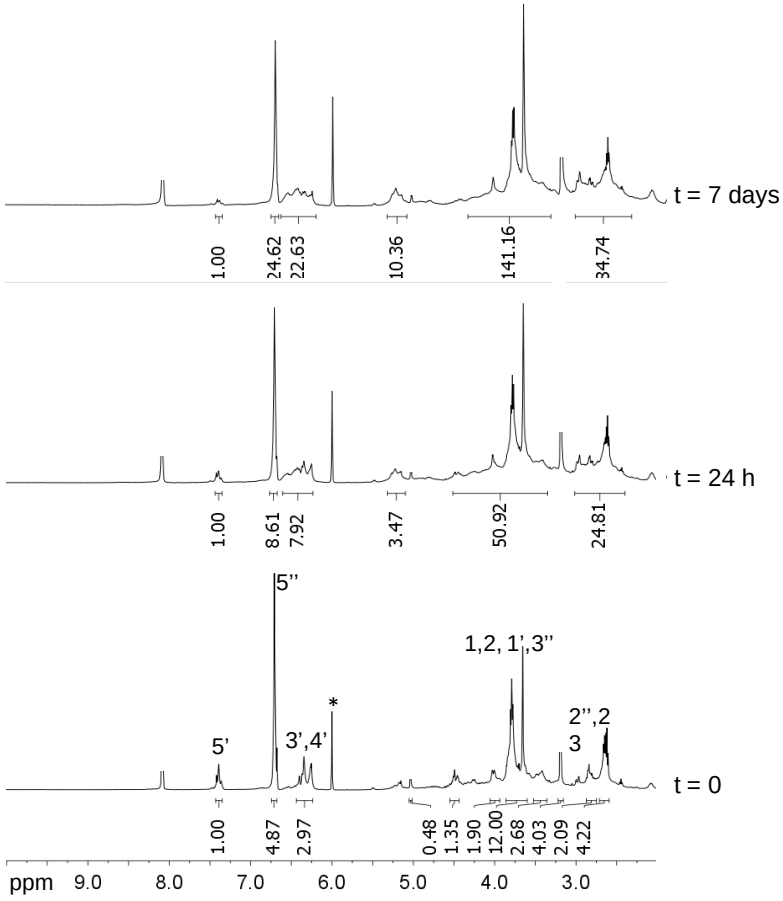

Figure 115. Time evolution of the ^{1}H NMR spectrum for the DA polimerization of 0.1 M **XVII** solution at 65ºC in *TCE-d_2. The initial spectrum (t = 0), taken at room temperature, corresponds to the unprotected AB_2 structure.

After reaching the equilibrium, the retro-DA reaction of this system was followed by ^{1}H NMR spectroscopy at 110ºC for 24 hours. Again, the expected behaviour is observed, viz. decrease of the adducts signals to the detriment of the corresponding growth of the unreacted furan and maleimide moieties (Figure 116). Thereafter, the systems were allowed to cool again to 65ºC, and left for three more days. The equilibrium was re-established and the systems thus returned to the initial state, with recovery of the polymer (Figure 116).

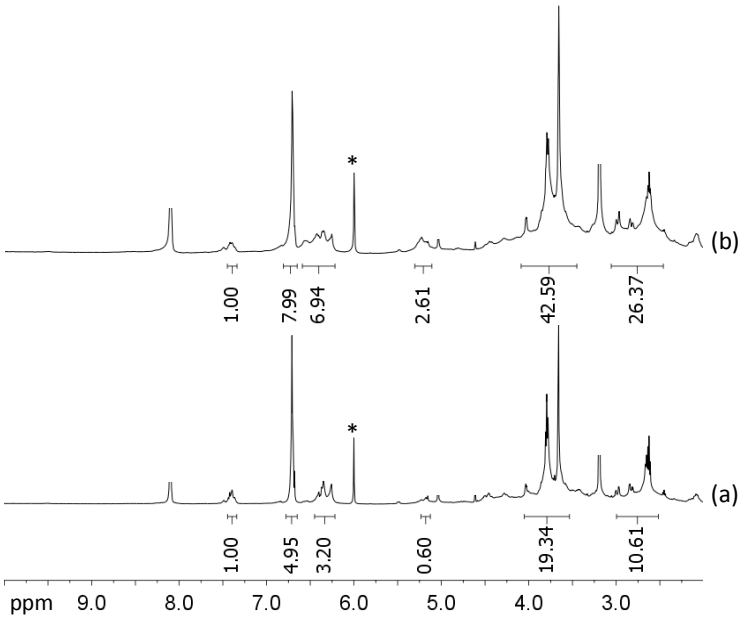

Figure 116. ^{1}H NMR spectra of the (**a**) depolimerized AB_2-polymer **XXVII** by retro-DA reaction (110ºC, 24 h) and (**b**) its second DA polimerization at 65ºC, in *TCE-d_2

4.3.3 Characterization of the AB_2 polymer

The hyperbranched polymer **XXVII** (Scheme 20) was precipitated in an excess of petroleum ether, dried under vacuum and then characterized by DSC and SEC (Table 23). Its thermogram displays a Tg around 58 ºC, in tune with the rather rigid polymer structure (Figure 117). The SEC tracing of this polymer suggests the presence of cyclic oligomers, together with the mixture of hyperbranched macromolecules, which can explain the relatively low polymer molecular weight (Table 23) and PD value.

Table 23. DSC and SEC results for non linear polymer **XXVII**.

polymer	Tg /ºC	Mw	Mn	PD = Mw/Mn
XXVII	58	5650	2360	2.4

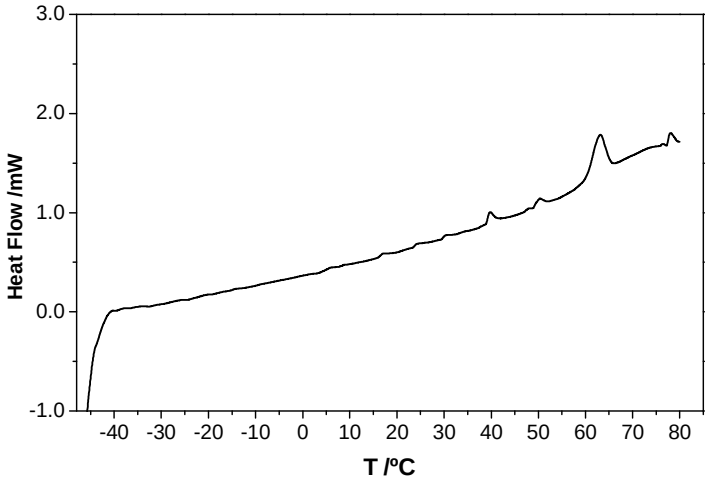

Figure 117. DSC thermogram for polymer **XXVII**.

4.4 CONCLUSIONS

The non-linear polymerization studied here, namely A_2+B_3 and A_3+B_2, displayed the same behaviour pattern. In general, the reactions conducted with r = 1.0 produced the most rapid thickening and gel formation within a few days, while their counterpart with r = 0.75 displayed similar features, albeit in a slower mode, and the reduction of r to 0.50 only showed a slow progressive increase in viscosity without attaining a gel point, which is in tune with the fact that crosslinking would only be reached at 100% conversion in the absence of ring formation. Thus, the use of complementary moiety stoichiometry produced a gel (network), whereas as the relative amount of trifunctional monomer was decreased, the reactions stopped short of crosslinking, i.e. gave soluble highly branched polymers.

Although, the viscosity was not measured, it was possible to control visually its change, that is, the solution viscosity increased during the DA reaction, and decreased during the retro-DA reaction.

As expected, the results obtained from both UV and ^{1}H NMR studies for these non-linear systems corroborated the feasibility of multiple DA/retro-DA cycles.

Although the DA polycondensation involving the assymmetrically substituted AB_2 monomer was only a preliminary study, the results obtained were promising**.** Obviously much remains to be done to unravel its features as well as to obtain and characterize the ensuing materials.

As in the linear systems, the use of relatively low concentrations (<1M) led to cyclization, which influenced negatively the final non-linear polymer molecular weights, as well as lowered their Tg values.

PART IV

EXPERIMENTAL

1 REAGENTS AND EQUIPMENT

The commercially available compounds and solvents were used without further purification; except in the cases where an anhydrous solvent was required. The solvent drying was carried out as described in the literature [262]. Thin-layer chromatography was applied with Merck silica gel 60 F_{254} and column chromatography called upon Merck silica gel 60, 170–230 mesh.

The monomers' structures were characterized by FTIR, NMR spectroscopy, mass spectrometry, and melting point, when applicable. Their intermediate structures were only characterized by FTIR and NMR.

FTIR spectra were recorded with a Mattson 7000 galaxy series spectrophotometer working in the ATR mode. UV spectra were taken with a temperature controlled Jasco V-560 spectrophotometer using 1 cm Hellma Suprasil cells equipped with 9.9 mm quartz spacers and a quartz-to-pyrex graded seal. Most of the ^{1}H and ^{13}C NMR spectra were acquired with a Bruker Avance 300 spectrometer working at 300.13 MHz and 75.47 MHz, respectively; others, properly indicated in the text, were acquired with a Bruker Avance 500 spectrometer working at 500.13 MHz and 125.76 MHz, respectively. TMS was used as internal standard.

DSC experiments were performed in a Power Compensation Dynamic Scanning Calorimeter, Perkin Elmer Diamond DSC, using a scanning rate of 10ºC/min both when heating and cooling, in a temperature range from -90 to 200ºC, adapted to the specific sample. The equipment calibration was performed with In and Pb standards. The software used was Pyris v.7.0.0.0110 2004. The Tg values were approximated to the closest degree, as the standard practice for polymers.

The determinations of polymers molecular weights and their distributions by size-exclusion chromatography (SEC) were performed in a Varian PL-GPC 110 equipped with an IR-PD 2020 light scattering detector. THF, DMF and DMA were used as solvents. The samples' concentration was about 6 mg/mL. A calibration curve was obtained with five

polystyrene standards (1mg/mL) in a narrow-range of molecular weights comprised between 1700 and 66000.

HRMS analyses were performed at the “C.A.C.T.I. - Unidad de Espectrometría de Masas”, University of Vigo, Spain, on a Bruker Daltonics APEX-Qe FT-ICR mass spectrometer, equipped with an actively shielded 7 T superconducting magnet, and a Combi MALDI-ESI source. Sample ionization was achieved by electrospray (ESI), using a voltage of 4500 V applied to the needle, and a counter voltage of 300 V applied to the capillary. A mixture of methanol/water containing 0.01% of formic acid 70:30 (v/v) was used as the carrier solvent. Data acquisition was performed using the ApexControl 3.0.0 software, and data processing used the Data Analysis 4.0 software.

2 SYNTHESIS OF FURAN MONOMERS

2.1 AA MONOMERS

Synthesis of difurfuryl adipate (I)

The first AA monomer was obtained by adding dropwise a solution of adipoyl chloride (1 g, 5.5 mmol) to a stirred solution of furfuryl alcohol (1.08 g, 11.0 mmol) and triethylamine (1.53 mL, 11.0 mmol) in dichloromethane (10 mL) under a gentle stream of dry nitrogen, while keeping the temperature of the medium close to 0ºC for 3 hours. An intense exothermic reaction was observed. The ensuing solution was extracted with water and the organic fraction dried over sodium sulphate before removing the volatile components. The oily residue was purified by column chromatography on SiO_2, eluting with petroleum ether/ethyl acetate 1:1 v:v. The final product (**I**) was obtained as a brown viscous liquid with a yield of 82% [178]. The final product was store in a refrigerator.

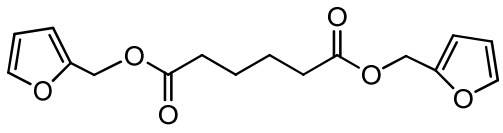

I

I: Tg = -63.4ºC (DSC). **^{1}H NMR** (300MHz, $CDCl_3$, TMS) δ/ppm: 7.42 (dd; *J* =2.0, 0.8 Hz; 1H; furan H-5'), 6.40 (d; *J* =3.3 Hz; 1H; furan H-3'), 6.36 (dd; *J* =3.3, 1.8 Hz; 1H; furan H-4'), 5.06 (s; 2H; furan-2-C$\underline{H_2}$), 2.34 (m; 2H; CC$\underline{H_2}$), 1.65 (m; 2H; $CCH_2C\underline{H_2}$). **^{13}C NMR** (75MHz, $CDCl_3$, TMS) δ/ppm: 172.85 (C=O), 149.40 (furan C-2'), 143.19 (furan C-5'), 110.54, 110.48 (furan C-3', C-4'), 57.90 (furan-2-$\underline{C}H_2$), 33.61 ($C\underline{C}H_2$), 24.13 ($CCH_2\underline{C}H_2$). **FTIR-ATR** (cm^{-1}): 3117, 2931, 2862, 1732, 1589, 1504, 1454, 1381, 1350, 1226, 1141, 1010, 918, 813, 736, 597. **ESI - HRMS** for $C_{16}H_{18}O_6Na$ $[M+Na]^+$: *m/z* calcd: 329.09956; found: 329.09926 [error: 0.9 ppm].

Synthesis of N,N'-difurfuryl-4,7,10-trioxa-1,13-tridecanediamine (III)

The second AA monomer was synthesized in two steps, namely synthesis of a Schiff base derivative and its *in situ* reduction, following an already reported procedure [249,250] with some modifications.

i) *Synthesis of the Schiff base* II: In a round-bottom flask kept under N_2, were introduced 10 mL of methanol (absolute), 2.3 mmol of 4,7,10-trioxa-1,13-tridecanediamine (0.51 g) and a molar excess of 20% of furfural (0.53 g). The mixture was stirred for 5 hours at room temperature. In a first experiment, in order to characterize this structure by NMR and FTIR, the solvent was evaporated and the ensuing product dried under vacuum, with the subsequent elimination of the excess of furfural.

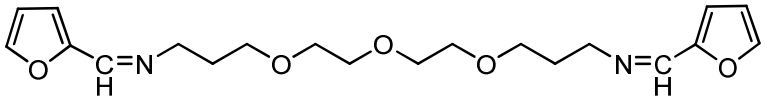

II

II: **^{1}H NMR** (300MHz, $CDCl_3$, TMS) δ/ppm: 8.10 (s; 1H; C*H*=N), 7.50 (d; *J* =1.6 Hz; 1H; furan H-5'), 6.72 (d; *J* =3.4 Hz; 1H; furan H-3'), 6.46 (dd; *J* =3.4, 1.8 Hz; 1H; furan H-4'), 3.51-3.68 (m; 8H; =NC*H*$_2$, (OC*H*$_2$)$_3$), 2.0 (quintet; *J* =6.5 Hz; 2H; $CH_2CH_2CH_2$). **^{13}C NMR** (75MHz, $CDCl_3$, TMS) δ /ppm: 151.45 (furan C-2), 150.05 (*C*H=N), 144.59 (furan C-5), 113.70, 111.04 (furan C-3, C-4), 70.51, 70.07 (O*C*H$_2$*C*H$_2$O), 68.69 (*C*H$_2$OCH$_2$), 58.20 (=N*C*H$_2$,), 30.54 ($CH_2CH_2CH_2$). **FTIR-ATR** (cm^{-1}): 3109, 2916, 2862, 1643, 1585, 1481, 1469, 1396, 1357, 1269, 1099, 1014, 929, 879, 748, 594.

ii) *Reduction of the Schiff base*: The *in situ* reduction of the Schiff base **II** was conducted in methanol with an excess of sodium borohydride (0.18 g, 4.6 mmol). After approximately 2 hours (when the H_2 release had stopped), the solution was concentrated and chloroform was added. This solution was left overnight, while a precipitate accumulated. After filtration and extraction with water/chloroform, the organic fraction was dried with anhydrous sodium sulphate. The solvent was evaporated and the final product vacuum dried. The ensuing product (**III**) was obtained as a brown viscous liquid with an overall yield of 80%.

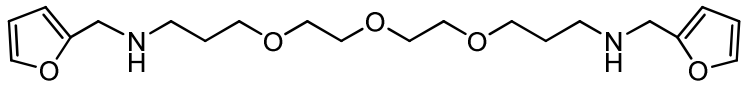

III

III: Tg = -70.8ºC (DSC). **^{1}H NMR** (300MHz, $CDCl_3$, TMS) δ/ppm: 7.35 (dd; *J* =1.6, 0.8 Hz; 1H; furan H-5'), 6.30 (dd; *J* =3.1, 1.9 Hz; 1H; furan H-4'), 6.16 (d, *J* =2.9 Hz; 1H; furan H-3'), 3.77 (s; 2H; furan-2-C$\underline{H_2}$), 3.66 – 3.48 (m; 6H; (OC$\underline{H_2}$)$_3$), 2.70 (t; *J* =6.9 Hz; 2H; NHC$\underline{H_2}$CH$_2$), 1.78 (quintet; *J* =6.6 Hz; 2H; NHCH$_2$C$\underline{H_2}$), 1.63 (bs; 1H; N*H*). **^{13}C NMR** (75MHz, $CDCl_3$, TMS) δ /ppm: 154.02 (furan C-2'), 141.65 (furan C-5'), 110.02 (furan C-4'), 106.69 (furan C-3'), 70.56, 70.15 (O$\underline{C}$H$_2\underline{C}$H$_2$O), 69.78 ($\underline{C}$H$_2$OCH$_2$), 46.48 (furan-2-$\underline{C}$H$_2$), 46.22 (NH$\underline{C}$H$_2$CH$_2$), 29.84 (NHCH$_2\underline{C}$H$_2$). **FTIR-ATR** (cm^{-1}): 3305, 3109, 2912, 2862, 1598, 1454, 1346, 1241, 1176, 1103, 1010, 914, 798, 740, 715, 597. **ESI -HRMS** for $C_{20}H_{33}N_2O_5$ $[M+H]^+$: *m/z* calcd: 381.23840; found: 381.23769 [error: 1.9 ppm].

2.2 A_3 MONOMERS

Synthesis of tris(N-furfuryl-2-aminoethyl)amine (VI) and N, N', N''-trisfurfuryl Jeffamine derivative (VII)

A_3 monomers were prepared according to the procedure described above for the bisfuran monomer **III** [249,250], using in this case trisubstituted amines as starting reagents.

i) ***Synthesis of the Schiff bases*** **IV** ***and*** **V:** In a round-bottom flask kept under N_2, were introduced 10 mL of methanol (absolute), 2.3 mmol of tris(2-aminoethyl)amine (0.34 g) or Jeffamine T-403 (1.10 g) and a 20% molar excess of furfural (0.80 g). The mixture was stirred for 5 hours at room temperature. In a first experiment, in order to characterize this structure by NMR and FTIR, the solvent was evaporated and the ensuing products dried under vacuum, with the subsequent elimination of the excess of furfural.

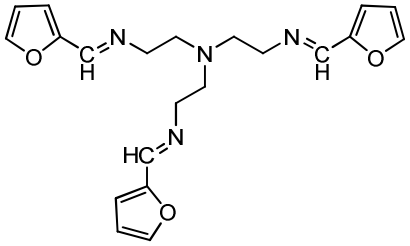

IV

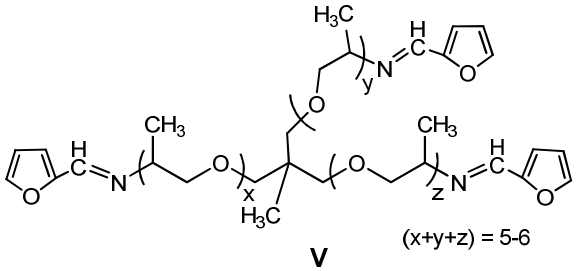

V

IV: **^{1}H NMR** (300MHz, $CDCl_3$, TMS) δ/ppm: 7.93 (s; 1H; C*H*=N), 7.49 (d; *J* =1.5 Hz; 1H; furan H-5'), 6.48 (d; *J* =3.4 Hz; 1H; furan H-3'), 6.44 (dd; *J* =3.4, 1.7 Hz; 1H; furan H-4'), 3.64 (t; *J* =6.0 Hz; 2H; $=NCH_2CH_2N$), 2.89 (t; *J* =6.4 Hz; 2H; $=NCH_2CH_2N$). **^{13}C NMR** (75MHz, $CDCl_3$, TMS) δ/ppm: 151.56 (furan C-2), 150.54 (*C*H=N), 144.49 (furan C-5), 113.79 (furan C-3), 111.47 (furan C-4), 59.70 ($=NCH_2CH_2N$), 55.29 ($=NCH_2CH_2CH_2N$). **FTIR-ATR** (cm^{-1}): 3108, 2940, 2883, 2836, 1643, 1568, 1482, 1439, 1388, 1346, 1269, 1153, 1060, 1012, 930, 816, 743, 595.

V: **^{1}H NMR** (300MHz, $CDCl_3$, TMS) δ/ppm: 8.13 (s; 1H; C*H*=N), 7.49 (s; 1H; furan H-5'), 6.70 (s; 1H; furan H-3'), 6.45 (s; 1H; furan H-4'), 3.77-2.89 (m; 9H; core jeffamine protons), 1.54 – 0.60 (m; 9H; core jeffamine protons). **^{13}C NMR** (75MHz, $CDCl_3$, TMS) δ/ppm: 151.47 (furan C-2'), 149.19 (*C*H=N), 144.53 (furan C-5'), 114.20 (furan C-3'), 111.43 (furan C-4'), 80-10 (core jeffamine carbons). **FTIR-ATR** (cm^{-1}): 3117, 2967, 2931, 2867, 1643, 1560, 1482, 1453, 1372, 1100, 1011, 930, 880, 818, 747, 596.

ii) *Reduction of the Schiff bases*: The *in situ* reduction of the Schiff bases **IV** and **V** was carried out in methanol with an excess of sodium borohydride (0.26 g, 6.9 mmol). After approximately 2 hours (when the H_2 release had stopped), the solution was concentrated and chloroform was added. This solution was left overnight, while a precipitate accumulated. After filtration and extraction with water/chloroform, the organic fraction was dried over anhydrous sodium sulphate. The solvent was evaporated and the final products dried under vacuum. Both ensuing products (**VI** and **VII**) were obtained as brown viscous liquids with overall yields higher than 90%.

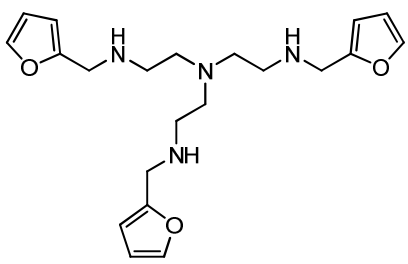

VI

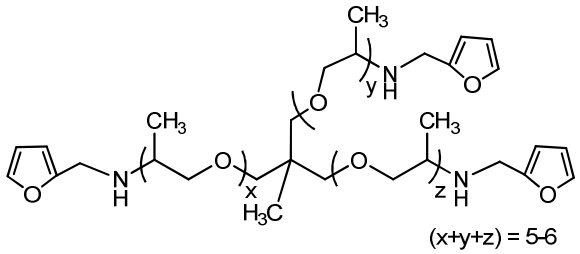

VII

VI: Tg = -61.6ºC (DSC). **^{1}H NMR** (300MHz, $CDCl_3$, TMS) δ/ppm: 7.33 (dd; *J* =1.8, 0.9 Hz; 1H; furan H-5'), 6.29 (dd; *J* =3.0, 2.1Hz; 1H; furan H-4'), 6.14 (d; *J* =3.2 Hz; 1H; furan H-3'), 3.78 (s; 2H; furan-2-C*H*$_2$), 2.68 (t; *J* =5.8 Hz; 2H; NHC*H*$_2$*C*H$_2$N), 2.56 (t; *J* =5.9 Hz; 2H; NHCH$_2$C*H*$_2$N), 2.06 (br s; 1H; N*H*). **^{13}C NMR** (75MHz, $CDCl_3$) δ/ppm: 153.87 (furan C-2'), 141.65 (furan C-5'), 110.04 (furan C-4'), 106.77 (furan C-3'), 54.22 (NHCH$_2$*C*H$_2$N), 46.69 (furan-2-*C*H$_2$), 46.05 (NH*C*H$_2$CH$_2$N). **FTIR-ATR** (cm^{-1}): 3305, 3113, 2923, 2819, 1590, 1504, 1452, 1384, 1330, 1192, 1146, 1051, 1008, 916, 880, 796, 728, 598. **ESI - HRMS** for $C_{21}H_{31}N_4O_3$ $[M+H]^+$: *m/z* calcd: 387.23907; found: 387.23855 [error: 1.3 ppm].

VII: Tg = -60.1ºC (DSC). **^{1}H NMR** (300MHz, $CDCl_3$, TMS) δ/ppm: 7.34 (s; 1H; furan H-5'), 6.29 (m; 1H; furan H-4'), 6.15 (m; 1H; furan H-3'), 3.80 ('*AB quartet*'; *J* =14.5Hz; 2H; furan-2-C*H*$_2$), 3.61 – 2.80 (m; 9H; core jeffamine protons), 1.46 – 0.71 (m; 9H; core jeffamine protons), 2.06 (bs; 1H; N*H*). **^{13}C NMR** (75MHz, $CDCl_3$, TMS) δ/ppm: 154.60 (furan C-2'), 142.09 (furan C-5'), 110.48 (furan C-4'), 106.95 (furan C-3'), 80-10 (core jeffamine carbons), 44.13 (furan-2-*C*H$_2$). **FTIR-ATR** (cm^{-1}): 3315, 3113, 2966, 2938, 2867, 1607, 1455, 1374, 1264, 1146, 1100, 1010, 917, 802, 730, 715, 599. **ESI - HRMS** for *(x+y+z)=5*, $C_{42}H_{72}N_3O_{10}$ $[M+CH_3]^+$: *m/z* calcd 778.52122; found: 778.52029 [error: 1.2 ppm]; for *(x+y+z)=6*, $C_{45}H_{78}N_3O_{11}$ $[M+CH_3]^+$: *m/z* calcd 836.56309; found: 836.56344 [error: -0.4 ppm].

3 SYNTHESIS OF MALEIMIDE MONOMERS

3.1 BB MONOMER

Synthesis of N,N'-hexamethylenebismaleimide (IX)

The monomer with two maleimide moieties was prepared in a two step-procedure, as follows [203,251]. A bismaleamic acid derivative was prepared using a diamine as precursor, followed by its intra-molecular cyclization, which originated the corresponding bismaleimide structure.

i) ***Synthesis of the N,N'-hexamethylenebismaleamic acid*** **(VIII):** One equivalent of 1,6-hexamethylenediamine (0.53 g, 4.5 mmol) in diethyl ether (20 mL) was added dropwise to two equivalents of maleic anhydride (0.88 g, 9.0 mmol) in diethyl ether (30 mL). The reaction mixture was stirred for 3 hours at room temperature and a further 3 hours under reflux. The ensuing white precipitate was filtered, washed with diethyl ether and dried [253]. The final product (**VIII**) was obtained as white solid with a yield of 87%.

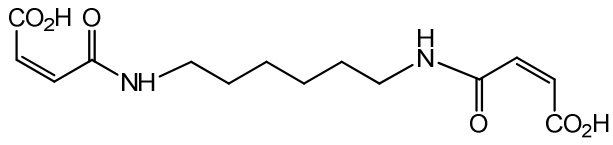

VIII

VIII: **^{1}H NMR** (300MHz, methanol-d_4, TMS) δ/ppm 6.43 (d; *J* =12.6 Hz; 1H; =C*H*), 6.26 (d; *J* =12.9 Hz; 1H; =C*H*), 3.31 (t; *J* =4.8 Hz; 2H; NHCH_2CH$_2$CH$_2$), 1.66 – 1.55 (m; 2H; NHCH$_2$CH_2CH$_2$), 1.45 – 1.40 (m; 2H; NHCH$_2$CH$_2$CH_2). **^{13}C NMR** (75MHz, $CDCl_3$, TMS) δ/ppm: 168.67, 167.71 (C=O$_{acid}$, C=O$_{amide}$), 134.14, 133.54 (*C*H=*C*H), 40.70 (NH*C*H$_2$CH$_2$CH$_2$), 29.70

($NHCH_2\underline{C}H_2CH_2$), 27.47 ($NHCH_2CH_2\underline{C}H_2$). **FTIR-ATR** ($cm^{-1}$): 3300, 3286, 3059, 2954, 2858, 1705, 1627, 1531, 1469, 1458, 1404, 1372, 1253, 1053, 956, 864, 786, 690, 632, 594.

ii) ***Intramolecular cyclization*****:** The bismaleamic acid **VIII** (1g), anhydrous sodium acetate (1.3 g) and acetic anhydride (15 mL) were stirred at 100ºC for 4-5 hours under a gentle stream of nitrogen. The ensuing mixture was poured onto cold water and the precipitate filtered, washed with water and dissolved in methylene chloride. This solution was again washed with water and the organic fraction dried over sodium sulphate. The solvent was removed under reduced pressure and the ensuing residue washed with toluene (3x10mL). The brown solid thus isolated was purified by column chromatography on SiO_2 and eluting with petroleum ether/ethyl acetate 1:2 v:v [253]. The final product (**IX**) was obtained as a white solid with a yield of 44%.

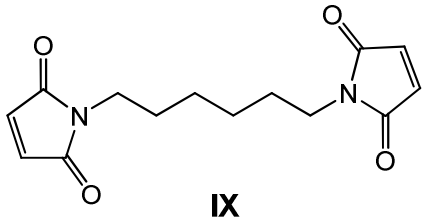

IX

IX: m.p. = 115.5ºC (DSC). **^{1}H NMR** (300MHz, $CDCl_3$, TMS) δ/ppm: 6.69 (s; 2H; C$\underline{H}$=C$\underline{H}$), 3.50 (t; *J* =7.2 Hz; 2H; NHC$\underline{H}_2CH_2CH_2$), 1.60 – 1.52 (m; 2H; $NCH_2C\underline{H}_2CH_2$), 1.32 – 1.27 (m; 2H; $NCH_2CH_2C\underline{H}_2$). **^{13}C-NMR** (75MHz, $CDCl_3$, TMS) δ/ppm: 170.85 ($C=O_{maleimide}$), 134.02 ($\underline{C}H=\underline{C}H$), 37.66 ($N\underline{C}H_2CH_2CH_2$), 28.32 ($NCH_2\underline{C}H_2CH_2$), 26.14 ($NHCH_2CH_2\underline{C}H_2$). **FTIR-ATR** ($cm^{-1}$): 3088, 2938, 2857, 1747, 1687, 1450, 1405, 1368, 1326, 1129, 853, 782, 695, 597. **ESI – HRMS** for $C_{14}H_{17}N_2O_4$ $[M+H]^+$: *m/z* calcd: 277.11828; found: 277.11839 [error: -0.4 ppm].

3.2 B_3 MONOMER

Synthesis of tris(2-maleimidoethyl)amine (XI)

The trismaleimide monomer was prepared according to a two-step procedure previously described in the literature, with some modifications [258,263].

i) ***Synthesis of the tris(2-(exo-3,6-epoxy-1,2,3,6-tetrahydrophthalimido)ethyl)amine*** **(X):** Tris-(2-aminoethyl)amine (3.96 g, 27.1 mmol) was added dropwise to a solution of *exo*-3,6-epoxy-1,2,3,6-tetrahydrophthalic anhydride (furan-maleic anhydride Diels-Alder adduct) (13.5 g, 81.3 mmol) in methanol (250 mL). The solution was stirred at 56ºC for 3 days and a precipitate formed progressively. The suspension was filtered and the pale yellow solid residue washed with methanol. The final product (**X**) was dried under vacuum and obtained with a yield of 50%.

ii) ***Deprotection of the maleimide groups by retro-Diels-Alder:*** The retro-DA was applied to the final product with the purpose of unprotecting the maleimide groups. A solution of **X** (2.12 g, 3.6 mmol) in toluene (250 mL) was heated to reflux during 24 hours. The solvent was then removed under reduced pressure and the ensuing yellow solid washed with *n*-hexane. The final product (**XI**) was dried under vacuum and obtained with a yield of 96%.

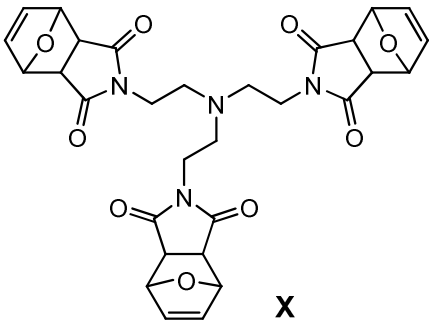

X

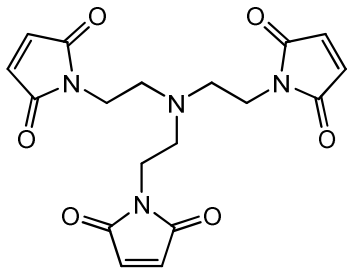

XI

X: **^{1}H NMR** (300MHz, $CDCl_3$, TMS) δ/ppm: 6.51 (s; 1H; =C*H*CHCH), 5.21 (s; 1H; =CHC*H*CH), 3.42 (t; *J* =5.8 Hz; 1H; $N_{maleimide}C\underline{H_2}CH_2N$), 2.91 (s; 1H; =CHCHC*H*), 2.60 (t; *J* =5.9 Hz; 1H; $N_{maleimide}CH_2C\underline{H_2}N$). **^{13}C NMR** (75MHz, $CDCl_3$, TMS) δ/ppm: 176.46 ($C{=}O_{maleimide}$), 136.47 (=*C*HCHCH), 80.68 (=CH*C*HCH), 51.62 ($N_{maleimide}\underline{C}H_2CH_2N$), 47.67 (=CHCH*C*H), 36.92 ($N_{maleimide}CH_2\underline{C}H_2N$). **FTIR-ATR** ($cm^{-1}$): 3017, 2957, 2835, 1767, 1687, 1415, 1401, 1344, 1148, 1018, 877, 851, 802, 723, 645, 595.

XI: m.p. = 167.7ºC (DSC). **^{1}H NMR** (300MHz, $CDCl_3$, TMS) δ/ppm: 6.68 (s; 2H; C*H*=C*H*), 3.52 (t; *J* =6.6 Hz; 2H; $N_{maleimide}C\underline{H_2}CH_2N$), 2.71 (t; *J* =6.6 Hz; 2H; $N_{maleimide}CH_2C\underline{H_2}N$). **^{13}C NMR** (75MHz, $CDCl_3$, TMS) δ/ppm: 170.61 ($C{=}O_{maleimide}$), 134.03 (*C*H=*C*H), 51.65 ($N_{maleimide}\underline{C}H_2CH_2N$), 35.67 ($N_{maleimide}CH_2\underline{C}H_2N$). **FTIR-ATR** ($cm^{-1}$): 3098, 2950, 2858, 1762, 1687, 1442, 1405, 1382, 1328, 1121, 826, 734, 691, 620. **ESI - HRMS** for $C_{18}H_{19}N_4O_6$ $[M+H]^+$: *m/z* calcd: 387.12991; found: 387.12924 [error: 1.7 ppm].

4 SYNTHESIS OF FURAN-MALEIMIDE MONOMERS

4.1 AB MONOMERS

The AB-type structures (**XIII** and **XIV**) were synthesised in a two-step procedure using an aminoacid, namely β-alanine, as their precursor, as described below.

Synthesis of 3-(exo-3,6-epoxy-1,2,3,6-tetrahydrophthalimido)propanoic acid (XII)

3-Aminopropanoic acid (β-ALA) (2.41 g, 27.1 mmol) was slowly added to a solution of *exo*-3,6-epoxy-1,2,3,6-tetrahydrophthalic anhydride (furan-maleic anhydride DA adduct) (4.50 g, 27.1 mmol) and Na_2CO_3 (2.87 g, 27.1 mmol) in methanol (200 mL). The solution was stirred at 56ºC for 6 days. Then the solvent was removed under reduced pressure and the white residue dissolved in 100 mL of dichloromethane and washed with 3×100 mL of 0.6 M aqueous HCl. The organic layer was dried over anhydrous sodium sulphate and concentrated under reduced pressure. The expected product (**XII**) was obtained as white crystals with a yield of 59% [258]. This compound was also used in the synthesis of the AB_2-type monomer (section **4.2**).

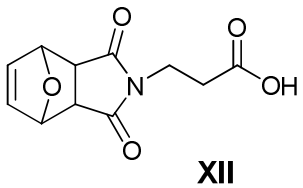

XII

XII: **^{1}H NMR** (300MHz, acetone-d_6, TMS) δ/ppm: 6.58 (s; 2H; =C*H*CHCH), 5.13 (s; 2H; =CHC*H*CH), 3.67 (t; *J* =7.8 Hz; 2H; NC*H*$_2$CH$_2$), 2.92 (s; 2H; =CHCHC*H*), 2.55 (t; *J* =7.7 Hz; 2H; NCH$_2$C*H*$_2$). **^{13}C NMR** (75MHz, acetone-d_6, TMS) δ/ppm: 176.78 (C=O$_{acid}$), 171.90 (C=O$_{maleimide}$), 137.33 (=*C*HCHCH), 81.68 (=CH*C*HCH), 48.24 (=CHCH*C*H), 34.82 (N$_{maleimide}$*C*H$_2$CH$_2$), 31.98

($N_{maleimide}CH_2\underline{C}H_2$). **FTIR-ATR** ($cm^{-1}$): 3000 - 3100, 3012, 2931, 2873, 1779, 1690, 1443, 1402, 1341, 1212, 1158, 1012, 954, 877, 712, 640, 589.

Reaction of 3-(exo-3,6-epoxy-1,2,3,6-tetrahydrophthalimido)propanoic acid XII with a monofunctional furan derivative

In this step, two different routes were followed, viz. the previously synthesized acid **XII** reacted, on one hand, with furfuryl alcohol, which led to an ester derivative, and on the other hand, with furfuryl amine, which originated an amide derivative. Their syntheses were carried out as follows.

Synthesis of furfuryl-3-(exo-3,6-epoxy-1,2,3,6-tetrahydrophthalimido)propanoate (XIII)

A solution of **XII** (4.74 g, 20 mmol), furfuryl alcohol (5.89 g, 60 mmol) and DMAP (1.95 g, 16 mmol) in dry dichloromethane (20 mL) was prepared and after 5 minutes stirring, DCC (4.54 g, 22 mmol) was added to it and the reaction mixture left overnight at room temperature under N_2. The precipitated *N*,*N'*-dicyclohexylurea (DCU) formed during the reaction was removed by filtration and the filtrate washed with 0.5 M aqueous HCl (2x5 mL) and a saturated sodium hydrogen carbonate aqueous solution (2x5 mL). The organic phase was dried over anhydrous sodium sulphate before vacuum removal of the solvent. Additional DCU was precipitated by adding ethyl acetate to the obtained residue. The suspension was filtrated and concentrated under reduced pressure. The expected product was obtained as a brownish solid with a yield of 90.0%. Compound **XIII** was stable and could not undergo DA self-condensation since the maleimide moiety was protected as its furan adduct [260].

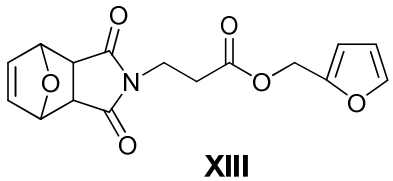

XIII

XIII: m.p. = 67.4ºC (DSC). **^{1}H NMR** (300MHz, $CDCl_3$, TMS) δ/ppm: 7.41 (dd; *J* =1.6, 0.6 Hz; 1H; furan H-5'), 6.51 (s; 2H; =C*H*CHCH), 6.41 (d; *J* =3.3 Hz; 1H; furan H-3'); 6.36 (dd; *J* =3.2, 1.9 Hz; furan H-4'), 5.26 (s; 2H; =CHC*H*CH), 5.05 (s; 2H; OC*H*$_2$-2-Furan), 3.78 (t; *J* =7.4 Hz; 2H; NC*H*$_2$$CH_2$), 2.83 (s; 2H; =CHCHC*H*), 2.64 (t; *J* =7.3 Hz; 2H; NCH_2C*H*$_2$). **^{13}C NMR** (75MHz, $CDCl_3$, TMS) δ/ppm: 175.78 ($C=O_{ester}$), 170.19 ($C=O_{maleimide}$), 149.02 (furan C-2'), 143.30 (furan C-5'), 136.50 (=*C*HCHCH), 110.88, 110.57 (furan C-3',C-4'), 80.84 (=CH*C*HCH), 58.30 (O*C*H_2-2-Furan), 47.3 (=CHCH*C*H), 34.44 (N*C*H_2CH_2), 31.79 (NCH_2*C*H_2). **FTIR-ATR** (cm^{-1}): 3120, 3000, 2933, 2857, 1775, 1736, 1693, 1437, 1407, 1382, 1347, 1274, 1226, 1150, 1015, 915, 877, 809, 734, 658, 593. **ESI - HRMS** for $C_{16}H_{15}NO_6Na$ $[M+Na]^+$: *m/z* calcd: 340.07916; found: 340.07908 [error: 0.2 ppm].

Synthesis of N-furfuryl-3-(exo-3,6-epoxy-1,2,3,6-tetrahydrophthalimido)propanamide (XIV)

A solution of **XII** (4.74 g, 20 mmol), furfuryl amine (3.85 g, 40 mmol) and DMAP (1.95 g, 16 mmol) in dry dichloromethane (20 mL) was prepared and after 5 minutes stirring, DCC (4.54 g, 22 mmol) was added to it and the reaction mixture left 4 hours at room temperature under N_2. The precipitated DCU formed during the reaction was removed by filtration and the filtrate washed with 0.5 M aqueous HCl (2x5 mL) and a saturated sodium hydrogen carbonate aqueous solution (2x5 mL). The organic phase was dried over anhydrous sodium sulphate before vacuum removal of the solvent. Additional DCU was precipitated by adding ethyl acetate to the obtained residue. The suspension was filtrated and concentrated under reduced pressure. The expected product was obtained as a white solid white a yield of 97%. Compound **XIV** was stable and could not undergo DA self-condensation since the maleimide moiety was protected as its furan adduct [260].

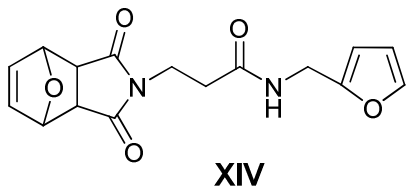

XIV

XIV: m.p. = 138.3ºC (DSC) **^{1}H NMR** (300MHz, $CDCl_3$, TMS) δ/ppm: 7.34 (d; *J* =2.0 Hz; 1H; furan H-5'), 6.50 (s; 2H; =C*H*CHCH), 6.32 (dd; *J* =3.2, 1.8 Hz; 1H; furan H-4'), 6.23 (d; *J* =3.6

Hz; 1H; furan H-3'), 6.01 (bs; 1H), 5.22 (s; 2H; =CHC*H*CH), 4.39 (d; *J* =5.5 Hz; 2H; NHC*H*$_2$-2-Furan), 3.80 (t; *J* =7.1 Hz; 2H; NC*H*$_2$CH$_2$), 2.83 (s; 2H; =CHCHC*H*), 2.49 (t; *J* =7.1 Hz; 2H; NCH$_2$C*H*$_2$). **^{13}C NMR** (75MHz, $CDCl_3$, TMS) δ/ppm: 175.93 ($C{=}O_{amide}$), 169.27 ($C{=}O_{maleimide}$), 151.02 (furan C-2'), 142.15 (furan C-5'), 136.46 (=*C*HCHCH), 110.46, 107.59 (furan C-3',C-4'), 80.94 (=CH*C*HCH), 47.32 (=CHCH*C*H), 36.47 (N*C*H$_2$CH$_2$), 35.21 (NH*C*H$_2$-2-Furan), 34.04 (NCH$_2$*C*H$_2$). **FTIR-ATR** (cm^{-1}): 3337, 3117, 3006, 2933, 2857, 1770, 1694, 1644, 1539, 1429, 1407, 1376, 1340, 1221, 1169, 1016, 918, 877, 851, 723, 689, 654, 598. **ESI - HRMS** for $C_{16}H_{17}N_2O_5$ $[M+H]^+$: *m/z* calcd: 317.11320; found: 317.11317 [error: 0.1 ppm].

4.2 AB_2 MONOMER

The AB_2 monomer (**XVII**) was prepared in a three step-procedure by using an amino-diol derivative as precursor, viz. first a Schiff base was synthesized, then it was reduced *in situ* [249,250], and finally an ester derivative was obtained by reacting the ensuing product with an acid [260].

Synthesis of 3-furfurylamino-1,2-propanediyl-bis(3(exo-3,6-epoxy-1,2,3,6-tetrahydro-phthalimido)propanoate) (XVII)

i) ***Synthesis of the Schiff base*** **XV:** In a round-bottom flask kept under N_2, 10 mL of methanol (absolute), 2.3 mmol of 3-amino-1,2-propanediol (0.21 g) and a 20% molar excess of furfural (0.26 g) were introduced. The mixture was stirred for 5 hours at room temperature. In a first experiment, in order to characterize this structure by NMR and FTIR, a fraction was taken. The solvent was evaporated and the ensuing product dried under vacuum, with the subsequent elimination of the excess of furfural.

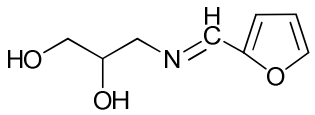

XV

XV: **^{1}H NMR** (500MHz, $CDCl_3$, TMS) δ/ppm: 8.10 (s; 1H; N=CH), 7.52 (d; *J* = 1.8 Hz; 1H; furan H-5'), 6.78 (d; *J* =3.3 Hz; 1H; furan H-3'), 6.48 (dd; *J* =3.1, 1.6 Hz; 1H; furan H-4'), 4.05 – 3.70 (m; 5H; HOC*H*$_2$, C*H*OH, $(OH)_2$), 2.84 (m; 2H; C*H*$_2$N=). **^{13}C NMR** (75MHz, $CDCl_3$, TMS) δ/ppm: 151.98 (NH*C*H_2-2-furan), 151.15 (furan C-2'), 145.09 (furan C-5'), 114.86, 111.81 (furan C-3', C-4'), 71.44 (*C*HOH), 64.86 (HO*C*H_2), 64.07 (*C*H_2NH). **FTIR-ATR** (cm^{-1}): 3500 - 3100, 3112, 2862, 2839, 1643, 1560, 1481, 1418, 1392, 1348, 1272, 1103, 1026, 1014, 931, 883, 746, 592.

ii) ***Reduction of the Schiff base*****:** The *in situ* reduction of the Schiff base **XV** was conducted in methanol with an excess of sodium borohydride (0.087 g, 2.3 mmol). After approximately 2 hours (when the H_2 release had stopped), the solution was concentrated and chloroform was added. This solution was left overnight. After filtration, the solvent was evaporated and the final product vacuum dried. The ensuing product (**XVI**) was obtained as a brownish yellow viscous liquid with an overall yield of 84%.

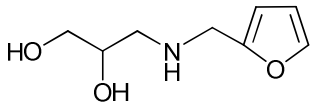

XVI

XVI: **^{1}H NMR** (500MHz, $CDCl_3$, TMS) δ/ppm: 7.36 (d; *J* =1.9 Hz; 1H; furan H-5'), 6.30 (d; *J* =3.3 Hz; 1H; furan H-3'), 6.20 (dd; *J* =2.2, 2.0 Hz; 1H; furan H-4'), 4.11 - 3.39 (m; 6H; NHC*H*$_2$-2-furan, HOC*H*$_2$, C*H*OH, OH), 2.69 (m; 2H; C*H*$_2$NH). **^{13}C NMR** (126MHz, $CDCl_3$, TMS) δ/ppm: 153.52 (furan C-2'), 141.95 (furan C-5'), 110.19, 107.19 (furan C-3', C-4'), 72.26 (*C*HOH), 66.22 (HO*C*H_2), 53.49 (NH*C*H_2-2-furan), 46.16 (*C*H_2NH). **FTIR-ATR** (cm^{-1}): 3500-3100, 3106, 2898, 2836, 1569, 1504, 1436, 1388, 1330, 1180, 1041, 1008, 914, 802, 721, 598.

iii) ***Esterification of the aminodiol XVI with the acid XII*****:** A solution of compound **XII** (4.74 g, 20 mmol), **XVI** (1.71 g, 10 mmol) and DMAP (1.95 g, 16 mmol) in dry dichloromethane (20 mL) was prepared, and after 5 minutes stirring, DCC (4.54 g, 22 mmol) was added to it and the reaction mixture left overnight at room temperature under N_2. The precipitated DCU formed during the reaction was removed by filtration and the filtrate washed with 0.5 M aqueous HCl (2x5 mL) and a saturated sodium hydrogen carbonate aqueous solution (2x5 mL). The organic phase was dried over anhydrous sodium sulphate before vacuum removal of the solvent. Additional DCU was precipitated by

adding ethyl acetate to the obtained residue. The suspension was filtrated and concentrated under reduced pressure. The expected product was obtained as a sticky brownish-yellow solid with a yield of 30%. Compound **XVII** was stable and could not undergo DA condensation since the maleimide moiety was protected as its furan adduct.

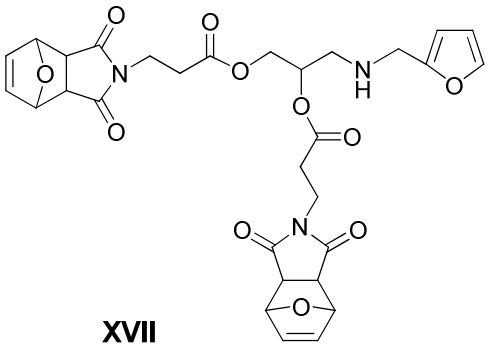

XVII

XVII: Tg = -1.3ºC (DSC) **^{1}H NMR** (500MHz, TCE-d_2, TMS) δ/ppm: 7.41 (s; 1H; furan H-5'), 6.52 (m; 5H; =C*H*CHCH), 6.36 - 6.26 (m; 2H; furan H-4',H-3'), 5.25 (m; 5H; =CHC*H*CH), 4.06 - 3.64 (m; 10H; C*H*O, OC*H*$_2$, CH_2C*H*$_2$N, NHC*H*$_2$-2-furan), 2.91 – 2.58 (m; 11H; =CHCHC*H*, C*H*$_2$NH, C*H*$_2$$CH_2$N). **^{13}C NMR** (126 MHz, TCE-d_2, TMS) δ/ppm: 176.25, 176.02, 170.67 (C=O), 149.58 (furan C-2'), 143.26 (furan C-5'), 136.77 (=*C*HCHCH), 110.78, 108.88 (furan C-3',C-4'), 81.09 (=CH*C*HCH), 66.93 (*C*H-O), 58.58 (O*C*H_2), 52.23 (NH*C*H_2-2-furan), 47.61 (=CHCH*C*H), 46.44 (*C*H_2NH), 34.79 (N*C*$H_2$$CH_2$), 32.08 ($NCH_2$*C*$H_2$). **FTIR-ATR** ($cm^{-1}$): 3430, 3069, 2989, 2933, 2856, 1757, 1732, 1690, 1589, 1435, 1399, 1363, 1341, 1307, 1236, 1161, 1084, 1015, 916, 876, 732, 715, 647, 592. **ESI - HRMS** for $C_{30}H_{32}N_3O_{11}$ $[M+H]^+$: *m/z* calcd: 610.20314; found: 610.20296 [error: 0.3 ppm].

5 DIELS-ALDER POLYCONDENSATIONS

5.1 MODEL SYSTEM (-A+-B)

Monofunctional compounds, namely furfuryl acetate (FA) and *N*-methylmaleimide (MM) were used as complementary DA reagents in the model system.

5.1.1 Determination of the molar extinction coefficient, ε

The maleimide moiety absorbs in the near UV because of its chromophore made up of the two carbonyl groups conjugated with the C=C unsaturation. A calibration curve was constructed using several standard solutions of MM, as indicated in Table 24, in order to determinate the value of the molar extinction coefficient, ε, for the maleimide group. The solvent used was TCE. The absorption maximum was recorded at 293 nm.

Table 24. Standard solutions of MM and the correspondent values of absorbance obtained at λ_{max}= 293 nm.

	[MM] x10^{-3} mol.dm^{-3}	Abs_{293nm}
	0.00	0.024
1	1.07	0.811
2	2.14	1.558
3	3.21	2.352

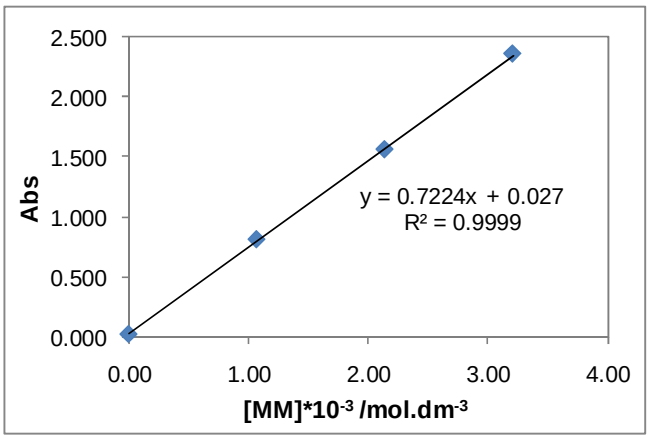

Graph 1. Graphical representation of Abs *vs* [MM], according to Table 24.

Clearly, Beer-Lambert law (3) was obeyed, viz.

$$Abs = \varepsilon bc \quad (3)$$

where *Abs* is the absorbance, ε the molar absortivity or extinction coefficient with units of dm^{-3} mol^{-1} cm^{-1}, *b* the path length, expressed in cm, and *c* the concentration of the compound, expressed in $mol.dm^{-3}$. Hence, from the slope of linear Graph 1, ε_{MM} was calculated as 720 dm^3 mol^{-1} cm^{-1}.

5.1.2 UV spectroscopy

2 M FA (1.40 g, 10 mmol) and 0.2 M MM (0.11 g, 1.0 mmol) solutions were prepared separately in 5.0 mL volumetric flasks, using TCE as solvent. Then 0.5 mL of each solution was mixed in a 0.1 mm Suprasil cell, which was left in the temperature controlled spectrophotometer at constant temperature. Spectra where taken every 30 minutes during 24 hours, with the purpose of evaluate the order of the reaction and the rate constant for the formation of adduct. Three different temperatures were applied, viz. 35, 50 and 65ºC, in order to determine the activation energy associated with this reaction.

In order to study the retro-DA reaction, the adduct **XVIII** was precipitated into an excess of diethyl ether and the ensuing solid product dried under vacuum. Thereafter, a 0.1 M solution of **XVIII** (12.6 mg, 0.05 mmol) in TCE (0.5 mL) was prepared under nitrogen, and its initial UV spectrum taken. The solution was then left in an oil bath at 90ºC for 24 hours and at regular times, a spectrum was taken (at room temperature). In order to reach again the equilibrium, the system was allowed to cool to room temperature and a UV spectrum was taken after 3 days.

5.1.3 NMR spectroscopy

Equimolar solutions, viz. 0.6 M, of FA (42.0 mg, 0.3 mmol) and MM (33.3 mg, 0.3 mmol) in TCE-d_2 (0.5 mL) were prepared directly in the NMR tubes under nitrogen and their initial ^1H NMR spectra taken. Then, the solutions were mixed and a sequence of ^1H

NMR spectra recorded at constant temperature of 65ºC. After the system had been left at this temperature for 72 hours, it was allowed to return to room temperature and left for ten more days. The ensuing solution was then left in an oil bath at 90ºC during 24 hours and at regular times a spectrum taken (at room temperature). In order to reach again the equilibrium, the system was allowed to cool to room temperature where ^{1}H NMR spectra were taken after 3, 7 and 12 days.

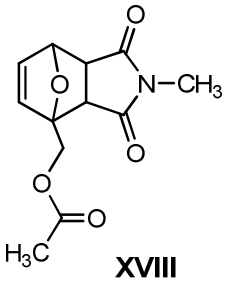

XVIII

5.2 LINEAR SYSTEMS

5.2.1 A-A+B-B system

The linear polymerization procedure was similar to that described above for the model system. Nevertheless, here equimolar solutions of difuran monomer A-A and complementary bismaleimide counterpart B-B were used for both UV and NMR spectroscopy.

5.2.1.1 UV spectroscopy

I and **IX** solutions, each one with a concentration of 0.2 M (0.31 g, 1.0 mmol, and 0.28 g, 1.0 mmol, respectively), were prepared in 5.0 mL volumetric flasks, using TCE as solvent. Then 0.5 mL of each solution was mixed in a 0.1 mm Suprasil cell, which was left in the temperature controlled spectrophotometer at 65ºC. The UV measurements where

made every hour during 62 hours. Thereafter, the UV cell was left in an oil bath at 110ºC for another 24 hours and, at regular times, a spectrum was taken (at room temperature).

5.2.1.2 NMR spectroscopy

0.6 M solutions of **I** (91.9 mg, 0.3 mmol) and **IX** (82.8 mg, 0.3 mmol) in TCE-d_2 (0.5 mL) were prepared directly in the NMR tubes under nitrogen, and their initial ^{1}H NMR spectra taken. Then, the solutions were mixed and a sequence of ^{1}H NMR spectra recorded at constant temperature of 65ºC. After the system had reached its equilibrium, it was allowed to return to room temperature and left for seven more days, when its ^{1}H NMR spectrum suggested near-complete reaction.

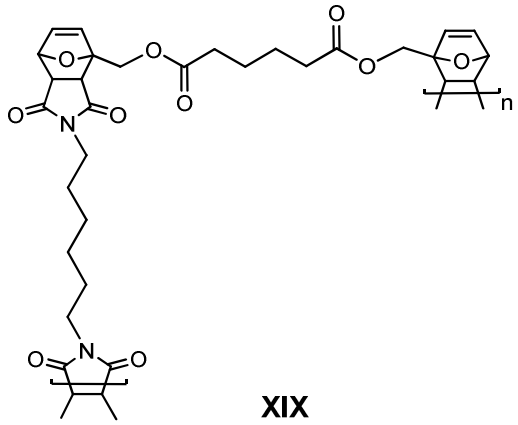

XIX

The polymer **XIX**, from both sections **5.2.1.1** and **5.2.1.2**, was then precipitated in an excess of petroleum ether and dissolved in dichloromethane. The solvent was removed and the solid product dried under vacuum.

A fraction of the ensuing polymer (**XIX**) (60 mg) was dissolved in toluene (1.0 mL) and heated at 120ºC for 24 hours. After this time, a tenfold excess of DMFu (1.0 mL) was added to the solution and the temperature was decreased to 65ºC. The reaction was left for another 24 hours in nitrogen atmosphere. The final mixture, which contained the structures **I, XX** and the excess of DMFu, was dried under vacuum in order to remove the latter.

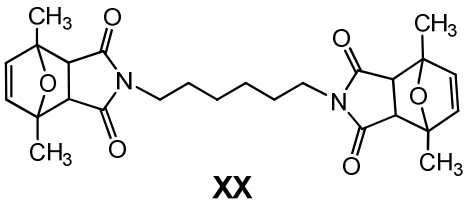

XX

5.2.1.3 Non-equimolar polymerizations

In this study, two linear systems were considered, viz. difuran monomers **I** and **III** were reacted with the bismaleimide **IX** in three different stoichiometric ratios, namely 1:1, 0.95:1 and 1:0.95 for both systems, yielding the polymers **XIX** and **XXI**, respectively.

For each monomer, two solutions with concentration 1.0 and 0.95 M were prepared (Table 25) in 5.0 mL volumetric flasks using TCE-d_2 as solvent. Then, 0.5 mL of each was mixed in the proportion indicated in Table 26 and transferred to an NMR tube. The tubes were left in a bath at 65ºC for 5 days, while spectra were taken at regular intervals. After this time, they were allowed to return to room temperature and left for seven more days, when the corresponding ^{1}H NMR spectra suggested near-complete reaction.

Table 25. Preparation of the 1.0 and 0.95 mol.dm^{-3} solutions used in the systems **I**+**IX** and **III**+**IX**.

		m /g		
[monomer] /mol.dm^{-3}	n /mmol	I (AA)	III (AA)	IX (BB)
1.0	5.00	1.5317	1.9027	1.3816
0.95	4.75	1.4551	1.8076	1.3125

Table 26. Monomers proportions used in the systems **I**+**IX** and **III**+**IX**.

V /mL		I		III	
		1	0.95	1	0.95
IX	1	1.0	1.0	1.0	1.0
	0.95	1.0	-	1.0	-

The ensuing polymers **XIX** and **XXI** were precipitated in an excess of petroleum ether and dissolved in dichloromethane. The solvent was removed and the ensuing product dried under vacuum.

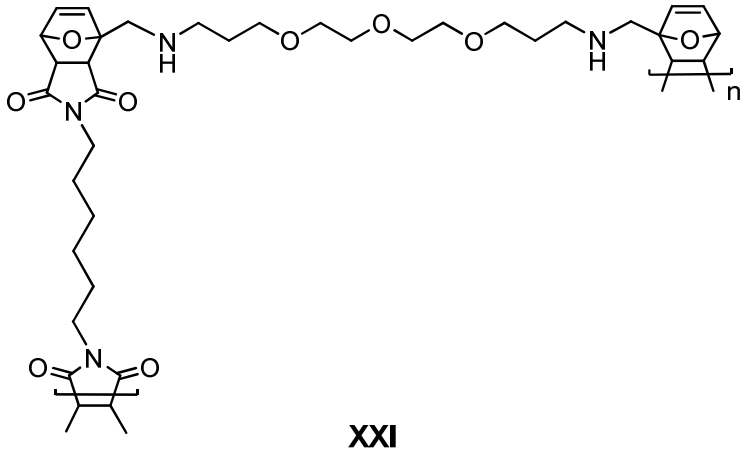

XXI

5.2.2 A-B systems

The previously described procedures were applied to the both A-B systems.

5.2.2.1 UV spectroscopy

0.2 M solution of **XIII** (31.7 mg, 0.1 mmol) or **XIV** (31.6 mg, 0.1 mmol) was prepared using TCE (0.5 mL) as solvent and left at 110ºC for 24 hours. This step promoted the retro-DA elimination of furan from the adduct moiety and the ensuing maleimide function was hence set free to polymerize. The solution was then transferred to a 0.1 mm Suprasil cell, which was left in the temperature-controlled spectrophotometer at 65ºC. UV spectra where taken every 30 minutes during the first 3 hours, then every hour until reaching 24 hours and finally after 3 days.

5.2.2.2 NMR spectroscopy

0.2 M solution of **XIII** (63.5 mg, 0.2 mmol) or **XIV** (63.3 mg, 0.2 mmol)in TCE-d_2 (1.0 mL) was prepared and left at 110 ºC for 24 hours under nitrogen atmosphere, in order to promoted the elimination of furan from the adduct moiety and set free the ensuing maleimide function. The solution was transferred to an NMR tube and the corresponding ^{1}H NMR spectrum taken immediately at room temperature. The tube was then left in a bath at 65ºC, while spectra were taken at regular intervals. After the system had been left at this

temperature for 72 hours, it was allowed to return to room temperature and left for seven more days, when its ^{1}H NMR spectrum suggested near-complete reaction.

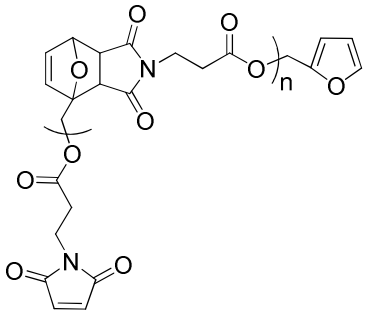

XXII

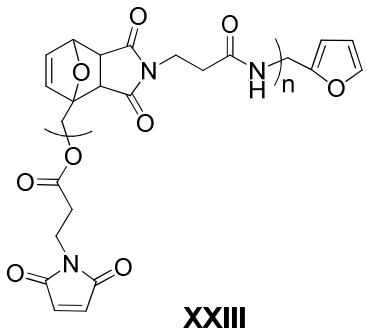

XXIII

The ensuing polymers **XXII** and **XXIII** were precipitated in an excess of petroleum ether and dissolved in dichloromethane. The solvent was removed and the ensuing product dried under vacuum, before being characterized.

5.3 NON-LINEAR SYSTEMS - A_n+B_m

5.3.1 A_2 + B_3 system

The non-linear polymerization was carried out using the bisfuran **I** and the trismaleimide **XI** monomers in different stoichiometric ratios, which were calculated according to the *Flory-Stockmayer equation* (2):

$$Pc = \frac{1}{[r + r\rho(m-2)]^{1/2}} \qquad (2)$$

where *Pc* is the crosslinking critical point, this is, the yield at which crosslinking occurs (more specifically the degree of consumption of the moiety which is in default), *r* the stoichiometric ratio between B and A groups [$r = N_B/N_A < 1$], ρ the crosslinking parameter [$\rho = N_{B(m)}/N_{B(total)}$], and *m* the functionality of the B_m monomer. For a system with only A_2 and B_3, m = 3 and ρ = 1.

The stoichiometric ratios used here are given in Table 27, together with the predicted conversions at which the gel point (partial crosslinking) should occur if no cyclisation takes place, i.e. following strictly equation 3.

Table 27. Stoichiometric ratios of the A_2 and B_3 monomers.

r ($N_B/N_A < 1$)		Pc (%)
4mol B_3/6 mol A_2 = 12/12 =	1.0	71
3mol B_3/6 mol A_2 = 9/12 =	0.75	81
2mol B_3/6 mol A_2 = 6/12 =	0.5	100

The initial concentrations of both monomers are given in Table 28. The concentration of the difuran monomer **I** was the same for the three experiments.

Table 28. Concentration of **I** and **XI** for the three different stoichiometric ratios r.

Monomer	r	V /mL	n /mmol	[monomer] /mol.dm^{-3}
I	1, 0.75 and 0.5	5.0	6.0	1.2
XI	1	5.0	4.0	0.8
	0.75		3.0	0.6
	0.5		2.0	0.4

5.3.1.1 UV spectroscopy

All solutions with the concentration indicated in Table 28 were prepared in 5 mL volumetric flasks using TCE as solvent. The mass of each monomer is given in Table 29.

Table 29. Mass monomers **I** and **XI** used to prepare the solutions for the UV study.

Monomer	r	m /g
I	1; 0.75; 0.5	1.8380
XI	1	1.5454
	0.75	1.1591
	0.5	0.7727

Due to the high concentration for the UV measurements, a fivefold dilution of each solution was made. The new concentrations are given in Table 30.

Table 30. Concentration of **I** and **XI** solutions after fivefold dilution.

Monomer	*r*	$[monomer]_{initial}$ /mol.dm^{-3}	$[monomer]_{dilution}$ /mol.dm^{-3}
I	1; 0.75; 0.5	1.2	0.24
XI	1	0.8	0.16
	0.75	0.6	0.12
	0.5	0.4	0.08

Then, 0.5 mL diluted solution of each complementary pairs were mixed in a 0.1 mm Suprasil cell, which was left in the temperature controlled spectrophotometer for 24 h at 65ºC. Spectra were taken every 30 minutes during the first 3 hours, then every hour until reaching 24 hours and finally after 48 hours.

5.3.1.2 NMR spectroscopy

The solutions were prepared directly in NMR tubes under nitrogen, in TCE-d_2 (0.5mL) and their initial ^{1}H NMR spectra taken. Their concentrations are given in Table 31.

Table 31. Concentrations used in the ^{1}H NMR study for the three experiments.

Monomer	*r*	$[monomer]_{initial}$ /mol.dm^{-3}	m /g
I	1; 0.75; 0.5	1.2	0.1838
XI	1	0.8	0.1545
	0.75	0.6	0.1159
	0.5	0.4	0.0773

The various solution pairs were then mixed and left in a bath at 65ºC during 72 hours. The corresponding spectra were taken twice a day at room temperature. Thereafter, they were allowed to return to room temperature and left for seven more days. After each system had reached its equilibrium, the NMR tubes containing the ensuing polymers were left in an oil bath at 110ºC for 24 hours and spectra taken after 2, 6 and 24 hours. Finally,

in order to attain the equilibrium once again, the system was allowed to cool to 65ºC and ^{1}H NMR spectra were taken after 72 hours.

The ensuing polymers **XXIV** were precipitated into an excess of petroleum ether and recovered precipitates dissolved in dichloromethane. The solvent was removed and the solid products dried under vacuum. When an insoluble fraction was observed, the suspension was filtered and the residue washed with dichloromethane. The residue was dried under vacuum, whereas the filtrate was precipitated again with petroleum ether, filtered and dried under vacuum.

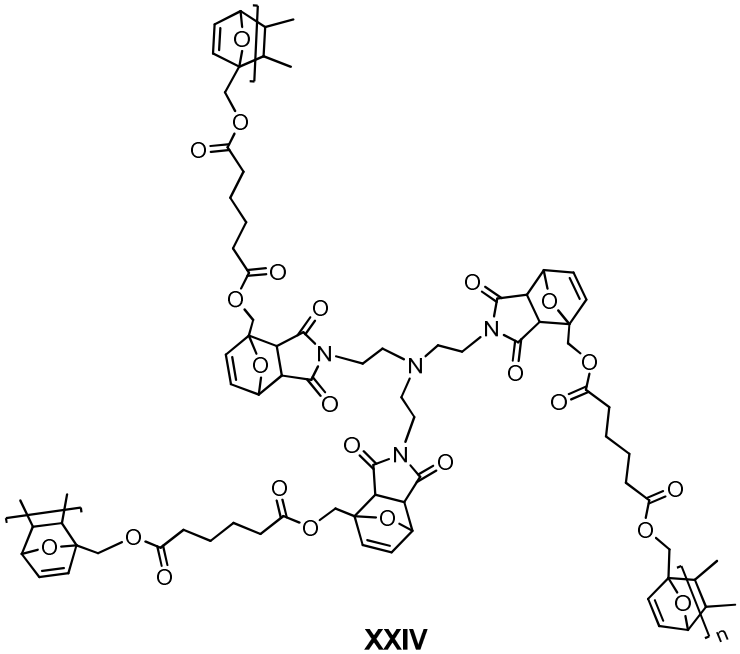

XXIV

5.3.2 $A_3 + B_2$ systems

In this study, two systems were investigated using the same procedure as described above. The trisfuran monomers **VI** and **VII** were reacted with the bismaleimide **IX** in three different stoichiometric ratios, viz. 1, 0.75 and 0.5 (Table 27).

5.3.2.1 UV spectroscopy

All solutions were prepared in 5 mL volumetric flasks using TCE as solvent, according to Table 32. The concentration of the bismaleimide **IX** was the same in all experiments. However, due to the high concentration for the UV measurements, a fivefold dilution of each solution was carried out. The new concentrations are given in Table 33.

Table 32. Preparation of the **VI**, **VII** and **IX** solutions used in the UV study.

Monomer	*r*	[monomer] /mol.dm^{-3}	m /g
IX	1, 0.75 and 0.5	1.2	1.6577
VI	1	0.8	3.0600
	0.75	0.6	2.2950
	0.5	0.4	1.5300
VII	1	1.2	1.5460
	0.75	0.8	1.1595
	0.5	0.6	0.7730

Table 33. Concentration of **VI**, **VII** and **IX** solutions after fivefold dilution.

Monomer	*r*	$[monomer]_{initial}$ /mol.dm^{-3}	$[monomer]_{dilution}$ /mol.dm^{-3}
IX	1, 0.75 and 0.5	1.2	0.24
VI	1	0.8	0.16
	0.75	0.6	0.12
	0.5	0.4	0.08
VII	1	0.8	0.16
	0.75	0.6	0.12
	0.5	0.4	0.08

Then, 0.5 mL diluted solution of each complementary pairs were mixed in a 0.1 mm Suprasil cell, which was left in the temperature controlled spectrophotometer for 24 hours at 65ºC. Spectra were taken every 30 minutes during the first 3 hours, then every hour until reaching 24 hours and finally after 48 hours.

5.3.2.2 NMR spectroscopy

The solutions were prepared directly in NMR tubes under nitrogen in TCE-d_2 (0.5mL) and their initial ^{1}H NMR spectra taken. Their concentrations are given in Table 34.

Table 34. Concentrations used in the ^{1}H NMR study for the three experiments.

Monomer	*r*	[monomer] /mol.dm^{-3}	m /g
IX	1, 0.75 and 0.5	1.2	0.1658
VI	1	0.8	0.3060
	0.75	0.6	0.2295
	0.5	0.4	0.1530
VII	1	1.2	0.1546
	0.75	0.8	0.1159
	0.5	0.6	0.0773

The different solution pairs were then mixed and left in a bath at 65ºC during 72 hours. The corresponding spectra were taken twice a day at room temperature. They were thereafter allowed to return to room temperature and left for seven more days. After the system had reached its equilibrium, the NMR tubes containing the ensuing polymers were left in an oil bath at 110ºC for 24 hours and spectra were taken after 2, 6 and 24 hours. Finally, in order to attain the equilibrium once again, the system was allowed to cool to 65ºC and ^{1}H NMR spectra were taken after 72 hours.

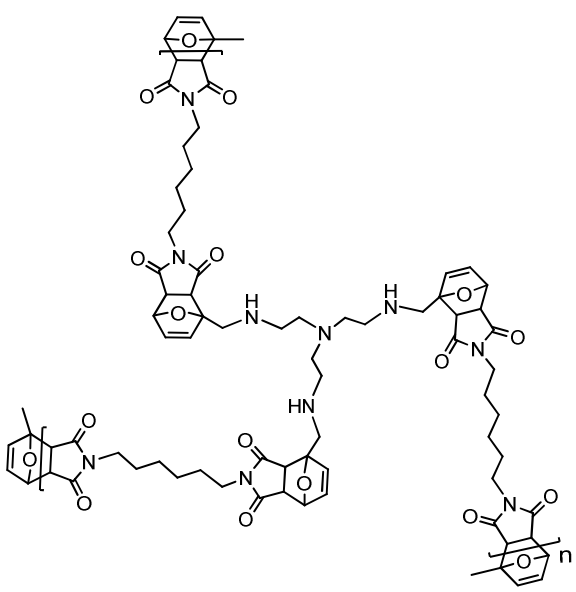

XXV

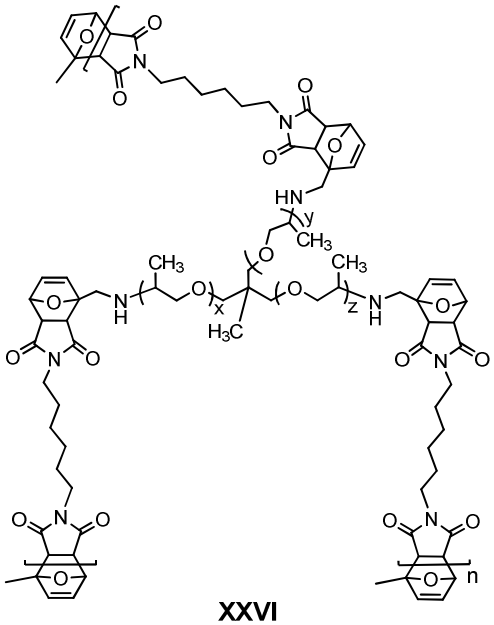

XXVI

Both **XXV** and **XXVI** polymers were precipitated in an excess of petroleum ether. Each precipitate was dissolved in dichloromethane, the solvent was removed and the ensuing solid product dried under vacuum. When an insoluble fraction was observed, a filtration was carried out and the residue washed with dichloromethane. The residue was dried under vacuum, whereas the filtrate was precipitated again with petroleum ether, filtered and dried under vacuum.

5.3.3 AB_2 System

5.3.3.1 UV spectroscopy

0.1 M solution of **XVII** (30.5 mg, 0.1 mmol) was prepared using TCE (0.5 mL) as solvent and left at 110ºC for 24 hours. This step promoted the retro-DA elimination of furan from the adduct moiety and the ensuing maleimide function was hence set free to polymerize. The solution was then transferred to a 0.1 mm Suprasil cell, which was left in the temperature controlled spectrophotometer at 65ºC. UV spectra where taken every 30 minutes during the first 3 hours, then every hour until reaching 24 hours and finally after 3 days.

5.3.3.2 NMR spectroscopy

0.1 M solution of **XVII** (61.0 mg, 0.1 mmol) in TCE-d_2 (1.0 mL) was prepared and left at 110 ºC for 24 hours under nitrogen atmosphere, in order to promoted the elimination of furan from the adduct moiety and set free the ensuing maleimide function. The solution was transferred to an NMR tube and the corresponding ^{1}H NMR spectrum taken immediately at room temperature. The tube was then left in a bath at 65ºC, while spectra were taken at regular intervals. After the system had reached its equilibrium, it was allowed to return to room temperature and left for seven more days, when its ^{1}H NMR spectrum suggested near-complete reaction.

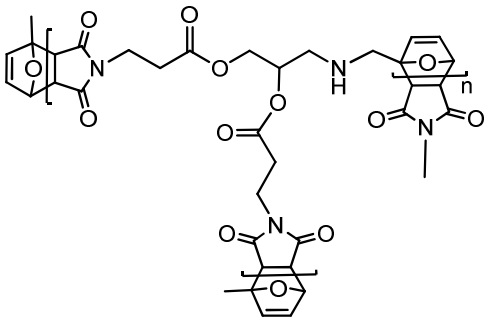

XXVII

The ensuing polymer **XXVII** was precipitated in an excess of petroleum ether and dissolved in dichloromethane. The solvent was removed and the ensuing product dried under vacuum.

GENERAL CONCLUSIONS

GENERAL CONCLUSIONS

This research focused on the synthesis and characterization of novel thermally reversible polymeric materials by means of the DA reaction applied to monomers bearing complementary furan (diene) and maleimide (dienophile) moieties.

The interest in exploiting the reversible DA reaction in the context of furan chemistry has been clearly shown by (*i*) the renewable character of the sources of these heterocyclic compounds, viz. vegetable biomass; (*ii*) the pronounced dienic nature of the furan ring which makes it particularly suitable in terms of kinetics and yields; and (iii) the vast array of specific polymeric structures, not readily available via petrochemistry.

The thermal reversibility of the DA reaction, which implies that adducts can be readily reverted to their precursors by heating, is one of the most relevant aspects of this reaction and represents the basic working hypothesis for the systems involved in this study, because it opens the way to temperature-sensitive materials with promising applications, which can cover numerous domains associated with self-mendability and network recyclability through reversible cross-linking.

All the furan and maleimide monomers used in this study were synthesized, purified and characterized before their use in the DA polymerizations. They bore structures with different spacing moieties separating the reactive functions, viz. aliphatic or oligoether bridges, incorporating in some instances ester and amide groups.

The furan monomers bearing two or three furan ring were obtained as highly viscous liquids, showing low Tg values due to the flexible nature of their bridging groups. The complementary structures bearing two and three maleimide moieties were obtained as solids with relatively high melting points. The simple furan-maleimide A-B monomers, as well as the more complex AB_2-type counterpart prepared here, were the first examples of such structures suitable for DA polymerizations. Indeed, the protection of the maleimide group in the form of a furan-DA adduct, until the incorporation of the furan moiety, proved

to be effective in the synthesis of these structures, because it avoided the DA polymerization of these intrinsically reactive monomers during their synthesis, purification and storage. Their polycondensation could then easily be achieved through the *in situ* retro-DA deprotection at high temperature, followed by the return of the now bared AB monomers to the appropriate temperature for their DA polymerization.

A systematic study followed on the application of the DA and retro-DA reaction, first to model monofunctional system (-A+-B), then to linear polymerizations using both A-A+B-B and A-B monomers, as well as to non-linear systems using both An+Bm systems with n or m >2 (leading to networks under appropriate stoichiometric conditions), and a AB_2 monomer (leading to hyperbranched macromolecules which do not crosslink). The emphasis here was on the role of the temperatures chosen to shift appropriately the equilibrium from predominant adduct formation (polymerisation by DA), viz. around 65ºC for a reasonable reaction rate, to the predominant reversion to its precursors (depolymerisation by retro-DA), viz. above 100ºC.

It was from the preliminary study on the equilibrium position and kinetics related to the model compounds that the choice of these forward and backward reaction temperatures was made for the subsequent polymerizations. Moreover, the study of the model monofunctional system provided clear-cut evidence of the intermediate structures involved and of the absence of significant side reactions in both forward and backward pathways, even after several cycles.

The original application of UV spectroscopy, never applied to these types of studies, coupled with the more classical use of the ^{1}H NMR counterpart, were exploited successfully to follow the kinetics and equilibrium of formation and decoupling of the DA adducts.

The use of single monomers bearing both the furan and the maleimide moieties in their structures, i.e. the A-B systems, represented a novel interesting alternative to the difunctional A-A+B-B linear polymerizations, because they ensured intrinsically the ideal functional stoichiometry.

The different non-linear polymerizations studied here displayed the same behaviour pattern, namely the reactions conducted with $r = 1.0$, i.e. a stoichiometric balance between furan and maleimide functions, produced the most rapid thickening and gel formation

within a few days, while their counterparts with r = 0.75 displayed similar features, albeit in a slower mode, and the reduction of r to 0.50 only resulted in a slow progressive increase in viscosity, without attaining a gel point, which is in tune with the fact that crosslinking was calculated to be reached at 100% conversion in the absence of ring formation. Thus, as expected, the use of complementary moiety stoichiometry produced a gel (network), whereas as the relative amount of trifunctional monomer was decreased, the reactions stopped short of crosslinking, i.e. gave soluble highly branched polymers. Visually, this could be observed by the increase and decrease of the solution viscosity during the DA and retro-DA reaction, respectively.

Although the DA polycondensation involving the asymmetrically substituted AB_2 monomer was only a preliminary study, the results obtained were promising**.** Obviously much remains to be done to unravel its quantitative features, as well as to obtain and characterize the ensuing materials.

In a general way, the polymers with flexible backbone between adducts had Tg values lower than those of homologues bearing bridges capable of establish intermolecular hydrogen bonding, like those incorporating amide groups. In addition, for all DA systems, since relatively low concentrations were used (<1M), a tendency to cyclization was observed, which influenced negatively their final polymer molecular weights and hence reduced Tg values correspondingly.

In conclusion, the outcome of this study allowed, on the one hand, the assess of extent of useful applications of furans, i.e. compounds derived from renewable resources which can be used as alternative to fossil-based materials, and, on the other hand, the establishment of quantitative criteria about the synthesis, properties, and controlled thermal depolymerization of all these materials, as well as the reproducibility of the DA and retro-DA cycles.

These DA systems are excellent examples of reversible click chemistry applied to macromolecular synthesis and represent an important contribution to the realm of novel materials based on renewable resources. Among the possible applications of these intelligent and functional materials are green ink-jet inks without solvent, based on the equilibrium between linear polymers (solid at room temperature) and its monomers/oligomers (liquids at the ink head temperature), both glassy and plastic

mendable materials, and the recycling of polymer networks. The latter potential process is particularly important, because it allows the recovery of the initial thermoplastic precursors used for preparing crosslinked elastomers like tyres, i.e. materials which cannot be recovered by the present technological know-how.

Among the possible lines of pursuit of this investigations, it seems appropriate to include (*i*) the completion of the work on AB_2 monomers, which represent a major original contribution to the field of hyperbranched materials, with the hitherto unexplored additional feature of controlled thermal destructuring of the macromolecules through the retro-DA reaction; (*ii*) the study of aqueous systems bearing a greener character to prepare reversible hydrogels, among other novel systems; (*iii*) the study of the role of catalysts to accelerate the DA and retro-DA reactions, particularly in such contexts as the application to inkjet inks, which require a fast response.

BIBLIOGRAPHY

BIBLIOGRAPHY

1. S. Sukhatme (**2008**) *Solar Energy: Principles of Thermal Collection and Storage*, Tata McGraw Hill, New Delhi.

2. V. Smil (**2004**) "World history and energy", In: Cleveland, C.J. (ed.) *Encyclopedia of Energy*, Elsevier Academic Press, Oxford.

3. C. Ngô and J. Natowitz (**2009**) *Our Energy Future: Resources, Alternatives and the Environment*, John Wiley & Sons, New Jersey.

4. D.L. Klass (**1998**) *Biomass for Renewable Energy, Fuels, and Chemicals*, Academic Press, San Diego.

5. D.L. Klass (**1998**) "Energy consumption, reserves, depletion, and environmental issues", In: Klass, D.L. (ed.) *Biomass for Renewable Energy, Fuels, and Chemicals*, Academic Press, San Diego.

6. F.W. Lichtenthaler and S. Peters (**2004**) Carbohydrates as green raw materials for the chemical industry, *C. R. Chimie*. 7, 65-90.

7. C. Okkerse and H.V. Bekkum (**1999**) From fossil to green, *Green Chem*. 1, 107-114.

8. J.B. Binder and R.T. Raines (**2009**) Simple chemical transformation of lignocellulosic biomass into furans for fuels and chemicals, *J. Am. Chem. Soc.* 131, 1979-1985.

9. B. Kamm, P.R. Gruber, and M. Kamm (**2010**) *Biorefineries - Industrial Processes and Products: Status Quo and Future Directions*, Wiley-VCH, Weinheim.

10. National Petroleum Council (**2007**) "Facing the Hard Truths about Energy" [report available on http://www.npchardtruthsreport.org/], acessed in August 2010, .

11. BP (**2009**) "Statistical Review of World Energy, June 2009" [report available online at www.bp.com/statisticalreview], acessed in August 2010, .

12. L.A. Lucia, D.S. Argyropoulos, L. Adamopoulos, and A.R. Gaspar (**2007**) Chemicals, materials, and energy from biomass: a review, *ACS Symp. Ser.* 954, 2-30.

13. D. Hammes and D. Wills (**2005**) Black gold - The end of bretton woods and the oil-price shocks of the 1970s, *Independent Rev. IX*, 501- 511.

14. C.J. Campbell and J.H. Laherrère (**1998**) The end of cheap oil, *Scientific American Magazine*. 78-83.

15. D.L. Klass (**2004**) "Biomass for renewable energy and fuels", In: Cleveland, C.J. (ed.) *Encyclopedia of Energy*, Elsevier Academic Press, Oxford.

16. A. Gandini, D. Coelho, M. Gomes, B. Reis, and A. Silvestre (**2009**) Materials from renewable resources based on furan monomers and furan chemistry: work in progress, *J. Mater. Chem.* 19, 8656-8664.

17. A. Gandini (**2010**) "Monomers and macromonomers from renewable resources", In: Look, K. (ed.) *Biocatalysis in Polymer Chemistry*, Wiley-VCH, Weinheim.

18. A. Gandini (**2010**) "Epoxy polymers based on renewable resources", In: Pascault, J.-P. and Williams, R.J. (eds.) E*poxy Polymers: New Materials and Inovations*, Wiley-VCH, Weinheim.

19. J. Twidell and T. Weir (**2006**) *Renewable Energy Resources*, Taylor & Francis, New York.

20. M.N. Belgacem and A. Gandini, Eds, (**2008**) *Monomers, Polymers and Composites from Renewable Resources*, Elsevier Ltd, Oxford.

21. A. Gandini (**2008**) Polymers from renewable resources: a challenge for the future of macromolecular materials, *Macromolecules*. 41, 9491-9504.

22. D.C. Elliott (**2004**) Biomass, chemicals from, In: Cleveland, C.J. (ed.) *Encyclopedia of Energy*, Elsevier Academic Press, Oxford.

23. A. Gandini (**2010**) Furans as offspring of sugars and polysaccharides and progenitors of a family of remarkable polymers: a review of recent progress, *Polym. Chem.* 1, 245-251.

24. S. Hussain, A.H. Fawcett, and P. Taylor (2002) Use of polymers from biomass in paints, *Prog. Org. Coat.* 45, 435-439.

25. M. Paster, J.L. Pellegrino, and T.M. Carole (**2004**) "Industrial Bioproducts: Today and Tomorrow" [report available online at http://www.energetics.com/], acessed in August 2010, .

26. A. Gandini (**1990**) Polymers and oligomers containing furan rings, *ACS Symp. Ser.* 433, 195-208.

27. R.D. Perlack, L.L. Wright, A.F. Turhollow, R.L. Graham, B. Stokes, and D.C. Erbach (**2005**) "Biomass as Feedstock for a Bioenergy and Bioproducts Industry:

The Technical Feasibility of a Billion-Ton Annual Supply" [report available online at http://www.osti.gov/bridge], acessed in August 2010, .

28. S. Zafar "Biomass wastes" [available online at http://www.altenergymag.com/emagazine.php?art_id=1359], access in August 2010.

29. J.H. Clark, V. Budarin, F.E.I. Deswarte, J.J.E. Hardy, F.M. Kerton, A.J. Hunt, R. Luque, D.J. Macquarrie, K. Milkowski, A. Rodriguez, O. Samuel, S.J. Tavener, R.J. White, and A.J. Wilson (**2006**) Green chemistry and the biorefinery: a partnership for a sustainable future, *Green Chem.* 8, 853-860.

30. P. McKendry (**2002**) Energy production from biomass (part 1): overview of biomass, *Bioresource Techn.* 83, 37-46.

31. F.W. Lichtenthaler (**2006**) "The key sugars of biomass: availability, present non-food uses and potential future development lines", In: Kamm, B., Gruber, P.R., and Kamm, M. (eds.) *Biorefineries - Industrial Processes and Products. Status Quo and Future Directions*, Wiley-VCH, Weinheim.

32. B. Kamm and M. Kamm (**2004**) Principles of biorefineries, *Appl. Microbiol. Biotechnol*. 64, 137-145.

33. J.J. Bozell (**2008**) Biomass as a source of carbon: the conversion of renewable feedstocks into chemicals and materials, *NABC 20: Reshaping American Agriculture to Meet its Biofuel and Biopolymer Roles*, National Agricultural Biotechnology Council, Ohio.

34. S. Fernando, S. Adhikari, C. Chandrapal, and N. Murali (**2006**) Biorefineries: current status, challenges, and future direction, *Energy Fuels.* 20, 1727-1737.

35. National Renewable Energy Laboratory (NREL) [available online: http://www.nrel.gov/biomass/biorefinery.html], acessed in June 2010.

36. D.L. Klass (**1998**) "Organic Commodity Chemicals from Biomass", In: Klass, D.L. (ed.) *Biomass for Renewable Energy, Fuels, and Chemicals*, Academic Press, San Diego.

37. U.S. Department of Energy - Energy Efficiency & Renewable Energy [available online: http://www1.eere.energy.gov/biomass/technologies.html], acessed in August 2010.

38. J.J. Bozell (**2001**) Chemicals and materials from renewable resources, *ACS Symp. Ser.* 784, 1-9.

39. J.J. Bozell and G.R. Petersen (**2010**) Technology development for the production of biobased products from biorefinery carbohydrates - the US Department of Energy's "Top 10" revisited, *Green Chem.* 12, 539-554.

40. F.W. Lichtenthaler (**2007**) "Carbohydrates as renewable raw materials: a major challenge of green chemistry", In: Tundo, P., Perosa, A., and Zecchini, F. (eds.) *Methods and Reagents for Green Chemistry: An Introduction*, John Wiley & Sons, New Jersey.

41. A. Gandini and M.N. Belgacem (**2008**) "Furan derivatives and furan chemistry at the service of macromolecular materials", In: Gandini, A. and Belgacem, M.N. (eds.) *Monomers, Polymers and Composites from Renewable Resources*, Elsevier, Amsterdam.

42. A. Gandini (**2011**) "Furans as offsprings of sugars and polysaccharides and progenitors of an emblematic family of polymer siblings", In: Mathers, R.T. and Meier, M.A. (eds.) *Green Polymerization Methods: Renewable Starting Materials, Catalysis and Waste Reduction*, Wiley-VCH, Weinheim.

43. A. Gandini (**1977**) The behaviour of furan derivatives in polymerization reactions, *Adv. Polym. Sci.* 25, 47-96.

44. A.P. Dunlop and F.N. Peters (**1953**) *The Furans*, Reinhold Publishing Co., New York.

45. A. Gandini and M.N. Belgacem (**1997**) Furans in polymer chemistry, *Prog. Polym. Sci.* 22, 1203-1379.

46. A. Gandini (**2011**) "Furan monomers and their polymer: synthesis, properties and applications", In: Plackett, D. (ed.) *Biopolymers: New Materials for Sustainable Films and Coatings*, John Wiley & Sons.

47. A. Corma, S. Iborra, and A. Velty (**2007**) Chemical routes for the transformation of biomass into chemicals, *Chem. Rev.* 107, 2411-2502.

48. S. Zafar "Woody biomass utilization for power generation - An overview" [available online at http://www.energypulse.net/centers/article/article_display.cfm?a_id=1911], acessed July 2010.

49. B. Kamm and M. Kamm (**2004**) Biorefinery – Systems, Chem. Biochem. *Eng. Q.* 18, 1-6.

50. F.W. Lichtenthaler (**2002**) "Carbohydrates", *Ullmann s - Encyclopedia of Industrial Chemistry*, Wiley-VCH, Weinheim.

51. C. Moreau, M. Naceur, and A. Gandini (**2004**) Recent catalytic advances in the chemistry of substituted furans from carbohydrates and in the ensuing polymers, *Top. Catal.* 27, 11-30.

52. TransFurans Chemicals bvba [available online: http://www.furan.com/tfc.html], acessed in June 2010.

53. D.T. Win (**2005**) Furfural - gold from garbage, *AU J. T.* 8, 185-190.

54. H.E. Hoydonckx, W.M. van Rhijn, W.V. van Rhijn, D.E. de Vos, and P.A. Jacobs (**2007**) "Furfural and Derivatives", *Ullmann s Encyclopedia of Industrial Chemistry: Electronic Release*, Wiley-VCH, Weinheim.

55. M. Choura, N.M. Belgacem, and A. Gandini (**1996**) Acid-catalyzed polycondensation of furfuryl alcohol: mechanisms of chromophore formation and cross-linking, *Macromolecules.* 29, 3839-3850.

56. J.N. Chheda, Y. Román-Leshkov, and J.A. Dumesic (**2007**) Production of 5-hydroxymethylfurfural and furfural by dehydration of biomass-derived mono- and poly-saccharides, *Green Chem.* 9, 342-350.

57. K.J. Zeitsch (**2000**) *The Chemistry and Technology of Furfural and its Many By-Products*, Elsevier, Amsterdam.

58. A. Gandini (**1986**) "Furan polymers", In: Mark, H., Bikales, N., Overberger, C., Menges, G., and Kroschwitz, J.I. (eds.) *Encyclopedia of Polymer Science and Engineering*, John Wiley & Sons, New York.

59. W.J. McKillip (**1989**) Chemistry of furan polymers, *ACS Symp.* Ser. 385, 408-423.

60. F.W. Lichtenthaler (**2002**) Unsaturated O- and N-heterocycles from carbohydrate feedstocks, *Acc. Chem. Res.* 35, 728-737.

61. B.H. Lipshutz (**1986**) Five-membered heteroaromatic rings as intermediates in organic synthesis, *Chem. Rev.* 86, 795-819.

62. A. Gandini (**2005**) The application of the Diels-Alder reaction to polymer syntheses based on furan/maleimide reversible couplings, *Polímeros: Ciência e Tecnologia.* 15, 95-101.

63. F. Fringuelli and A. Taticchi (**1990**) *Dienes in the Diels-Alder Reaction*, Wiley-VCH, New York.

64. F. Fringuelli and A. Taticchi (**2002**) T*he Diels-Alder Reaction: Selected Practical Methods*, John Wiley & Sons, West Sussex.

65. O. Diels and K. Alder (**1928**) Synthesen in der hydroaromatischen Reihe, L*iebigs Ann.* 460, 98–122.

66. E.M. Carreira and L. Kvaerno (**2009**) *Classics in Stereoselective Synthesis*, Wiley-VCH, Weinheim.

67. F.A. Carey and R.J. Sundberg (**2007**) *Advanced Organic Chemistry. Part B: Reactions and Synthesis*, Springer, New York.

68. W. Carruthers and I. Coldham (**2004**) *Cycloaddition Reactions in Organic Synthesis*, Cambridge University Press, Cambridge.

69. C.P. Dell (**1998**) Cycloadditions in synthesis, *J. Chem. Soc., Perkin Trans. 1*. 3873-3905.

70. K.N. Houk, J. Gonzalez, and Y. Li (**1995**) Pericyclic reaction transition states: passions and punctilios, 1935-1995, *Acc. Chem. Res.* 28, 81-90.

71. C.O. Kappe, S.S. Murphree, and A. Padwa (**1997**) Synthetic applications of furan Diels-Alder chemistry, *Tetrahedron.* 53, 14179-14233.

72. H. Kwart and K. King (**1968**) The reverse Diels-Alder or retrodiene reaction, *Chem. Rev.* 68, 415-447.

73. T.J. Brocksom, J. Nakamura, M.L. Ferreira, and U. Brocksom (**2001**) The Diels-Alder reaction: an update, *J. Braz. Chem. Soc.* 12, 597-622.

74. S. Kobayashi and K.A. Jørgensen, Eds, (**2001**) *Cycloaddition Reactions in Organic Synthesis*, Wiley-VCH, Weinheim.

75. A.I. Konovalov and V.D. Kiselev (**2003**) Diels-Alder reaction: Effect of internal and external factors on the reactivity of diene-dienophile systems, *Russ. Chem. Bull., Int. Ed.* 52, 293-311.

76. K.C. Nicolaou, S.A. Snyder, T. Montagnon, and G. Vassilikogiannakis (**2002**) The Diels-Alder reaction in total synthesis, *Angew. Chem. Int. Ed.* 41, 1668-1698.

77. J. March (**1992**) *Advanced Organic Chemistry. Reactions, Mechanism, and Structures*, John Wiley & Sons, New York.

78. W. Oppolzer (**1991**) "Intermolecular Diels-Alder reaction", In: Trost, B.M., Flemming, I., and Paquette, L.A. (eds.) *Comprehensive Organic Synthesis*, pp. 315-399 Pergamon Press, Oxford.

79. J. Sauer (**1967**) Diels-Alder reactions II: the reaction mechanism, *Angew. Chem. Int. Ed. Engl.* 6, 16-33.

80. J. Sauer and R. Sustmann (**1980**) Mechanistic aspects of Diels-Alder reactions: a critical survey, Angew. Chem. Int. Ed. Engl. 19, 779-807.

81. F.A. Carey and R.J. Sundberg (**2007**) A*dvanced Organic Chemistry. Part A: Structure and Mechanisms*, Springer, New York.

82. I. Fleming (**1998**) *Pericyclic Reactions*, Oxford University Press, New York.

83. T.L. Gilchrist and R.C. Storr (**1979**) *Organic Reactions and Orbital Symmetry*, Cambridge University Press, New York.

84. R.B. Woodward (**1942**) The mechanism of the Diels-Alder reaction, *J. Am. Chem. Soc.* 64, 3058-3059.

85. R.A. Firestone (**1977**) The diradical mechanism for 1,3-dipolar cycloadditions and related thermal pericyclic reactions, *Tetrahedron.* 33, 3009-3039.

86. M.J.S. Dewar and A.B. Pierini (**1984**) Mechanism of the Diels-Alder reaction. Studies of the addition of maleic anhydride to furan and methylfurans, *J. Am. Chem. Soc.* 106, 203-208.

87. S. Seltzer (**1965**) The mechanism of the Diels-Alder reaction of 2-methylfuran with maleic anhydride, *J. Am. Chem. Soc.* 87, 1534–1540.

88. R. Huisgen (**1976**) The concerted nature of 1,3-dipolar cycloadditions and the question of diradical intermediates, *J. Org. Chem.* 41, 403-419.

89. I. Fleming (**2010**) *Molecular Orbitals and Organic Chemical Reactions*, Wiley, West Sussex.

90. H. Fujimoto, S. Inagaki, and K. Fukui (**1976**) On the donor-acceptor relationship in cyclic additions, *J. Am. Chem.* 98, 2670-2671.

91. M.J.S. Dewar and R.S. Pyron (**1970**) Nature of the transition state in some Diels-Alder reactions, *J. Am. Chem. Soc.* 92, 3098-3103.

92. K.N. Houk (**1975**) The Frontier Molecular Orbital theory of cycloaddition reactions, *Acc. Chem. Res.* 8, 361-369.

93. R.B. Woodward and R. Hoffmann (**1969**) The conservation of orbital symmetry, *Angew. Chem. Int. Ed. Engl.* 8, 781-932.

94. R. Hoffmann and R.B. Woodward (**1965**) Selection rules for concerted cycloaddition reactions, *J. Am. Chem. Soc.* 87, 2046–2048.

95. K. Fukui (**1982**) Role of frontier orbitals in chemical reactions, *Angew. Chem. Int. Ed. Engl.* 21, 801-876.

96. K. Fukui (**1971**) Recognition of stereochemical paths by orbital interaction, *Acc. Chem. Res.* 4, 57-64.

97. R. Sustmann (**1971**) A simple model for substituent effects in cycloaddition reactions. II. The Diels-Alder reaction, *Tetrahedron Lett.* 12, 2721-2724.

98. G.J. Bodwell and Z. Pi (**1997**) Electron deficient dienes I. Normal and inverse electron demand Diels-Alder reaction of the same carbon skeleton, *Tetrahedron Lett.* 38, 309-312.

99. R. Hoffmann and R.B. Woodward (**1965**) Orbital symmetries and endo/exo relationships in concerted cycloaddition reactions, *J. Am. Chem. Soc.* 87, 4388-4389.

100. D. Ginsburg (**1983**) The role of secondary orbital interactions in control of organic reactions, *Tetrahedron.* 39, 2095-2135.

101. W. Herndon and L.H. Hall (**1967**) Endo and exo transition states in the Diels-Alder reaction, *Tetrahedron Lett.* 8, 3095-3100.

102. R.B. Woodward and H. Baer (**1944**) Studies on diene-addition reactions. II. The reaction of 6,6-pentamethylenefulvene with maleic anhydride, *J. Am. Chem. Soc.* 66, 645-649.

103. H. Kwart and I. Burchuk (**1952**) Isomerism and adduct stability in the Diels-Alder reaction. I.The adducts of furan and maleimide, *J. Am. Chem. Soc.* 74, 3094–3097.

104. U. Pindur (**1993**) Acceleration and selectivity enhancement of Diels-Alder reactions by special and catalytic methods, *Chem. Rev.* 93, 741-761.

105. P. Yates and E. Philip (**1960**) Acceleration of the Diels-Alder reaction by aluminum chloride, *J. Am. Chem. Soc.* 82, 4436-4437.

106. F. Fringuelli, L. Minuti, F. Pizzo, and A. Taticchi (**1993**) Reactivity and selectivity in Lewis-acid-catalyzed Diels-Alder reactions of 2-cyclohexenones, *Acta Chem. Scand.* 47, 255-263.

107. P.J. Stevenson (**1999**) Synthetic methods. Part ii. Pericyclic Methods, A*nnu. Rep. Prog. Chem., Sect. B: Org. Chem.* 95, 19-38.

108. D.J. Nelson (**1986**) An MNDO investigation of the complexes of carbonyl compounds with Lewis Acids, *J. Org. Chem.* 51, 3185-3186.

109. F. Fringuelli, O. Piermatti, F. Pizzo, and L. Vaccaro (**2001**) Recent advances in Lewis acid catalyzed Diels-Alder reactions in aqueous media, *Eur. J. Org. Chem.* 2001, 439-455.

110. V. Caprio and J.M.J. Williams (**2009**) *Catalysis in Asymmetric Synthesis (Postgraduate Chemistry Series)*, Wiley-Blackwell, New York.

111. S. Kobayashi and K. Manabe (**2002**) Development of novel Lewis Acid catalysts for selective organic reactions in aqueous media, *Acc. Chem. Res.* 35, 209-217.

112. L.C. Dias (**1997**) Chiral Lewis acid catalysts in Diels-Alder cycloadditions: mechanistic aspects and synthetic applications of recent systems, *J. Braz. Chem. Soc.* 8, 289-332.

113. K.N. Houk and R.W. Strozier (**1973**) Lewis acid catalysis of Diels-Alder reactions, *J. Am. Chem. Soc.* 95, 4094-4096.

114. D.A. Evans and J.S. Johnson (1999) Diels-Alder reactions, In: Jacobsen, E.N., Pfaltz, A., and Yamamoto, H. (eds.) *Comprehensive Asymmetric Catalysis I-III*, pp. 1177-1235 Springer-Verlag, Heidelberg.

115. P.V. Bonnesen, C.L. Puckett, R.V. Honeychuck, and W.H. Hersh (**1989**) Catalysis of Diels-Alder reactions by low oxidation state transition-metal Lewis acids: fact and fiction, *J. Am. Chem. Soc.* 111, 6070-6081.

116. T.R. Kelly, S.K. Maity, P. Meghani, and N.S. Chandrakumar (**1989**) New Lewis acid catalysts for the Diels-Alder reaction, *Tetrahedron Lett.* 30, 1357-1360.

117. J.W. Faller and Y. Ma (**1991**) Strong Lewis acids derived from molybdenum and tungsten nitrosyls containing the tri-2-pyridylmethane ligand. Dynamic NMR studies of their adducts with aldehydes, ketones, and esters, *J. Am. Chem. Soc.* 113, 1579-1586.

118. T.K. Hollis, N.P. Robinson, and B. Bosnich (**1992**) Homogeneous catalysis. titanium complex [Ti(Cp)2(CF3SO3)2] and zirconium complex [Zr(Cp)2(CF3SO3)2THF], efficient catalysts for the Diels-Alder reaction, *Organometallics.* 11, 2745-2748.

119. D.J. Bellville, D.D. Wirth, and N.L. Bauld (**1981**) The cation-radical catalyzed Diels-Alder reaction, *J. Am. Chem. Soc.* 103, 718-720.

120. D. Carmona, M.P. Lamata, and L.A. Oro (**2000**) Recent advances in homogeneous enantioselective Diels-Alder reactions catalyzed by chiral transition-metal complexes, *Coord. Chem. Rev.* 200-202, 717-772.

121. H.B. Kagan and O. Riant (**1992**) Catalytic asymmetric Diels-Alder reactions, *Chem. Rev.* 92, 1007-1019.

122. S. Kobayashi (**1998**) New types of Lewis acids used in organic synthesis, *Pure Appl. Chem.* 70, 1019-1026.

123. K. Kamahori, S. Tada, K. Ito, and S. Itsuno (**1999**) Optically active polymer synthesis by Diels-Alder polymerization with chirally modified Lewis acid catalyst, *Macromolecules.* 32, 541-547.

124. A. Vaccari (**1999**) Clays and catalysis: a promising future, *Appl. Clay Sci.* 14, 161-198.

125. R.M. Dessau (**1986**) Catalysis of Diels-Alder reactions by zeolites, *J. Chem. Soc., Chem. Commun.* 1167-1168.

126. C. Cativiela, J.M. Fraile, J.I. García, J.A. Mayoral, E. Pires, A.J. Royo, F. Figueras, and L.C.D. Ménorval (**1993**) Silica and alumina modified by Lewis acids as catalysts in Diels-Alder reactions of carbonyl-containing dienophiles, *Tetrahedron.* 49, 4073-4084.

127. K.-ichi Fujita, T. Muraki, H. Hattori, and T. Sakakura (**2006**) Diels-Alder reaction using a dendritic copper (II) triflate-catalyst: a positive dendritic effect on the chemical yield, *Tetrahedron Lett.* 47, 4831-4834.

128. I. López, G. Silvero, M.J. Arévalo, R. Babiano, J.C. Palacios, and J.L. Bravo (**2007**) Enhanced Diels-Alder reactions: on the role of mineral catalysts and microwave irradiation in ionic liquids as recyclable media, *Tetrahedron.* 63, 2901-2906.

129. C. Cativiela, J.I. Garcia, J.A. Mayoral, E. Pires, A.J. Royo, and F. Figueras (**1995**) Diels-Alder reactions of a-amino acid precursors by heterogeneous catalysis: thermal vs. microwave activation, *Appl. Catal., A.* 131, 159-166.

130. E.V.D. Eycken, P. Appukkuttan, W.D. Borggraeve, W. Dehaen, D. Dallinger, and C.O. Kappe (**2002**) High-speed microwave-promoted hetero-Diels-Alder reactions of 2(1H)-pyrazinones in ionic liquid doped, *J. Org. Chem.* 67, 7904-7907.

131. P. Lidstrom, J. Tierney, B. Wathey, and J. Westman (**2001**) Microwave assisted organic synthesis - a review, *Tetrahedron.* 57, 9225-9283.

132. J.R. McCabe and C.A. Eckert (**1974**) The role of high-pressure kinetics in studies, *Acc. Chem. Res.* 7, 251-257.

133. F.-G. Klarner and F. Wurche (**2000**) The Effect of pressure on organic reactions: basic principles and mechanistic applications, *J. Prakt. Chem.* 342, 609-636.

134. G. Jenner (**2002**) Comparative activation modes in organic synthesis. The specific role of high pressure, *Tetrahedron*. 58, 5185-5202.

135. V.M. Zhulin, V.S. Bogdanov, M.V. Keltseva, E.B. Kabotyanskaya, and Y.D. Koreshkov (**1990**) Effect of high pressure on the composition of stereoisomers of the Diels-Alder reaction between furan and maleic anhydride, *Russ. Chem. Bull.* 38, 2303-2308.

136. V.M. Zhulin, M.V. Keltseva, V.S. Bogdanov, Y.D. Koreshkov, and E.B. Kabotyanskaya (**1990**) Effect of high pressure on the rate constant of the Diels-Alder reaction between furan and maleic anhydride, *Russ. Chem. Bull.* 39, 456-459.

137. A. Drljaca, C.D. Hubbard, R.V. Eldik, T. Asano, M.V. Basilevsky, and W.J.L. Noble (**1998**) Activation and reaction volumes in Solution. 3, *Chem. Rev.* 98, 2167−2289.

138. T. Asano and W.J.L. Noble (**1978**) Activation and reaction volumes in solution, *Chem. Rev.* 78, 407-489.

139. J. Bertrán (**1998**) Some fundamental questions in chemical reactivity, T*heor. Chem. Acc.* 99, 143-150.

140. D.C. Rideout and R. Breslow (**1980**) Hydrophobic acceleration of Diels-Alder reactions, *J. Am. Chem. Soc.* 102, 7816-7817.

141. G. Silvero, M. Arevalo, J. Bravo, M. Avalos, J. Jimenez, and I. Lopez (**2005**) An in-depth look at the effect of Lewis acid catalysts on Diels-Alder cycloadditions in ionic liquids, *Tetrahedron.* 61, 7105-7111.

142. F.M.D. Silva and J. Jones Jr (**2001**) Organic reactions in aqueous media, *Quim. Nova.* 24, 646-657.

143. A. Kumar (**2001**) Salt effects on Diels-Alder reaction kinetics, *Chem. Rev.* 101, 1-19.

144. S. Otto and J.B. Engberts (**2000**) Diels-Alder reactions in water, *Pure Appl. Chem.* 72, 1365-1372.

145. C.-J. Li (**1993**) Organic reactions in aqueous media - with a focus on carbon-carbon bond formation, *Chem. Rev.* 93, 2023-2035.

146. T. Fischer, A. Sethi, T. Welton, and J. Woolf (**1999**) Diels-Alder reactions in room-temperature ionic liquids, *Tetrahedron Lett.* 40, 793-796.

147. M.F. Ruiz-Lopez, X. Assfeld, J.I. Garcia, J.A. Mayoral, and L. Salvatella (**1993**) Solvent effects on the mechanism and selectivities of asymmetric Diels-Alder reactions, *J. Am. Chem. Soc.* 115, 8780–8787.

148. C. Reichardt (**2003**) *Solvents and Solvent Effects in Organic Chemistry*, Wiley-VCH, Weinheim.

149. R. Breslow (**1991**) Hydrophobic effects on simple organic reactions in water, *Acc. Chem. Res*. 24, 159-164.

150. C. Cativiela, J.I. García, J.A. Mayoral, and L. Salvatella (**1996**) Modelling of solvent effects on the Diels-Alder reaction, *Chem. Soc. Rev.* 25, 209.

151. R.W. Sweger and A.W. Czarnik (**1991**) "Retrograde Diels-Alder reactions", In: Trost, B.M., Flemming, I., and Paquette, L.A. (eds.) *Comprehensive Organic Synthesis*, pp. 4-5 Pergamon Press, Oxford.

152. J.L. Ripoll, A. Rouessac, and F. Rouessac (**1978**) Applications recentes de la reaction de retro-Diels-Alder en synthese organique, *Tetrahedron*. 34, 19-40.

153. A. Ichihara (**1987**) Retro-Diels-Alder strategy in natural product synthesis, *Synthesis.* 1987, 207-222.

154. S. Kotha, S. Banerjee, M.P. Patil, and R.B. Sunoj (**2006**) Retro Diels-Alder reaction under mild conditions: experimental and theoretical studies, *Org. Biomol. Chem.* 4, 1854-6.

155. A. Ichihara and H. Oikawa (**1998**) Diels-Alder type natural products - structures and biosynthesis, *Curr. Org. Chem.* 2, 365-394.

156. W.R. Roush (**1991**) "Intramolecular Diels-Alder Reactions", In: Trost, B.M., Flemming, I., and Paquette, L.A. (eds.) *Comprehensive Organic Synthesis*, pp. 513-550 Pergamon Press, Oxford.

157. M. Juhl and D. Tanner (**2009**) Recent applications of intramolecular Diels-Alder reactions to natural product synthesis, *Chem. Soc. Rev.* 38, 2983-2992.

158. G. Brieger and J.N. Bennett (**1980**) The intramolecular Diels-Alder reaction, *Chem. Rev.* 80, 63-97.

159. W. Zhao (**2010**) Novel syntheses of bridge-containing organic compounds, *Chem. Rev.* 110, 1706-45.

160. K.A. Jørgensen (**2004**) Hetero-Diels-Alder reactions of ketones - a challenge for chemists, *Eur. J. Org. Chem.* 2004, 2093-2102.

161. L.E. Tietze and G. Kettschau (**1997**) Hetero Diels-Alder reactions in organic chemistry, *Top. Curr. Chem.* 189, 1-120.

162. S.M. Weinreb (**1991**) "Heterodienophile additions to dienes", In: Trost, B.M., Flemming, I., and Paquette, L.A. (eds.) *Comprehensive Organic Synthesis*, pp. 401-449 Pergamon Press, Oxford.

163. D.L. Boger (**1991**) Heterodiene additions, In: Trost, B.M., Flemming, I., and Paquette, L.A. (eds.) *Comprehensive Organic Synthesis*, pp. 451-512 Pergamon Press, Oxford.

164. H. Pellissier (**2009**) Asymmetric hetero-Diels-Alder reactions of carbonyl compounds, *Tetrahedron.* 65, 2839-2877.

165. J.D. Winkler (**1996**) Tandem Diels-Alder cycloadditions in organic synthesis, *Chem. Rev.* 96, 167-176.

166. L.F. Tietze (**1996**) Domino reactions in organic synthesis, *Chem. Rev.* 96, 115-136.

167. A. Gandini and M.N. Belgacem (**2007**) Furan chemistry at the service of functional macromolecular materials: the reversible Diels-Alder reaction, *ACS Symp. Ser.* 954, 280-295.

168. S.D. Bergman and F. Wudl (**2008**) Mendable polymers, *J. Mater. Chem.* 18, 41-62.

169. J.A. Berson and R. Swidler (**1953**) The sterochemistry of the furan-maleic acid reaction, *J. Am. Chem. Soc.* 75, 1721–1726.

170. M.W. Lee and W.C. Herndon (**1978**) Stereochemistry of the furan-maleic anhydride cycloaddition, *J. Org. Chem.* 43, 518.

171. R.B. Woodward and H. Baer (**1948**) The reaction of furan with maleic anhydride, *J. Am. Chem. Soc.* 70, 1161–1166.

172. L. Rulisek, P. Sebek, Z. Havlas, R. Hrabal, P. Capek, and A. Svatos (**2005**) An experimental and theoretical study of stereoselectivity of furan-maleic anhydride and furan-maleimide Diels-Alder reactions, *J. Org. Chem.* 70, 6295-6302.

173. G.C. Tesoro and V.R. Sastri (**1986**) Synthesis of siloxane-containing bis(furans) and polymerization with bis(maleimides), *Ind. Eng. Prod. Res. Dev.* 25, 444-448.

174. X. He, V.R. Sastri, and G.C. Tesoro (**1988**) 1,4-Bis(5-methylfurfuryl)benzene: Polymerization with siloxane containing dimaleimides, *Makromol. Chem. Rapid. Commun.* 9, 191-194.

175. H.S. Patel and B.D. Lad (**1989**) Polyimides based on poly(2,5-furandiylmethylene), 1, *Makromol. Chem.* 190, 2055–2061.

176. C.D. Diakoumakos and J.A. Mikroyannidis (**1992**) Polyimides derived from Diels-Alder polymerization of furfuryl-substituted maleamic acids or from the reaction of bismaleamic with bisfurfurylpyromellitamic acids, *J. Polym. Sci., Part A: Polym. Chem.* 30, 2559–2567.

177. C.D. Diakoumakos and J.A. Mikroyannidis (**1994**) Heat-resistant resins derived from cyano-substituted Diels-Alder polymers, *Eur. Polym. J.* 30, 465-472.

178. N. Kuramoto, K. Hayashi, and K. Nagai (**1994**) Thermoreversible reaction of Diels-Alder polymer composed of difurufuryladipate with bismaleimidodiphenylmethane, *J. Polym. Sci., Part A: Polym. Chem.* 32, 2501-2504.

179. C. Goussé and A. Gandini (**1999**) Diels-Alder polymerization of difurans with bismaleimides, *Polym. Int.* 48, 723-731.

180. T. Brand and M. Klapper (**1999**) Control of viscosity through reversible addition of telechelics via repetitive Diels-Alder reaction in bulk, *Des. Monomers Polym.* 2, 287-309.

181. N. Teramoto, Y. Arai, and M. Shibata (**2006**) Thermo-reversible Diels–Alder polymerization of difurfurylidene trehalose and bismaleimides, *Carbohydr. Polym.* 64, 78-84.

182. C.P. Berumen (**2003**), "Nouveaux materiaux polymeres bases sur la chimie furanique", PhD Thesis, PAGORA - Institut National Polytechnique de Grenoble, France.

183. J.A. Mikroyannidis (**1992**) Synthesis and Diels–Alder polymerization of furfurylidene and furfuryl-substituted maleamic acids, *J. Polym. Sci., Part A: Polym. Chem.* 30, 125-132.

184. J.A. Mikroyannidis (**1992**) Furyl-maleimide in situ generated ab-monomers: Synthesis, characterization, and Diels-Alder polymerization, *J. Polym. Sci., Part A: Polym. Chem.* 30, 2017–2024.

185. C. Goussé and A. Gandini (**1998**) Synthesis of 2-furfurylmaleimide and preliminary study of its Diels-Alder polycondensation, *Polym. Bull.* 40, 389-394.

186. V. Gaina and C. Gaina (**2003**) AB monomers. I. Synthesis and polymerization of furyl-maleimide monomers, *Rev. Roum. Chim.* 48, 881-890.

187. X. Chen, M.A. Dam, K. Ono, A. Mal, H. Shen, S.R. Nutt, K. Sheran, and F. Wudl (**2002**) A thermally re-mendable cross-linked polymeric material, *Science.* 295, 1698-1702.

188. X. Chen, F. Wudl, A.K. Mal, H. Shen, and S.R. Nutt (**2003**) New thermally remendable highly cross-linked polymeric materials, *Macromolecules.* 36, 1802-1807.

189. R. Gheneim, C. Perez-Berumen, and A. Gandini (**2002**) Diels-Alder reactions with novel polymeric dienes and dienophiles: synthesis of reversibly cross-linked elastomers, *Macromolecules.* 35, 7246-7253.

190. C. Goussé, A. Gandini, and P. Hodge (**1998**) Application of the Diels-Alder reaction to polymers bearing furan moieties. 2 .Diels-Alder and retro-Diels-Alder reactions involving furan rings in some styrene copolymers, *Macromolecules.* 31, 314-321.

191. H. Laita, S. Boufi, and A. Gandini (**1997**) The application of the Diels-Alder reaction to polymers bearing furan moieties. 1.Reactions with maleimides, *Eur. Polym. J.* 33, 1203-1211.

192. S.A. Canary and M.P. Stevens (**1992**) Thermally reversible crosslinking of polystyrene via the furan-maleimide Diels–Alder reaction, J. *Polym. Sci., Part A: Polym. Chem.* 30, 1755–1760.

193. Y. Chujo, K. Sada, and T. Saegusa (**1990**) Reversible gelation of polyoxazoline by means of Diels-Alder reaction, *Macromolecules.* 23, 2636-2641.

194. H.S. Patel, B.D. Lad, and H.S. Vyas (**1990**) Polyimides Based on Poly(2,5-furandiylmethylene). II, *High Perform. Polym.* 2, 113-120.

195. M.P. Stevens and A.D. Jenkins (**1979**) Crosslinking of polystyrene via pendant maleimide groups, *J. Polym. Sci. Polym. Chem. Ed.* 17, 3675–3685.

196. Y. Zhang, A.A. Broekhuis, and F. Picchioni (**2009**) Thermally self-healing polymeric materials: the next step to recycling thermoset polymers?, *Macromolecules.* 42, 1906-1912.

197. E. Goiti, M.B. Huglin, and J.M. Rego (**2001**) Some observations on the copolymerization of styrene with furfuryl methacrylate, *Polymer.* 42, 10187-10193.

198. E. Goiti, M.B. Huglin, and J.M. Rego (**2003**) Thermal Breakdown by the Retro Diels–Alder Reaction of Crosslinking in Poly[styrene-co-(furfuryl methacrylate)], *Macromol. Rapid Commun.* 24, 692-696.

199. E. Goiti, M.B. Huglin, and J.M. Rego (**2004**) Some properties of networks produced by the Diels–Alder reaction between poly(styrene-co-furfuryl methacrylate) and bismaleimide, *Eur. Polym. J.* 40, 219-226.

200. E. Goiti, F. Heatley, M.B. Huglin, and J.M. Rego (**2004**) Kinetic aspects of the Diels-Alder reaction between poly(styrene-co-furfuryl methacrylate) and bismaleimide, *Eur. Polym. J.* 40, 1451-1460.

201. Y. Imai, H. Itoh, K. Naka, and Y. Chujo (**2000**) Thermally reversible IPN organic-inorganic polymer hybrids utilizing the Diels-Alder reaction, *Macromolecules.* 33, 4343-4346.

202. T.E. Zewert and M.G. Harrington (**1999**) Cross-linked poly(N-acetylethylenimine) as an isoelectric focusing matrix, *Electrophoresis.* 20, 1339-1348.

203. R. Gheneim (**2002**), "Synthese et caracterisation de materiaux elastomeres a reticulation reversible basee sur la reaction de Diels-Alder", PhD Thesis, PAGORA - Institut National Polytechnique de Grenoble, France.

204. J.R. McElhanon, E.M. Russick, D.R. Wheeler, D.A. Loy, and J.H. Aubert (**2002**) Removable foams based on an epoxy resin incorporating reversible Diels-Alder adducts, *J. Appl. Polym. Sci.* 85, 1496-1502.

205. J.H. Aubert (**2003**) Thermally removable epoxy adhesives incorporating thermally reversible Diels-Alder adducts, *J. Adhes.* 79, 609-616.

206. N. Yoshie, M. Watanabe, H. Araki, and K. Ishida (**2010**) Thermo-responsive mending of polymers crosslinked by thermally reversible covalent bond: polymers from bisfuranic terminated poly(ethylene adipate) and tris-maleimide, *Polym. Degrad. Stab.* 95, 826-829.

207. Q. Tian, Y.C. Yuan, M.Z. Rong, and M.Q. Zhang (**2009**) A thermally remendable epoxy resin, *J. Mater. Chem.* 19, 1289.

208. Y.H. Kim (**1998**) Hyperbranched polymers 10 years after, *J. Polym. Sci., Part A: Polym. Chem.* 36, 1685-1698.

209. C. Yates (**2004**) Synthesis and applications of hyperbranched polymers, *Eur. Polym. J.* 40, 1257-1281.

210. J.R. McElhanon and D.R. Wheeler (**2001**) Thermally responsive dendrons and dendrimers based on reversible furan-maleimide Diels-Alder adducts, *Org. Lett.* 3, 2681-2683.

211. G. Franc and A.K. Kakkar (**2009**) Diels-Alder "click" chemistry in designing dendritic macromolecules., *Chem. Eur. J.* 15, 5630-9.

212. M.M. Kose, G. Yesilbag, and A. Sanyal (**2008**) Segment block dendrimers via Diels-Alder cycloaddition, *Org. Lett.* 10, 2353-2356.

213. M.L. Szalai, D.V. Mcgrath, D.R. Wheeler, T. Zifer, and J.R. Mcelhanon (**2007**) Dendrimers based on thermally reversible furan-maleimide Diels-Alder Adducts, *Macromolecules.* 40, 818-823.

214. B.I. Voit and A. Lederer (**2009**) Hyperbranched and highly branched polymer architectures-synthetic strategies and major characterization aspects, *Chem. Rev.* 109, 5924-5973.

215. B. Gotsmann, U. Duerig, J. Frommer, and C.J. Hawker (**2006**) Exploiting chemical switching in a Diels-Alder polymer for nanoscale probe lithography and data storage, *Adv. Funct. Mater.* 16, 1499-1505.

216. K. Adachi, A.K. Achimuthu, and Y. Chujo (**2004**) Synthesis of organic-inorganic polymer hybrids controlled by Diels-Alder reaction, *Polymer.* 37, 9793-9797.

217. K. Inoue, M. Yamashiro, and M. Iji (**2009**) Recyclable shape-memory polymer: poly(lactic acid) crosslinked by a thermoreversible Diels-Alder reaction, J. *Appl. Polym. Sci.* 112, 876-885.

218. F. Wudl and X. Chen (**2005**), "Thermally re-mendable cross-linked polymers", US patent 6933361 B2.

219. M. Watanabe and N. Yoshie (**2006**) Synthesis and properties of readily recyclable polymers from bisfuranic terminated poly(ethylene adipate) and multi-maleimide linkers, *Polymer.* 47, 4946-4952.

220. C. Tarducci, J.P.S. Badyal, S.A. Brewer, and C. Willis (**2005**) Diels-Alder chemistry at furan ring functionalized solid surfaces, *Chem. Commun.* 406-408.

221. P.J. Costanzo, J.D. Demaree, and F.L. Beyer (**2006**) Controlling dispersion and migration of particulate additives with block copolymers and Diels-Alder chemistry, *Langmuir.* 22, 10251-10257.

222. F. He, Y. Tang, M. Yu, S. Wang, Y. Li, and D. Zhu (**2007**) A Strategy for the detection of Diels–Alder reactions using fluorescence quenching of conjugated polymers, *Adv. Funct. Mater.* 17, 996-1002.

223. Y. Liu, C. Hsieh, and Y. Chen (**2006**) Thermally reversible cross-linked polyamides and thermo-responsive gels by means of Diels-Alder reaction, *Polymer.* 47, 2581-2586.

224. Y.-L. Liu and Y.-W. Chen (**2007**) Thermally Reversible Cross-Linked Polyamides with High Toughness and Self-Repairing Ability from Maleimide- and Furan-Functionalized Aromatic Polyamides, *Macromol. Chem. Phys.* 208, 224-232.

225. Y.-L. Liu and C.-Y. Hsieh (**2006**) Crosslinked epoxy materials exhibiting thermal remendablility and removability from multifunctional maleimide and furan compounds, *J. Polym. Sci., Part A: Polym. Chem.* 44, 905-913.

226. A.A. Kavitha and N.K. Singha (**2007**) A tailor-made polymethacrylate bearing a reactive diene in reversible Diels-Alder reaction, *J. Polym. Sci., Part A: Polym. Chem.* 45, 4441-4449.

227. M. Yamashiro, K. Inoue, and M. Iji (**2008**) Recyclable Shape-memory and Mechanical Strength of Poly(lactic acid) Compounds Cross-linked by Thermo-reversible Diels-Alder Reaction, *Polymer J.* 40, 657-662.

228. A.M. Peterson, R.E. Jensen, and G.R. Palmese (**2009**) Reversibly cross-linked polymer gels as healing agents for epoxy-amine thermosets., *ACS Appl. Mater. Interfaces.* 1, 992-5.

229. P.G. Parzuchowski, M. Kiźlińska, and G. Rokicki (**2007**) New hyperbranched polyether containing cyclic carbonate groups as a toughening agent for epoxy resin, *Polymer.* 48, 1857-1865.

230. H.-L. Wei, Z. Yang, L.-M. Zheng, and Y.-M. Shen (**2009**) Thermosensitive hydrogels synthesized by fast Diels-Alder reaction in water, *Polymer.* 50, 2836-2840.

231. K. Ishida and N. Yoshie (**2008**) Synthesis of readily recyclable biobased plastics by Diels-Alder reaction, *Macromol. Biosci.* 8, 916-22.

232. C.S. Chiu, J.M. Lin, Y.K. Chen, S.H. Wu, B.S. Peng, and K.Y. Hsu (**2003**) Thermally cleavable epoxy resins for electronic and optoelectronic applications, *Electronics Packaging Technology, 2003 5th Conference* (EPTC 2003), pp. 425-428.

233. N. Aumsuwan and M. Urban (**2009**) Reversible releasing of arms from star morphology polymers, *Polymer.* 50, 33-36.

234. C. Jegat and N. Mignard (**2008**) Effect of the polymer matrix on the thermal behaviour of a furan-maleimide type adduct in the molten state, *Polym. Bull.* 60, 799-808.

235. C.-M. Chang and Y.-L. Liu (**2009**) Functionalization of multi-walled carbon nanotubes with furan and maleimide compounds through Diels–Alder cycloaddition, *Carbon*. 47, 3041-3049.

236. J.R. McElhanon, T. Zifer, S.R. Kline, D.R. Wheeler, D.A. Loy, G.M. Jamison, T.M. Long, K. Rahimian, and B.A. Simmons (**2005**) Thermally cleavable surfactants based on furan-maleimide Diels-Alder adducts, *Langmuir.* 21, 3259-3266.

237. I. Bicu, Mustata¸F. (**2000**) Water soluble polymers from Diels-Alder adducts of abietic acid as paper additives, *Macromol. Mater. Eng.* 280, 47-53.

238. V. Balzani, P. Ceroni, S. Gestermann, C. Kauffmann, and M.G.A.F. Vögtle (**2000**) Dendrimers as fluorescent sensors with signal amplification, *Chem. Commun.* 853-854.

239. X. Zhang, Z.-C. Li, K.-B. Li, F.-S. Du, and F.-M. Li (**2004**) Multi-maleimides bearing electron-donating chromophores: reversible fluorescence and aggregation behavior, *J. Am. Chem. Soc.* 126, 12200-12201.

240. M. Shi and M.S. Shoichet (**2008**) Furan-functionalized co-polymers for targeted drug delivery: characterization, self-assembly and drug encapsulation, *J. Biomater. Sci., Polymer Ed.* 19, 1143- 1157.

241. M. Shi, J.H. Wosnick, K. Ho, A. Keating, and M.S. Shoichet (**2007**) Immuno-polymeric nanoparticles by Diels-Alder chemistry, *Angew. Chem. Int. Ed.* 46, 6126-31.

242. L.J. Bellamy (**1975**) *The Infrared Spectra of Complex Molecules*, Chapman and Hall Ltd., London.

243. N.E. Jacobsen (**2007**) *NMR Spectroscopy Explained*, John Wiley & Sons, New Jersey.

244. M. Balci (**2005**) *Basic ^{1}H- and ^{13}C-NMR Spectroscopy*, Elsevier B.V., Amsterdam.

245. R.J. Abraham and H.J. Bernstein (**1959**) The proton resonance spectra of furan and pyrrole, *Can. J. Chem.* 37, 1056-1065.

246. R.J. Abraham and H.J. Bernstein (**1961**) The proton resonance spectra of some substituted furans and pyrroles, *Can. J. Chem.* 39, 905-914.

247. E. Breitmaier and W. Voelter (**1987**) *Carbon-13 NMR Spectroscopy*, VCH, Weinheim.

248. D.L. Pavia, G.M. Lampman, G.S. Kriz, and J.R. Vyvyan (**2009**) *Introduction to Spectroscopy*, Brooks/Cole, Belmont.

249. A. Gandini, S. Hariri, and J. Le Nest (**2003**) Furan-polyether-modified chitosans as photosensitive polymer electrolytes, *Polymer.* 44, 7565-7572.

250. S. Hariri (**2001**), "Électrolytes polymères photoréticulables à base de chitosane polyéthers et chromophores furaniques conjugués", PhD Thesis, PAGORA - Institut National Polytechnique de Grenoble, France.

251. T.P. Kogan (**1992**) The synthesis of substituted methoxy-poly(ethyleneglycol) derivatives suitable for selective protein modification, *Synth. Commun.* 22, 2417-2424.

252. K. Popov-Pergal, M. Pergal, D. Babic, M. Marinovic-Cincovic, and R. Jovanovic (**2000**) Thermal, oxidative and radiation stability of polyimides I. Bismaleimidoethane and different diamine-based polyimides, *Polym. Degrad. Stab.* 67, 547-552.

253. A. Gandini, D. Coelho, and A. Silvestre (**2008**) Reversible click chemistry at the service of macromolecular materials. Part 1: Kinetics of the Diels-Alder reaction applied to furan-maleimide model compounds and linear polymerizations, *Eur. Polym. J.* 44, 4029-4036.

254. C.K. Sauers (**1969**) Dehydration of N-arylmaleamic acids with acetic anhydride, *J. Org. Chem.* 34, 2275-2279.

255. M. Sava, C. Gaina, V. Gaina, and D. Timpu (**2001**) Synthesis and characterization of some bismaleimides containing ether groups in the backbone, *Macromol. Chem. Phys.* 202, 2601-2605.

256. G. Socrates (**2001**) *Infrared and Raman Characteristic Group Frequencies: Tables and Charts*, John Wiley & Sons, West Sussex.

257. G. Mantovani, F. Lecolley, L. Tao, D.M. Haddleton, J. Clerx, J.J.L.M. Cornelissen, and K. Velonia (**2005**) Design and synthesis of N-maleimido-functionalized hydrophilic polymers via copper-mediated living radical polymerization: a suitable alternative to PEGylation chemistry, *J. Am. Chem. Soc.* 127, 2966-2973.

258. B.J. Neubert and B.B. Snider (**2003**) Synthesis of (±)-phloeodictine A1, *Org. Lett.* 5, 765-768.

259. G. Mantovani, F. Lecolley, L. Tao, D.M. Haddleton, J. Clerx, J.J.L.M. Cornelissen, and K. Velonia (**2005**) Supporting information: Design and synthesis of new N-maleimido-functionalized hydrophilic polymers via copper-mediated living radical polymerization: a suitable alternative to PEGylation chemistry, *J. Am. Chem. Soc.* 127, 1-17.

260. D.J. Berry, C.V. DiGiovanna, S.S. Metrick, and R. Murugan (**2001**) Catalysis by 4-dialkylaminopyridines, *ARKIVOC.* 2001, 201-226.

261. W. Steglich (**1990**) Esterification of carboxylic acids with dicyclohexylcarbodiimide/4-dimethylaminopyridine: tert-butyl ethyl fumarate, *Org. Synth.* 7, 93-95.

262. A. Vogel, A. Tatchell, B. Furnis, A. Hannaford, and P. Smith (**1989**) *Vogel s textbook of practical organic chemistry,* Longman Scientific & Technical, Essex.

263. Z. Zhou and R. Chen (**2000**) Synthesis of glycerophospholipid conjugates of cantharidin and its analogues, *Synth. Commun.* 30, 3527-3533.

APPENDIX

Publications

SCI papers

Alessandro Gandini, Dora Coelho and Armando Silvestre (**2008**) Reversible click chemistry at the service of macromolecular materials. Part 1: Kinetics of the Diels–Alder reaction applied to furan–maleimide model compounds and linear polymerizations, *Eur. Polym. J.*, 44, 4029–4036.

Alessandro Gandini, Dora Coelho, Mónica Gomes, Bruno Reis and Armando Silvestre (**2009**) Materials from renewable resources based on furan monomers and furan chemistry: work in progress, *J. Mater. Chem.*, 19, 8656-8664.

Alessandro Gandini, Armando Silvestre and Dora Coelho (**2010**) Reversible Click Chemistry at the Service of Macromolecular Materials. II. Thermoreversible Polymers Based on the Diels-Alder Reaction of an A-B Furan/Maleimide Monomer, *J. Polym. Sci., Part A: Polym. Chem.*, 48, 2053-2056.

Alessandro Gandini, Armando Silvestre and Dora Coelho (**2011**) Reversible Click Chemistry at the Service of Macromolecular Materials. Thermoreversible Polymers Based on the Diels-Alder Reaction of A-B Furan/Maleimide Monomers, *Polym. Chem.*, *submitted*.

Proceeding

Dora Coelho, Alessandro Gandini and Armando Silvestre (**2010**) *Thermoreversible polymers based on the Diels-Alder reaction between furan and maleimide monomers. AB and A_n+B_m systems*, Polycondensation 2010 Conference, Kerkrade, The Netherlands, September 5-8.

Abstracts (Oral presentations)

Dora Coelho, Alessandro Gandini and Armando Silvestre, *Novel Furan Polymeric Materials Based on the reversible Diels-Alder Reaction*, XI Simposio Latinoamericano y IX Congreso Iberoamericano de Polímeros – SLAP 2008, Lima, Peru, July 15-18, **2008**.

Dora Coelho, Alessandro Gandini and Armando Silvestre, *Thermoreversible polymers based on the Diels-Alder reaction between furan and maleimide monomers*, EPF'09 – European Polymer Congress, Graz, Austria, July 12-17, **2009**.

Dora Coelho, Alessandro Gandini and Armando Silvestre, *Novel Furan Polymer Materials: An alternative based on renewable resources*, 1st G7 CICECO meeting, University of Aveiro, Portugal, July 21, **2009**.

Dora Coelho, Alessandro Gandini and Armando Silvestre, *Thermoreversible polymers based on the Diels-Alder reaction between furan and maleimide monomers. AB and A_2B_3 systems*, 2nd International Conference on Biodegradable Polymers and Sustainable Composites (BIOPOL), Alicante, Spain, September 30 – October 2, **2009**.

Dora Coelho, Mónica Gomes, Alessandro Gandini and Armando Silvestre, *New Polymers from furan monomers*, VII CICECO meeting, University of Aveiro, Portugal, January 28-29, **2010**.

Alessandro Gandini, Dora Coelho and Armando Silvestre, *Furan as monomers in Diels-Alder polymerizations with maleimides*, Biomass derived pentoses: from biotechnology to fine chemistry, Reims, France, November 14-16, **2010**.

Abstracts (Poster Presentations)

Dora Coelho, Alessandro Gandini and Armando Silvestre, *New thermoreversible materials based on the Diels-Alder reaction applied to furan derivatives*, 1st International Conference on Biodegradable Polymers and Sustainable Composites (BIOPOL), Alicante, Spain, October 3-5, **2007**.

Dora Coelho, Alessandro Gandini and Armando Silvestre, *Thermoreversible materials based on the Diels-Alder reaction of furan monomers,* XXI Encontro da Sociedade Portuguesa de Química (SPQ), Porto, Portugal, June 11-13, **2008**.

Dora Coelho, Alessandro Gandini and Armando Silvestre, *Thermoreversible materials based on the Diels-Alder reaction of furan monomers,* VI CICECO meeting, University of Aveiro, Portugal, March 5-6, **2009**.

Dora Coelho, Alessandro Gandini and Armando Silvestre, *Thermoreversible polymers based on the Diels-Alder reaction between furan and maleimide monomers. AB and A_n+B_m systems*, Polycondensation 2010 conference, Kerkrade, The Netherlands, September 5-8, **2010**.